UNIVERSITÀ
DEGLI STUDI
DI BRESCIA

DOTTORATO DI RICERCA IN PRECISION MEDICINE

settore scientifico disciplinare MED/04

XXXIV CICLO

MÜLLER GLIAL CELLS IN EPIRETINAL MEMBRANE FORMATION

DOTTORANDO: ADWAID MANU KRISHNA CHANDRAN

RELATORE: PROF. MARCO PRESTA

TUTOR: Dr. MIRELLA BELLERI

TABLE OF CONTENTS

ACKNOWLEDGMENTS i

ABBREVIATIONS AND ACRONYMS ii

SUMMARY iv

RIASSUNTO vi

INTRODUCTION 1

- **ERM PREVALENCE** 1
- **DIAGNOSIS AND CLASSIFICATION** 2
- **IDIOPATHIC EPIRETINAL MEMBRANE** 4
  - **CLINICAL FEATURES** 5
  - **PATHOGENESIS OF iERM** 6
  - **TREATMENT** 7
- **DIABETES MELLITUS** 8
  - **DIABETIC RETINOPATHY** 8
  - **PREVALENCE OF PDR** 9
  - **PATHOGENESIS OF PDR** 9
  - **TREATMENT** 11
- **RETINA** 12
- **INNER LIMITING MEMBRANE** 14
- **MÜLLER GLIAL CELLS** 14
- **ROLE OF MÜLLER GLIAL CELLS IN ERM** 16
- **EPITHELIAL-MESENCHYMAL TRANSITION (EMT)** 19

RESULTS 21

- **GENE EXPRESSION ANALYSIS IDENTIFIES TWO DISTINCT MOLECULAR CLUSTERS OF IDIOPATHIC EPIRETINAL MEMBRANES** 21
- **VEGF-INDEPENDENT ACTIVATION OF MÜLLER CELLS BY THE VITREOUS FROM PROLIFERATIVE DIABETIC RETINOPATHY PATIENTS** 50

CONCLUSIONS 69

- **MOLECULAR CLASSIFICATION OF iERMs** 69

- **iERMs VITREOUS INDUCES GMT IN MÜLLER MIO-M1 CELLS** 69
- **PDR VITREOUS-INDUCED ACTIVATION OF MÜLLER CELLS IS INDEPENDENT OF VEGF** 70

BIBLIOGRAPHY 72

ADDENDUM 83

- ***β*-GALACTOSYLCERAMIDASE DEFICIENCY CAUSES UPREGULATION OF LONG PENTRAXIN-3 IN THE CENTRAL NERVOUS SYSTEM OF *TWITCHER* MICE AND KRABBE PATIENTS.** 84

CURRICULUM VITAE 114

ACKNOWLEDGMENTS

The success of this project depends largely on the encouragement and guidelines of many others. I take this opportunity to express my gratitude to the people who have been instrumental in the successful completion of my Ph.D.

With immense pleasure, I wish to express my profound sense of reverence, gratitude, and obligation to my esteemed guide Prof. Marco Presta, Department of Molecular and Translational Medicine (DMMT), University of Brescia, for his research guidance, close supervision, relevant suggestion, bolstering encouragement, constructive criticism, timely advice and help throughout the period of investigation and preparation of this thesis despite his hectic schedule. I am proud and fortunate for having worked under his guidance.

With profound respect, I convey my sincere thanks to my tutor Dr. Mirella Belleri, for invaluable guidance, teaching, encouragement, and constant support at every step throughout my Ph.D.

I sincerely convey my gratitude to Dr. Daniela Coltrini and Dr. Sara Rezzola for their help and support in all my endeavours to complete my doctoral work.

I express my sincere obligation to the management of the University of Brescia for permitting and providing me with the necessary facilities and fellowship to carry out my research.

In the end, I express my heartiest devotion and a deep sense of gratitude to my family, my parents, sister for their encouragement, moral support, and the love bestowed on me, without which the present thesis would not have been successful.

ABBREVIATIONS AND ACRONYMS

ACTA2	Actin2
BCVA	Best-Corrected Visual Acuity
BRB	Blood-Retinal Barrier
ECM	Extracellular Matrix
EMT	Epithelial-to-Mesenchymal Transition
FGF2	Fibroblast Growth Factor 2
FGFR	Fibroblast growth factor receptor
GFAP	Glial Fibrillary Acid-Protein
GMT	Glial-to-Mesenchymal Transition
iERM	Idiopatic Epiretinal Membrane
ILM	Inner Limiting Membrane
IS/OS	Inner Segment/Outer Segment
KIR4.1	Inward Rectifier K+ Channel 10
NPDR	Non-Proliferative Diabetic Retinopathy
PDR	Proliferative Diabetic Retinopathy
PRP	Pan-Retinal Photocoagulation
PVD	Posterior Vitreous Detachment
RLBP1	Retinaldehyde-Binding Protein 1
RPE	Retinal Pigment Epithelial

S100A4	S100 calcium-binding protein A4
SD-OCT	Spectral-Domain Optical Coherence Tomography
TGFβ	Transforming Growth Factor β
TNFα	Tumor Necrosis Factor α
VEGF	Vascular Endothelial Growth Factor
VEGFR	Vascular Endothelial Growth Factor Receptor
VIM	Vimentin
αSMA	α-Smooth Muscle Actin

SUMMARY

An epiretinal membrane (ERM) is a thin layer of fibrous tissue that can form on the surface of the retina macular area and cause vision problems. ERMs can be classified as idiopathic, primary, or secondary based on their underlying etiology. Idiopathic ERM is the most common type of epiretinal membrane that occur in the absence of an identifiable etiology, which is more relevant for patients over the age of 50. The secondary ERM is commonly associated with ocular eye diseases like age-related macular degeneration, glaucoma, diabetic retinopathy. The most severe level of ERM is observed in patients with proliferative diabetic retinopathy (PDR), the major complication of diabetes mellitus and the leading cause of blindness among working adults worldwide. Müller glial cells appear to play a pivotal role in the pathogenesis of ERM, where various cytokines and growth factors may act as autocrine and paracrine modulators by triggering Müller cell proliferation, migration, collagen contraction, transdifferentiation, and increased expression of gliosis markers. Vitreous humor may represent a reservoir of pathological mediators that accumulate during the progression of retinal diseases. Here, the vitreous fluid obtained from iERM and PDR patients was used as a tool to investigate the activation that occurs in Müller cells in disease progression.

During the first part of my Ph.D. thesis work, I participated in a research project in which we showed that surgically removed iERMs are characterized by a different pattern of expression of a series of the cell population, extracellular matrix, and cytokine/growth factor biomarkers relevant to the pathogenesis of the disease. Further, the hierarchical clustering of the gene expression data identified two molecular clusters of iERM membranes associated with distinct clinical and SD-OCT features (named iERM-A and iERM-B). iERM-A patients are characterized by less severe clinical features and a more "quiescent" iERM gene expression profile when compared to iERM-B patients.

Further, I focused on understanding the role of Müller glial cells in the pathogenesis of iERM. During the progression of iERM, Müller glial cells undergo a glial-to-mesenchymal transition (GMT), a transdifferentiation process characterized by the downregulation of Müller cell markers paralleled by the upregulation of pro-fibrotic myofibroblast markers. The present study demonstrated that the vitreous fluid obtained from the iERM patients induces proliferation, migration, and GMT in MIO-M1 Müller cells, a phenotype consistent with Müller cell behaviour during iERM progression. However, even though the vitreous fluid obtained from iERM-A patients could induce a complete GMT in MIO-M1 cells, iERM-B samples caused only a partial GMT, characterized by the

downregulation of Müller cell markers in the absence of upregulation of pro-fibrotic myofibroblast markers.

For the final part of my thesis work, the vitreous fluid obtained from PDR patients was used as a tool to investigate the activation that occurs in Müller cells during PDR. The results show that PDR vitreous induces the acquisition of an activated phenotype in Müller cells, characterized by an increase in cell proliferation and migration, intracellular signalling activation, and proinflammatory cytokine/chemokine expression. Surprisingly, we found that the acquisition of this phenotype is not related to VEGF stimulation, whereas treatment of Müller cells with basic fibroblast growth factor (FGF2) induces a significant increase in the expression of various cytokines/chemokines in MIO-M1 cells. Accordingly, the anti-VEGF drug ranibizumab does not affect Müller cell activation mediated by PDR vitreous whereas treatment with the FGF receptor (FGFR) tyrosine kinase inhibitor BGJ398, the pan-FGF trap NSC12, the multi-target heparin-binding protein antagonist N-tert-butyloxycarbonyl-Phe-Leu-Phe-Leu-Phe Boc2, or the anti-inflammatory drug hydrocortisone inhibits, at least in part, the activity of PDR vitreous samples.

Together, the results indicate that a relationship may exist among the ability of iERM vitreous to modulate GMT in Müller cells, the molecular profile of the corresponding iERMs, and the clinical features of iERM patients. Also, these data point to a role for various mediators besides VEGF in the response elicited by PDR vitreous in Müller cells.

RIASSUNTO

Una membrana epiretinica (ERM) è un sottile strato di tessuto fibroso che può formarsi sulla superficie dell'area maculare della retina e causare problemi alla vista. Le ERM possono essere classificate come idiopatiche, primarie o secondarie in base alla loro eziologia. L'ERM idiopatica è il tipo più comune di membrana epiretinica; essa si verifica in assenza di un'eziologia identificabile ed è la più rilevante per i pazienti di età superiore ai 50 anni. L'ERM secondaria è comunemente associata a malattie oculari come la degenerazione maculare senile, il glaucoma , o la retinopatia diabetica. Il livello più grave di ERM si osserva nei pazienti con retinopatia diabetica proliferativa (PDR), la principale complicanza del diabete mellito e la principale causa di cecità tra gli adulti. Le cellule gliali di Müller sembrano svolgere un ruolo fondamentale nella patogenesi dell'ERM, dove varie citochine e fattori di crescita possono agire come modulatori autocrini e paracrini innescando la proliferazione, la migrazione, la contrazione del collagene, la transdifferenziazione e l'aumento dell'espressione dei marcatori della gliosi delle cellule di Müller. L'umor vitreo può rappresentare un serbatoio di mediatori patologici che si accumulano durante la progressione delle malattie retiniche. L'umor vitreo ottenuto da pazienti con iERM e PDR è stato utilizzato come strumento per studiare l'attivazione che si verifica nelle cellule di Müller nella progressione della malattia.

Durante la prima parte del mio dottorato di ricerca ho partecipato a un progetto in cui abbiamo dimostrato che gli iERM rimossi chirurgicamente sono caratterizzati da un diverso pattern di espressione di geni associati a diverse popolazioni cellulari, matrice extracellulare e biomarcatori di citochine/fattori di crescita rilevanti per la patogenesi della malattia. Inoltre, il raggruppamento gerarchico dei dati di espressione genica ha identificato due cluster molecolari di membrane iERM associati a caratteristiche cliniche e SD-OCT distinte (denominate iERM-A e iERM-B). I pazienti iERM-A sono caratterizzati da manifestazioni cliniche meno gravi e un profilo di espressione genica iERM più "quiescente" rispetto ai pazienti iERM-B.

Inoltre, mi sono concentrato sulla comprensione del ruolo delle cellule gliali di Müller nella patogenesi di iERM. Durante la progressione di iERM, le cellule gliali di Müller subiscono una transizione gliale-mesenchimale (GMT), un processo di transdifferenziazione caratterizzato dalla sottoregolazione dei marcatori delle cellule di Müller parallela alla sovraregolazione dei marcatori dei miofibroblasti pro-fibrotici. Il presente studio ha dimostrato che il fluido vitreo ottenuto dai pazienti iERM induce proliferazione, migrazione e GMT nelle cellule MIO-M1 Müller, un fenotipo coerente con il comportamento delle cellule Müller durante la progressione iERM. Tuttavia, anche se

il fluido vitreo ottenuto dai pazienti iERM-A potrebbe indurre un GMT completo nelle cellule MIO-M1, i campioni iERM-B hanno causato solo un GMT parziale, caratterizzato dalla downregulation dei marker cellulari di Müller in assenza di upregulation di pro- marcatori fibrotici di miofibroblasti.

Per la parte finale del mio lavoro di tesi, ho utilizzato il fluido vitreo ottenuto da pazienti con PDR come strumento per studiare l'attivazione che si verifica nelle cellule di Müller durante la PDR. I risultati mostrano che il vitreo PDR induce l'acquisizione di un fenotipo attivato nelle cellule di Müller, caratterizzato da un aumento della proliferazione e della migrazione cellulare, dall'attivazione del segnale intracellulare e dall'espressione di citochine/chemochine proinfiammatorie. Sorprendentemente, abbiamo scoperto che l'acquisizione di questo fenotipo non è correlata alla stimolazione del VEGF, mentre il trattamento delle cellule di Müller con il fattore di crescita dei fibroblasti di base (FGF2) induce un aumento significativo dell'espressione di varie citochine/chemochine nelle cellule MIO-M1. Di conseguenza, il farmaco anti-VEGF ranibizumab non influenza l'attivazione delle cellule di Müller mediata dal vitreo PDR mentre il trattamento con l'inibitore della tirosin-chinasi del recettore dell'FGF (FGFR) BGJ398, la trappola pan-FGF NSC12, l'antagonista della proteina legante l'eparina multi-target N- tert-butyloxycarbonyl-Phe-Leu-Phe-Leu-Phe Boc2, o il farmaco antinfiammatorio idrocortisone inibisce, almeno in parte, l'attività dei campioni vitrei PDR.

Insieme, i risultati indicano che potrebbe esistere una relazione tra la capacità del vitreo iERM di modulare il GMT nelle cellule di Müller, il profilo molecolare dei corrispondenti iERM e le caratteristiche cliniche dei pazienti iERM. Inoltre, questi dati indicano un ruolo per vari mediatori oltre al VEGF nella risposta suscitata dal vitreo PDR nelle cellule di Müller.

INTRODUCTION

Epiretinal membranes (ERMs) are a thin layer of scar tissue formed on the macular or perimacular regions of the retina mainly due to the development of fibrocellular tissue on the inner limiting membrane, which can lead to visual loss in the elderly population [1, 2]. Iwanoff first described ERM in 1865 [2-4]. ERMs have a detrimental effect on one's quality of life, resulting in severe vision damage. The majority of ERM affects people over the age of 50, and the rate of ERM rises with age. Occasionally, epiretinal membranes can develop in children and young adults. Race, ethnicity, sex, smoking, diabetes, hypercholesterolemia, and arteriolar narrowing are reported to be possible risk factors for developing ERM. Clinically, ERMs have also been distinguished by various structural alterations in the vitreoretinal junction on ophthalmoscopic inspection. The early type of ERM, which is marked by a semitranslucent membrane, usually is asymptomatic or can cause mild changes in visual acuity, which is rarely below 20/200. Nevertheless, the more extreme cases, which have also been characterized by a semitranslucent, thick, and contractile membrane, may cause a significant loss in visual acuity and a variety of visual symptoms like metamorphopsia, micropsia, diplopia, aniseikonia, and vision loss. Since ERMs usually exert traction on the underlying retina, decreasing visual acuity, which results in tractional detachment of the macula, they will even induce vitreoretinal tractions or perhaps tractional Retinal Detachment. Individual symptoms can vary depending on the duration and severity of the disease [1, 2, 4].

ERM PREVALENCE

There is significant variability in the reported prevalence of ERM amongst different racial groups and countries. Reported rates are Australia 7% (Blue Mountains Eye Study (BMES)), 8.9% (MCCS); USA 11.8% (BDES), 18.7% (Los Angeles Latino Eye Study (LALES)); Singapore 7.6% (Singapore Indian Eye Study (SINDI)), 7.9% (Singapore Malay Eye Study (SiMES) Group), 12.1% (Singapore Epidemiology of Eye Disease (SEED)); China 1.02% (Beixinjing Blocks, Shanghai), 2.2% (Beijing Eye Study),3.4% (Handan Study, rural China), 7.3% (Jiangning Eye Study, urban Shanghai), 7.6% (Kailuan Eye Study); Japan 4.0% (Hisayama Study), 5.7% (Funagata Study) and Korea 2.9% (Korea National Health and Nutrition Examination Survey) [1, 5, 6].

In a 2011 multi-ethnic survey of the U.S. population involving 5960 participants aged 45 to 84 years, it was discovered that Chinese (39%) had a slightly higher prevalence than Hispanics (29.3%),

Whites (27.5%), and Blacks (26.2 %) [7]. Prevalence of epiretinal membranes increased significantly by age 0.5% for persons 40 to 49 years of age, 2.6% for persons 50 to 59 years of age, 9.4% for persons 60 to 69 years of age, 15.1% for persons 70 to 79 years of age, and 11.3% for persons aged 80 years or older. ERM epidemiology varies with a different population [1, 2, 5].

Reasons for such variation between the different racial and ethnic groups are unclear but may be due to different research designs, sampling methodology, photography methods, and rates of detection and definition of ERM, mainly when the earliest stages are present. As a result, it is unknown if there is a racial or cultural disparity in the incidence of ERM.

DIAGNOSIS AND CLASSIFICATION

Historically, ERMs were identified and classified only based on clinical examination findings. Recent breakthroughs in imaging, on the other hand, have allowed clinicians to diagnose and characterize ERM more precisely. The most effective ancillary test in clinical practice for diagnosing and classifying ERM is optical coherence tomography (OCT). OCT is a non-invasive high-resolution cross-sectional imaging technique used in medicine to obtain images of biological tissues. For diagnosing various disorders of the vitreomacular interface, including ERM, OCT has proved to be more sensitive. The increased scanning speed and detection sensitivity of spectral-domain optical coherence tomography (SD-OCT) have replaced mainly time-domain OCT in clinical practice [8-10].

Based on the severity of the ERM, the SD-OCT images present as a highly reflective layer along the surface of the inner limiting membrane that is consistent with retinal folds or changes in foveal depression. Further SD-OCT allows an accurate follow-up and careful monitoring. Clinicians have classified ERMs on the basis of morphological, ultrastructural, clinical, and immunocytochemical features based on OCT findings. Govetto et al. [11] suggested a more recent classification of ERMs, in which they were divided into four stages based on the progression of anatomical changes observed with OCT analysis. Stage 1: ERMs were mild and thin, with a foveal depression. Stage 2: ERMs were linked to the loss of the foveal depression and widening the outer nuclear layer. Stage 3: ERMs were linked to continuous ectopic inner foveal layers that crossed the entire foveal region. Stage 4: ERMs were dense and connected with ectopic inner foveal layers that were continuous.

Another OCT-based ERM classification system has been proposed by Konidaris et al. [12] based on extensive morphologic classification and subclassification. ERMs were divided into two groups: A, which included posterior vitreous detachment (PVD), and B, which did not include PVD. Category A was subdivided into two subcategories: A1, which had no ERM contraction, and A2, which had membrane contraction. A2 was further subdivided into A2.1, with retinal folding, A2.2, with edema, A2.3, with cystoid macular edema, and A2.4, with lamellar macular hole. Category B was divided into two subcategories: B1, without vitreomacular traction (VMT), and B2, with the presence of VMT. Category B2 was subdivided into B2.1, with edema, B2.2, presenting retinal detachment, and B2.3, with schisis. Though this classification system provides a framework for fully characterizing an ERM's morphologic properties nonetheless, there is no universally agreed ERM classification.

The current ERM classification system is based on understanding the pathogenesis of ERMs and the clinically relevant SD-OCT findings. ERMs can be classified as idiopathic, primary, or secondary based on their underlying etiology. Idiopathic ERMs are those that occur in the absence of an identifiable etiology. Though primary ERMs may have been associated with ocular conditions, their pathogenesis remains unidentified. The terms used to describe ERM are Primary retinal folds, wrinkling of the inner retinal surface, silent central retinal vein obstruction, preretinal macular fibrosis (PMF) or gliosis, or macular pucker cellophane maculopathy. The secondary ERMs are commonly associated with eye diseases like retinal vascular occlusion, diabetic retinopathy, retinal vein occlusion, blunt force trauma, retinal detachment, and cataract surgery [13].

The most common type of epiretinal membrane is idiopathic, which is more relevant for patients over the age of 50. Idiopathic ERMs do not have an identifiable cause [1]. The most severe level of ERM is observed in proliferative diabetic retinopathy (PDR), patients with one of the most severe complications of diabetes and are potentially sight-threatening in patients aged 20–75 years. The incidence of PDR in adult diabetic patients is higher than 40%, and approximately 5%- 10% of PDR cases progress to severe visual impairment [14, 15]. iERM are mainly characterized by non-angiogenic fibro glial tissue characteristics, whereas PDR ERMs are characterized primarily by neovascularization, both lead to lead to significant visual loss. Pathogenesis of the iERM and PDR ERMs is yet to be elucidated.

IDIOPATHIC EPIRETINAL MEMBRANE

Idiopathic epiretinal membrane (iERM) is a chronic disease with an estimated prevalence of 1.02–28.9% across the different ethnic populations [5, 16, 17]. iERM is the most common form of ERM, characterized by fibrocellular tissue development on the inner limiting membrane, strongly linked to aging. While patients with iERM can be asymptomatic when the membrane is thin and translucent, the development of the membrane to a semitranslucent, thick, and contractile state may cause macular distortion and metamorphopsia. "Macular pucker," "preretinal macular fibrosis," "epiretinal fibrosis" or "gliosis," "surface wrinkling retinopathy," or "cellophane maculopathy" have all been used to describe this clinical condition. iERM can be classified into two types where type 1 refers to the cases where collagens in vitreous intervene between ILM and ERM, and type 2 refers to cases where cell proliferation takes place with only a sparse or even no collagen-containing layer forming between the ILM and ERM surface.

Epidemiologic studies have found that the factors for iERM formation are aging, posterior vitreous detachment (PVD), genetic and lifestyle factors. The onset and progression of iERM are usually slow. A 5-year cumulative study conducted in Blue Mountain Eye Study population has reported that the overall progression, stability, and regression rates were 28.6, 38.8, and 25.7 %, respectively, and that the progression rate of iERM from grade 0 to grade 2 was 9.3% [18].

Figure 1: Representative images **A)** fundus photo of an iERM **B)** SD-OCT image of an iERM

CLINICAL FEATURES

A grading system introduced by Govetto et al. [11] has been commonly used in clinical practice to classify the various phases of the iERM.

Grade 0: Cellophane Maculopathy

A translucent membrane can be seen, with no distortion of the underlying retina. The patient has no symptoms, and the condition is usually discovered by chance through a regular ophthalmic examination.

Grade 1: Crinkled Cellophane Maculopathy

In this condition, the iERM shrinks or contracts, causing frequent wrinkling of the retina's inner layers and resulting mainly in the loss of optical acuity and blurred central vision. The optical acuity loss is primarily driven by the distortion of inner retinal membranes, not by the thickness of the membrane. Other symptoms recorded are binocular, photopsia, and macropsia.

Grade 2: Preretinal Macular Fibrosis

This iERM has a thicker, opaque membrane obscures the underlying retinal vasculature and a full-thick retinal distortion. Small retinal hemorrhages, cotton-wool spots, retinal edema, and exudates are observed in patients. Blurred vision or metamorphopsia is observed in 80% of patients. Grade 2 iERM is also referred to as macular pucker.

The diagnosis of iERM is primarily based on clinical findings. Many objective examination techniques have been applied to assess the extent of functional and morphological changes of iERM. To analyse the morphological changes qualitatively and quantitatively in iERM OCT has been extensively used. Based on OCT findings, clinicians have classified iERM based on morphological, ultrastructural, clinical, and immunocytochemical features.

Huwang et al. [19] have proposed an OCT-based idiopathic ERM classification system on foveal morphology. The classification includes

GROUP 1A - fovea-involving ERM with outer retinal thickening and minimal inner retinal change

GROUP 1B - fovea-involving ERM with outer retinal inward projection and inner retinal thickening

GROUP 1C - fovea-involving ERM with prominent thickening of the inner retinal layer

GROUP 2A - fovea-sparing ERM with the formation of a macular pseudo hole

GROUP 2B - fovea-sparing ERM with schisis-like intraretinal splitting

Above mentioned classifications have provided a detailed description of the morphologic/structural alterations in the retina of iERM patients. However, the pathogenesis of this clinical entity has not been completely defined, and a globally accepted ERM classification system is still lacking.

PATHOGENESIS OF iERM

The exact pathogenesis of iERMs is uncertain. The generally accepted risk factors in the iERM pathogenesis are older age and posterior vitreous detachment (PVD) [20]. In 95% of the cases, cell proliferation appears following PVD also forms a break in inter limiting membrane. Other factors that might play a role in iERM formation are altered microvascular retinal blood flow and metabolic stress, together with genetic and lifestyle-related factors like smoking [21].

iERMs are composed of two main components: retinal and extraretinal cells and Extra Cellular Matrix (ECM) proteins. In iERM, ECM is mainly constituted by collagen, laminin, vitronectin, tenascin, thrombospondin, and fibronectin. The primary cell constituent in iERM are glial cells (retinal Müller cells, astrocytes, and microglia), hyalocytes, macrophages, retinal pigment epithelial (RPE) cells, fibroblasts, and myofibroblasts. The essential pathogenic process in iERM formation is mainly considered the ability of precursor cells like retinal Müller cells, hyalocytes, and RPE cells to differentiate into a myofibroblast-like phenotype, resulting in a myofibroblast-like phenotype in excessive proliferation, collagen production, and deposition. Evidence of myofibroblastic transdifferentiation is characterized by a reduction in cell-specific proteins such as glial fibrillary acidic protein (GFAP) and the upregulation of proteins involved in myofibroblast proliferation and membrane contractility such as α-smooth muscle actin (SMA). Other cell lines, such as hyalocytes in cortical vitreous remnants, contribute to the ERM formation and contraction [22]. Microglia and laminocytes are different cell types with fundamental involvement in the pathology of iERMs which

also play a crucial role in inflammatory and degenerative diseases [23, 24]. Different growth factors enhance myofibroblast differentiation, cellular proliferation, and ERM contraction.

The predominant cell types in ERMs differ between studies. This may reflect different aetiological factors involved in ERM formation and different methods (such as histology, electron microscopy, and immunofluorescence) in identifying cell types. A significant question is what stimulates these cells in idiopathic ERM formation. The most widely accepted proposed theory is that posterior vitreous detachment (PVD) plays an essential role in the formation of iERM formation. PVD appears to be a critical pathogenic component in the development of idiopathic ERM, as it is found in 70% of patients in the early stages of the disease [25]. Various cytokines and growth factors activate the hyalocytes that reside in cortical vitreous remnants on the ILM. This might result in myofibroblast differentiation and cellular proliferation, thus leading to iERM formation. There is also uncertainty about which cell types are responsible for idiopathic ERMs and how they move to the retinal surface. So, a detailed study is still required to understand the pathogenesis of the disease.

TREATMENT

Pars plana vitrectomy and epiretinal membrane peeling have been done as a cure for ERM. Pars plana vitrectomy is often indicated in patients affected with decreased visual acuity, metamorphopsia, double vision, or difficulty using their eyes together. Vitrectomy surgery for ERM usually leads to improvement of the metamorphopsia and visual acuity. Recurrent ERM is thought to result from incomplete removal showed that ERM removal alone does not separate the fibrocellular tissue from the macula. Therefore, additional ILM peeling is advised to eradicate epi-ILM and sub- ILM proliferation, thus eliminating the scaffold for further proliferation. Several clinical series reported that ILM peeling seems to give better results than non-ILM peeling [26].

The current surgical management of ERMs is inadequate, and better treatment is needed. When vitrectomy is paired with ERM/ILM peeling, the visual recovery is rarely complete. ILM/ERM peeling is a complex procedure that can result in iatrogenic macular damage, infectious endophthalmitis, and cataract development during and after the procedure. The pathophysiology of fibrosis in vitreoretinal interface disease must be explained to establish effective strategies to prevent membrane contraction [26, 27].

DIABETES MELLITUS

Diabetes mellitus (D.M.), commonly known as diabetes, is one of the leading health problems in the 21st century. It is a metabolic disease, which involves elevated blood glucose levels. The worldwide incidence of diabetes is set to rise dramatically from 171 million people to an estimated 366 million in 2030 [28]. D.M. is mainly classified into several categories, and the two main subtypes are Type 1 Diabetes Mellitus and Type 2 Diabetes Mellitus. Type 1 Diabetes Mellitus presents in children or adolescents, primarily due to autoimmune-mediated destruction of pancreatic β-cells, which leads to insulin deficiency. Type 2 Diabetes Mellitus mainly affects middle-aged and older adults who have prolonged hyperglycemia due to poor lifestyle and dietary choices. Globally, 1 in 11 adults has D.M. in that 90% have Type 2 Diabetes Mellitus. Clinically, D.M. is a metabolic disease and, in the long-term, damage macro and microvessels of the heart, nerves, kidney, and retina. The pathogenesis of diabetes-associated complications is exceptionally complex. Diabetes-associated complications include nephropathy, neuropathy, and diabetic retinopathy.

DIABETIC RETINOPATHY

Diabetic retinopathy remains a leading cause of visual impairment in many developing countries as the global prevalence of diabetes mellitus rises. Following 20 years of diabetes, nearly all patients with Type 1 diabetes will have at least some retinopathy. Moreover, ∼80% of insulin-dependent Type 2 diabetic patients and 50% of Type 2 diabetic patients not requiring exogenous insulin will have retinopathy after 20 years of diabetes [29, 30]. Diabetic retinopathy is a condition that affects the retina's tiny blood vessels (the light-sensitive tissue that lines the back of the eye). Diabetic retinopathy is primarily asymptomatic, worsening vision is experienced by time, and there will be significantly advanced pathology. So, there is a need for screening to assess the progression and presence of the condition [31].

Clinicians have used various classifications to grade the severity of diabetic retinopathy, but traditionally diabetic retinopathy is classified into an early, non-proliferative diabetic retinopathy (NPDR) and a later, advanced stage proliferative diabetic retinopathy (PDR). Micro aneurysms and microhemorrhages, increased vessel permeability, and the development of soft and hard exudates are all signs of NPDR. Progressive damage to the retinal microvascular network results in tissue ischemia. Diabetic macular edema (DME), which occurs due to the breakdown of the blood-retinal barrier (BRB), is secondary to increased retinal vascular permeability and is the most common cause

of vision loss in NPDR. PDR is the advanced-stage diabetic retinopathy characterized by neovascularization or preretinal/vitreous hemorrhages. PDR will become complicated by vitreous hemorrhage or tractional retinal detachment, resulting in fibrovascular epiretinal membrane formation. Excessive neuro-vascular damage, retinal ischemia/hypoxia, and leukostasis are significant players in the initiation and progression, leading to permanent vision loss [31].When high-risk PDR is left untreated for five years, there is a 60% likelihood of severe vision loss [31].

PREVALENCE OF PDR

Diabetic retinopathy becomes more common as diabetes progresses, and it affects most diabetic patients who have had the disease for at least 20 years. After 20 years of diabetes, PDR affects about 50% of patients with type 1 diabetes, 5–10% of patients with noninsulin-dependent type 2 diabetes, and 30% of patients with insulin-dependent type 2 diabetes [28-30]. The significant risk factors for the progression of diabetic retinopathy are the duration of diabetes mellitus, poor glucose control, high blood pressure, and elevated cholesterol. In Europe and the U.S. alone, the WHO (World Health Organization) has estimated that diabetic retinopathy accounts for approximately 15–17% of total blindness. Worldwide diabetic retinopathy is an even bigger problem, and a comprehensive study by Yau et al. [14] based on 22,896 individuals from 35 studies in the U.S., Australia, Europe, and Asia demonstrated that the prevalence of diabetic retinopathy was almost 35% with the increased risk associated with diabetes duration, higher HbA1c (glycated haemoglobin) and hypertension. The prevalence of the PDR (proliferative diabetic retinopathy) was ~7%.

PATHOGENESIS OF PDR

The pathophysiology of diabetic retinopathy is multifactorial and complex. The main systemic factors involved are hyperglycemia, hypertension, hyperlipidemia, and genetic background. Whereas Hyperglycemia was accepted early on as central to the pathology and structural changes seen in diabetic retinopathy, other aspects, such as inflammation and neuronal dysfunction, have only more recently been identified as contributing elements. Increasing evidence indicates that neurodegeneration could be an early event in the pathogenesis of diabetic retinopathy [32]. The decrease in oscillating potential in electroretinograms is the first detectable difference in retinal function in diabetic patients [32, 33]. As a result, diabetic retinal dysfunction can be considered an impairment with the retinal neurovascular unit [34]. The retinal neurovascular unit comprises the

physical and biochemical interactions between neurons, glia, and blood vessels, as well as the retina's and central nervous system's close interdependency.

The retinal neurovascular unit consists of the neural unit and vascular unit. The neural unit mainly consists of RGCs and Glial cells, whereas Glial cells include Microglia, Müller cells, and astrocytes. The vascular unit mainly has two types of cells, endothelial cells, and pericytes. Together with Müller cells and astrocytes, they become the body of the inner blood-retina barrier (iBRB). The RPE, which severs as the outer blood-retina barrier (oBRB), is critical for maintaining retinal homeostasis.

In the diabetic environment, cell dysfunction is induced by hyperglycemia; this leads to structural defects and functional disorders developing in the neurovascular unit, leading to further cell impairment. Diabetic retinopathy has complex pathogenesis, and a number of independent hypotheses have been proposed to explain the adverse effects of hyperglycemia, including increased inflammation, increased hexosamine pathway flux, increased polyol pathway flux, increased advanced glycation end products (AGEs) formation, overactive PKC (protein kinase C), activation of renninangiotens in the system (RAS) and production of excess reactive oxygen species (ROS) [35-38].

The role of inflammation in diabetic retinopathy has received considerable attention in recent years. Neurovascular dysfunction and acellular capillaries' development have been related to abnormal expression of proinflammatory cytokines within the neural retina and up-regulation of adhesion molecules on the microvasculature leading to leukostatic responses. Proinflammatory factors such as IL-1a, IL-1ß, IL-6, and TNFα (tumor necrosis factor-alpha) and angiogenic factors such as angiopoietin, erythropoietin, fibroblast growth factor (FGF), insulin-like growth factor (IGF), tumor growth factor (TGF), and platelet-derived growth factor (PDGF) have stimulatory or modulating activities during the development of PDR. Retinal glial cells like microglia and müller glial cells may play an essential role in diabetes-mediated retinal inflammation by inducing inflammatory cytokine expression and pathological responses [39-42]. The primary angiogenic stimulus that plays a central role in PDR development is hypothesized to be relative retinal ischemia. The ischemia-driven angiogenic pathology in PDR is modulated by the vascular endothelial growth factor (VEGF) [41].

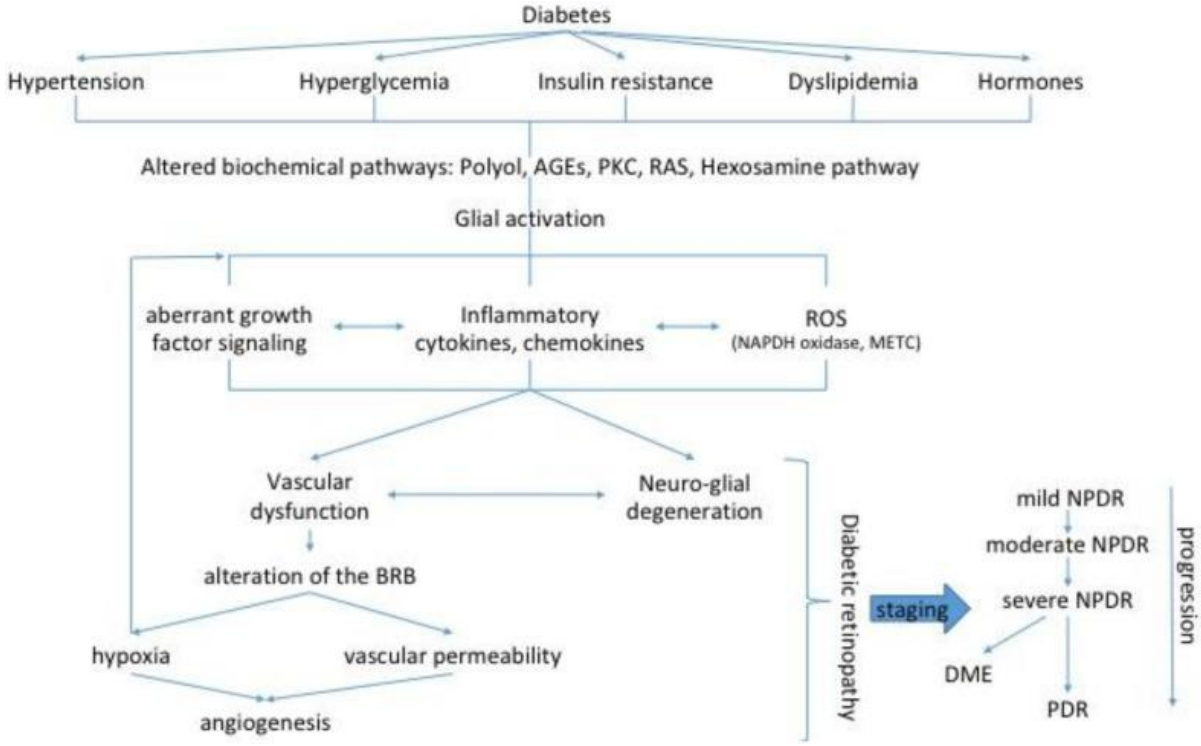

Figure 2. Schematic representation of the pathogenic mechanisms leading to sight-threatening endpoints of diabetic retinopathy, proliferative diabetic retinopathy (PDR), and diabetic macular edema (DME).

TREATMENT

Glycemic and hypertension regulation are critical for diabetic patients and achieving blood glucose and blood pressure control has been shown to significantly reduce the risk of diabetic retinopathy development and progression. However, in some patients, strict glycemic regulation is difficult or impossible to obtain. Treatment advancements in the management of PDR have been more restricted. In the early stages of diabetic retinopathy, vitrectomy surgery is successful in reducing vision loss. Vitrectomy is a valuable treatment for preventing vision loss and restoring vision since it uses a laser administered from inside the eye at the time of surgery and other advanced surgical techniques [43]. The mainstay treatment of PDR is PRP (pan-retinal photocoagulation). Although PRP is a highly effective treatment for PDR, which leads to disease quiescence and prevents severe vision loss, it is inherently destructive, resulting in loss of photoreceptors, particularly rods, leading to loss of peripheral field well as night vision [44]. The other approach is administrating intravitreally delivered pharmaceuticals that inhibit VEGF, reducing the number of patients reaching the proliferative stage. The main benefit of anti-VEGF pharmacotherapy is that it avoids the destructive nature of PRP. This translates into less severe, even though progressive, visual field loss with anti-

VEGF pharmacotherapy than PRP [44, 45]. The downside to anti-VEGF pharmacotherapy is that the effects are short-lived and require multiple intravitreal injections. There have also been clinical reports that some patients with diabetic retinopathy may respond poorly to VEGF inhibition, and it could even be associated with poor visual outcomes [46]. There are also concerns raised that anti-VEGF pharmacotherapy could compromise retinal neuroglial and resident microvascular survival. However, many therapeutic strategies are simply attempting more convenient or better-tolerated ways of impacting the VEGF pathway. Besides VEGF, many other pathogenic mechanisms are involved and play an important role in diabetic retinopathy, including PDR.

Consequently, therapeutics targeted at non-VEGF mechanisms are perhaps the more exciting and offer the greatest hope for more comprehensive treatment response in D.M. patients. In the context of diabetic retinopathy, this is an increasing concern. For this reason, the development of therapies capable of preventing or slowing the onset and progression of diabetic retinopathy remains a priority.

RETINA

The retina is a spatial information processor built upon a mosaic of rod and cone photoreceptors, the light-responsive elements that initiate signalling using graded electrical signals. It lines the back of the eye and is around 0.5 mm thick. A fragile nervous membrane that lines the inside of the eyeball. Its outer surface is in contact with the choroid, and its inner surface is in contact with the vitreous body's hyaloid membrane. The retina is a layered structure with a wide variety of component cells that form morphologically and functionally distinct circuits that act in parallel and in combination to produce vision. The outer nuclear layer (ONL) contains the cell bodies of photoreceptors, both rods and cones. The inner nuclear layer (INL) contains horizontal, bipolar, amacrine, and radial glial (or Müller) cells.

An exterior pigmented layer and an inner nervous stratum, or retina proper, constitute the retina. It is a layered structure made up of ten distinct layers of neurons linked by synapses. The three primary cell types are photoreceptor cells, neuronal cells, and glial cells [47, 48]. From the front anterior of the head towards the rear posterior of the head, the layers are as follows:

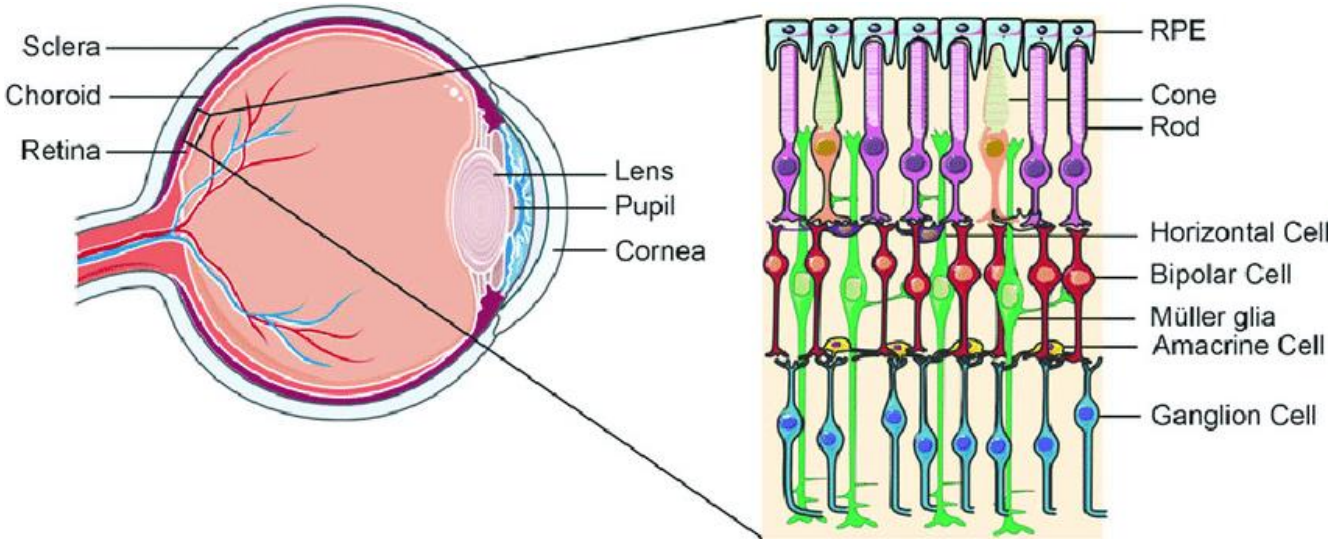

Figure 3: Schematic representation of photoreceptor cells in the retina of the eye

1. Inner limiting membrane
2. Nerve fiber layer (NFL)
3. Ganglion cell layer
4. Inner plexiform layer
5. Inner nuclear layer
6. Middle limiting membrane
7. Outer plexiform layer
8. Outer nuclear layer
9. External limiting membrane
10. The layer of rods and cones

The retina of a mammal does not have the ability to self-repair. As a result, human retinal diseases that cause neuronal cell death result in irreversible visual impairment. Nonetheless, under pathological conditions, multiple cell types in various locations of the adult mammalian retina can demonstrate some degree of neurogenic potential. Ciliary margin cells, RPE, and Müller glial cells are among them.

INNER LIMITING MEMBRANE

The inner limiting membrane (ILM) is a basement membrane (B.M.) that structurally constitutes the border between the retina and the vitreous and is composed of collagen fibers, glycosaminoglycans, laminin, and fibronectin. It forms the B.M. of the Müller cells and, as a result, aligns with their end feet across the entire eye. The ILM serves as a scaffold for the cellular proliferation of myofibroblasts, fibrocytes, and retinal pigment epithelium (RPE) cells [49]. The ILM is an intriguing structure from a clinical point of view since it is connected to various ocular diseases such as macular hole formation and proliferative vitreoretinal diseases. Since the ILM is the site that defines vitreoretinal adhesion, it also plays a crucial role in pathological traction. The latter will largely depend on the morphological and mechanical properties of the ILM. Interestingly, the very same features also determine the course and success of ILM peeling, a commonly performed procedure among vitreoretinal surgeons. The fact that ILM characteristics are highly influenced by aging and disease (e.g., diabetes) adds to the complexity of these clinical disorders and their therapies [50].

MÜLLER GLIAL CELLS

Cellular migration and proliferation on the inner retinal surface, ECM production, and tissue contraction are all characteristics of ERMs. According to histopathological investigations, RPE cells, glial cells, macrophages, endothelial cells, fibrocytes, fibrous astrocytes, myofibroblast-like cells, and trophic and transcription factors contribute to ERM formation. The critical cell type having a central role in ERM contraction are Müller cells, which can express α-smooth muscle actin (α-SMA), which is involved in membrane contraction and produces diverse collagens. As Müller cells proliferate and transdifferentiate, it leads to the development of idiopathic ERM. They also play a role in developing diabetic ERM, linked to gliosis, fibrosis, and migration. Müller glial cells are the major glial component of the retina discovered by the German anatomist Heinrich Müller, in 1851. Müller glia represents approximately 4–5% of retinal cells. They form architectural support structures stretching radially across the thickness of the retina and are the limits of the retina at the outer and inner limiting membrane, respectively. The primary function is to maintain retinal homeostasis and integrity, and Müller glial cells are the last retinal cell types to be born during development. Müller glia responds to retinal injury in various ways that can be either protective or detrimental to retinal function. Müller glia thus acquires some specialized glial functions but maintains a molecular signature of late-stage progenitor cells.

Müller cells and astrocytes together maintain the integrity of the blood-retinal barrier by stabilizing tight junctions between endothelial cells and ensuring the immune privilege of the eye. They also provide essential nutrients, such as lactate and amino acids, from the circulation to neurons while participating in the retinal regulation of neurotransmitters, glucose metabolism, and blood flow in response to the retinal injury[51]. Müller cells undergo reactive gliosis, upregulating intermediate filaments, namely glial fibrillary acidic protein (GFAP), vimentin and nestin, and becoming more rigid [52]. This increased rigidness of both macroglia is mediated by signal transducer and activator of transcription 3 (STAT3), which is known as the master regulator of glial scar formation [53]. The rigidness allows for the glial scar formation, establishing the physical and chemical barrier to RGC axon regeneration. Müller cells contain glycogen, mitochondria, and intermediate filaments, which are immunoreactive for vimentin and, to some extent to glial fibrillary acidic protein (GFAP). The latter filaments are usually in the inner half of the retinal Müller cells and their end feet, but following trauma to the retina such as retinal detachment, both vimentin and GFAP are massively upregulated throughout the cell [54].

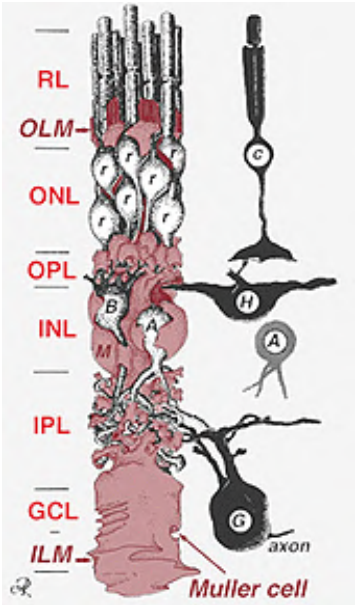

Figure 4: Schematic Drawing of the Relationship Between Müller Cells and Retinal Neurons

Müller cells serve a variety of activities, many of which are critical to the retinal neurons' health. Müller cells and neurons work together in a symbiotic way [55]. The following are some of the functions of Müller cells:

1. Providing anaerobic metabolism end products (glycogen breakdown) to feed aerobic metabolism in nerve cells.

2. Müller cells clean up carbon dioxide and ammonia from the brain and recycle used amino acid transmitters.

3. Müller cells protect neurons from excess neurotransmitters like glutamate by recycling this transmitter through well-developed absorption systems. They are primarily distinguished by the presence of elevated glutamine synthase concentrations.

4. Müller cells may have a role in the phagocytosis of neuronal debris and the release of neuroactive chemicals like GABA, taurine, and dopamine.

5. Müller cells are thought to make retinoic acid from retinol (retinoic acid is known to play a role in ocular and nervous system development) [56]

6. Müller cells regulate homeostasis and protect neurons from harmful changes in their ionic environment by absorbing and redistributing extracellular K+.

7. They help to generate the electroretinogram (ERG) b-wave, the slow P3 component of the ER, and the scotopic threshold response (STR). They do so via controlling K+ distribution across the retinal-vitreous boundary, across the retina, and locally in the retina's inner plexiform layer.

ROLE OF MÜLLER GLIAL CELLS IN ERM

The primary cellular source for myofibroblastic differentiation is suggested to be Müller glial cells, whose presence and pro-fibrotic role in iERM have been demonstrated in several immunohistochemical and in vitro studies. Moreover, Müller cells undergo reactive gliosis characterized by cell proliferation and cytoplasmic extension, contributing to the epiretinal membrane [57]. Activated Müller cells also have more direct cytotoxic effects by releasing soluble factors such as the proinflammatory cytokines TNF and monocyte chemoattractant protein (MCP)-1 (Ccl-2). Cytotoxic effects of Müller cells contribute to retinal degeneration in various retinopathies [58].

Vitreous hemorrhage resulting in activation of glial cells can be a causative factor in epiretinal membrane formation. A breakdown of blood-ocular barriers occurs in cases of ocular inflammation, ischemia, and trauma and in the presence of mechanical stress to Müller cells after detachment of the

posterior vitreous from the retina. The aberrant proliferation of retinal glial cells is one major causative factor for the formation of fibroproliferative tissues associated with PVR and PDR [59, 60] and for the formation of epiretinal membranes in idiopathic surface wrinkling maculopathy [61]. Glial cells undergo mitosis in the retina, and the nuclei of the cells migrate, passing through the inner limiting membrane onto the retinal surface. The vitreoretinal gradient of chemoattractants and growth factors, which were found to be present at high concentration in the vitreous [59, 62], may represent a significant factor that direct the process extension and migration of Müller cells. Increases in vitreous growth factor and cytokine activity are suggested to precede the development of PVR and PDR [59, 62, 63]. Growth and inflammatory factors released from infiltrating immune cells, platelets, and plasma-derived factors may activate Müller cells. Müller cells can be activated by various pathogenic factors, such as mechanical traction, retinal trauma, hyperglycemia, and the release of cytokines and growth factors because of blood-retinal barrier breakdown [64].

Müller cells appear to play a pivotal role in the pathogenesis of iERM [59], where various cytokines and growth factors may act as autocrine and paracrine modulators by triggering Müller cell proliferation, migration, collagen contraction, and transdifferentiation [65-71]. In particular, transforming growth factor-beta (TGFβ) has been shown to induce glial-to-mesenchymal transition (GMT) in Müller cells, a transdifferentiation process characterized by the downregulation of Müller cell glial markers, paralleled by the upregulation pro-fibrotic myofibroblast markers [57].

During PDR, high blood glucose levels may induce retinal dysfunctions caused by increased levels of oxidative stress, which triggers early neurodegeneration, activation of inflammatory responses, and abnormal neovessel formation [72]. Because of the pathological changes in the retina during PDR, activated Müller cells may undergo reactive gliosis, a non-specific reactive response of glial cells to damage characterized by uncontrolled proliferation, migration, and increased expression gliosis markers [54, 59]. Moreover, Müller cells may undertake a fibrotic trans-differentiation, contributing to the formation of a fibrovascular epiretinal membrane (ERM), which can exert tractional forces on the retinal surface, thus causing retinal detachment [73, 74]. In addition, activated Müller cells produce several cytokines and chemokines, contributing to maintaining the inflammatory environment, altering the blood-retinal barrier (BRB) integrity, and neovascularization [75, 76].

VITREOUS HUMOR

The vitreous humor (V.H.), a transparent gel that fills the posterior cavity of the eye, plays a vital role in maintaining visual function. Structural and molecular alterations of the vitreous, observed during ERM progression, are consequences of metabolic and functional modifications of the retinal tissue[72]. The posterior segment (the space between the lens and the retina) is filled with vitreous; unlike the aqueous humour, the vitreous is not continually drained and re-generated. The vitreous, permanently formed at birth, is a delicate transparent gel composed of water (99%) and salts (0.9%); other constituents include various proteins and polysaccharides (mainly collagen molecules and glycosaminoglycans (GAGs)) [77].

Because of the proximity/interaction between the vitreous humor and retina, physiological and pathological conditions of this tissue should be reflected in its protein content. Therefore, vitreous humor provides a means of indirectly studying the events at the retina [72]. Vitreous humor has a vital role in the progression of several ocular pathologies. It is a fact that proteins retained in the vitreous humor are altered in disease states, and therefore identifying proteins that could be early diagnostic tools or therapeutic targets is justified. Some diseases are thought only to affect the vitreous in the late stages of progression, and this would be the case of retinal vasculopathies such as diabetic retinopathy and other vitreoretinal proliferation. In other cases, the disease may be triggered in more small structures of the eye but still reverberate in the vitreous chamber, causing symptoms and helping in the diagnosis in the more accessible vitreous humor. Significant breakthroughs in this area may undoubtedly arise from the proteomic approach, which is still constrained by the limited knowledge available about the key events leading to disease progression. Several molecules have already been identified in the vitreous humor, which may be putatively involved in the physiopathology of specific ocular diseases. Although each vitreoretinal disease has changed a unique set of proteins, several general tendencies have been pointed. That is the case of increased protein concentration and increased levels of inflammation-associated proteins, which supports the importance of inflammation in some vitreoretinal diseases [78, 79].

Changes in the vitreous proteins could affect the pathological mechanism and development of the disease. The metabolic and functional modifications of the retinal tissue, and systemic responses that occur during ERM progression, can result in structural and molecular alterations of the vitreous [2, 72]. These alterations reflect the pathological events that occur at the vitreoretinal interface and characterize the diabetic condition. For instance, recent studies have shown that the vitreous from

patients with proliferative diabetic retinopathy can be used as a tool to investigate the molecular events triggered by vitreal mediators in endothelial cells and to evaluate the anti-angiogenic/anti-inflammatory activity of established therapeutics or novel drug candidates [80-85]. In addition, vitreous from diabetic retinopathy patients has been demonstrated to trigger Müller cell activation in a vascular endothelial growth factor (VEGF) independent manner. However, little data are available about the effect exerted on these cells by iERM vitreous, mainly focusing on its capacity to stimulate tractional force generation.

Aretz and colleagues have discovered the proteins in vitreous humor samples from patients with epiretinal gliosis by [86]. Through VH-based proteomics, two investigations targeting idiopathic epiretinal membrane, a result of fibrocellular tissue proliferation along the vitreal surface of the retina, were conducted in the same year. Another study analyzed the vitreous humor and aqueous fluid from eyes with epiretinal membrane [120] and found 12 distinct proteins expressed [87]. The authors, on the other hand, sought to highlight the parallels between the two ocular chambers.

The vitreous humor contains a variety of soluble proteins and has a close relationship with the progress of diabetic retinopathy. Besides, and vitreous humor is the first site in the eye where anti-VEGF agents exert their curative effects. Many studies have demonstrated that label-free quantitative proteomics analysis can detect proteins in the vitreous humor and provided quantitatively mapped proteome changes of the vitreous humor in diabetic retinopathy patients [72, 80]. However, these data have not been fully used for further analysis and research to understand the complexity of pathophysiological mechanisms and molecular events contributing to the disease.

EPITHELIAL-MESENCHYMAL TRANSITION (EMT)

The epithelial-mesenchymal transition (EMT) plays crucial roles in pathophysiological processes in adults, including wound healing, tissue fibrosis, and cancer progression [88, 89]. Based on the biological context, EMT has been classified into three types. During type 1 EMT, the mesoderm, endoderm, and mobile neural crest cells are formed, associated with implantation and embryonic trulation. Type-2 EMT is associated with wound healing, tissue regeneration, and organ fibrosis. If the expression of type 2 EMT is over an extended period, it can eventually destroy an affected organ if the primary inflammatory insult is not removed or attenuated. Type 3 EMT promotes carcinogenesis in terms of cell motility and growth, which contributes to tumor progression, metastasis, and invasion [90, 91]. In Type 2 EMT-mediated tissue fibrosis, highly transdifferentiated

myofibroblasts acquire the following pathogenic characteristics: aberrant cell migration and proliferation, ECM overproduction, and cytoskeletal muscle contraction culminating in tissue deformation and organ dysfunction [91, 92].

EMT is generally described when epithelial cells lose E-cadherin expression and gain expression of mesenchymal cell components such as vimentin and N-cadherin [92, 93], even though the phenomena have not been formally expressed defined. The spatiotemporally controlled process of keratinocyte production, in which keratinocytes can transit into a mesenchymal state and then revert to an epithelial state, is hypothesized to constitute partial EMT and is crucial for the reepithelization mechanism in wound healing associated EMT [93, 94]. EMT in cancer progression has received much attention, and it is often likened to EMT in wound healing, owing to the molecular alterations and cell plasticity that both processes share. EMT associated with cancer progression involves a niche of intermediate states between the epithelium and the mesenchymal such as partial EMT on wound healing [95]. Snai2, a zinc-finger transcriptional repressor that belongs to the Snai1 superfamily, is the most studied molecule in wound healing EMT and is assumed to be the significant EMT-inducing transcription factor in cutaneous wound healing [94, 96, 97].

The primary cause for EMT and tissue fibrosis in various organs to be identified are the cytokines and growth factors, including connective tissue growth factor (CTGF), fibroblast growth factor (FGF), and platelet-derived growth factor (PDGF), transforming growth factor (TGF) signaling via the TGF receptor [98, 99]. In ocular fibrosis diseases like proliferative vitreoretinopathy, age-related macular degeneration, and iERM, TGF -β-induced EMT was shown to occur in RPE cells. TGF -β has been shown to induce glial-to-mesenchymal transition (GMT) in Müller cells, a transdifferentiation process characterized by the downregulation of Müller cell glial markers, paralleled by the upregulation pro-fibrotic myofibroblast markers [57, 100]. Thus, the Type 2 EMT program may be formed based on pro-fibrotic stimuli, transcription factors, and the cellular phenotypes that result, such as cell motility, ECM production, and cytoskeleton contractility.

RESULTS

GENE EXPRESSION ANALYSIS IDENTIFIES TWO DISTINCT MOLECULAR CLUSTERS OF IDIOPATHIC EPIRETINAL MEMBRANES

Idiopathic epiretinal membranes (ERMs) are fibrocellular membranes that comprise extracellular matrix proteins and epiretinal cells from both the retina and the extraretinal space. The

pathophysiology of iERMs, which cause lower visual acuity, is still unknown. The goal of this study was to use gene expression analysis to provide a molecular characterization of iERMs. In the present work, a list of 20 genes relevant to the pathogenesis of iERM was established based on educated guess after extensive searching of the scientific literature. These genes encode for proteins representing putative biomarkers of the cellular and molecular events occurring in iERMs, including cell population markers, ECM components, cytokines, and growth factors. Next, we performed a retrospective study in which we assessed the levels of expression of these genes by real-time quantitative polymerase chain reaction (RT-qPCR) analysis in a cohort of surgically removed iERM samples. Hierarchical clustering of the gene expression data allowed the identification of two major clusters of iERM specimens. Compared to Cluster A samples, Cluster B iERMs were characterized by a higher expression of most of the genes investigated, accompanied by more severe clinical and SD-OCT features. This work paves the way to future prospective whole-genome transcriptomic studies to define a molecular classification of iERMs and identify molecular signature(s) of prognostic and therapeutic significance.

BBA - Molecular Basis of Disease 1866 (2020) 165938

Contents lists available at ScienceDirect

BBA - Molecular Basis of Disease

journal homepage: www.elsevier.com/locate/bbadis

Gene expression analysis identifies two distinct molecular clusters of idiopatic epiretinal membranes

Daniela Coltrini[a], Mirella Belleri[a], Elena Gambicorti[b], Davide Romano[b], Francesco Morescalchi[b], Adwaid Manu Krishna Chandran[a], Stefano Calza[a], Francesco Semeraro[b,*], Marco Presta[a,*]

[a] Department of Molecular and Translational Medicine, University of Brescia, Viale Europa 11, 25123 Brescia, Italy
[b] Eye Clinic, Department of Neurological and Vision Sciences, University of Brescia, Piazzale Spedali Civili 1, 25123 Brescia, Italy

ARTICLE INFO

Keywords:
Epiretinal membrane
Gene expression
Retina
Eye disease

ABSTRACT

Idiopathic epiretinal membranes (ERMs) are fibrocellular membranes containing extracellular matrix proteins and epiretinal cells of retinal and extraretinal origin. iERMs lead to decreased visual acuity and their pathogenesis has not been completely defined. Aim of this study was to provide a molecular characterization of iERMs by gene expression analysis. To this purpose, 56 iERMs obtained by *pars plana* vitrectomy were analyzed for the expression levels of genes encoding biomarkers of the cellular and molecular events occurring in iERMs. RT-qPCR analysis showed significant differences in the levels of cell population, extracellular matrix and cytokine/growth factor biomarkers among the iERMs investigated. Hierarchical clustering of RT-qPCR data identified two distinct iERM clusters, Cluster B samples representing transcriptionally "activated" iERMs when compared to transcriptionally "quiescent" Cluster A specimens. Further, Cluster B could be subdivided in two subgroups, Cluster B1 iERMs, characterized by a marked glial cell activation, and Cluster B2 samples characterized by a more pro-fibrotic phenotype. Preoperative decimal best-corrected visual acuity and post-surgery inner segment/outer grading values were higher in Cluster A patients, that showed a prevalence of fovea-attached type iERMs with near-normal inner retina, than in Cluster B patients, that presented more severe clinical and spectral domain optical coherence tomography (SD-OCT) features. In conclusion, this molecular characterization has identified two major clusters of iERM specimens with distinct transcriptional activities that reflect different clinical and SD-OCT features of iERM patients. This retrospective work paves the way to prospective whole-genome transcriptomic studies to allow a molecular classification of iERMs and for the identification of molecular signature(s) of prognostic and therapeutic significance.

1. Introduction

Epiretinal membranes (ERMs) are fibrocellular membranes containing extracellular matrix (ECM) proteins and epiretinal cells of retinal and extraretinal origin [1,2]. ERMs are characterized by the growth of fibrocellular tissue on the inner limiting membrane (ILM) of the retina and are defined as idiopathic ERMs (iERM) when they are not associated with any other ocular disease such as trauma, intraocular inflammation, retinal detachment, and retinal vascular pathologies [3].

Vision disturbance resulting from decreased visual acuity with or without metamorphopsia is the main indication for ERM surgery [4]. Even though this may lead to an improvement of vision, successful ERM removal may result in a limited improvement of visual acuity in a significant percentage of patients [5]. This calls for a classification of ERMs that may provide useful prognostic information for more successful therapeutic approaches to a disease whose prevalence is approximately 6% in patients aged over 60 years and tends to increase with aging [6,7].

Thus far, various classification strategies have been proposed for iERMs based on spectral domain optical coherence tomography (SD-OCT) biomarkers that may represent predictive factors for postsurgical visual outcomes [1,8–13]. These studies have provided a detailed description of the morphologic/structural alterations that occur in the retina of iERM patients. However, the pathogenesis of this clinical entity has not been completely defined and a globally accepted ERM classification system is still lacking [1]. Morphological and

Abbreviations: BCVA, best-corrected visual acuity; ECM, extracellular matrix; iERM, idiopatic epiretinal membrane; ILM, inner limiting membrane; IS/OS, inner segment/outer; segment SD-OCT, spectral domain optical coherence tomography

* Corresponding authors.
E-mail addresses: francesco.semeraro@unibs.it (F. Semeraro), marco.presta@unibs.it (M. Presta).

https://doi.org/10.1016/j.bbadis.2020.165938
Received 22 May 2020; Received in revised form 30 July 2020; Accepted 17 August 2020
Available online 20 August 2020

immunohistochemical analyses have demonstrated the presence of a variety of cell types in iERMs, including hyalocytes, fibroblasts, myofibroblasts, retinal pigment epithelial cells, and glial cells (Müller cells, astrocytes, and microglia) [14–16]. Cell proliferation, transdifferentiation and deposition of ECM proteins characterize iERM formation that appears to be driven by various cytokines/growth factors that accumulate in the humor vitreous [16,17].

In the present work, a list of 20 genes relevant to the pathogenesis of iERM was established based on educated guess after an extensive searching of the scientific literature. These genes encode for proteins that represent putative biomarkers of the cellular and molecular events occurring in iERMs, including cell population markers, ECM components, cytokines and growth factors. Next, we performed a retrospective study in which we assessed the levels of expression of these genes by real-time quantitative polymerase chain reaction (RT-qPCR) analysis in a cohort of surgically removed iERM samples. Hierarchical clustering of the gene expression data allowed the identification of two major clusters of iERM specimens. When compared to Cluster A samples, Cluster B iERMs were characterized by a higher expression of most of the genes investigated that was accompanied by more severe clinical and SD-OCT features. This work paves the way to future prospective whole-genome transcriptomic studies to define a molecular classification of iERMs and for the identification of molecular signature(s) of prognostic and therapeutic significance.

2. Materials and methods

2.1. iERM samples

Membrane peeling was performed by an experienced surgeon (F.M.) at the Clinics of Ophthalmology of the University of Brescia on 56 iERM patients [gender (m/f): 26/30; age: 73 ± 7.4; phakic (%)/pseudofakic (%) = 77%/23%; preoperative decimal best-corrected visual acuity (BCVA) at Snellen chart: 0.35 ± 0.15] during the period from August 2017 to April 2019. 56 iERM samples were collected, immediately frozen and stored at −80 °C. Collection and analysis of human samples was approved by the internal review board of the Spedali Civili of Brescia, Italy, and followed the principles of the Declaration of Helsinki.

We included iERM patients older than 18 years, decimal BCVA lower than 0.63 (20/30) using the Snell chart, and clear evidence of ERM traction on sagittal OCT scans. The exclusion criteria were pregnancy, history of diabetes mellitus, connective tissue diseases, malignancies, or other systemic disorders, prior vitreoretinal surgery, ocular trauma, any corneal pathology. Patients with dry or wet age-related macular degeneration were also excluded.

SD-OCT scans were performed by one of two masked physicians (*E.G.* or D.R.) before, one month and 3 months after surgery to evaluate iERM staging, central macular thickness (CMT), and the visibility of the inner segment/outer segment (IS/OS) junction. The clinical ocular examination, including BCVA test by using the Snellen chart, slit-lamp biomicroscopy, and dilated fundoscopy, was conducted only at baseline visit, before surgery.

2.2. SD-OCT scan protocol and analysis

The macula raster scanning was performed in all eyes with 21 B-scans over 12 × 4 mm area. Combined spectral OCT/SLO topography and microperimetry (OPKO/OTI, Miami, FL) were used and images were considered suitable when signal strength index was ≥7/10. ERM was defined as single, irregular and hyperreflective band anterior to neurosensory retina, above the ILM, often associated with underlying retinal wrinkling and the presence of hyporeflective space between ERM and ILM.

CMT was measured manually using the “caliper function”, tracking a vertical perpendicular line from the midpoint of the retinal pigment epithelium/choriocapillaris band to the retinal surface and the foveal pit. When the foveal pit was absent, the measurement was taken at the central point of the fovea where the inner layers became tented.

The iERM stage was defined following the criteria used by Hwang et al. [9], while the evaluation of the IS/OS junction was defined following the criteria used by Sheales et al. [18]. The IS/OS junction was observed as a hyperreflective band in front of the retinal pigment epithelium/choriocapillaris unit. A score equal to 0, 1, or 2 was given when the intensity of the line IS /OS junction within 1.5 mm of the central fovea was < 10%, between 10 and 50%, or > 50%, respectively.

Of the 56 iERM collected, 9 samples were excluded from the SD-OCT classification due to low imaging quality (< 7/10) and the presence of cystoid macular edema (defined as the presence of multiple hyporeflective intraretinal cystoids spaces). All OCT images were quantitatively and qualitatively evaluated by two independent and masked observers (*E.G.* or D.R.) and disagreements were resolved by the intervention of a third observer (F.S.).

2.3. Surgical technique

A transconjunctival sutureless *pars plana* vitrectomy was performed in all patients with the Constellation 25 G+ Total Plus Vitrectomy Pak (Alcon Laboratories, Fort Worth, TX). The main steps of PPV were induction of posterior hyaloids detachment using the active suction of the vitreous cutter, core and peripheral vitreous gel removal, peeling of the ERM and peeling of the ILM. The posterior hyaloids was detached increasing the suction of the vitrectomy probe to 600 mmHg near the optic nerve head and pulling the vitreous cortex until the equatorial periphery of the retina. A first intravitreal staining with Blu Dual (DORC, Zuiland, The Netherlands) was performed for approximately 1 min and the epiretinal proliferation was centripetally removed from the macula using 25-Gauge vitreoretinal forceps. After ERM removal, a second one-minute Blu Dual intravitreal staining was performed to completely remove the ILM if still present. The retina was then inspected with scleral depression and any iatrogenic retinal holes or tears were treated with argon laser photocoagulation. A combined phacovitrectomy was performed in all phakic patients.

2.4. RT-qPCR analysis

For mRNA expression analysis, iERM were processed and total RNA was extracted using the ReliaPrep™ RNA Cell Miniprep System according to manufacturer's instructions (Promega). Total RNA was retrotranscribed with SuperScript™ VILO™ MasterMix (Invitrogen) using random hexaprimers in a final 20 µL volume. Then, RT-qPCR was performed with a ViiA™ 7 Real-Time PCR Detection System (Applied Biosystems) using iQ™ SYBR Green Supermix (Biorad) according to manufacturer's instructions. Expression levels of selected genes were normalized to *GAPDH* expression. An arbitrary value equal to 1.0 was assigned to the levels of expression of the genes measured in one iERM specimen that was used as reference sample for all the experiments. The primers used for RT-qPCR are listed in Suppl. Table 1.

2.5. Statistical analysis

Hierarchical clustering was performed on gene expression values expressed on $\log_2$ scale. Gene expression levels were then standardized in order to have comparable dynamic ranges. Clustering was performed on Euclidean distances using Ward's hierarchical agglomerative clustering method [19]. Missing data were assigned using median value imputation.

Gene expression level comparison between groups was performed on $\log_2$ expression values using linear models with moderated t-statistic [20]. *P* values were adjusted for multiple testing using the false discovery rate (FDR) [21]. As for IS/OS scores and retinal thickness data, comparison among molecular clusters without distinction of timing of

Table 1
Genes analyzed in the present study.

Gene	Protein abbreviation	Putative biological significance in iERM
Cell population markers		
GLUL	GLUL (Glutamate-Ammonia Ligase)	Muller cell marker
RLBP1	CRALBP (Cellular retinaldehyde binding protein)	Muller cell marker
GFAP	GFAP (Glial fibrillary acid protein)	Activated glial cell marker
ACTA2	αSMA (α-Smooth muscle actin)	Myofibroblast marker
TAGLN	SM22/Transgelin	Myofibroblast marker
S100A4/FSP1	S100 (Fibroblast-specific protein 1)	Fibroblast marker
PTPRC	CD45	Hyalocyte marker
CD163	CD163	Macrophage marker
Biological markers		
CCND1	Cyclin D1	Cell proliferation marker
SNAI1	SNAIL	EMT and GMT marker
HIF1A	HIF1α (Hypoxia Inducible Factor 1 subunit alpha)	Hypoxia marker/cytokine expression mediator
ECM proteins		
COL1A1	COLL1α (Collagen type I alpha 1 chain)	ECM deposition marker
COL6A1	COLL6α (Collagen type VI alpha 1 chain)	ECM deposition marker
Cytokines and growth factors		
TGFB1 and *TGFB2*	TGFβ1 and TGFβ2 (Transforming growth factor beta 1 and 2)	Pro-fibrogenic factors, EMT and GMT inducers, cell-mediated collagen contraction inducers.
VEGFA	VEGF (Vascular endothelial growth factor-A)	Pro-angiogenic factor
FGF2	FGF2 (Fibroblast growth factor 2)	Autocrine Muller cell growth factor, pro-angiogenic and pro-fibrogenic factor
PDGFB	PDGF (Platelet derived growth factor beta)	Autocrine Muller cell growth factor and contractility inducer, pro-fibrogenic factor
NGF	NGF (Nerve growth factor)	Myofibroblast contractility inducer, pro-fibrogenic factor
IGF1	IGF1 (Insulin like growth factor 1)	Muller cell growth factor and contractility inducer

ECM, extracellular matrix; EMT, epithelial-mesenchymal transition; GMT, glial-mesenchymal transition.

measurement were performed using generalized estimating equations (GEE) models to account for within patient correlation. IS/OS was modelled as an ordinal variable, while retinal thickness was modelled assuming a Gaussian distribution.

All tests were two sided and analyses were performed using PRISM and R software (version 4.0).

3. Results

3.1. iERM gene selection

A PubMed search using "Epiretinal membrane" as keyword retrieved more than 3.600 publications. Among them, approximately 100 papers focused on the classification of ERMs (PubMed search, 20/03/2020). Based on literature data, we used a hypothesis-driven approach to select a set of genes that may represent putative biomarkers of the cellular and molecular events that occur in the iERM in order to analyze their levels of expression in a cohort of surgically removed iERM samples.

The selected genes encode for proteins belonging to the following biological categories: a) markers of different cell populations forming the iERM; b) markers of biological events relevant to the pathogenesis of iERM; c) ECM components of the iERM; d) cytokines and growth factors (Table 1).

3.1.1. Cell population markers

GLUL and *RLBP1* were selected as Müller cell markers. *GLUL* encodes for the glutamate-ammonia ligase/glutamine synthase (GLUL) protein. *GLUL* is expressed by Müller cells and is involved in the rapid conversion of glutamate into glutamine, which is subsequently exported from the glia for recycling by neighboring neurons back into glutamate [22]. *RLBP1* encodes for the cellular retinaldehyde binding protein (CRALBP) that supports chromophore recycling in Müller cells to help cone cells to function in high light intensities [23]. *GFAP* encodes for the intermediate filament glial fibrillary acid protein (GFAP) which is a marker of glial cell activation in response to retinal injuries [24]. *ACTA2* and *TAGLN* are two myofibroblast markers encoding for α-smooth muscle actin (αSMA) and SM22/transgelin proteins, respectively, whereas *S100A4/FSP1*, encoding for the S100/fibroblast-specific protein 1, is considered as a fibroblast marker [25–27]. Finally, *PTPRC/CD45* and *CD163* were used as hyalocyte and macrophage markers, respectively [14,28].

3.1.2. Biological markers

CCND1, encoding for the Cyclin D1 protein required for the progression through the G1 phase of the cell cycle, was used as a cell proliferation marker in iERM [29]. *SNAI1* encodes for the transcription factor SNAIL1 that plays a pivotal role in the epithelial-to-mesenchymal transition (EMT) and glial-to-mesenchymal transition (GMT) processes [27]. Hypoxia inducible factor-1 subunit alpha (HIF1α) is encoded by the *HIFA* gene and its expression is a widely used marker of hypoxia in different pathophysiological conditions, including eye diseases [30]. HIF1α, together with the HIF1β subunit, forms the HIF transcription factor heterodimer that triggers the activation of a large number of proteins, including VEGF and angiopoietin-2, and its expression has been reported in diabetic ERMs [31].

3.1.3. ECM proteins

ECM production and remodeling plays a pivotal role in the pathogenesis of iERM [3,32]. In the present work, *COL1A1* and *COL6A1* were utilized as markers of ECM production. *COL1A1* encodes for the alpha-1 chain of Type I collagen that appears to form, together with Type II collagen, the bulk of ECM in late ERMs; *COL6A1* encodes for the alpha-1 chain of Type VI collagen that anchors the ERM to the retinal ILM [33].

3.1.4. Cytokines and growth factors

A variety of cytokines and growth factors, acting on different retinal cell components in an autocrine and/or paracrine fashion, have been implicated in the pathogenesis of iERM [16,17]. Here, iERM samples were analyzed for the levels of expression of *TGFB1*, *TGFB2*, *VEGFA*, *FGF2*, *PDGFB*, *NGF* and *IGF1* genes. Transforming growth factor beta (TGFβ) is thought to play an important role in iERM formation due to its pro-fibrogenic activity and its capacity to induce collagen contraction mediated by Müller cells [25,34,35]. In addition, TGFβ induces EMT [36] and the TGFβ/SNAIL axis has been shown to trigger GMT in

Müller cells [27]. Notably, TGFβ2 appears to be present in the vitreous fluid of iERM patients at concentrations significantly higher than those of the TGFβ1 subtype, pointing to a significant role of this cytokine in iERM evolution (see [37] and references therein). Upregulation of the pro-angiogenic vascular endothelial growth factor-A (VEGF) occurs in several cell components of ERMs in diabetic and proliferative vitreoretinopathy patients, including Müller and retinal pigment epithelial cells [38,39] and it is part of the pro-survival responses triggered by HIF during hypoxia [40]. Fibroblast growth factor 2 (FGF2) is detected in ERMs [41,42] and pro-inflammatory mediators can induce *FGF2* expression by Müller cells [43,44]. In turn, FGF2 may induce proliferation, *VEGF* and *GFAP* upregulation in Müller cells and may stimulate fibroblast/myofibroblast migration and proliferation [45,46]. Cellular components of fibrovascular and avascular ERMs, including Müller cells, produce platelet-derived growth factor B (PDGFB) [47,48]. Besides its stimulatory effects on fibroblasts/myofibroblasts, PDGF acts as an autocrine factor for Müller cells, triggering cell proliferation, migration, VEGF secretion, and collagen contraction [35,48]. As observed for TGFβ, increasing evidence indicates that nerve growth factor (NGF) is endowed with pro-fibrogenic activity by inducing fibroblast migration and their differentiation into myofibroblasts [49,50]. *NGF* expression has been observed in iERMs where it is thought to play a role in its evolution and in myofibroblast-mediated contractility [51,52]. Finally, insulin like growth factor-1 (IGF1) is endowed with the capacity to trigger Müller cell proliferation and contractility [35,53,54].

3.2. iERM gene expression analysis

A series of 56 iERMs samples collected from August 2017 to April 2019 were evaluated by RT-qPCR for the relative expression levels of the 20 selected genes, leading to more than 1.000 gene expression data. Expression levels of all the selected genes, normalized for *GAPDH* expression, were compared to those measured in one iERM sample that was used as reference sample in all the experiments. The results indicate that a high variability of the steady state mRNA levels exists for each of the analyzed genes in the sample series, the expression of some of them differing by more than 100-fold among the iERMs samples (Fig. 1).

On this basis, a linear regression analysis was performed to correlate the expression levels of each gene with those calculated for the other 19 genes in all the iERM samples (Suppl. Table 2). The results indicate that

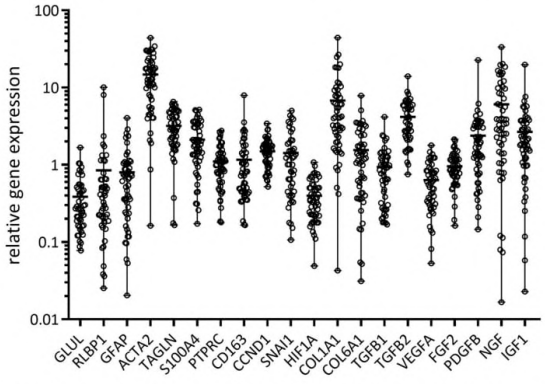

Fig. 1. Gene expression levels in iERM. iERM samples (n = 56) were analyzed by RT-qPCR and the levels of expression of the 20 indicated genes were normalized to *GAPDH* and compared to those measured in one iERM specimen that was used as a reference samples in all the experiments and in which the levels of gene expression were arbitrarily set equal to 1.0 for all the genes investigated. Data are shown as mean ± range.

a significant correlation exists between the expression levels of the Müller cell/glial markers *GLUL* and *RLBP1*, as well as with the expression levels of the glial activation marker *GFAP*. Notably, both *GLUL* and *GFAP* expression are related with *HIF1A* mRNA levels and with the HIF target genes *VEGFA* and *FGF2* (Fig. 2A).

A significant correlation was observed also among the fibroblast/myofibroblast markers *ACTA2*, *TAGLN* and *S100A4* that encode for αSMA, SM22 and S100 proteins, respectively (Fig. 2B). In keeping with the ECM deposition activity of these cells, *ACTA2* and *TAGLN* expression levels were directly related to *COL1A1* mRNA levels. In turn, *COL1A1* expression correlates with *COL6A1* expression, both transcripts being related to the expression levels of various pro-fibrogenic genes, including *TGFB1*, *FGF2*, and *PDGFB* (Fig. 2C).

As anticipated, a significant correlation occurs between the hyalocyte/macrophage markers *PTPRC* (encoding for the CD45 antigen) and *CD163*, both related to the mRNA levels of *HIF1A*, *TGFB1*, *TGFB2*, and *FGF2* (Fig. 2D).

In keeping with previous observations [29], cell proliferation occurs in iERMs, as confirmed by the expression of *CCND1* that encodes for the cyclin D1 protein. Notably, cell proliferation goes in parallel with the expression of all the cytokines/growth factors investigated (Fig. 2E). In addition, *CCDN1* mRNA levels correlate with the fibrosis-related markers *TAGLN*, *COL1A1* and *COL6A1*, as well as with the hypoxia and EMT markers *HIF1A* and *SNAI1*, respectively (Fig. 2F). Surprisingly, *SNAI1* expression did not seem to be related to the levels of expression of the EMT/GMT inducers *TGFB1 and TGFB2*, being instead related to the expression of the growth factor-encoding genes *FGF2*, *PDGFB*, *NGF* and *IGF1* and with *HIF1A* (Fig. 2G). The importance of the transcription factor HIF in iERMs was further supported by the direct correlation observed among *HIF1A* mRNA levels and the expression of the glial markers *GLUL* and *GFAP* (Fig. 2A) and of the myofibroblast marker *TAGLN* (Fig. 2H).

Finally, a direct correlation was observed among most of the cytokine/growth factor encoding genes tested, including a significant correlation between *TGFB1* and *TGFB2* subtypes, suggesting that a tight cross-talk may exit among these genes that appears to be related, at least in part, to the expression of the transcription factor *HIF1A* (Suppl. Table 2).

3.3. Cluster analysis of the iERM gene expression data

A hierarchical cluster analysis was performed on our RT-qPCR data in order to assess whether iERM samples could be grouped according to similar patterns of gene expression. The results, shown in Fig. 3A, indicate that iERMs could be divided in two clusters hereinafter referred to as Cluster A and Cluster B. Cluster A (n = 25) shows lower expression levels for most of the genes investigated when compared to Cluster B (n = 30). In addition, the analysis indicates that Cluster B can be subdivided in two distinct subgroups (Clusters B1 and B2, n = 16 and n = 14, respectively) based on the different levels of expression of a subset of genes that includes the growth factor-encoding genes *IGF1*, *NGF*, and *VEGFA*, the glial markers *RLBP1*, *GLUL*, and *GFAP*, and the pro-fibrogenic markers *ACTA2*, *TAGLN* and *COL1A1*. It must be pointed out that Clusters A, B, B1 and B2 showed similar expression levels of the housekeeping gene *GAPDH*, ruling out the possibility that such clustering was the mere consequence of differences in the cell content of the analyzed samples (data not shown).

On this basis, the gene expression levels measured in Cluster B iERMs were compared to the corresponding mean levels in Cluster A samples. As shown in Fig. 3B, the results of such analysis confirmed that iERMs belonging to Cluster B are characterized by higher mRNA transcript levels for all the genes investigated, the only exception being represented by the *ACTA2*, *TAGLN*, *S100A4* and *PTPRC* transcripts, encoding for the myofibroblast/fibroblast markers αSMA, SM22/transgelin and S100 and for the hyalocyte marker CD45, respectively.

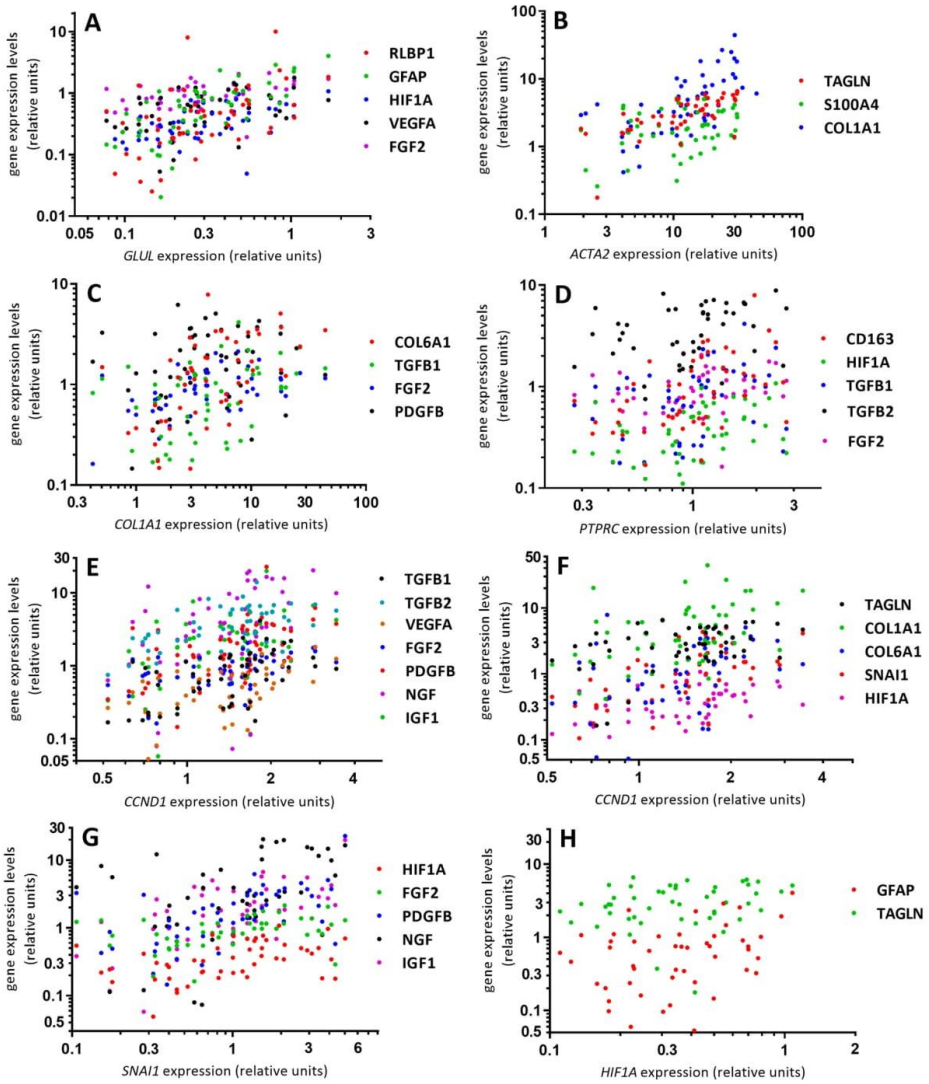

Fig. 2. Gene expression relationships in iERMs. A linear regression analysis was performed to correlate the expression levels of the gene indicated on the "x" axis with those listed in the inset legend of each panel. Each dot represents one iERM sample. R^2 and *P* values are shown in **Supplementary Table 2**.

Finally, we analyzed the expression levels of the different genes in the B1 ($n = 16$) and B2 ($n = 14$) subgroups. As shown in Fig. 4A, the Muller/glial markers *GLUL*, *RLBP1* and *GFAP* are upregulated in Cluster B1 when compared to Cluster B2 and Cluster A samples whereas the pro-fibrotic markers *ACTA2*, *TAGLN*, and *COL1A1*, as well as the cytokines/growth factors *TGFB1*, *NGF* and *IGF* are more expressed in Cluster B2 samples when compared to Cluster B1 and Cluster A iERMs (Fig. 4B). Finally, the *CD163*, *CCND1*, *SNAI1*, *COL6A1* and *HIF1A* genes and the growth factors *VEGFA*, *FGF2, TGFB2* and *PDGFB* are modulated in B1 and B2 subgroups in a similar manner (Fig. 4C).

Together, these results confirm the data obtained by hierarchical cluster analysis and indicate that iERMs can be clustered at the molecular level based on the expression levels of the analyzed genes.

3.4. Clinical features of molecular iERM clusters

We reviewed the clinical charts of the patients investigated in this retrospective study and we assessed whether the molecular iERM clustering could reflect different clinical features of the disease. As shown in Fig. 5A, preoperative decimal BCVA was higher in Cluster A than in Cluster B patients. In addition, a better and faster improvement of IS/OS visualization was observed following ERM peeling in Cluster A patients when compared to Cluster B patients (Fig. 5B). However, no significant difference was observed between A and B clusters in terms of pre-surgical and post-surgical central macular thickness (Fig. 5C).

Next, we assessed whether significant differences could exist between the two molecular iERM subgroups B1 and B2. Notably, a more

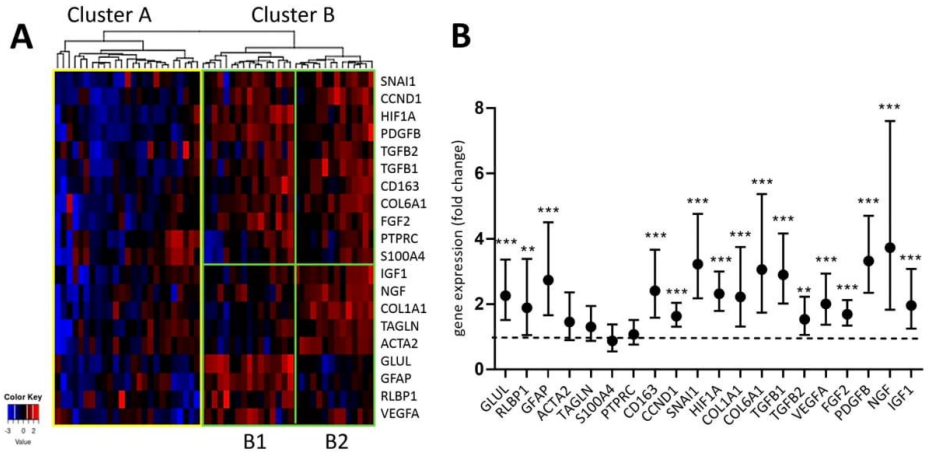

Fig. 3. Hierarchical cluster analysis of gene expression data in iERM samples. **A)** Heatmap depicting the relative expression of the genes investigated in the 55 iERM samples grouped by hierarchical cluster analysis. Each column represents one iERM sample and each row represents the indicated gene. The expression level of each gene in a single sample is depicted according to the color scale. **B)** Fold change of mean gene expression levels in Cluster B (n = 30) *versus* Cluster A (n = 25) samples. Data are shown as mean ± 95% CI. B *versus* A: *, FDR < 0.1; **, FDR < 0.05; ***, FDR < 0.01, moderated *t*-test.

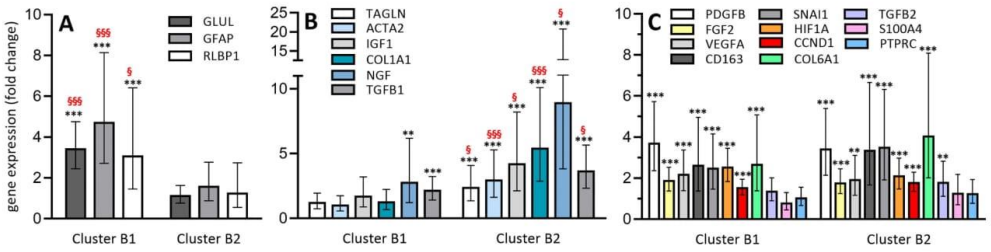

Fig. 4. Gene expression analysis in B1 and B2 iERM subgroups. Fold change of mean gene expression levels in Cluster B1 (n = 16) and Cluster B2 (n = 14) iERMs *versus* Cluster A (n = 25) samples. Data are shown as mean ± 95% CI. B1 or B2 *versus* A: *, FDR < 0.1; **, FDR < 0.05; ***, FDR < 0.01. B1 *versus* B2: §, FDR < 0.1; §§, FDR < 0.05; §§§, FDR < 0.01, moderated t-test.

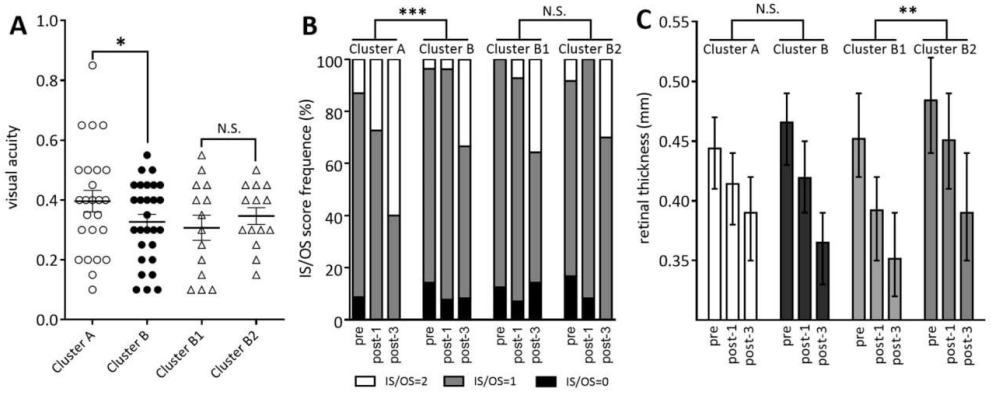

Fig. 5. Visual acuity, IS/OS, and mean central macular thickness in the different molecular iERM clusters. **A)** Preoperative decimal BCVA. Data are the mean ± S.E.M. *, P = 0.11, Student's t-test. **(B)** Stacked bar plot showing the frequency of pre-surgical (pre), 1-month post-surgery (post-1) and 3-month post-surgery (post-3) IS/OS score levels. ***, P < 0.01, GEE model. **C)** Central macular thickness. Data are shown as mean ± 95% CI. **, P < 0.05, GEE model. Values were obtained from the clinical charts of patients belonging to molecular iERM Cluster A (n = 20–25), Cluster B (n = 20–28), Cluster B1 (n = 14–16) and Cluster B2 (n = 10–14).

Table 2
Distribution of iERMs based on SD-OCT-based classification and molecular clustering.

SD-OCT-based iERM classification	Molecular Cluster A (*n* = 23)	Molecular Cluster B[a] (*n* = 24)	Molecular Cluster B1 (n = 14)	Molecular Cluster B2[b] (n = 10)	Total (*n* = 47)
Group 1A	6 (26.1%)	0 (0%)	0 (0%)	0 (0%)	6
Group 1B	9 (39.1%)	9 (37.5%)	8 (57.1%)	1 (10.0%)	18
Group 1C	7 (30.4%)	9 (37.5%)	3 (21.4%)	6 (60.0%)	16
Group 2A	0 (0%)	0 (0%)	0 (0%)	0 (0%)	0
Group 2B	1 (4.4%)	6 (25.0%)	3 (21.4%)	3 (30%)	7

iERMs belonging to molecular clusters A and B were distributed according their SD-OCT features as classified by Hwang et al. [9].
[a] $P < 0.05$, Cluster B *vs* Cluster A.
[b] $P < 0.05$, Cluster B2 *vs* Cluster B1, contingency table Chi-Square test.

relevant reduction of postoperative central macular thickness occurred in Cluster B1 patients when compared to Cluster B2 (Fig. 5C), even though no statistical differences were observed between the two subgroups in terms of decimal BCVA and IS/OS grading (Fig. 5A,B).

Various iERM classification strategies have been proposed based on SD-OCT findings. Information present in the clinical charts allowed us to apply the SD-OCT-based classification proposed by Hwang et al. [9] to 47 out of the 56 iERMs analyzed in our study, 23 of them belonging to the molecular Cluster A and 24 to the molecular Cluster B (Table 2). We found that 6 out of the total 47 iERMs belonged to the fovea-attached type ERM Group 1A, characterized by an ERM with outer retinal thickening and near-normal inner retina [9], whereas 18 and 16 samples were part of the more severe SD-OCT Groups 1B and 1C, respectively. The remaining 7 samples belonged to the pseudohole type ERM

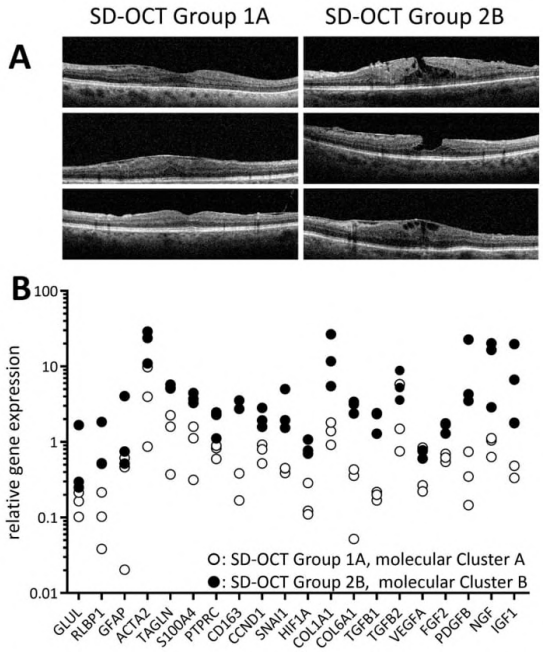

Fig. 6. Representative SD-OCT images and gene expression data showing examples of molecular Cluster A and Cluster B iERMs. **A)** SD-OCT images of Group 1A and Group 2B iERMs according to the morphologic classification by Hwang et al. [9]. **B)** Gene expression analysis of the corresponding iERMs belonging to the molecular Cluster A (open symbols) and Cluster B (closed symbols), respectively.

Group 2B, characterized by the presence of a macular pseudohole accompanied by marked intraretinal splitting [9].

When the molecular iERM Clusters A and B were analyzed separately, all SD-OCT Group 1A samples were part of the molecular Cluster A whereas 6 out of the 7 SD-OCT Group 2B samples belonged to the molecular Cluster B (Table 2 and Fig. 6). In addition, when the SD-OCT-based classification was applied to the molecular iERM subgroups B1 and B2, Cluster B2 iERMs showed more severe SD-OCT features when compared to Cluster B1 samples (Table 2).

Together these data indicate that iERMs of the molecular Cluster B present more severe clinical and morphological features when compared to Cluster A specimens. Table 3 summarizes the main molecular and clinical differences between Cluster A and Cluster B iERMs.

4. Discussion

In the present work, we performed a retrospective study in which the levels of expression of iERM-related genes were analyzed in a cohort of 56 iERM samples. The genes encode for proteins representing biomarkers of different aspects of the pathogenesis of iERM, including markers of iERM cell populations and ECM components and markers of the biological events relevant to the pathogenesis of iERM, including various cytokines and growth factors.

The results showed a high variability in the expression levels of all the genes investigated. Our data and previous experimental evidences [14–16,55] indicate that such variability may reflect significant differences in the cell populations representing the different iERM samples, with consequent differences in ECM protein synthesis and cytokine/growth factor production. Indeed, we observed a significant correlation between the expression levels of the Müller cell/glial markers *GLUL* and *RLBP1*. Similarly, a significant correlation was observed among the fibroblast/myofibroblast markers *ACTA2*, *TAGLN* and *S100A4*, as well as between the hyalocyte/macrophage markers *PTPRC* and *CD163*. These data confirm and extend previous morphological and immunohistochemical analyses showing the presence of these cell types in iERMs [14–16].

Gliosis, hypoxia, fibrosis, and EMT/GMT differentiation are part of the biological processes that characterize the pathogenesis of iERM [3,56]. Accordingly, iERMs express the glial activation marker *GFAP* whose transcript levels correlate with the expression of *GLUL* and *RLBP1* and with that of *HIF1A*. The importance of the hypoxia-inducible transcription factor HIF in iERMs was supported by the direct correlation occurring among *HIF1A* mRNA levels and the expression of the glial marker *GLUL*, the myofibroblast marker *TAGLN*, the EMT/GMT inducer *SNAI1*, and with the cell proliferation marker *CCND1*, encoding for the cyclin D1 protein. In parallel, the occurrence of pro-fibrotic events in iERMs was substantiated by the expression of the collagen-encoding genes *COL1A1* and *COL6A1*. The expression of these genes correlated directly with the expression of fibroblast/myofibroblast markers as well as with that of pro-fibrogenic genes, including *FGF2*, *PDGFB* and *TGFB1*, but not *TGFB2,* pointing to a different biological function of TGFβ1 and TGFβ2 subtypes in iERMs.

In keeping with the pivotal role played by EMT/GMT processes in the pathogenesis of iERM [27,56], we observed that the expression of *SNAI1*, encoding for the EMT/GMT inducer SNAIL1, correlates with the expression of the growth factor-encoding genes *FGF2*, *PDGF*, *NGF* and *IGF1* and with that of *HIF1A*. Several experimental evidences indicate that TGFβ induces EMT in different pathological conditions and it is able to trigger GMT when administered *in vitro* to Müller cells [27,36]. However, we did not find any relationship between *SNAI1* and *TGFB1/TGFB2* expression in our iERM samples, suggesting that also different growth factors/cytokines may play a role in the iERM transdifferentiation processes. FGF2, PDGF, NGF and IGF1 have been shown to act as mitogenic and pro-fibrogenic factors. Their role as transdifferentiating factors in iERMs will deserve further investigation.

When a hierarchical cluster analysis of the gene expression data was

Table 3
Summary of the main molecular and clinical differences between Cluster A and Cluster B iERMs.

Molecular cluster	Relative gene expression				
	Myofibroblast/fibroblast markers	Hyalocyte markers	Glial markers	Fibrogenic markers	Growth factors/cytokines
Cluster A	=	=	-	-	-
Cluster B	=	=	+	+	+

Molecular cluster	Clinical features		
	Preoperative decimal BCVA	Postoperative IS/OS improvement	SD-OCT severity
Cluster A	+	+	-
Cluster B	-	-	+

performed, two clusters were identified in which iERM samples could be grouped according to distinct patterns of gene expression. Notably, when compared to Cluster A, iERMs belonging to Cluster B are characterized by higher mRNA transcript levels for all the genes investigated, the only exception being represented by the genes encoding for the myofibroblast/fibroblast markers αSMA, SM22/transgelin and S100 and the hyalocyte marker *PTPRC/CD45*. It must be pointed out that no difference in total cellularity appears to occur between the two clusters, as indicated by the similar levels of expression of the housekeeping *GAPDH* gene. In addition, iERM patients belonging to Clusters A and B did not differ in terms of gender, age and previous cataract surgery. Thus, these data suggest that Cluster A is characterized by iERM specimens with a more "quiescent" status whereas Cluster B samples represent transcriptionally "activated" iERMs, possibly because of the higher levels of expression of various pro-inflammatory/pro-fibrotic cytokines and growth factors.

The hierarchical cluster analysis also indicated that Cluster B could be subdivided in two distinct subgroups based on the different levels of expression of a subset of the analyzed genes. Indeed, the subgroup B1 was characterized by a higher expression of the Muller/glial markers *GLUL*, *RLBP1* and *GFAP* when compared to Cluster B2 and Cluster A. Cluster B2 iERMs express instead higher levels of the pro-fibrotic markers *ACTA2*, *TAGLN*, and *COL1A1*, as well as of the cytokines/growth factors *TGFB1*, *NGF* and *IGF*. Based on these observations, it seems possible to hypothesize that two different statuses of activation may exist in iERMs, one characterized by a more pro-fibrotic phenotype driven, among others, by *TGFB1*, *NGF* and *IGF* gene products, and a second one in which glial cell activation plays a prominent role.

Pars plana vitrectomy with double peeling of the ILM and ERM is a common procedure for patients affected by ERM [55,57]. iERMs cause a tractional stress force on the retina which results in increasing retinal thickness and centripetal displacement of inner retinal layers [58]. This mechanic stress acts on Müller cells, inducing the activation of different signal transduction pathways and reactive internal gliosis [37]. Müller cells act as living optical fibers that guide light through the inner retinal tissue and the loss of their function may lead to a reduction of quantity and quality of the light reaching the photoreceptors, causing a reduced BCVA [59].

In an attempt to assess whether the results of the hierarchical cluster analysis may reflect different clinical features of the iERM patients analyzed in this study, we reviewed retrospectively their clinical charts. Notably, despite the equal average age and percentage of phakic and pseudophakic patients, preoperative decimal BCVA was lower for iERM patients belonging to Cluster B when compared to Cluster A. This could reflect the more activated status of Cluster B iERMs, with consequent retinal cell transdifferentiation and acquisition of a pro-inflammatory/pro-fibrotic phenotype driven by the overexpression of cytokines and growth factors.

In keeping with previous observations, we observed an improvement of IS/OS visualization following ERM peeling related to a possible restoration of cone outer tips after the removal of the tractional force [60–63]. Even though this improvement occurred in both Cluster A and B patients, the percentage of patients with better post-surgery IS/OS grading values were higher in Cluster A patients when compared to Cluster B patients. We hypothesize that the different integrity of IS/OS junction in the two clusters could be related to a stronger tractional damage caused by Cluster B iERMs in respect to Cluster A membranes. No significant difference was instead observed between Cluster A and B patients in terms of baseline central macular thickness and of its improvement after surgery.

Various SD-OCT-based classification strategies have been proposed to identify predictive factors for postsurgical visual outcomes in iERM patients [1,8–13]. Inclusion criteria and information present in the clinical charts allowed us to apply to our cohort of patients the SD-OCT-based iERM classification proposed by Hwang et al. [9]. According to these classification criteria, specimens belonging to Cluster A show a prevalence of fovea-attached type iERMs, characterized by outer retinal thickening and near-normal inner retina. Cluster B iERMs include instead more severe SD-OCT features, characterized by the presence of a macular pseudohole accompanied by schisis-like intraretinal splitting. Again, these differences might be explained, at least in part, by the different activation status of the iERMs belonging to the two molecular clusters, more quiescent iERMs showing less severe SD-OCT findings due to differences in the expression levels of pro-fibrotic genes, with consequent differences in tractional forces between the two groups. This hypothesis is supported by the observation that Cluster B2 iERMs, characterized by a more pro-fibrotic phenotype, showed more severe SD-OCT features when compared to Cluster B1 samples, characterized instead by a marked glial cell activation. In this frame, it is worth noticing that the observed post-surgery decrease in central macular thickness appears to occur more efficiently in Cluster B1 patients when compared to Cluster B2 patients.

Steady state levels of a given gene transcript do not necessarily reflect the amount and biological impact of the corresponding protein. Indeed, translational modulation, prost-translational modifications and/or extracellular protein activation may determine the biological significance of the gene products herewith investigated. For instance, the activity of the transcription factor HIF-1 depends on its intracellular stability [30] whereas NGF and TGFβs are synthesized in a latent form that requires extracellular activation [57,58]. This may explain, at least in part, the lack of correlation that we observed at the transcriptional level between *SNAI1* and *TGFB1/2* expression. In addition, the activity of cytokines and growth factors strictly depends on the expression of the cognate receptors and co-receptors in target cells and consequent activation of various intracellular signaling pathways. Thus, the study of iERM proteome [59] may provide useful information about the pathogenesis of the disease, complemental to gene expression data. In this frame, to the best of our knowledge our study represents the first attempt to characterize iERMs at a gene transcription level. Performed retrospectively on a limited number of genes, this work paves the way

to future prospective proteome and whole-genome transcriptome studies to allow a molecular classification of iERMs and for the identification of molecular signature(s) of prognostic and therapeutic significance.

CRediT authorship contribution statement

Daniela Coltrini: Investigation, Data curation.**Mirella Belleri:** Investigation.**Elena Gambicorti:**Resources, Investigation.**Davide Romano:**Resources, Investigation.**Francesco Morescalchi:** Resources.**Krishna Chandran Adwaid Manu:**Investigation.**Stefano Calza:**Formal analysis.**Francesco Semeraro:**Supervision, Funding acquisition.**Marco Presta:**Supervision, Funding acquisition, Writing - original draft, Writing - review & editing.

Declaration of competing interest

The authors declare that they have no known competing financial interests or personal relationships that could have appeared to influence the work reported in this paper.

Acknowledgements

This work was supported in part by grant CAAR (Health and Wealth Project) from the University of Brescia (Italy) to F.S.

Appendix A. Supplementary data

Supplementary data to this article can be found online at https://doi.org/10.1016/j.bbadis.2020.165938.

References

[1] W. Stevenson, C.M. Prospero Ponce, D.R. Agarwal, R. Gelman, J.B. Christoforidis, Epiretinal membrane: optical coherence tomography-based diagnosis and classification, Clin. Ophthalmol. 10 (2016) 527–534.
[2] M. Inoue, K. Kadonosono, Macular diseases: epiretinal membrane, Dev. Ophthalmol. 54 (2014) 159–163.
[3] S.C. Bu, R. Kuijer, X.R. Li, J.M. Hooymans, L.I. Los, Idiopathic epiretinal membrane, Retina 34 (2014) 2317–2335.
[4] P. Massin, C. Allouch, B. Haouchine, F. Metge, M. Paques, L. Tangui, A. Erginay, A. Gaudric, Optical coherence tomography of idiopathic macular epiretinal membranes before and after surgery, Am J. Ophthalmol. 130 (2000) 732–739.
[5] J.G. Wong, N. Sachdev, P.E. Beaumont, A.A. Chang, Visual outcomes following vitrectomy and peeling of epiretinal membrane, Clin. Exp. Ophthalmol. 33 (2005) 373–378.
[6] C.H. Ng, N. Cheung, J.J. Wang, A.F. Islam, R. Kawasaki, S.M. Meuer, M.F. Cotch, B.E. Klein, R. Klein, T.Y. Wong, Prevalence and risk factors for epiretinal membranes in a multi-ethnic United States population, Ophthalmology 118 (2011) 694–699.
[7] N. Cheung, S.P. Tan, S.Y. Lee, G.C.M. Cheung, G. Tan, N. Kumar, C.Y. Cheng, T.Y. Wong, Prevalence and risk factors for epiretinal membrane: the Singapore epidemiology of eye disease study, Br. J. Ophthalmol. 101 (2017) 371–376.
[8] L. Arias, N. Padron-Perez, I. Flores-Moreno, L. Giralt, E. Cobos, D. Lorenzo, P. Garcia-Bru, B. Dias, J.M. Caminal, Internal limiting membrane peeling versus nonpeeling to prevent epiretinal membrane development in primary rhegmatogenous retinal detachment: a swept-source optical coherence tomography study with a new postoperative classification system, Retina 40 (2020) 1286–1298.
[9] J.U. Hwang, J. Sohn, B.G. Moon, S.G. Joe, J.Y. Lee, J.G. Kim, Y.H. Yoon, Assessment of macular function for idiopathic epiretinal membranes classified by spectral-domain optical coherence tomography, Invest. Ophthalmol. Vis. Sci. 53 (2012) 3562–3569.
[10] V. Konidaris, S. Androudi, A. Alexandridis, A. Dastiridou, P. Brazitikos, Optical coherence tomography-guided classification of epiretinal membranes, Int. Ophthalmol. 35 (2015) 495–501.
[11] G. Gonzalez-Saldivar, A. Berger, D. Wong, V. Juncal, D.R. Chow, Ectopic inner foveal layer classification scheme predicts visual outcomes after epiretinal membrane surgery, Retina 40 (2020) 710–717.
[12] A. Govetto, R.A. Lalane 3rd, D. Sarraf, M.S. Figueroa, J.P. Hubschman, Insights into epiretinal membranes: presence of ectopic inner foveal layers and a new optical coherence tomography staging scheme, Am J. Ophthalmol. 175 (2017) 99–113.
[13] J.D.M. Gass, Macular dysfunction caused by epiretinal membrane contraction, Stereoscopic Atlas of Macular Diseases: Diagnosis and Treatment, vol. 2, Mosby, St Louis, MO, 1997, pp. 938–950.
[14] R.G. Schumann, A. Gandorfer, J. Ziada, R. Scheler, M.M. Schaumberger, A. Wolf, A. Kampik, C. Haritoglou, Hyalocytes in idiopathic epiretinal membranes: a correlative light and electron microscopic study, Graefes Arch. Clin. Exp. Ophthalmol. 252 (2014) 1887–1894.
[15] F. Zhao, A. Gandorfer, C. Haritoglou, R. Scheler, M.M. Schaumberger, A. Kampik, R.G. Schumann, Epiretinal cell proliferation in macular pucker and vitreomacular traction syndrome: analysis of flat-mounted internal limiting membrane specimens, Retina 33 (2013) 77–88.
[16] M. Joshi, S. Agrawal, J.B. Christoforidis, Inflammatory mechanisms of idiopathic epiretinal membrane formation, Mediat. Inflamm. 2013 (2013) 192582.
[17] E. Tsotridou, E. Loukovitis, K. Zapsalis, I. Pentara, S. Koronis, P. Tranos, S. Asteriadis, M. Balidis, T. Sousouras, T. Vakalis, Z. Zachariadis, G. Anogeianakis, Update on the cellular, genetic and cytokine basis of epiretinal membrane pathogenesis, J. Biol. Regul. Homeost. Agents 33 (2019) 1879–1884.
[18] M.P. Sheales, Z.S. Kingston, R.W. Essex, Associations between preoperative OCT parameters and visual outcome 3 months postoperatively in patients undergoing vitrectomy for idiopathic epiretinal membrane, Graefes Arch. Clin. Exp. Ophthalmol. 254 (2016) 1909–1917.
[19] F. Murtagh, P. Legendre, Ward's hierarchical agglomerative clustering method: which algorithms implement Ward's criterion? J. Classif. 31 (2014) 274–295.
[20] M.E. Ritchie, B. Phipson, D. Wu, Y. Hu, C.W. Law, W. Shi, G.K. Smyth, limma powers differential expression analyses for RNA-sequencing and microarray studies, Nucleic Acids Res., 43 (2015) e47.
[21] Y. Benjamini, Y. Hochberg, Controlling the false discovery rate: a practical and powerful approach to multiple testing, J. Royal Stat. Soc. Series B 57 (1995) 289–300.
[22] M.M. Jablonski, N.E. Freeman, W.E. Orr, J.P. Templeton, L. Lu, R.W. Williams, E.E. Geisert, Genetic pathways regulating glutamate levels in retinal Muller cells, Neurochem. Res. 36 (2011) 594–603.
[23] Y. Xue, S.Q. Shen, J. Jui, A.C. Rupp, L.C. Byrne, S. Hattar, J.G. Flannery, J.C. Corbo, V.J. Kefalov, CRALBP supports the mammalian retinal visual cycle and cone vision, J. Clin. Invest. 125 (2015) 727–738.
[24] A.G. Junemann, R. Rejdak, C. Huchzermeyer, R. Maciejewski, P. Grieb, F.E. Kruse, E. Zrenner, K. Rejdak, A. Petzold, Elevated vitreous body glial fibrillary acidic protein in retinal diseases, Graefes Arch. Clin. Exp. Ophthalmol. 253 (2015) 2181–2186.
[25] S.C. Bu, R. Kuijer, R.J. van der Worp, G. Postma, V.W. Renardel de Lavalette, X.R. Li, J.M. Hooymans, L.I. Los, Immunohistochemical evaluation of idiopathic epiretinal membranes and in vitro studies on the effect of TGF-beta on Muller cells, Invest. Ophthalmol. Vis. Sci. 56 (2015) 6506–6514.
[26] A.M. Abu El-Asrar, M.I. Nawaz, G. De Hertogh, K. Alam, M.M. Siddiquei, K. Van den Eynde, A. Mousa, G. Mohammad, K. Geboes, G. Opdenakker, S100A4 is upregulated in proliferative diabetic retinopathy and correlates with markers of angiogenesis and fibrogenesis, Mol. Vis. 20 (2014) 1209–1224.
[27] A. Kanda, K. Noda, I. Hirose, S. Ishida, TGF-beta-SNAIL axis induces Muller glial-mesenchymal transition in the pathogenesis of idiopathic epiretinal membrane, Sci. Rep. 9 (2019) 673.
[28] Y. Kobayashi, S. Yoshida, T. Nakama, Y. Zhou, K. Ishikawa, R. Arita, S. Nakao, M. Miyazaki, Y. Sassa, Y. Oshima, K. Izuhara, T. Kono, T. Ishibashi, Overexpression of CD163 in vitreous and fibrovascular membranes of patients with proliferative diabetic retinopathy: possible involvement of periostin, Br. J. Ophthalmol. 99 (2015) 451–456.
[29] S. Kase, W. Saito, M. Yokoi, K. Yoshida, N. Furudate, M. Muramatsu, A. Saito, M. Kase, S. Ohno, Expression of glutamine synthetase and cell proliferation in human idiopathic epiretinal membrane, Br. J. Ophthalmol. 90 (2006) 96–98.
[30] D.J. Peet, T. Kittipassorn, J.P. Wood, G. Chidlow, R.J. Casson, HIF signalling: the eyes have it, Exp. Cell Res. 356 (2017) 136–140.
[31] A.M. Abu El-Asrar, L. Missotten, K. Geboes, Expression of hypoxia-inducible factor-1alpha and the protein products of its target genes in diabetic fibrovascular epiretinal membranes, Br. J. Ophthalmol. 91 (2007) 822–826.
[32] S.C. Bu, R. Kuijer, R.J. van der Worp, E.A. Huiskamp, V.W. Renardel de Lavalette, X.R. Li, J.M. Hooymans, L.I. Los, Glial cells and collagens in epiretinal membranes associated with idiopathic macular holes, Retina 34 (2014) 897–906.
[33] M. Kritzenberger, B. Junglas, C. Framme, H. Helbig, V.P. Gabel, R. Fuchshofer, E.R. Tamm, J. Hillenkamp, Different collagen types define two types of idiopathic epiretinal membranes, Histopathology 58 (2011) 953–965.
[34] C.J. Guerin, L. Hu, G. Scicli, A.G. Scicli, Transforming growth factor beta in experimentally detached retina and periretinal membranes, Exp. Eye Res. 73 (2001) 753–764.
[35] C. Guidry, K.M. Bradley, J.L. King, Tractional force generation by human muller cells: growth factor responsiveness and integrin receptor involvement, Invest. Ophthalmol. Vis. Sci. 44 (2003) 1355–1363.
[36] S. Lamouille, J. Xu, R. Derynck, Molecular mechanisms of epithelial-mesenchymal transition, Nat. Rev. Mol. Cell. Biol. 15 (2014) 178–196.
[37] S. Zandi, C. Tappeiner, I.B. Pfister, A. Despont, R. Rieben, J.G. Garweg, Vitreal cytokine profile differences between eyes with epiretinal membranes or macular holes, Invest. Ophthalmol. Vis. Sci. 57 (2016) 6320–6326.
[38] Y.S. Chen, S.F. Hackett, C.L. Schoenfeld, M.A. Vinores, S.A. Vinores, P.A. Campochiaro, Localisation of vascular endothelial growth factor and its receptors to cells of vascular and avascular epiretinal membranes, Br. J. Ophthalmol. 81 (1997) 919–926.
[39] D. Armstrong, A.J. Augustin, R. Spengler, A. Al-Jada, T. Nickola, F. Grus, F. Koch, Detection of vascular endothelial growth factor and tumor necrosis factor alpha in epiretinal membranes of proliferative diabetic retinopathy, proliferative vitreoretinopathy and macular pucker, Ophthalmologica 212 (1998) 410–414.
[40] A.A. Tirpe, D. Gulei, S.M. Ciortea, C. Crivii, I. Berindan-Neagoe, Hypoxia: overview on hypoxia-mediated mechanisms with a focus on the role of HIF genes, Int. J. Mol.

Sci. 20 (2019) 6140.
[41] A. Hueber, P. Wiedemann, P. Esser, K. Heimann, Basic fibroblast growth factor mRNA, bFGF peptide and FGF receptor in epiretinal membranes of intraocular proliferative disorders (PVR and PDR), Int. Ophthalmol. 20 (1996) 345–350.
[42] X. Liang, C. Li, Y. Li, J. Huang, S. Tang, R. Gao, S. Li, Platelet-derived growth factor and basic fibroblast growth factor immunolocalized in proliferative retinal diseases, Chin. Med. J. 113 (2000) 144–147.
[43] S. Yoshida, A. Yoshida, T. Ishibashi, Induction of IL-8, MCP-1, and bFGF by TNF-alpha in retinal glial cells: implications for retinal neovascularization during post-ischemic inflammation, Graefes Arch. Clin. Exp. Ophthalmol. 242 (2004) 409–413.
[44] T. Cheng, W. Cao, R. Wen, R.H. Steinberg, M.M. LaVail, Prostaglandin E2 induces vascular endothelial growth factor and basic fibroblast growth factor mRNA expression in cultured rat Muller cells, Invest. Ophthalmol. Vis. Sci. 39 (1998) 581–591.
[45] M. Hollborn, K. Jahn, G.A. Limb, L. Kohen, P. Wiedemann, A. Bringmann, Characterization of the basic fibroblast growth factor-evoked proliferation of the human Muller cell line, MIO-M1, Graefes Arch. Clin. Exp. Ophthalmol. 242 (2004) 414–422.
[46] H. Kimura, C. Spee, T. Sakamoto, D.R. Hinton, Y. Ogura, Y. Tabata, Y. Ikada, S.J. Ryan, Cellular response in subretinal neovascularization induced by bFGF-impregnated microspheres, Invest. Ophthalmol. Vis. Sci. 40 (1999) 524–528.
[47] S.G. Robbins, R.N. Mixon, D.J. Wilson, C.E. Hart, J.E. Robertson, I. Westra, S.R. Planck, J.T. Rosenbaum, Platelet-derived growth factor ligands and receptors immunolocalized in proliferative retinal diseases, Invest. Ophthalmol. Vis. Sci. 35 (1994) 3649–3663.
[48] A. Bringmann, P. Wiedemann, Involvement of Muller glial cells in epiretinal membrane formation, Graefes Arch. Clin. Exp. Ophthalmol. 247 (2009) 865–883.
[49] Z. Liu, Y. Cao, G. Liu, S. Yin, J. Ma, J. Liu, M. Zhang, Y. Wang, p75 neurotrophin receptor regulates NGF-induced myofibroblast differentiation and collagen synthesis through MRTF-A, Exp. Cell Res. 383 (2019) 111504.
[50] E. Palazzo, A. Marconi, F. Truzzi, K. Dallaglio, T. Petrachi, P. Humbert, S. Schnebert, E. Perrier, M. Dumas, C. Pincelli, Role of neurotrophins on dermal fibroblast survival and differentiation, J. Cell. Physiol. 227 (2012) 1017–1025.
[51] S. Minchiotti, B. Stampachiacchiere, A. Micera, A. Lambiase, G. Ripandelli, B. Billi, S. Bonini, Human idiopathic epiretinal membranes express NGF and NGF receptors, Retina 28 (2008) 628–637.
[52] L. Iannetti, M. Accorinti, R. Malagola, F. Bozzoni-Pantaleoni, S. Da Dalt, F. Nicoletti, R. Gradini, A. Traficante, M. Campanella, P. Pivetti-Pezzi, Role of the intravitreal growth factors in the pathogenesis of idiopathic epiretinal membrane, Invest. Ophthalmol. Vis. Sci. 52 (2011) 5786–5789.
[53] C. Guidry, R. Feist, R. Morris, C.W. Hardwick, Changes in IGF activities in human diabetic vitreous, Diabetes 53 (2004) 2428–2435.
[54] D. Romaniuk, M.W. Kimsa, B. Strzalka-Mrozik, M.C. Kimsa, A. Kabiesz, W. Romaniuk, U. Mazurek, Gene expression of IGF1, IGF1R, and IGFBP3 in epiretinal membranes of patients with proliferative diabetic retinopathy: preliminary study, Mediat. Inflamm. 2013 (2013) 986217.
[55] R.G. Schumann, K.H. Eibl, F. Zhao, M. Scheerbaum, R. Scheler, M.M. Schaumberger, H. Wehnes, A.K. Walch, C. Haritoglou, A. Kampik, A. Gandorfer, Immunocytochemical and ultrastructural evidence of glial cells and hyalocytes in internal limiting membrane specimens of idiopathic macular holes, Invest. Ophthalmol. Vis. Sci. 52 (2011) 7822–7834.
[56] S. Tamiya, H.J. Kaplan, Role of epithelial-mesenchymal transition in proliferative vitreoretinopathy, Exp. Eye Res. 142 (2016) 26–31.
[57] M. Fahnestock, G. Yu, M.D. Coughlin, ProNGF: a neurotrophic or an apoptotic molecule? Prog. Brain Res. 146 (2004) 101–110.
[58] M.A. Travis, D. Sheppard, TGF-beta activation and function in immunity, Annu. Rev. Immunol. 32 (2014) 51–82.
[59] C. Christakopoulos, L.J. Cehofski, S.R. Christensen, H. Vorum, B. Honore, Proteomics reveals a set of highly enriched proteins in epiretinal membrane compared with inner limiting membrane, Exp. Eye Res. 186 (2019) 107722.
[60] Y. Itoh, M. Inoue, T. Rii, T. Hiraoka, A. Hirakata, Significant correlation between visual acuity and recovery of foveal cone microstructures after macular hole surgery, Am J. Ophthalmol. 153 (2012) 111–119.
[61] T. Wakabayashi, M. Fujiwara, H. Sakaguchi, S. Kusaka, Y. Oshima, Foveal microstructure and visual acuity in surgically closed macular holes: spectral-domain optical coherence tomographic analysis, Ophthalmology 117 (2010) 1815–1824.
[62] M. Shimozono, A. Oishi, M. Hata, T. Matsuki, S. Ito, K. Ishida, Y. Kurimoto, The significance of cone outer segment tips as a prognostic factor in epiretinal membrane surgery, Am J. Ophthalmol. 153 (2012) 698–704.
[63] W.J. Mayer, M. Vogel, A. Neubauer, M. Kernt, A. Kampik, A. Wolf, C. Haritoglou, Pars plana vitrectomy and internal limiting membrane peeling in epimacular membranes: correlation of function and morphology across the macula, Ophthalmologica 230 (2013) 9–17.

Supplementary Table 1. Primers used for RT-qPCR analysis

Gene	Forward	Reverse
GLUL	5′-ATGCGGGAGGAGAATGGT-3′	5′-CGTTGATGTTGGAGGTTTCA-3′
RLBP1	5′-GCTGCTGGAGAATGAGGAAA-3′	5′-TGGTGGATGAAGTGGATGG-3′
GFAP	5′-ATCAACTCACCGCCAACAG-3′	5′-CCAGCGACTCAATCTTCCTC-3′
ACTA2	5′-AATGGCTCTGGGCTCTGTAA-3′	5′-TTTTGCTCTGTGCTTCGTCA-3′
TAGLN	5′-AGCAGGTGGCTCAGTTCCT-3′	5′-CGGTAGTGCCCATCATTCTT-3′
S100A4/FSP1	5′-CCTGGATGTGATGGTGTCC-3′	5′-TCGTTGTCCCTGTTGCTGT-3′
PTPRC	5′-CTCTTGGCATTTGGCTTTG-3′	5′-GGGAAGGTGTTGGGCTTT-3′
CD163	5′-CACTGGTTCTGCTCATTTTGG-3′	5′-TCTGCTGGCTTCACTGGTC-3′
CCND1	5′-ATCGTCGCCACCTGGAT-3′	5′-GACCTCCTCCTCGCACTTC-3′
SNAI1	5′-AATCGGAAGCCTAACTACAGCG-3′	5′-GTCCCAGATGAGCATTGGCA-3′
HIF1A	5′-AAGAACAAAACACACAGCGAAG-3′	5′-AAATCAGCACCAAGCAGGTC-3′
COL1A1	5′-AAGAGGAAGGCCAAGTCGAG-3′	5′-AGATCACGTCATCGCACAAC-3′
COL6A1	5′-CGGAGACGATAACAACGACA-3′	5′-CACAGCAAGAGCACATTTTCA-3′
TGFB1	5′-GCAACAATTCCTGGCGATAC-3′	5′-GTAGTGAACCCGTTGATGTCC-3′
TGFB2	5′-GACCCCACATCTCCTGCTAA-3′	5′-GGGTTCGTGTATCCATTTCC-3′
VEGFA	5′-AGTGTGTGCCCACTGAGGA-3′	5′-GGTGAGGTTTGATCCGCATA-3′
FGF2	5′-TGTGTCTATCAAAGGAGTGTG-3′	5′-CCGTAACACATTTAGAAGCCA-3′
PDGFB	5′-CCTCATAGACCGCACCAAC-3′	5′-GGCTTCTTCCGCACAATCT-3′
NGF	5′-GAGGTGCATAGCGTAATGTCC-3′	5′-CAGTGTCAAGGGAATGCTGA-3′
IGF1	5′-ATCGTGGATGAGTGCTGCTT-3′	5′-TCCCTCTACTTGCGTTCTTCA-3′
GAPDH	5′-GAAGGTCGGAGTCAACGGATT-3′	5′-TGACGGTGCCATGGAATTTG-3′

Supplementary Table 2. Correlation between gene expression levels in iERMs.

	GLUL	*RLBP1*	*GFAP*	*ACTA2*	*SM22*	*S100A4*	*PTPRC*	*CD163*	*CCND1*	*SNAI1*	*HIF1A*	*COL1A1*	*COL6A1*	*TGFB1*	*TGFB2*	*VEGFA*	*FGF2*	*PDGFB*	*NGF*	*IGF1*
GLUL	-	(+) 0.14 *	(+) 0.63 **	(-) 0.05 NS	(-) 0.00 NS	(-) 0.00 NS	(+) 0.01 NS	(+) 0.10 NS	(+) 0.01 NS	(+) 0.02 NS	(+) 0.32 **	(-) 0.04 NS	(+) 0.00 NS	(+) 0.03 NS	(+) 0.02 NS	(+) 0.01 NS	(+) 0.01 NS	(+) 0.03 NS	(-) 0.01 NS	(-) 0.01 NS
RLBP1	(+) 0.14 *	-	(+) 0.22 **	(-) 0.02 NS	(-) 0.03 NS	(+) 0.00 NS	(-) 0.01 NS	(+) 0.00 NS	(-) 0.04 NS	(-) 0.04 NS	(+) 0.05 NS	(-) 0.03 NS	(-) 0.00 NS	(+) 0.01 NS	(-) 0.01 NS	(+) 0.01 NS	(+) 0.01 NS	(+) 0.03 NS	(-) 0.01 NS	(-) 0.01 NS
GFAP	(+) 0.63 **	(+) 0.22 **	-	(-) 0.06 NS	(-) 0.01 NS	(+) 0.00 NS	(+) 0.00 NS	(+) 0.03 NS	(+) 0.03 NS	(+) 0.04 NS	(+) 0.23 **	(-) 0.01 NS	(+) 0.02 NS	(+) 0.01 NS	(+) 0.01 NS	(+) 0.01 NS	(+) 0.01 NS	(+) 0.03 NS	(-) 0.00 NS	(-) 0.01 NS
ACTA2	(-) 0.05 NS	(-) 0.02 NS	(-) 0.06 NS	-	(+) 0.55 **	(+) 0.08 *	(+) 0.04 NS	(+) 0.11 *	(+) 0.03 NS	(+) 0.04 NS	(+) 0.01 NS	(+) 0.34 **	(+) 0.03 NS	(+) 0.07 *	(+) 0.03 NS	(+) 0.01 NS	(+) 0.01 NS	(+) 0.03 NS	(+) 0.12 *	(+) 0.09 *
SM22	(-) 0.00 NS	(-) 0.03 NS	(-) 0.01 NS	(+) 0.55 **	-	(+) 0.31 **	(+) 0.28 **	(+) 0.21 **	(+) 0.15 **	(+) 0.08 *	(+) 0.12 *	(+) 0.20 **	(+) 0.03 NS	(+) 0.17 **	(+) 0.20 **	(-) 0.02 NS	(+) 0.06 NS	(+) 0.05 NS	(+) 0.15 **	(+) 0.19 **
S100A4	(-) 0.00 NS	(+) 0.00 NS	(+) 0.00 NS	(+) 0.08 *	(+) 0.31 **	-	(+) 0.61 **	(+) 0.07 NS	(+) 0.01 NS	(+) 0.01 NS	(+) 0.04 NS	(+) 0.05 NS	(+) 0.01 NS	(+) 0.05 NS	(+) 0.06 NS	(-) 0.09 *	(+) 0.01 NS	(+) 0.01 NS	(+) 0.00 NS	(+) 0.09 *
PTPRC	(+) 0.01 NS	(-) 0.01 NS	(+) 0.00 NS	(+) 0.04 NS	(+) 0.28 **	(+) 0.61 **	-	(+) 0.19 **	(+) 0.02 NS	(+) 0.00 NS	(+) 0.16 **	(+) 0.01 NS	(+) 0.02 NS	(+) 0.12 **	(+) 0.09 *	(-) 0.10 *	(+) 0.08 *	(+) 0.00 NS	(+) 0.02 NS	(+) 0.06 NS
CD163	(+) 0.10 NS	(+) 0.00 NS	(+) 0.03 NS	(+) 0.11 *	(+) 0.21 **	(+) 0.07 NS	(+) 0.19 **	-	(+) 0.03 NS	(+) 0.07 NS	(+) 0.26 **	(+) 0.04 NS	(+) 0.05 NS	(+) 0.14 **	(+) 0.01 NS	(+) 0.00 NS	(+) 0.12 *	(+) 0.09 *	(+) 0.06 NS	(+) 0.15 **
CCND1	(+) 0.01 NS	(-) 0.04 NS	(+) 0.03 NS	(+) 0.03 NS	(+) 0.15 **	(+) 0.01 NS	(+) 0.02 NS	(+) 0.03 NS	-	(+) 0.24 **	(+) 0.15 **	(+) 0.11 *	(+) 0.10 *	(+) 0.17 **	(+) 0.18 **	(+) 0.26 **	(+) 0.24 **	(+) 0.13 **	(+) 0.15 **	(+) 0.07 *
SNAI1	(+) 0.02 NS	(-) 0.04 NS	(-) 0.04 NS	(-) 0.04 NS	(+) 0.08 *	(+) 0.01 NS	(+) 0.00 NS	(+) 0.07 NS	(+) 0.24 **	-	(+) 0.12 *	(+) 0.10 *	(+) 0.02 NS	(+) 0.05 NS	(+) 0.02 NS	(+) 0.04 NS	(+) 0.12 *	(+) 0.32 **	(+) 0.15 **	(+) 0.30 **
HIF1A	(+) 0.32 **	(+) 0.05 NS	(+) 0.23 **	(+) 0.01 NS	(+) 0.12 *	(+) 0.04 NS	(+) 0.16 **	(+) 0.26 **	(+) 0.15 **	(+) 0.12 *	-	(+) 0.01 NS	(+) 0.14 **	(+) 0.33 **	(+) 0.17 **	(+) 0.04 NS	(+) 0.48 **	(+) 0.24 **	(+) 0.07 NS	(+) 0.11 *
COL1A1	(-) 0.04 NS	(-) 0.03 NS	(-) 0.01 NS	(+) 0.34 **	(+) 0.20 **	(+) 0.05 NS	(+) 0.01 NS	(+) 0.04 NS	(+) 0.11 *	(+) 0.10 *	(+) 0.01 NS	-	(+) 0.18 **	(+) 0.13 **	(+) 0.05 NS	(+) 0.00 NS	(+) 0.06 NS	(+) 0.11 *	(+) 0.25 **	(+) 0.27 **
COL6A1	(+) 0.00 NS	(-) 0.00 NS	(+) 0.02 NS	(+) 0.03 NS	(+) 0.03 NS	(+) 0.01 NS	(+) 0.02 NS	(+) 0.05 NS	(+) 0.10 *	(+) 0.02 NS	(+) 0.14 **	(+) 0.18 **	-	(+) 0.11 *	(+) 0.03 NS	(+) 0.02 NS	(+) 0.31 **	(+) 0.07 *	(+) 0.12 **	(+) 0.03 NS
TGFB1	(+) 0.03 NS	(+) 0.01 NS	(+) 0.01 NS	(+) 0.07 *	(+) 0.17 **	(+) 0.05 NS	(+) 0.12 **	(+) 0.14 **	(+) 0.17 **	(+) 0.05 NS	(+) 0.33 **	(+) 0.13 **	(+) 0.11 *	-	(+) 0.21 **	(+) 0.01 NS	(+) 0.10 **	(+) 0.17 **	(+) 0.35 **	(+) 0.17 **
TGFB2	(+) 0.02 NS	(-) 0.01 NS	(+) 0.01 NS	(+) 0.03 NS	(+) 0.20 **	(+) 0.06 NS	(+) 0.09 *	(+) 0.01 NS	(+) 0.18 **	(+) 0.02 NS	(+) 0.17 **	(+) 0.05 NS	(+) 0.03 NS	(+) 0.21 **	-	(+) 0.03 NS	(+) 0.09 *	(+) 0.04 NS	(+) 0.03 NS	(+) 0.04 NS
VEGFA	(+) 0.15 **	(-) 0.00 NS	(+) 0.11 *	(-) 0.01 NS	(-) 0.02 NS	(-) 0.09 *	(-) 0.10 *	(+) 0.00 NS	(+) 0.26 **	(+) 0.04 NS	(+) 0.04 NS	(+) 0.00 NS	(+) 0.02 NS	(+) 0.01 NS	(+) 0.03 NS	-	(+) 0.08 *	(+) 0.06 NS	(+) 0.00 NS	(+) 0.00 NS
FGF2	(+) 0.18 **	(+) 0.01 NS	(+) 0.23 **	(+) 0.03 NS	(+) 0.06 NS	(+) 0.01 NS	(+) 0.08 *	(+) 0.12 *	(+) 0.24 **	(+) 0.12 *	(+) 0.48 **	(+) 0.06 NS	(+) 0.31 **	(+) 0.10 **	(+) 0.09 *	(+) 0.08 *	-	(+) 0.18 **	(+) 0.13 **	(+) 0.04 NS
PDGFB	(+) 0.03 NS	(+) 0.00 NS	(+) 0.05 NS	(+) 0.02 NS	(+) 0.05 NS	(+) 0.01 NS	(+) 0.00 NS	(+) 0.09 *	(+) 0.13 **	(+) 0.32 **	(+) 0.24 **	(+) 0.11 *	(+) 0.07 *	(+) 0.17 **	(+) 0.04 NS	(+) 0.06 NS	(+) 0.18 **	-	(+) 0.09 *	(+) 0.62 **
NGF	(-) 0.01 NS	(-) 0.01 NS	(-) 0.00 NS	(+) 0.12 *	(+) 0.15 **	(+) 0.00 NS	(+) 0.02 NS	(+) 0.06 NS	(+) 0.15 **	(+) 0.15 **	(+) 0.07 NS	(+) 0.25 **	(+) 0.12 **	(+) 0.35 **	(+) 0.03 NS	(+) 0.00 NS	(+) 0.13 **	(+) 0.09 *	-	(+) 0.18 **
IGF1	(-) 0.01 NS	(-) 0.01 NS	(-) 0.01 NS	(+) 0.09 *	(+) 0.19 **	(+) 0.09 *	(+) 0.06 NS	(+) 0.15 **	(+) 0.07 *	+) 0.30 **	(+) 0.11 *	(+) 0.27 **	(+) 0.03 NS	(+) 0.17 **	(+) 0.04 NS	(+) 0.00 NS	(+) 0.04 NS	(+) 0.62 **	(+) 0.18 **	-

A linear regression analysis was performed between the indicated couples of genes. Positive (+) or negative (-) correlation. R^2 and P values were calculated for each couple of genes. NS, not significant; *, P < 0.05; **, P < 0.01.

VITREOUS FROM IDIOPATHIC EPIRETINAL MEMBRANE PATIENTS INDUCES GLIAL-TO-MESENCHYMAL TRANSITION IN MÜLLER CELLS

Macroglial Müller cells appear to play a pivotal role in the pathogenesis of iERM, where they may undergo a glial-to-mesenchymal transition (GMT), a transdifferentiation process characterized by the downregulation of Müller cell markers, paralleled by the upregulation pro-fibrotic myofibroblast markers. Previous results mentioned above allowed us to identify the molecular identification of two major clusters of iERM patients (named iERM-A and iERM-B). IERM-A patients are characterized by less severe clinical features and a more "quiescent" iERM gene expression profile when compared to iERM-B patients. In the present work, Müller MIO-M1 cells were exposed to vitreous samples obtained before membrane peeling from the same cohort of iERM-A and iERM-B patients. The results demonstrate that iERM vitreous induces proliferation, migration, and GMT in MIO-M1 cells. In addition, the different capacity of individual iERM vitreous samples to affect the expression of Müller cell/glial and myofibroblast markers in MIO-M1 cells indicates that a relationship may exist among the ability of iERM vitreous to modulate GMT in Müller cells, the molecular profile of the corresponding iERMs, and the clinical features of iERM patients

BBA - Molecular Basis of Disease 1867 (2021) 166181

Contents lists available at ScienceDirect

BBA - Molecular Basis of Disease

journal homepage: www.elsevier.com/locate/bbadis

Vitreous from idiopathic epiretinal membrane patients induces glial-to-mesenchymal transition in Müller cells

Adwaid Manu Krishna Chandran [a], Daniela Coltrini [a], Mirella Belleri [a], Sara Rezzola [a], Elena Gambicorti [b], Davide Romano [b], Francesco Morescalchi [b], Stefano Calza [a], Francesco Semeraro [b,*], Marco Presta [a,c,**]

[a] Department of Molecular and Translational Medicine, University of Brescia, Viale Europa 11, 25123 Brescia, Italy
[b] Eye Clinic, Department of Neurological and Vision Sciences, University of Brescia, Piazzale Spedali Civili 1, 25123 Brescia, Italy
[c] Italian Consortium for Biotechnology (CIB), Unit of Brescia, Brescia, Italy

ARTICLE INFO

Keywords:
Epiretinal membrane
Gene expression
Retina
Eye disease
Müller cells
Vitreous

ABSTRACT

Idiopathic epiretinal membranes (ERMs) are fibrocellular membranes containing extracellular matrix proteins and epiretinal cells of retinal and extraretinal origin. iERMs lead to decreased visual acuity and their pathogenesis has not been completely defined. Macroglial Müller cells appear to play a pivotal role in the pathogenesis of iERM where they may undergo glial-to-mesenchymal transition (GMT), a transdifferentiation process characterized by the downregulation of Müller cell markers, paralleled by the upregulation of pro-fibrotic myofibroblast markers. Previous observations from our laboratory allowed the molecular identification of two major clusters of iERM patients (named iERM-A and iERM-B), iERM-A patients being characterized by less severe clinical features and a more "quiescent" iERM gene expression profile when compared to iERM-B patients. In the present work, Müller MIO-M1 cells were exposed to vitreous samples obtained before membrane peeling from the same cohort of iERM-A and iERM-B patients. The results demonstrate that iERM vitreous induces proliferation, migration, and GMT in MIO-M1 cells, a phenotype consistent with Müller cell behavior during iERM progression. However, even though the vitreous samples obtained from iERM-A patients were able to induce a complete GMT in MIO-M1 cells, iERM-B samples caused only a partial GMT, characterized by the downregulation of Müller cell markers in the absence of upregulation of pro-fibrotic myofibroblast markers. Together, the results indicate that a relationship may exist among the ability of iERM vitreous to modulate GMT in Müller cells, the molecular profile of the corresponding iERMs, and the clinical features of iERM patients.

1. Introduction

Epiretinal membranes (ERMs) are characterized by the growth of fibrocellular tissue on the inner limiting membrane of the retina [1,2]. ERMs are defined as idiopathic ERMs (iERMs) when they are not associated with any other ocular disease [3]. iERM prevalence is approximately 6% in patients aged over 60 years and increases with aging [4,5]. Decreased visual acuity with or without metamorphopsia is the main indication for ERM surgery, although successful ERM removal may provide only limited efficacy in a significant percentage of patients [6,7].

Even though spectral domain optical coherence tomography (SD-OCT) studies have provided a morphologic description of the alterations that occur in the iERM retina, the pathogenesis of the disease has not been fully elucidated. Morphological and immunohistochemical analyses have demonstrated the presence of retinal pigment epithelial cells,

Abbreviations: αSMA, α-smooth muscle actin; BCVA, best-corrected visual acuity; CRALBP, cellular retinaldehyde binding protein; EMT, epithelial-to mesenchymal transition; FGF2, fibroblast growth factor 2; GFAP, glial fibrillary acid-protein; GMT, glial-to-mesenchymal transition; iERM, idiopathic epiretinal membrane; IS/OS, inner segment/outer segment; KIR4.1, Inward Rectifier K^+ Channel 10; RRD, rhegmatogenous retinal detachment; SD-OCT, spectral domain optical coherence tomography; TGFβ, transforming growth factor β; TNFα, tumor necrosis factor α; VEGF, vascular endothelial growth factor..

** Correspondence to: F. Semeraro, Eye Clinic, Department of Neurological and Vision Sciences, University of Brescia, Piazzale Spedali Civili 1, 25123 Brescia, Italy.

** Correspondence to: M. Presta, Department of Molecular and Translational Medicine, University of Brescia, Viale Europa 11, 25123 Brescia, Italy.
E-mail addresses: francesco.semeraro@unibs.it (F. Semeraro), marco.presta@unibs.it (M. Presta).

https://doi.org/10.1016/j.bbadis.2021.166181
Received 9 March 2021; Received in revised form 10 May 2021; Accepted 24 May 2021
Available online 1 June 2021

hyalocytes, fibroblasts, myofibroblasts, and glial cells in iERMs [8–10]. Cell proliferation, epithelial-to mesenchymal transition (EMT) and deposition of extracellular matrix proteins characterize iERM formation, a process driven by cytokines and growth factors that may accumulate in the humor vitreous [3,10–12].

Retinal glia is constituted by astrocytes, macroglial Müller cells and resident microglia. Among them, Müller cells provide structural support to the neuroretina. They represent the anatomical link between blood vessels and vitreous body, creating a micro-unit involved in retinal homeostasis. In addition, Müller cells reallocate the metabolic waste of neuronal cells into the blood stream and vitreous. Finally, Müller cells are involved in microglial cell activation and in the regulation of vasodilation/vasoconstriction processes [13,14].

Müller cells appear to play a pivotal role in the pathogenesis of iERM [15], where various cytokines and growth factors may act as autocrine and paracrine modulators by triggering Müller cell proliferation, migration, collagen contraction, and transdifferentiation [16–22]. In particular, transforming growth factor beta (TGFβ) has been shown to induce glial-to-mesenchymal transition (GMT) in Müller cells, a transdifferentiation process characterized by the downregulation of Müller cell glial markers, paralleled by the upregulation of pro-fibrotic myofibroblast markers [23–25].

Vitreous humor, obtained by *pars plana* vitrectomy, may represent a reservoir of pathological mediators that accumulate during the progression of retinal diseases [26,27]. For instance, recent studies have shown that the vitreous from patients with proliferative diabetic retinopathy can be used as a tool to investigate the molecular events triggered by vitreal mediators in endothelial cells and to evaluate the anti-angiogenic/anti-inflammatory activity of established therapeutics or novel drug candidates (reviewed in [26]). In addition, vitreous from diabetic retinopathy patients has been demonstrated to trigger Müller cell activation in a vascular endothelial growth factor (VEGF)-independent manner [28]. However, few data are available about the effect exerted on these cells by iERM vitreous, mainly focusing on its capacity to stimulate tractional force generation [29,30].

Recently, a retrospective study from our laboratory has shown that surgically removed iERMs are characterized by a different pattern of expression of a series of cell population, extracellular matrix, and cytokine/growth factor biomarkers relevant to the pathogenesis of the disease. Hierarchical clustering of the gene expression data identified two molecular clusters of iERM membranes associated with distinct clinical and SD-OCT features [31]. In the present work, Müller MIO-M1 cells were exposed to vitreous samples obtained before membrane peeling from the same cohort of iERM patients. The results demonstrate that iERM vitreous induces proliferation, migration, and GMT in MIO-M1 cells. In addition, the different capacity of individual iERM vitreous samples to affect the expression of Müller cell/glial and myofibroblast markers in MIO-M1 cells indicates that a relationship may exist among the ability of iERM vitreous to modulate GMT in Müller cells, the molecular profile of the corresponding iERMs, and the clinical features of iERM patients.

2. Materials and methods

2.1. Human vitreous fluid samples

Vitreous fluid was collected from 28 iERM patients that underwent *pars plana* vitrectomy followed by membrane peeling at the Clinics of Ophthalmology (University of Brescia) [gender (m/f): 12/16; age: 72.9 ± 9.3; phakic (%)/pseudofakic (%) = 74%/26%; preoperative decimal best-corrected visual acuity (BCVA) at Snellen chart: 0.35 ± 0.14; average pre-operative central foveal thickness (mm): 0.47 ± 0.15]. The iERM patients included in this retrospective study were part of a previously investigated cohort of patients that underwent a molecular characterization of their iERMs [31]. Hierarchical clustering of the gene expression data allowed the molecular identification of two major clusters of iERM specimens (from here on named iERM-A and iERM-B), iERM-B samples representing transcriptionally "activated" iERMs when compared to transcriptionally "quiescent" iERM-A specimens. In addition, patients belonging to the iERM-B cluster were characterized by more severe clinical and SD-OCT features when compared to the iERM-A cluster (see Table 1 and [31]).

A pool of iERM vitreous was created by collecting 100 μl of fluid from each of the 28 harvested samples. Then, the final 2.8 ml pool was aliquoted. Aliquots and the residual fluid from each individual vitreous sample were stored at −80 °C until use. Heat-inactivated vitreous was prepared by incubating an aliquot of the vitreous pool for 20 min at 95 °C. A pool of vitreous samples obtained from patients affected by rhegmatogenous retinal detachment (RRD) was used as control. Indeed, recent observations have shown that RRD vitreous has a proteome profile distinct to that observed in other retinal diseases, such as pucker, macular hole, and proliferative diabetic retinopathy [32].

SD-OCT scans were performed before, one month and three months after surgery to evaluate iERM staging, central macular thickness, and the visibility of the inner segment/outer segment (IS/OS) junction. The clinical ocular examination, including BCVA test by using the Snellen chart, slit lamp biomicroscopy, and dilated fundoscopy, was conducted only at baseline visit, before surgery. The iERM stage was defined following the criteria used by Hwang et al. [33], while the IS/OS junction was scored as 0 = not visible, 1 = visible, and 2 = clearly visible following the criteria used by Sheales et al. [34]. See Ref. [31] for more details.

2.2. Cell cultures

The human Müller cell line Moorfields/Institute of Ophthalmology-Müller 1 (MIO-M1) was obtained at cell passage 29 from the UCL Institute of Ophthalmology, London, UK [35], and grown in Dulbecco's modified Eagle medium (DMEM) with 4.5 mg/ml glucose *plus* 10% fetal calf serum (FCS) and 1.0 mM glutamine. Cells were maintained in a humidified 5% CO_2 incubator at 37 °C, with medium replaced every 2–3 days until cells reached confluency. Cells were tested regularly for *Mycoplasma* negativity and were used up to cell passage 44 with no significant changes in their capacity to respond to iERM vitreous.

2.3. MIO-M1 proliferation assay

MIO-M1 cells were seeded at 5000 cells/cm^2 in DMEM *plus* 2.0% FCS. After 3 days, cells were treated with increasing amounts of saline or vitreous diluted in culture medium. Cells were counted 24, 48, or 72 h after treatment.

2.4. MIO-M1 wound healing assay

MIO-M1 cells were seeded at 50,000 cells/cm^2 in DMEM *plus* 2.0% FCS. After 3 days, MIO-M1 cell monolayers were scratched with a 200 μl tip to obtain a 2-mm-thick denuded area and cultured in the presence of saline or vitreous diluted with culture medium. After 24 h, wounded monolayers were photographed, and the percentage of repaired area was quantified with Fiji software [36].

2.5. MIO-M1 chemotaxis assay

MIO-M1 cells were seeded at 30,000 cells/cm^2 in DMEM *plus* 2.0% FCS. After 3 days, cells were resuspended in 2.0% FCS (1.0×10^6 cells/ml) and seeded in the upper compartment of a Boyden chamber containing 0.1% gelatin-coated PVP-free polycarbonate filters (5.0 μm pore size). Saline, iERM vitreous or heat-inactivated vitreous diluted in serum free DMEM (1:4, vol:vol) were placed in the lower compartment of the chamber. After 2 h and 4 h of incubation, cells migrated to the lower side of the filter were fixed with methanol and stained with haematoxylin and eosin (H&E). The number of migrated cells was determined by

Table 1
Summary of the molecular, clinical, and biological characterization of iERM patients. The vitreous samples utilized in the present study were obtained from Cluster iERM-A (n = 10) and Cluster iERM-B (n = 18) patients as defined in [31]. The table summarizes the main differences in iERM gene expression data and clinical features of the two clusters of patients [see [31] for more details], as well as the effect exerted by the corresponding vitreous fluid on Müller MIO-M1 cells (present work).

	iERM gene expression					Clinical features			Vitreous-induced MIO-M1 cell transdifferentiation
	Myofibroblast markers	Hyalocyte markers	Glial markers	Fibrogenic markers	Cytokines/ growth factors	Preoperative decimal BCVA	Postoperative IS/ OS improvement	SD-OCT severity	GMT
Cluster iERM-A	Equally expressed	Equally expressed	Down	Down	Down	Better	Better	Better	Complete
Cluster iERM-B			Up	Up	Up	Worse	Worse	Worse	Partial

counting 8 microscopic fields per well for each sample in triplicate.

2.6. Western blot analysis

MIO-M1 cells were seeded at 30,000 cells/cm^2 in DMEM *plus* 2.0% FCS. After 3 days of starvation, cells were treated with iERM, heat-inactivated iERM or RRD vitreous pools diluted 1:4 with culture medium. After 24 and 48 h of incubation, cell extracts (20 μg of protein) were analyzed by Western blotting using monoclonal anti-αSMA (1:1000 dilution, Sigma-Aldrich) or anti-GFAP (1:1000 dilution, Dako) antibodies. Uniform loading of the gel was confirmed with monoclonal anti-vinculin antibody (1:1000 dilution, Sigma-Aldrich).

2.7. Quantitative PCR (qPCR)

MIO-M1 cells were seeded at 30,000 cells/cm^2 in DMEM *plus* 2.0% FCS. After 3 days of starvation, cells were treated with the vitreous pool or individual vitreous samples diluted 1:4 with culture medium. At different time points of stimulation, total RNA was extracted from MIO-M1 cells using the ReliaPrep™ RNA Cell Miniprep System according to manufacturer's instructions (Promega). Total RNA was retrotranscribed with SuperScript™ VILO™ MasterMix (Invitrogen) using random hexaprimers in a final 20 μl volume. Then, qPCR was performed with a ViiA™ 7 Real-Time PCR Detection System (Applied Biosystems) using iQ™ SYBR Green Supermix (Biorad) according to manufacturer's instructions. Expression levels of selected genes were normalized to *GAPDH* expression and were compared to those measured in untreated MIO-M1 cells. Oligonucleotide primers are listed in Suppl. Table 1.

2.8. Statistical analysis

Data are expressed as mean ± SEM. Group differences were tested using Student's *t*-test or one-way ANOVA followed by post-hoc tests with Tukey's HSD correction for multiple comparison.

Hierarchical clustering was performed on gene expression values expressed on $\log_2$ scale. Gene expression levels were then standardized to have comparable dynamic ranges. Clustering was performed on Euclidean distances using Ward's hierarchical agglomerative clustering method [37].

IS/OS scores, considered as an ordinal variable, were compared among molecular clusters and of timing of measurement using Cumulative link mixed models [38] to account for within patient correlation. Similarly, retinal thickness was modelled using Linear Mixed Models, assuming a Gaussian distribution [39]. All analyses were performed using PRISM and R software (version 4.0).

3. Results

3.1. iERM vitreous induces GMT in Müller MIO-M1 cells

Previous observations from our laboratory allowed the molecular identification of two major clusters of iERM patients (named iERM-A and iERM-B), characterized by different clinical features and iERM gene expression profiles [31] (Table 1). Müller cell proliferation, migration, transdifferentiation (GMT) and extracellular matrix deposition are implicated in the pathogenesis of iERM.

To investigate the capacity of iERM vitreous to activate Müller cells, MIO-M1 cells were treated with a pool of vitreous samples obtained before membrane peeling from the same iERM-A (n = 10) and iERM-B (n = 18) patients investigated in our previous study [31]. As shown in Fig. 1A, the iERM vitreous pool stimulates MIO-M1 cell proliferation in a dose- and time-dependent manner. Moreover, iERM vitreous modulates Müller cell motility when assessed in chemotaxis and wound healing assays (Fig. 1B, 1C).

GMT is characterized by the downregulation of the expression of glial Müller cell markers, paralleled by the upregulation of pro-fibrotic myofibroblast markers [23,24]. Accordingly, treatment of MIO-M1 cells with iERM vitreous causes the downregulation of the Müller cell markers *RLBP1*, a gene that encodes for the cellular retinaldehyde binding protein (CRALBP) involved in chromophore recycling [40], and *KCNJ10*, a gene encoding for the ATP-Sensitive Inward Rectifier K^+ Channel 10 (KIR4.1) [41] (Fig. 2A). In addition, iERM vitreous-treated MIO-M1 cells showed decreased levels of the intermediate filament glial fibrillary acid-encoding *GFAP*, a marker of glial cell activation in response to retinal injuries [42]. In parallel, iERM vitreous induced the upregulation of the myofibroblast markers *ACTA2* and *TAGLN*, encoding for the α-smooth muscle actin (αSMA) and SM22/transgelin proteins, as well as of the α1 chain of Type I and Type IV collagen genes *COL1A1* and *COL4A1* (Fig. 2B). The capacity of iERM vitreous to modulate *ACTA2* and *GFAP* expression in MIO-M1 cells was confirmed at the protein level by Western blot analysis of αSMA and GFAP content in the cell extracts (Suppl. Fig. 1).

Previous observations had shown that the transcription factor SNAIL1 plays a pivotal role in EMT and GMT processes [23]. As observed for TGFβ-induced GMT in MIO-M1 cells [23,24], iERM vitreous induced a rapid and transient upregulation of the SNAIL1-encoding gene *SNAI1* along with the downregulation of *TWIST1*, with no significant changes in *SNAI2* expression, two genes that encode for the transcription factors TWIST and SLUG, respectively (Fig. 2C).

In all the assays, negligible activity was exerted by heat-inactivated iERM vitreous, pointing to a proteinaceous nature of the vitreal mediator(s) responsible for the biological activity exerted by iERM vitreous on MIO-M1 cells. In addition, a pool of vitreous samples obtained from patients affected by RRD was unable to induce GMT and a significant chemotactic response in Müller cells, its effect being limited to a modest

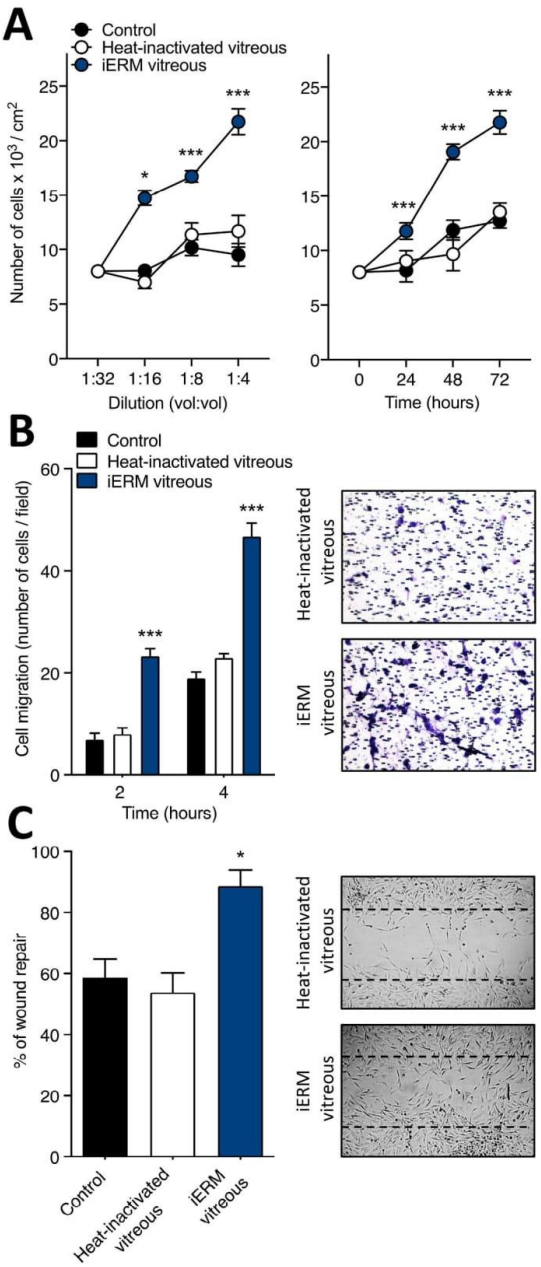

(caption on next column)

Fig. 1. Müller cell activation by iERM vitreous. A) MIO-M1 cells were treated with increasing amounts of iERM or heat-inactivated vitreous samples (vol:vol dilution in cell culture medium) and counted 72 h thereafter (left panel) or were incubated with 1:4 vitreous dilution and counted at different time points (right panel). Data are representative of 2 independent experiments in triplicate that gave similar results and are expressed as mean ± SEM. B) MIO-M1 cells were assessed for their capacity to migrate in response to iERM or heat-inactivated vitreous fluid in a Boyden chamber. After 2 and 4 h, cells migrated to the lower side of the filter were counted. Data are representative of 2 independent experiments in triplicate that gave similar results and are expressed as mean ± SEM. Inset: representative images of cell migration across the PVPF filter in heat-inactivated vitreous-treated cells (upper panel) and iERM vitreous-treated cells (lower panel). C) Wounded MIO-M1 monolayers were treated with iERM or heat-inactivated vitreous samples. After 24 h, MIO-M1 cells invading the wounded area were quantified by computerized analysis of the digitalized images. Data are the mean ± SEM of 8 microscopic fields per experimental point. Inset: representative images of the repaired area in heat-inactivated vitreous-treated cells (upper panel) and iERM vitreous-treated cells (lower panel). $*p < 0.05$ and $***p < 0.01$ *vs* control or heat-inactivated vitreous, one-way ANOVA.

stimulation of MIO-M1 cell proliferation (Suppl. Figs. 1 and 2). Together, these data point to the capacity of iERM vitreous to induce a GMT response in MIO-M1 cells.

3.2. Individual iERM vitreous samples show a different capacity to induce GMT in MIO-M1 cells

To assess whether differences might exist in the capacity of individual vitreous samples to induce GMT in MIO-M1 cells, the same 28 vitreous samples used to generate the vitreous pool tested above were independently assessed for their effect on the expression of the Müller cell/glial markers *RLBP1* and *GFAP* and the myofibroblast markers *ACTA2* and *TAGLN* in MIO-M1 cells, as well as on the expression of the cell proliferation marker *CCDN1* that encodes for the Cyclin D1 protein required for the progression through the G1 phase of the cell cycle [43]. Given the limited volume of vitreous available from each patient, gene expression levels were compared to those measured in untreated MIO-M1 cells rather than in cells treated with an aliquot of the corresponding heat-inactivated sample.

Consistent with the data obtained with the iERM vitreous pool, the results indicate that the 28 individual vitreous samples tested were able to induce an average increase of *ACTA2* and *TAGLN* transcripts and downregulation of *RLBP1* and *GFAP* expression, along with a significant *CCND1* upregulation, an index of the mitogenic activity exerted by iERM vitreous in MIO-M1 cells. However, a high individual variability was observed in the response elicited by these samples on MIO-M1 cells. Indeed, even though all iERM vitreous samples were able to cause the downregulation of the Müller cell/glial markers *RLBP1* and *GFAP*, some of them exerted no effect on the expression of *ACTA2*, *TAGLN* and *CCND1* or even triggered their downregulation, rather than inducing their upregulation (Fig. 3A).

Because of such high variability, we wondered whether the expression of the various GMT-related genes was modulated in a coordinated or in an independent manner by each individual vitreous sample. To this purpose, a linear regression analysis was performed to correlate the expression levels of each gene with those observed for the other four genes tested in MIO-M1 cells treated with each single iERM vitreous sample (Fig. 3B). The results indicate that a significant correlation exists between the expression levels of the fibroblast/myofibroblast markers *ACTA2* and *TAGLN* that, in turn, are inversely correlated with the expression of the proliferation marker *CCDN1*. In addition, even though downregulated by all the samples, *RLBP1* transcription levels appeared to correlate with *ACTA2* and *TAGLN* expression and to be inversely related to *CCDN1* expression (Fig. 3C). Together, these data indicate that individual iERM samples have a different capacity to induce a GMT-related phenotype in MIO-M1 cells and that those samples able to

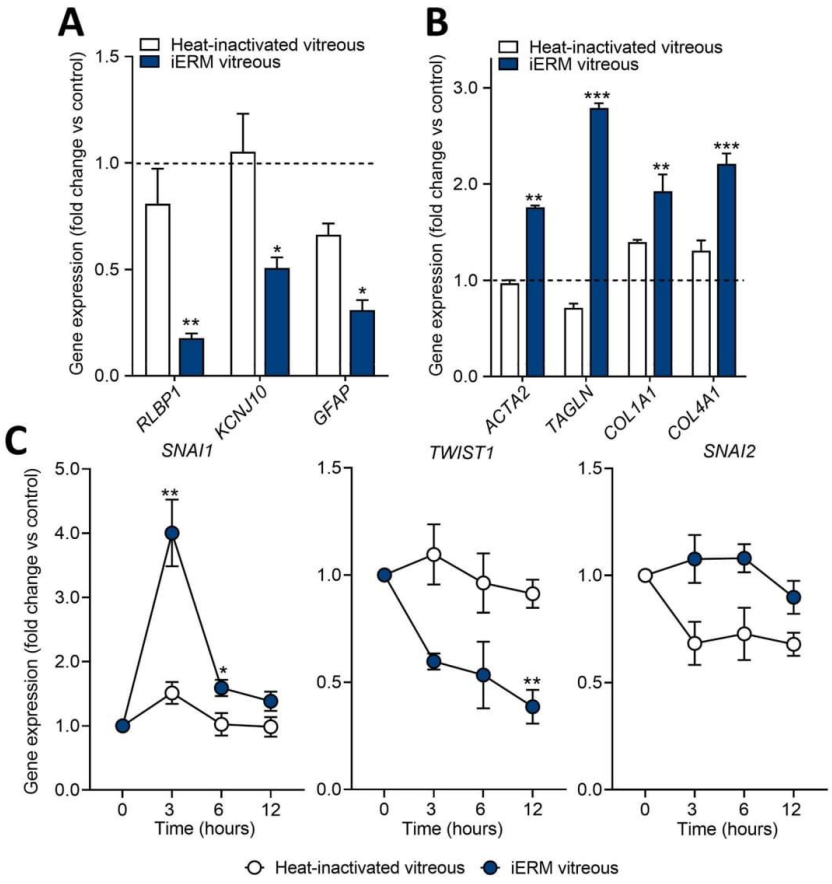

Fig. 2. Gene expression analysis of iERM vitreous-activated Müller cells. A–C) qPCR analysis of MIO-M1 cells treated with iERM or heat-inactivated vitreous pool samples. Glial/Müller cell markers *RLBP1*, *KCNJ10*, and *GFAP* (A) and myofibroblast markers *ACTA2*, *TAGLN*, *COL1A1*, and *COL4A1* (B) expression levels were assessed 24 h after treatment, whereas *SNAI1*, *TWIST1*, and *SNAI2* expression was evaluated at 3, 6, and 12 h of treatment (C). Data (mean ± SEM of 3 determinations) were normalized to *GAPDH* levels and expressed as fold change in respect to untreated MIO-M1 cells. $^{*}p < 0.05$, $^{**}p < 0.01$, and $^{***}p < 0.001$ *vs* untreated MIO-M1 cells, one-way ANOVA.

trigger a stronger mitogenic response were characterized by a more evident downregulation of the Müller cell marker *RLBP1*. This was paralleled by a less pronounced acquisition of a fibroblast/myofibroblast phenotype, as defined by the limited upregulation of *ACTA2* and *TAGLN* expression, raising the possibility that this may represent a partial transdifferentiation status of MIO-M1 cells (see below). At variance, no significant correlation was observed among *GFAP* downregulation and the expression levels of the other genes investigated. These data indicate that the vitreous fluid obtained from different iERM patients may exert diverse but coordinated GMT-related effects on MIO-M1 cells.

3.3. Cluster analysis of iERM vitreous-induced gene expression data

A hierarchical cluster analysis was performed on our qPCR data to assess whether iERM vitreous samples could be grouped according to similar patterns of modulation of gene expression in MIO-M1 cells. The results, shown in Fig. 4A, indicate that iERM vitreous samples could be divided in two clusters, hereinafter referred to as $GMT^{complete}$ and $GMT^{partial}$ clusters. One set of samples (n = 10) was characterized by the capacity to induce a consistent downregulation of Müller cell/glial markers *RLBP1* and *GFAP* in parallel with the upregulation of myofibroblast markers *ACTA2* and *TAGLN*, thus leading to a complete ($GMT^{complete}$) transdifferentiation response. A second set of samples (n = 18) caused instead MIO-M1 cell reprogramming toward a less differentiated state characterized by the upregulation of the proliferation marker *CCND1* and the downregulation of *RLBP1* and *GFAP*. However, this occurred in the absence of the acquisition of mesenchymal markers or in the presence of their further downregulation, pointing to a partial dedifferentiation ($GMT^{partial}$) response in MIO-M1 cells, as observed for the EMT process during embryo development and cancer progression [43]. In addition, the analysis indicates that the $GMT^{partial}$ cluster can be further subdivided in two subgroups ($GMT^{partialA}$ and $GMT^{partialB}$, n = 9 for both subgroups) based on the progressive decrease of the expression levels of both myofibroblast and glial markers.

On this basis, the average gene expression levels measured in the $GMT^{partial}$ cluster were compared to the corresponding average levels in $GMT^{complete}$ samples. As shown in Fig. 4B, the results of such analysis confirmed that MIO-M1 transcripts belonging to the $GMT^{partial}$ cluster are characterized by higher mRNA levels of the Cyclin1-encoding gene *CCDN1*, lower levels of *ACTA2* and *TAGLN* transcripts, and decreased expression of *RLBP1* and *GFAP*. Of note, the decreased expression of *ACTA2*, *TAGLN*, *RLBP1* and *GFAP* was even more evident in the $GMT^{partialB}$ subgroup when compared to the $GMT^{partialA}$ subgroup (Fig. 4C).

In keeping with these observations, $GMT^{partial}$ vitreous samples induced the coordinated upregulation of the collagen genes *COL1A1* and

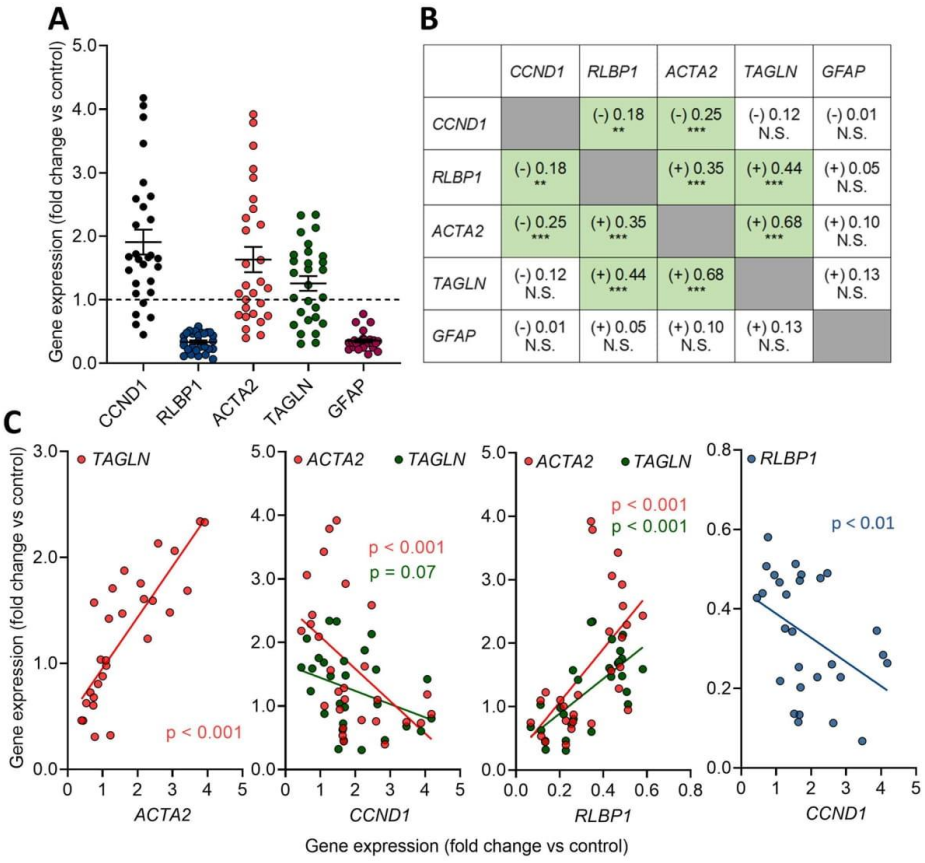

	CCND1	RLBP1	ACTA2	TAGLN	GFAP
CCND1		(-) 0.18 **	(-) 0.25 ***	(-) 0.12 N.S.	(-) 0.01 N.S.
RLBP1	(-) 0.18 **		(+) 0.35 ***	(+) 0.44 ***	(+) 0.05 N.S.
ACTA2	(-) 0.25 ***	(+) 0.35 ***		(+) 0.68 ***	(+) 0.10 N.S.
TAGLN	(-) 0.12 N.S.	(+) 0.44 ***	(+) 0.68 ***		(+) 0.13 N.S.
GFAP	(-) 0.01 N.S.	(+) 0.05 N.S.	(+) 0.10 N.S.	(+) 0.13 N.S.	

Fig. 3. Effect of individual iERM vitreous samples on Müller cells. A) The effect of individual iERM vitreous samples (n = 28) on gene expression in MIO-M1 cells was analyzed by qPCR after 24 h of treatment. The levels of expression of *CCDN1*, *RLBP1*, *ACTA2*, *TAGLN*, and *GFAP* were normalized to *GAPDH* and expressed as fold change in respect to untreated MIO-M1 cells. Each dot represents the effect of one iERM vitreous sample. Data are shown as mean ± SEM. B) Linear regression analysis of the expression of the indicated couples of genes. Positive (+) or negative (−) correlation. R^2 and *p* values were calculated for each couple of genes. $^{**}p < 0.01$ and $^{***}p < 0.001$ (green cells); *NS*, not significant (white cells). C) Linear regression analysis between the expression levels of the gene indicated on the *x* axis and those listed in the inset legend of each panel. Each dot represents the effect of one iERM vitreous sample.

COL4A1, the highest upregulation being observed for the $GMT^{partialA}$ subgroup, whereas $GMT^{complete}$ samples induced only a modest, not statistically significant upregulation of these genes (Suppl. Fig. 3).

Together, these results confirm the data obtained by hierarchical cluster analysis and indicate that iERM vitreous samples can be clustered based on their different capacity to induce a complete or partial GMT response in MIO-M1 cells.

3.4. Clinical features of $GMT^{complete}$ and $GMT^{partial}$ clusters

As stated above, the vitreous samples investigated in the present study were obtained from patients whose iERMs were analyzed for the expression of a set of genes encoding for biomarkers of the cellular and molecular events occurring in iERMs [31]. Hierarchical clustering of the gene expression data obtained by such analysis identified two groups of iERM patients, iERM-B patients being associated with more severe clinical and SD-OCT features when compared to iERM-A patients [31]. Unexpectedly, when the origin of the 28 vitreous samples analyzed in the present work was taken into account, all the 10 samples belonging to the $GMT^{complete}$ cluster were found to derive from iERM-A patients whereas all the 18 vitreous samples belonging to the $GMT^{partial}$ cluster were harvested from iERM-B patients ($p < 0.001$, Fisher exact test). These data suggest that a relationship may exist among the capacity of iERM vitreous to induce partial or complete GMT in Müller cells, the molecular profile of the corresponding iERMs, and the clinical features of iERM patients.

On this basis, we reviewed the clinical charts of the 28 iERM patients investigated in this retrospective study to assess whether the MIO-M1 clustering data could reflect different clinical features of the disease, as already observed for the gene expression analysis of their iERMs [31].

As shown in Fig. 5A, preoperative decimal BCVA was higher in patients belonging to the $GMT^{complete}$ group than in $GMT^{partial}$ patients. In addition, a better improvement of IS/OS visualization was observed following iERM peeling in $GMT^{complete}$ patients when compared to $GMT^{partial}$ patients (Fig. 5B), even though no significant difference was observed between the two clusters in terms of pre-surgical and post-surgical central macular thickness (data not shown).

In addition, we were able to apply the SD-OCT-based classification proposed by Hwang et al. [33] to 24 out of the 28 patients enrolled in this study. The results indicate that 2 iERM patients belonged to the

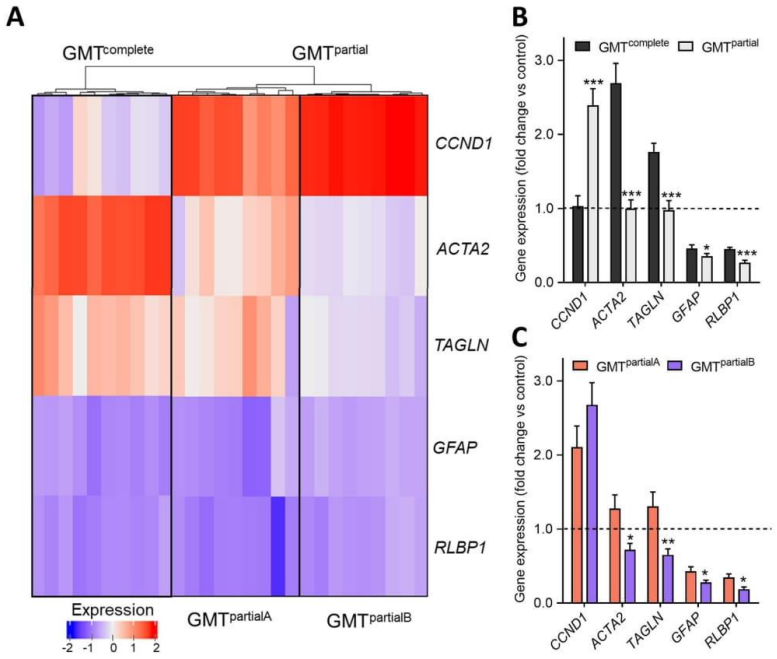

Fig. 4. Hierarchical cluster analysis of the effect of individual iERM vitreous samples on gene expression in MIO-M1 cells. A) Heatmap depicting the relative expression of the genes modulated in MIO-M1 cells by the 28 iERM vitreous samples grouped by hierarchical cluster analysis. Each column represents the effect of one vitreous sample and each row represents the indicated gene. The expression level of each gene is depicted according to the color scale. B) Fold change of mean gene expression levels in $GMT^{complete}$ (n = 10) *vs* $GMT^{partial}$ (n = 18) clusters. Data are shown as mean ± SEM. $*p < 0.05$ and $***p < 0.001$ *vs* $GMT^{complete}$, Student's *t*-test. C) Fold change of mean gene expression levels in $GMT^{partialA}$ (n = 9) *vs* $GMT^{partialB}$ (n = 9) clusters. Data are shown as mean ± SEM. $*p < 0.05$ and $**p < 0.01$ *vs* $GMT^{partialA}$, Student's *t*-test.

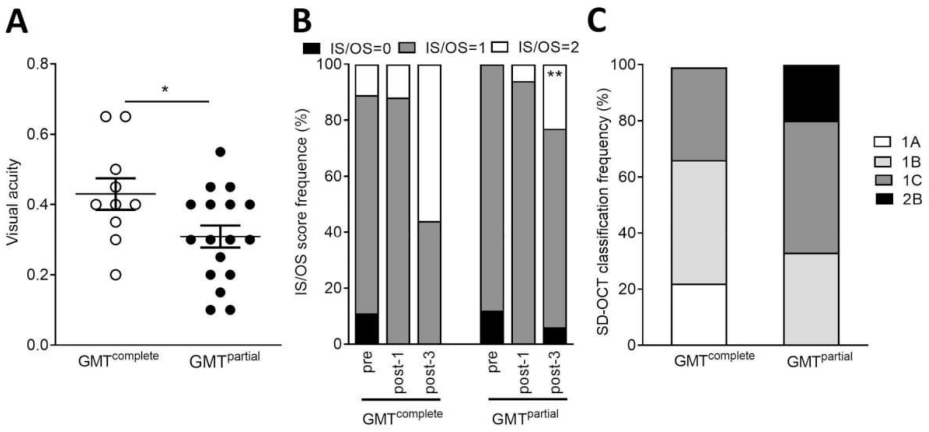

Fig. 5. Visual acuity, IS/OS, and SD-OCT-based classification of iERM patients belonging to $GMT^{complete}$ and $GMT^{partial}$ clusters. A) Preoperative decimal BCVA. Data are the mean ± SEM. $*p < 0.05$, Student's *t*-test. B) Stacked bar plot showing the frequency of pre-surgical (pre), 1-month post-surgery (post-1), and 3-month post-surgery (post-3) IS/OS score levels. $**p < 0.01$ *vs* post-3 $GMT^{complete}$, cumulative link mixed model. C) iERM patients belonging to $GMT^{complete}$ and $GMT^{partial}$ clusters were distributed according their SD-OCT features as classified by Hwang et al. [32]. Values were obtained from the clinical charts of patients belonging to molecular $GMT^{complete}$ (n = 9–10) and $GMT^{partial}$ (n = 15–18) clusters.

fovea-attached type ERM Group 1A, characterized by an ERM with outer retinal thickening and near-normal inner retina, whereas 9 and 10 patients were part of the more severe SD-OCT Groups 1B and 1C, respectively. The remaining 3 patients belonged to the pseudohole type ERM Group 2B, characterized by the presence of a macular pseudohole accompanied by marked intraretinal splitting [33]. When $GMT^{complete}$ and $GMT^{partial}$ patients were analyzed separately, $GMT^{partial}$ patients showed more severe SD-OCT-based morphological features when compared to $GMT^{complete}$ patients (Fig. 5C and Suppl. Table 2). At variance, no significant differences were observed for all the clinical parameters investigated between $GMT^{partialA}$ and $GMT^{partialB}$ subgroups (data not shown).

Together, these data indicate that iERM patients with vitreous fluid able to induce a $GMT^{partial}$ response in Müller cells are characterized by a distinct iERM gene expression profile and by more severe clinical and morphological features when compared to $GMT^{complete}$ patients

(Table 1).

4. Discussion

Müller cells appear to play a pivotal role in the pathogenesis of iERM [15]. Vitreal and retinal components may act on Müller cells, triggering cell proliferation, migration, collagen contraction, and transdifferentiation [16–22]. Recent observations have shown that Müller cells stimulated by TGFβ undergo GMT, a transdifferentiation process similar to EMT, characterized by the downregulation of Müller cell markers, paralleled by the upregulation of pro-fibrotic myofibroblast markers [23–25].

Here, we demonstrate that a pool of vitreous fluid harvested from iERM patients before membrane peeling induces proliferation, migration, and GMT in MIO-M1 cells, a phenotype consistent with Müller cell behavior during iERM progression. The specificity of the effect was confirmed by the fact that no or negligible responses were instead elicited by treatment with heat-inactivated iERM vitreous or with a vitreous pool obtained from RRD patients.

When aliquots of the same samples utilized to generate the iERM vitreous pool were assessed individually for their capacity to induce GMT in MIO-M1 cells, the results indicated that all iERM vitreous samples were able to cause the downregulation of the Müller cell/glial markers *RLBP1* and *GFAP*. However, these samples differ for their capacity to affect the expression of the myofibroblast markers *ACTA2* and *TAGLN*. Indeed, a cluster of iERM vitreous samples induced Müller cell/glial marker downregulation paralleled by a significant upregulation of the pro-fibrotic myofibroblast markers *ACTA2* and *TAGLN*, leading to a $GMT^{complete}$ response in MIO-M1 cells. A second cluster of iERM vitreous samples exerted instead no effect or an inhibitory response on the expression of *ACTA2* and *TAGLN* together with a significant upregulation of the Cyclin1-encoding gene *CCDN1*, thus inducing glial dedifferentiation in the absence of the acquisition of mesenchymal markers. This latter phenotype may represent a transitional $GMT^{partial}$ state, as observed for EMT in which cell dedifferentiation can be associated with proliferating cells undergoing a partial EMT (see [44] and references therein). Indeed, EMT proceeds *via* multiple partial intermediate states, known as partial or hybrid EMT states, during which cells sequentially lose apico-basal polarity and cell-cell adhesions and gain front-back polarity and enhanced cell-matrix interactions [45]. A partial EMT state, based on the existence of intermediate hybrid epithelial and mesenchymal phenotypes, has been noted in association with several developmental, wound healing, fibrosis, and cancer processes [45]. Thus, our findings rise the possibility that GMT may represent a transitional process during which Müller cells may move from a glial to a mesenchymal status *via* a quasi-stable dedifferentiated partial GMT through a spectrum of yet uncharacterized metastable intermediary phases.

Few data are available about the molecular mechanisms that control GMT in Müller cells. Previous observations had shown that TGFβ induces GMT in MIO-M1 cells *via* the activation of the transcription factor SNAIL [23]. Here, we have observed that iERM vitreous upregulates the expression of the SNAIL1-encoding gene *SNAI1* in MIO-M1 cells along with the downregulation of *TWIST1*, with no significant changes in *SNAI2* expression. At present, the signals responsible for the activation of a partial or complete GMT state in Müller cells remain largely unknown. The vitreous humor can be considered as a reservoir of biological mediators that accumulate during the progression of retinal diseases [26]. It derives that the effects exerted by iERM vitreous on MIO-M1 cells will result from the balance of the activity of all the agonists and antagonists accumulated during iERM progression rather than from the activity of a single growth factor or cytokine. Relevant to this point, preliminary data obtained with MIO-M1 cells treated with various recombinant cytokines/growth factors indicate that TGFβ causes the downregulation of the Müller cell marker *RLBP1* and the upregulation of *ACTA2*, *TAGLN*, *COL1A1* and *COL4A1* genes, with no effect on *GFAP* and *CCDN1* expression. At variance, both TNFα and FGF2 upregulate *CCDN1* expression and cause a strong downregulation of *RLBP1* and *GFAP*, with no significant consequence on *ACTA2*, *TAGLN*, *COL1A1* and *COL4A1* expression. Of note, no effect was instead exerted by VEGF treatment on any of the genes investigated (Suppl. Fig. 4). Thus, it seems possible to hypothesize that qualitative/quantitative differences of vitreal cytokines/growth factors may cause the induction of different transitional states in Müller cells during iERM. Further experiments will be required to elucidate this point.

In this work, we analyzed the vitreous fluid from iERM patients that were part of a cohort belonging to a previous retrospective study aimed to attempt the molecular characterization of iERM specimens obtained after membrane peeling [31]. In that study, qPCR analysis of the expression of genes encoding for putative biomarkers of the cellular and molecular events occurring in iERMs identified two molecular clusters of iERMs, herewith named iERM-A and iERM-B. When compared to iERM-A specimens, iERM-B samples showed higher levels of cytokine and growth factor transcripts and higher expression of glial and fibrogenic markers, with no difference in the levels of expression of myofibroblast and hyalocyte markers [31]. Notably, the information present in the clinical charts indicated that the patients belonging the iERM-A cluster showed less severe clinical features when compared to iERM-B patients, including higher preoperative decimal BCVA, a better and faster improvement of IS/OS visualization after surgery, and more favorable SD-OCT features following the Hwang et al. classification [33].

When the origin of the 28 vitreous samples analyzed in the present work was taken into account, all the 10 samples belonging to the $GMT^{complete}$ cluster were found to derive from iERM-A patients, whereas all the 18 vitreous samples belonging to the $GMT^{partial}$ cluster were obtained from iERM-B patients. In keeping with our previous observations, iERM-B patients with vitreous fluid able to induce a $GMT^{partial}$ response in MIO-M1 cells were characterized by more severe clinical and morphological features when compared to $GMT^{complete}$/iERM-A patients. Together, these data indicate that both the molecular analysis of iERMs and the study of the impact of the corresponding vitreous fluids on Müller cells provide congruent information that allow the identification of two clusters of iERM patients with distinct clinical features. This point deserves further discussion.

Morphological and immunohistochemical analyses have demonstrated the presence of a variety of cell types in iERMs beside Müller cells, including astrocytes, microglia, hyalocytes, fibroblasts, myofibroblasts, and retinal pigment epithelial cells [8–10]. Thus, the molecular profile of iERMs will reflect such heterogeneity and the results of the impact of long-lasting effects driven by systemic, vitreal, and retinal mediators on the different cell populations. It is therefore not surprising that the modulation of gene expression induced *in vitro* by iERM vitreous samples on Müller cells may not necessarily reflect the gene expression patterns observed in the corresponding iERMs. Indeed, we did not find any significant correlation between the expression levels of the various genes modulated by iERM vitreous samples in MIO-M1 cells and the levels of the same transcripts in the iERM specimens obtained from the same patients. Nevertheless, the results indicate that a relationship does exist among the ability of iERM vitreous to modulate GMT in Müller cells, the molecular profile of the corresponding iERMs, and the clinical features of iERM patients (Table 1). It seems therefore possible to hypothesize that the molecular characterization of the iERMs reflects their biological status that will determine, at least in part, the clinical features of the corresponding iERM patients. This will impact the qualitative/quantitative composition of biological mediators in the iERM vitreous fluid that, in turn, will affect the iERM/retinal environment. Such composition will determine the observed response elicited by iERM vitreous on MIO-M1 cells (Fig. 6).

In keeping with this hypothesis is the observation that the $GMT^{partial}$ response triggered by iERM-B vitreous samples in Müller cells is associated with more severe clinical and SD-OCT morphological features. As stated above, the $GMT^{partial}$ phenotype may represent a transitional

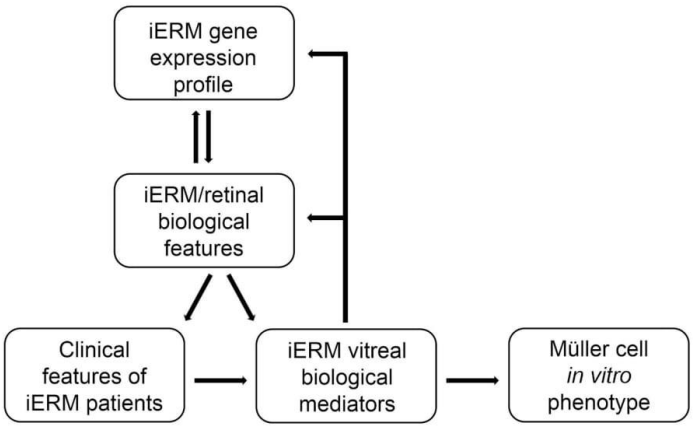

Fig. 6. Relationship among the iERM gene expression profile, iERM vitreous activity on Müller cells, and the clinical features of iERM patients. The molecular profile of iERMs reflects their biological status that will determine the clinical features of the patient. Together, they will affect the qualitative/quantitative composition of biological mediators in the iERM vitreous fluid that, in turn, will modulate the iERM/retinal environment and will govern the response elicited by iERM vitreous on Müller MIO-M1 cells.

dedifferentiation state like that observed for EMT in which cell dedifferentiation can be associated with a partial EMT state (see [44] and references therein). Notably, rather than complete EMT, partial EMT confers to cancer cells the highest tumor initiating potential [46] and partial EMT has been found to be critical for renal fibrosis [47]. By analogy, the capacity of iERM vitreous to confer a $GMT^{partial}$ phenotype to MIO-M1 cells may reflect a composition of vitreal mediators associated with distinct, more severe clinical conditions when compared to iERM vitreous samples able to induce a $GMT^{complete}$ phenotype. Accordingly, $GMT^{partial}$ vitreous samples were endowed with a stronger capacity to induce the upregulation of the collagen genes *COL1A1* and *COL4A1* in respect to $GMT^{complete}$ samples. This is in keeping with recent studies about the composition and structural arrangement of the extracellular matrix of iERMs, which is characterized by the accumulation of Type I and Type IV collagens together with other structural components [48,49]. Further experiments will be required to elucidate the role of Müller cells in the deposition and organization of the iERM extracellular matrix. In this frame, it must be pointed out that our observations were performed on the spontaneous immortalized MIO-M1 cell line [35]. Even though these cells are commonly used to investigate Müller cell biology, caution should be taken when extrapolating *in vitro* data obtained on this cell line to the Müller cell responses that may occur in the human eye under physiological and pathological conditions.

To the best of our knowledge, the data present in this and our previous work [31] represent a first attempt to correlate the biological potential of iERM vitreous fluid with the molecular profile of iERMs and the clinical features of iERM patients. Performed retrospectively on a limited number of patients, this work paves the way to future prospective studies about the impact of iERM vitreous on the different cell populations that form this fibrocellular tissue and to allow the identification of the biological mediators involved in iERM progression of therapeutic significance.

CRediT authorship contribution statement

Adwaid Manu Krishna Chandran: Investigation. **Daniela Coltrini:** Investigation. **Mirella Belleri:** Investigation. **Sara Rezzola:** Investigation. **Elena Gambicorti:** Resources, Investigation. **Davide Romano:** Resources, Investigation. **Francesco Morescalchi:** Resources. **Stefano Calza:** Formal analysis. **Francesco Semeraro:** Supervision, Funding acquisition. **Marco Presta:** Supervision, Funding acquisition, Writing – original draft, Writing – review & editing.

Declaration of competing interest

The authors declare that they have no known competing financial interests or personal relationships that could have appeared to influence the work reported in this paper.

Acknowledgements

This work was supported in part by grant CAAR (Health and Wealth Project) from the University of Brescia, Italy to F.S. S.R. was supported by a Fondazione Umberto Veronesi fellowship.

Appendix A. Supplementary data

Supplementary data to this article can be found online at https://doi.org/10.1016/j.bbadis.2021.166181.

References

[1] W. Stevenson, C.M. Prospero Ponce, D.R. Agarwal, R. Gelman, J.B. Christoforidis, Epiretinal membrane: optical coherence tomography-based diagnosis and classification, Clin. Ophthalmol. 10 (2016) 527–534, https://doi.org/10.2147/OPTH.S97722.
[2] M. Inoue, K. Kadonosono, Macular diseases: epiretinal membrane, Dev. Ophthalmol. 54 (2014) 159–163, https://doi.org/10.1159/000360462.
[3] S.C. Bu, R. Kuijer, X.R. Li, J.M. Hooymans, L.I. Los, Idiopathic epiretinal membrane, Retina 34 (2014) 2317–2335, https://doi.org/10.1097/IAE.0000000000000349.
[4] C.H. Ng, et al., Prevalence and risk factors for epiretinal membranes in a multi-ethnic United States population, Ophthalmology 118 (2011) 694–699, https://doi.org/10.1016/j.ophtha.2010.08.009.
[5] N. Cheung, S.P. Tan, S.Y. Lee, G.C.M. Cheung, G. Tan, N. Kumar, C.Y. Cheng, T. Y. Wong, Prevalence and risk factors for epiretinal membrane: the Singapore Epidemiology of Eye Disease study, Br. J. Ophthalmol. 101 (2017) 371–376, https://doi.org/10.1136/bjophthalmol-2016-308563.
[6] P. Massin, C. Allouch, B. Haouchine, F. Metge, M. Paques, L. Tangui, A. Erginay, A. Gaudric, Optical coherence tomography of idiopathic macular epiretinal membranes before and after surgery, Am J. Ophthalmol. 130 (2000) 732–739, https://doi.org/10.1016/s0002-9394(00)00574-2.
[7] J.G. Wong, N. Sachdev, P.E. Beaumont, A.A. Chang, Visual outcomes following vitrectomy and peeling of epiretinal membrane, Clin. Exp. Ophthalmol. 33 (2005) 373–378, https://doi.org/10.1111/j.1442-9071.2005.01025.x.
[8] R.G. Schumann, A. Gandorfer, J. Ziada, R. Scheler, M.M. Schaumberger, A. Wolf, A. Kampik, C. Haritoglou, Hyalocytes in idiopathic epiretinal membranes: a correlative light and electron microscopic study, Graefes Arch. Clin. Exp. Ophthalmol. 252 (2014) 1887–1894, https://doi.org/10.1007/s00417-014-2841-x.
[9] F. Zhao, A. Gandorfer, C. Haritoglou, R. Scheler, M.M. Schaumberger, A. Kampik, R.G. Schumann, Epiretinal cell proliferation in macular pucker and vitreomacular traction syndrome: analysis of flat-mounted internal limiting membrane specimens, Retina 33 (2013) 77–88, https://doi.org/10.1097/IAE.0b013e3182602087.

[10] M. Joshi, S. Agrawal, J.B. Christoforidis, Inflammatory mechanisms of idiopathic epiretinal membrane formation, Mediat. Inflamm. 2013 (2013), 192582, https://doi.org/10.1155/2013/192582.
[11] E. Tsotridou, E. Loukovitis, K. Zapsalis, I. Pentara, S. Koronis, P. Tranos, S. Asteriadis, M. Balidis, T. Sousouras, T. Vakalis, et al., Update on the cellular, genetic and cytokine basis of epiretinal membrane pathogenesis, J. Biol. Regul. Homeost. Agents 33 (2019) 1879–1884, https://doi.org/10.23812/19-275-L.
[12] S. Tamiya, H.J. Kaplan, Role of epithelial-mesenchymal transition in proliferative vitreoretinopathy, Exp. Eye Res. 142 (2016) 26–31, https://doi.org/10.1016/j.exer.2015.02.008.
[13] F.S. Sorrentino, M. Allkabes, G. Salsini, C. Bonifazzi, P. Perri, The importance of glial cells in the homeostasis of the retinal microenvironment and their pivotal role in the course of diabetic retinopathy, Life Sci. 162 (2016) 54–59, https://doi.org/10.1016/j.lfs.2016.08.001.
[14] E. Newman, A. Reichenbach, The Müller cell: a functional element of the retina, Trends Neurosci. 19 (1996) 307–312, https://doi.org/10.1016/0166-2236(96)10040-0.
[15] A. Bringmann, P. Wiedemann, Involvement of Müller glial cells in epiretinal membrane formation, Graefes Arch. Clin. Exp. Ophthalmol. 247 (2009) 865–883, https://doi.org/10.1007/s00417-009-1082-x.
[16] C. Guidry, R. Feist, R. Morris, C.W. Hardwick, Changes in IGF activities in human diabetic vitreous, Diabetes 53 (2004) 2428–2435, https://doi.org/10.2337/diabetes.53.9.2428.
[17] C. Guidry, K.M. Bradley, J.L. King, Tractional force generation by human müller cells: growth factor responsiveness and integrin receptor involvement, Invest. Ophthalmol. Vis. Sci. 44 (2003) 1355–1363, https://doi.org/10.1167/iovs.02-0046.
[18] D. Romaniuk, M.W. Kimsa, B. Strzalka-Mrozik, M.C. Kimsa, A. Kabiesz, W. Romaniuk, U. Mazurek, Gene expression of IGF1, IGF1R, and IGFBP3 in epiretinal membranes of patients with proliferative diabetic retinopathy: preliminary study, Mediat. Inflamm. 2013 (2013), 986217, https://doi.org/10.1155/2013/986217.
[19] M. Hollborn, K. Jahn, G.A. Limb, L. Kohen, P. Wiedemann, A. Bringmann, Characterization of the basic fibroblast growth factor-evoked proliferation of the human Müller cell line, MIO-M1, Graefes Arch. Clin. Exp. Ophthalmol. 242 (2004) 414–422, https://doi.org/10.1007/s00417-004-0879-x.
[20] H. Kimura, C. Spee, T. Sakamoto, D.R. Hinton, Y. Ogura, Y. Tabata, Y. Ikada, S. J. Ryan, Cellular response in subretinal neovascularization induced by bFGF-impregnated microspheres, Invest. Ophthalmol. Vis. Sci. 40 (1999) 524–528.
[21] S. Yoshida, A. Yoshida, T. Ishibashi, Induction of IL-8, MCP-1, and bFGF by TNF-α in retinal glial cells: implications for retinal neovascularization during post-ischemic inflammation, Graefes Arch. Clin. Exp. Ophthalmol. 242 (2004) 409–413, https://doi.org/10.1007/s00417-004-0874-2.
[22] T. Cheng, W. Cao, R. Wen, R.H. Steinberg, M.M. LaVail, Prostaglandin E2 induces vascular endothelial growth factor and basic fibroblast growth factor mRNA expression in cultured rat Müller cells, Invest. Ophthalmol. Vis. Sci. 39 (1998) 581–591.
[23] A. Kanda, K. Noda, I. Hirose, S. Ishida, TGF-β-SNAIL axis induces Müller glial-mesenchymal transition in the pathogenesis of idiopathic epiretinal membrane, Sci. Rep. 9 (2019) 673, https://doi.org/10.1038/s41598-018-36917-9.
[24] D. Wu, A. Kanda, Y. Liu, K. Noda, M. Murata, S. Ishida, Involvement of Müller glial autoinduction of TGF-β in diabetic fibrovascular proliferation via glial-mesenchymal transition, Invest. Ophthalmol. Vis. Sci. 61 (2020) 29, https://doi.org/10.1167/iovs.61.14.29.
[25] S.C. Bu, R. Kuijer, R.J. van der Worp, G. Postma, V.W. Renardel de Lavalette, X. R. Li, J.M. Hooymans, L.I. Los, Immunohistochemical evaluation of idiopathic epiretinal membranes and in vitro studies on the effect of TGF-β on Müller cells, Invest. Ophthalmol. Vis. Sci. 56 (2015) 6506–6514, https://doi.org/10.1167/iovs.14-15971.
[26] I.M. Nawaz, S. Rezzola, A. Cancarini, A. Russo, C. Costagliola, F. Semeraro, M. Presta, Human vitreous in proliferative diabetic retinopathy: characterization and translational implications, Prog. Retin. Eye Res. (2019), https://doi.org/10.1016/j.preteyeres.2019.03.002.
[27] S. Rezzola, M.I. Nawaz, A. Cancarini, F. Semeraro, M. Presta, Vascular endothelial growth factor in the vitreous of proliferative diabetic retinopathy patients: chasing a hiding prey? Diabetes Care 42 (2019) e105–e106, https://doi.org/10.2337/dc18-2527.
[28] S. Rezzola, J. Guerra, A.M. Krishna Chandran, A. Loda, A. Cancarini, P. Sacristani, F. Semeraro, M. Presta, VEGF-independent activation of Müller cells by the vitreous from Proliferative Diabetic Retinopathy patients, Int. J. Mol. Sci. 22 (2021) 2179, https://doi.org/10.3390/ijms22042179.
[29] C. Hardwick, R. Feist, R. Morris, M. White, D. Witherspoon, R. Angus, C. Guidry, Tractional force generation by porcine Müller cells: stimulation by growth factors in human vitreous, Invest. Ophthalmol. Vis. Sci. 38 (1997) 2053–2063.
[30] C. Guidry, The role of Müller cells in fibrocontractive retinal disorders, Prog. Retin. Eye Res. 24 (2005) 75–86, https://doi.org/10.1016/j.preteyeres.2004.07.001.
[31] D. Coltrini, M. Belleri, E. Gambicorti, D. Romano, F. Morescalchi, A.M. Krishna Chandran, S. Calza, F. Semeraro, M. Presta, Gene expression analysis identifies two distinct molecular clusters of idiopatic epiretinal membranes, Biochim. Biophys. Acta Mol. basis Dis. 1866 (2020), 165938, https://doi.org/10.1016/j.bbadis.2020.165938.
[32] T. Öhman, L. Gawriyski, S. Miettinen, M. Varjosalo, S. Loukovaara, Molecular pathogenesis of rhegmatogenous retinal detachment, Sci. Rep. 11 (2021) 966, https://doi.org/10.1038/s41598-020-80005-w.
[33] J.U. Hwang, J. Sohn, B.G. Moon, S.G. Joe, J.Y. Lee, J.G. Kim, Y.H. Yoon, Assessment of macular function for idiopathic epiretinal membranes classified by spectral-domain optical coherence tomography, Invest. Ophthalmol. Vis. Sci. 53 (2012) 3562–3569, https://doi.org/10.1167/iovs.12-9762.
[34] M.P. Sheales, Z.S. Kingston, R.W. Essex, Associations between preoperative OCT parameters and visual outcome 3 months postoperatively in patients undergoing vitrectomy for idiopathic epiretinal membrane, Graefes Arch. Clin. Exp. Ophthalmol. 254 (2016) 1909–1917, https://doi.org/10.1007/s00417-016-3326-x.
[35] G.A. Limb, T.E. Salt, P.M. Munro, S.E. Moss, P.T. Khaw, In vitro characterization of a spontaneously immortalized human Müller cell line (MIO-M1), Invest. Ophthalmol. Vis. Sci. 43 (2002) 864–869.
[36] J. Schindelin, et al., Fiji: an open-source platform for biological-image analysis, Nat. Methods 9 (2012) 676–682, https://doi.org/10.1038/nmeth.2019.
[37] F. Murtagh, P. Legendre, Ward's hierarchical agglomerative clustering method: which algorithms implement Ward's criterion? J. Classif. 31 (2014) 274–295.
[38] G. Tutz, W. Hennevogl, Random effects in ordinal regression models, Comput. Stat. Data Anal. 22 (1996) 537–557, https://doi.org/10.1016/0167-9473(96)00004-7.
[39] P. McCullagh, J.A. Nelder, Generalized Linear Models, 2nd ed., Chapman & Hall/CRC, Boca Raton, 1998.
[40] Y. Xue, S.Q. Shen, J. Jui, A.C. Rupp, L.C. Byrne, S. Hattar, J.G. Flannery, J. C. Corbo, V.J. Kefalov, CRALBP supports the mammalian retinal visual cycle and cone vision, J. Clin. Invest. 125 (2015) 727–738, https://doi.org/10.1172/JCI79651.
[41] A. Bringmann, T. Pannicke, J. Grosche, M. Francke, P. Wiedemann, S.N. Skatchkov, N.N. Osborne, A. Reichenbach, Müller cells in the healthy and diseased retina, Prog. Retin. Eye Res. 25 (2006) 397–424, https://doi.org/10.1016/j.preteyeres.2006.05.003.
[42] A.G. Junemann, R. Rejdak, C. Huchzermeyer, R. Maciejewski, P. Grieb, F.E. Kruse, E. Zrenner, K. Rejdak, A. Petzold, Elevated vitreous body glial fibrillary acidic protein in retinal diseases, Graefes Arch. Clin. Exp. Ophthalmol. 253 (2015) 2181–2186, https://doi.org/10.1007/s00417-015-3127-7.
[43] S. Kase, W. Saito, M. Yokoi, K. Yoshida, N. Furudate, M. Muramatsu, A. Saito, M. Kase, S. Ohno, Expression of glutamine synthetase and cell proliferation in human idiopathic epiretinal membrane, Br. J. Ophthalmol. 90 (2006) 96–98, https://doi.org/10.1136/bjo.2005.078394.
[44] H. Wang, J.J. Unternaehrer, Epithelial-mesenchymal transition and cancer stem cells: at the crossroads of differentiation and dedifferentiation, Dev. Dyn. 248 (2019) 10–20, https://doi.org/10.1002/dvdy.24678.
[45] M.A. Nieto, R.Y. Huang, R.A. Jackson, J.P. Thiery, EMT: 2016, Cell 166 (2016) 21–45, https://doi.org/10.1016/j.cell.2016.06.028.
[46] C.L. Chaffer, B.P. San Juan, E. Lim, R.A. Weinberg, EMT, cell plasticity and metastasis, Cancer Metastasis Rev. 35 (2016) 645–654, https://doi.org/10.1007/s10555-016-9648-7.
[47] S. Lovisa, V.S. LeBleu, B. Tampe, H. Sugimoto, K. Vadnagara, J.L. Carstens, C. C. Wu, Y. Hagos, B.C. Burckhardt, T. Pentcheva-Hoang, et al., Epithelial-to-mesenchymal transition induces cell cycle arrest and parenchymal damage in renal fibrosis, Nat. Med. 21 (2015) 998–1009, https://doi.org/10.1038/nm.3902.
[48] M. Regoli, G.M. Tosi, G. Neri, A. Altera, D. Orazioli, The peculiar pattern of type IV collagen deposition in epiretinal membranes, J. Histochem. Cytochem. 68 (2020) 149–162, https://doi.org/10.1369/0022155419897258.
[49] A. Altera, G.M. Tosi, M. Regoli, E. De Benedetto, E. Bertelli, The extracellular matrix complexity of idiopathic epiretinal membranes and the bilamiar arrangement of the associated internal limiting membrane in the posterior retina, Graefes Arch. Clin. Exp. Ophthalmol. (2021), https://doi.org/10.1007/s00417-021-05156-6.

Supplementary Table 1. Primers used for qPCR analysis

Gene	Forward	Reverse
RLBP1	5'-GCTGCTGGAGAATGAGGAAA-3'	5'-TGGTGGATGAAGTGGATGG-3'
KCNJ10	5'-CTTCTCCCTTGAATCCCAAA-3'	5'-ATGCTGGCTGAAACGAATG-3'
GFAP	5'-ATCAACTCACCGCCAACAG-3'	5'-CCAGCGACTCAATCTTCCTC-3'
ACTA2	5'-AATGGCTCTGGGCTCTGTAA-3'	5'-TTTTGCTCTGTGCTTCGTCA-3'
TAGLN	5'-AGCAGGTGGCTCAGTTCCT-3'	5'-CGGTAGTGCCCATCATTCTT-3'
S100A4/FSP1	5'-CCTGGATGTGATGGTGTCC-3'	5'-TCGTTGTCCCTGTTGCTGT-3'
CCND1	5'-ATCGTCGCCACCTGGAT-3'	5'-GACCTCCTCCTCGCACTTC-3'
SNAI1	5'-AATCGGAAGCCTAACTACAGCG-3'	5'-GTCCCAGATGAGCATTGGCA-3'
TWIST1	5'-GTCCGCAGTCTTACGAGGAG-3'	5'-GCTTGAGGGTCTGAATCTTGCT-3'
SNAI2	5'-TGACCTGTCTGCAAATGCTC-3'	5'-CAGACCCTGGTTGCTTCAA-3'
COL1A1	5'-AAGAGGAAGGCCAAGTCGAG-3'	5'-AGATCACGTCATCGCACAAC-3'
COL4A1	5'-ATGAAGGGTGATCCAGGTGA-3'	5'-TGGTGGTCCGGTAAATCCT-3'
GAPDH	5'-GAAGGTCGGAGTCAACGGATT-3'	5'-TGACGGTGCCATGGAATTTG-3'

Supplementary Table 2. Distribution of iERM patients based on SD-OCT-based classification and GMT clustering.

SD-OCT-based iERM classification	Cluster $GMT^{complete}$ (n = 9)	Cluster $GMT^{partial}$ (n = 15)	Total (n = 24)
Group 1A	2 (22 %)	0 (0%)	2
Group 1B	4 (44 %)	5 (33 %)	9
Group 1C	3 (33 %)	7 (47 %)	10
Group 2A	0 (0 %)	0 (0 %)	0
Group 2B	0 (0 %)	3 (20 %)	3

iERM patients belonging to the $GMT^{complete}$ and $GMT^{partial}$ clusters were distributed according their SD-OCT features as classified by Hwang et al. [32]

1

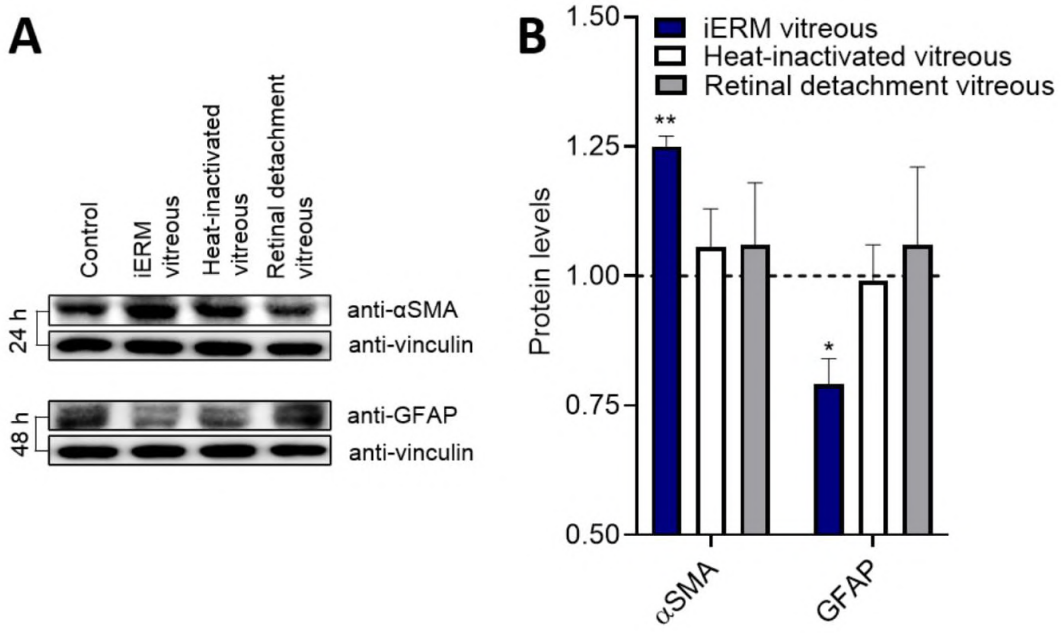

Supplementary Fig. 1. Analysis of αSMA and GFAP protein levels in MIO-M1 cells. **A**) Cells were treated for 24 or 48 hours with iERM, heat-inactivated iERM, or RRD vitreous pools diluted 1:4 with culture medium. Then, cell extracts (20 μg of protein) were analyzed by Western blotting using anti-αSMA and anti-GFAP antibodies. Uniform loading of the gel was confirmed with anti-vinculin antibody. **B**) αSMA and GFAP protein levels were quantified by densitometric analysis, normalized to vinculin levels, and expressed as fold change in respect to untreated cells. Data are the mean ± SEM of 2 determinations. * $p < 0.05$ and ** $p < 0.01$ *vs* untreated MIO-M1 cells.

2

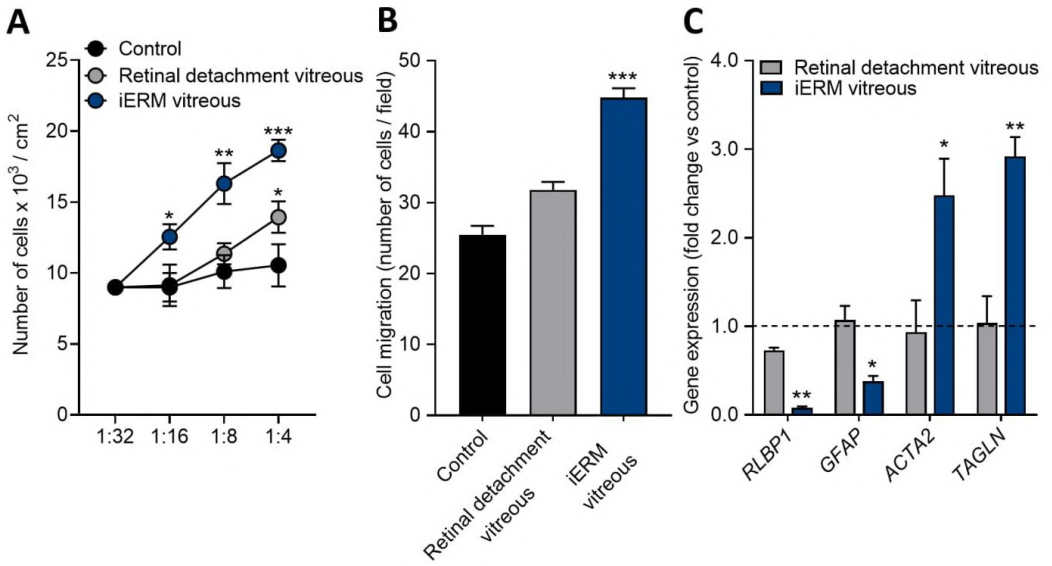

Supplementary Fig. 2. Rhegmatogenous retinal detachment (RRD) vitreous does not induce GMT in MIO-M1 cells. Different dilutions of iERM vitreous or RRD vitreous pools were assessed for the capacity to induce cell proliferation (**A**) and a chemotactic response (**B**) in MIO-M1 cells as described in the Materials and Methods section. **C**) MIO-M1 cells were incubated for 24 hours with a 1:4 dilution of iERM or RRD vitreous pools. At the end of incubation, the expression levels of the indicated genes were evaluated by qPCR and normalized to *GAPDH* expression. Data are the mean ± SEM of 3 determinations. * $p < 0.05$, ** $p < 0.01$, and *** $p < 0.001$ *vs* untreated MIO-M1 cells, one-way ANOVA.

3

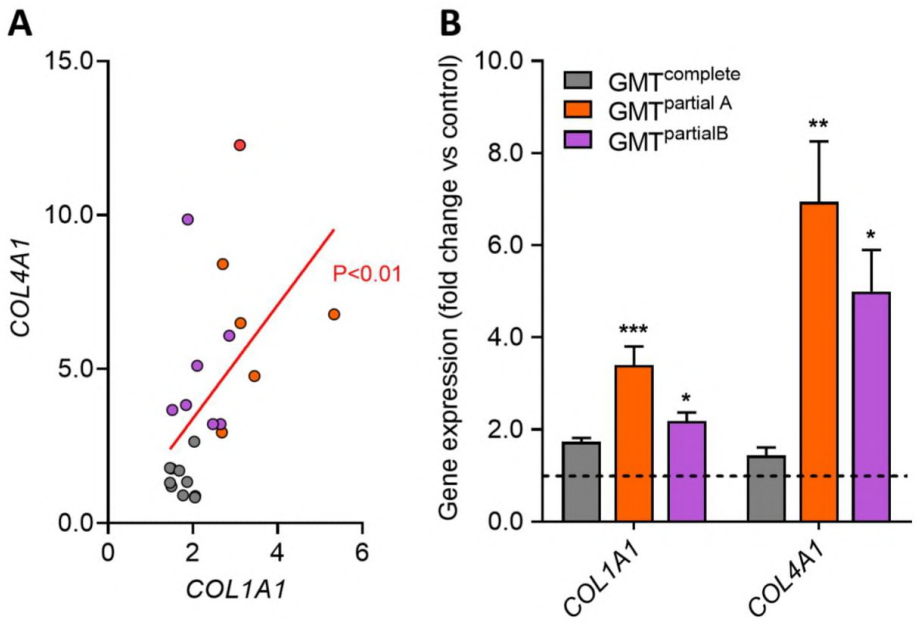

Supplementary Fig. 3. Individual iERM vitreous samples upregulate *COL1A1* and *COL4A1* gene expression in MIO-M1 cells. The effect of individual iERM vitreous samples belonging to $GMT^{complete}$ (n = 10), $GMT^{partialA}$ (n = 6), and $GMT^{partialB}$ (n = 7) clusters was analyzed by qPCR after 24 hours of treatment. Data were normalized to *GAPDH* and expressed as fold change in respect to untreated MIO-M1 cells. **A**) Linear regression analysis of the expression levels of *COL1A1 versus COL4A1*. Each dot represents the effect of one iERM vitreous sample. **B**) Fold change of mean gene expression levels. Data are shown as mean ± SEM. * $p < 0.05$, ** $p < 0.01$, and *** $p < 0.001$ *vs* untreated MIO-M1 cells, one-way ANOVA.

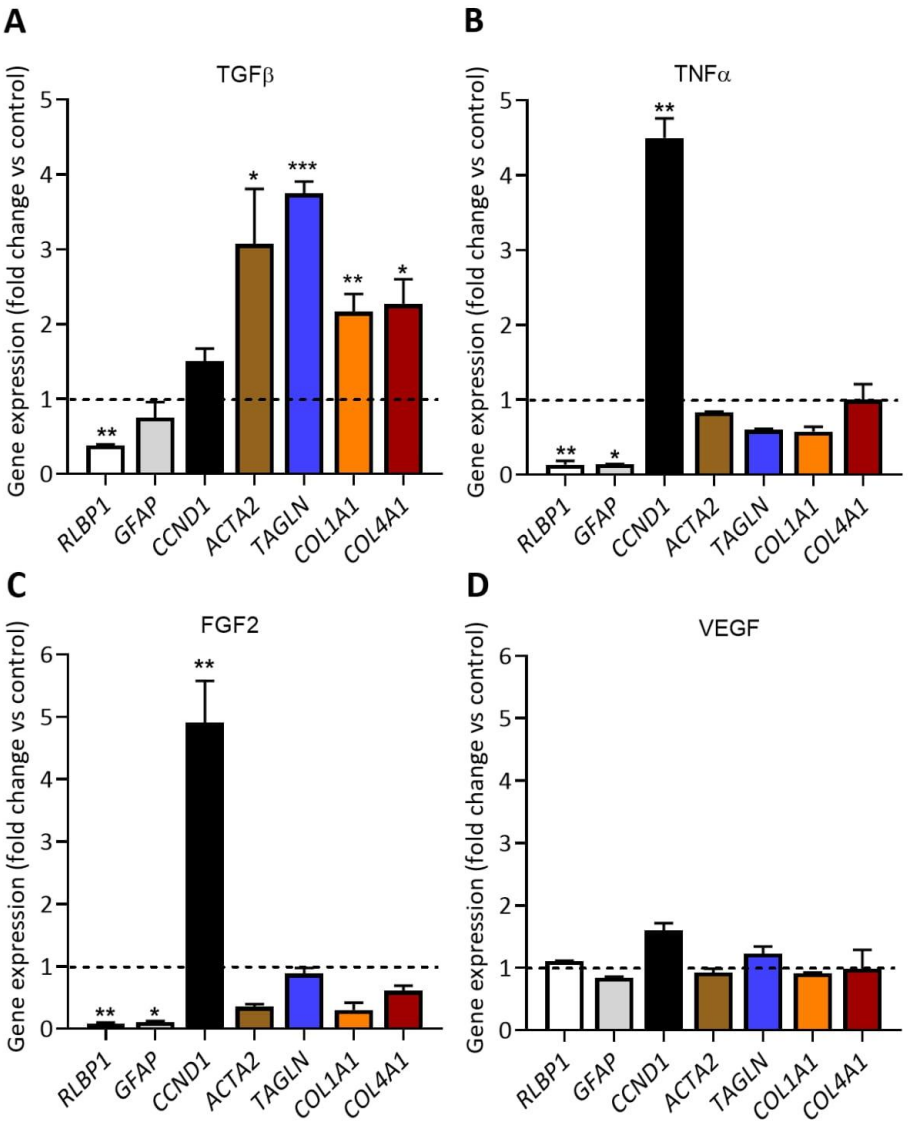

Supplementary Fig. 4. Effect of different cytokines/growth factors on MIO-M1 cells. MIO-M1 cells were treated for 24 hours with recombinant TGFβ, TNFα, FGF2, or VEGF (all at 30 ng/ml). Data (mean ± SEM of 3 determinations) were normalized to *GAPDH* levels and expressed as fold change in respect to untreated MIO-M1 cells. * $p < 0.05$, ** $p < 0.01$, and *** $p < 0.001$ *vs* untreated MIO-M1 cells, one-way ANOVA.

5

VEGF-INDEPENDENT ACTIVATION OF MÜLLER CELLS BY THE VITREOUS FROM PROLIFERATIVE DIABETIC RETINOPATHY PATIENTS

Proliferative diabetic retinopathy (PDR), a significant complication of diabetes mellitus, results from an inflammation-sustained interplay among endothelial cells, neurons, and glia. Even though anti-vascular endothelial growth factor (VEGF) interventions represent the therapeutic option for PDR, they are only partially efficacious. In PDR, Müller cells undergo reactive gliosis, produce inflammatory cytokines/chemokines, and contribute to scar formation and retinal neovascularization. However, the impact of anti-VEGF interventions on Müller cell activation has not been fully elucidated. Here, we show that treatment of MIO-M1 Müller cells with vitreous obtained from PDR patients stimulates cell proliferation and motility and activates various intracellular signaling pathways. The results show that PDR vitreous induces the acquisition of an activated phenotype in Müller cells, characterized by an increase of cell proliferation and migration, intracellular signaling activation, and proinflammatory cytokine/chemokine expression. Surprisingly, we found that the acquisition of this phenotype is not related to VEGF stimulation.

In contrast, fibroblast growth factor-2 (FGF2) induced a significant overexpression of various cytokines/chemokines in MIO-M1 cells. Accordingly, the anti-VEGF drug ranibizumab does not affect Müller cell activation mediated by PDR vitreous. In contrast, treatment with the FGF receptor (FGFR) tyrosine kinase inhibitor BGJ398, the pan-FGF trap NSC12, the multi-target heparin-binding protein antagonist N-tert-butyloxycarbonyl-Phe-Leu-Phe-Leu-Phe Boc2, or the anti-inflammatory drug hydrocortisone inhibits, at least in part, the activity of PDR vitreous samples. Together, these data point to a role for various mediators besides VEGF in the response elicited by PDR vitreous in Müller cells.

International Journal of
Molecular Sciences

MDPI

Article

VEGF-Independent Activation of Müller Cells by the Vitreous from Proliferative Diabetic Retinopathy Patients

Sara Rezzola [1,*], Jessica Guerra [1], Adwaid Manu Krishna Chandran [1], Alessandra Loda [1], Anna Cancarini [2], Piergiuseppe Sacristani [2], Francesco Semeraro [2] and Marco Presta [1,3,*]

[1] Department of Molecular and Translational Medicine, School of Medicine, University of Brescia, 25123 Brescia, Italy; j.guerra@unibs.it (J.G.); adwaid.krishna@unibs.it (A.M.K.C.); a.loda025@unibs.it (A.L.)
[2] Eye Clinic, Department of Neurological and Vision Sciences, University of Brescia, 25123 Brescia, Italy; acancarini@gmail.com (A.C.); piergiuseppe.sacristani@gmail.com (P.S.); francesco.semeraro@unibs.it (F.S.)
[3] Italian Consortium for Biotechnology (CIB), Unit of Brescia, 25123 Brescia, Italy
* Correspondence: sara.rezzola@unibs.it (S.R.); marco.presta@unibs.it (M.P.); Tel.: +39-030-3717311

Abstract: Proliferative diabetic retinopathy (PDR), a major complication of diabetes mellitus, results from an inflammation-sustained interplay among endothelial cells, neurons, and glia. Even though anti-vascular endothelial growth factor (VEGF) interventions represent the therapeutic option for PDR, they are only partially efficacious. In PDR, Müller cells undergo reactive gliosis, produce inflammatory cytokines/chemokines, and contribute to scar formation and retinal neovascularization. However, the impact of anti-VEGF interventions on Müller cell activation has not been fully elucidated. Here, we show that treatment of MIO-M1 Müller cells with vitreous obtained from PDR patients stimulates cell proliferation and motility, and activates various intracellular signaling pathways. This leads to cytokine/chemokine upregulation, a response that was not mimicked by treatment with recombinant VEGF nor inhibited by the anti-VEGF drug ranibizumab. In contrast, fibroblast growth factor-2 (FGF2) induced a significant overexpression of various cytokines/chemokines in MIO-M1 cells. In addition, the FGF receptor tyrosine kinase inhibitor BGJ398, the pan-FGF trap NSC12, the heparin-binding protein antagonist N-tert-butyloxycarbonyl-Phe-Leu-Phe-Leu-Phe Boc2, and the anti-inflammatory hydrocortisone all inhibited Müller cell activation mediated by PDR vitreous. These findings point to a role for various modulators beside VEGF in Müller cell activation and pave the way to the search for novel therapeutic strategies in PDR.

Keywords: diabetic retinopathy; inflammation; Müller cells; VEGF; vitreous humor

Citation: Rezzola, S.; Guerra, J.; Krishna Chandran, A.M.; Loda, A.; Cancarini, A.; Sacristani, P.; Semeraro, F.; Presta, M. VEGF-Independent Activation of Müller Cells by the Vitreous from Proliferative Diabetic Retinopathy Patients. *Int. J. Mol. Sci.* **2021**, *22*, 2179. https://doi.org/10.3390/ijms22042179

Academic Editor: Young Sook Kim

Received: 7 January 2021
Accepted: 19 February 2021
Published: 22 February 2021

1. Introduction

Proliferative diabetic retinopathy (PDR) is an ocular microvascular complication of diabetes [1]. Currently, it affects more than 93 million people in the world, and it represents the leading cause of acquired blindness in the working age population of industrialized regions [1]. PDR is considered as a multifactorial disease, albeit its pathogenesis is not yet fully understood. Indeed, numerous factors contribute to PDR development, including hyperglycemia, oxidative stress, inflammation, and hypoxia, leading to the damage of the vasculature, as well as of neurons and glial cells in the retina [2,3]. Anti-vascular endothelial growth factor (VEGF) drugs represent the pharmacologic option for PDR treatment to this day [4]. Even though anti-VEGF interventions have shown better outcomes than alternative treatments, limitations to anti-VEGF therapies do exist, including poor response in a significant percentage of patients [5–7]. Indeed, VEGF-driven pathways are only part of the complex machinery regulating angiogenesis and inflammation in the eye and the production of other factors may cause resistance to anti-VEGF therapies and limit their efficacy [8]. This creates an unmet need for a better understanding of the pathogenesis of PDR in order to develop more efficacious therapeutic strategies.

Müller cells represent the main glial population of the retina and provide structural support to the neuroretina, radially stretching across its entire thickness. They are the anatomical link between blood vessels and vitreous body, creating a micro-unit involved in the exchange of nourishing molecules and oxygen and in the maintenance of retinal homeostasis [9,10]. During PDR, high blood glucose levels may induce retinal dysfunctions caused by increased levels of oxidative stress, which triggers early neurodegeneration, activation of inflammatory responses, and abnormal neovessel formation [3]. Because of the pathological changes that occur in the retina during PDR, activated Müller cells may undergo reactive gliosis, a non-specific reactive response of glial cells to damage characterized by uncontrolled proliferation, migration, and increased expression of gliosis markers [11,12]. Moreover, Müller cells may undertake a fibrotic trans-differentiation, contributing to the formation of a fibrovascular epiretinal membrane (ERM), which can exert tractional forces on the retinal surface, thus causing retinal detachment [13,14]. In addition, activated Müller cells produce several cytokines and chemokines, contributing to the maintenance of the inflammatory environment, alteration of the blood–retinal barrier (BRB) integrity, and neovascularization [12,15,16].

The vitreous humor undergoes structural and molecular alterations during chronic diabetic conditions that may significantly impact the progression of PDR [3]. Thus, the vitreous obtained via pars plana vitrectomy from patients with PDR can represent a sort of receptacle where pro-angiogenic and proinflammatory mediators with pathological effects on retinal cells accumulate [3,17]. By mimicking the microenvironment facing the diabetic retina, PDR vitreous may therefore represent a valuable tool for a better understanding of the pathogenesis of PDR. Indeed, it has been demonstrated that PDR vitreous induces potent angiogenic and inflammatory responses in endothelial cells [3,18], suitable for the identification of novel pharmacological targets and the evaluation of the efficacy of new drug candidates [3,17–23].

Here, vitreous fluid obtained from PDR patients was used as a tool to investigate the activation that occurs in Müller cells during PDR. The results show that PDR vitreous induces the acquisition of an activated phenotype in Müller cells, characterized by an increase of cell proliferation and migration, intracellular signaling activation, and proinflammatory cytokine/chemokine expression. Surprisingly, we found that the acquisition of this phenotype is not related to VEGF stimulation, whereas treatment of Müller cells with basic fibroblast growth factor (FGF2), a prototypic member of the FGF family [24], induces a significant increase of the expression of various cytokines/chemokines in MIO-M1 cells. Accordingly, the anti-VEGF drug ranibizumab does not affect Müller cell activation mediated by PDR vitreous whereas treatment with the FGF receptor (FGFR) tyrosine kinase inhibitor BGJ398 [25], the pan-FGF trap NSC12 [26], the multi-target heparin-binding protein antagonist N-tert-butyloxycarbonyl-Phe-Leu-Phe-Leu-Phe Boc2 [20], or the anti-inflammatory drug hydrocortisone inhibits, at least in part, the activity of PDR vitreous samples. Together, these data point to a role for various mediators beside VEGF in the response elicited by PDR vitreous in Müller cells.

2. Results

2.1. MIO-M1 Müller Cells Are Activated by PDR Vitreous

In order to investigate the capacity of PDR vitreous to induce Müller cell activation, MIO-M1 cells were treated with vitreous samples, each pooled from 5–6 diabetic patients. As shown in Figure 1A,B, PDR vitreous stimulates MIO-M1 cell proliferation in a dose- and time-dependent manner. Moreover, it modulates Müller cell motility when assessed in an in vitro wound healing assay (Figure 1C). No significant stimulation of cell proliferation and motility was instead observed when Müller cells were treated with a pool of vitreous samples obtained from patients affected by rhegmatogenous retinal detachment (Figure S1). It must be pointed out that MIO-M1 cells were maintained in culture medium containing 25 mM glucose in these and all the following experiments, thus mimicking more closely a "diabetic-like" microenvironment when cells were treated with PDR vitreous.

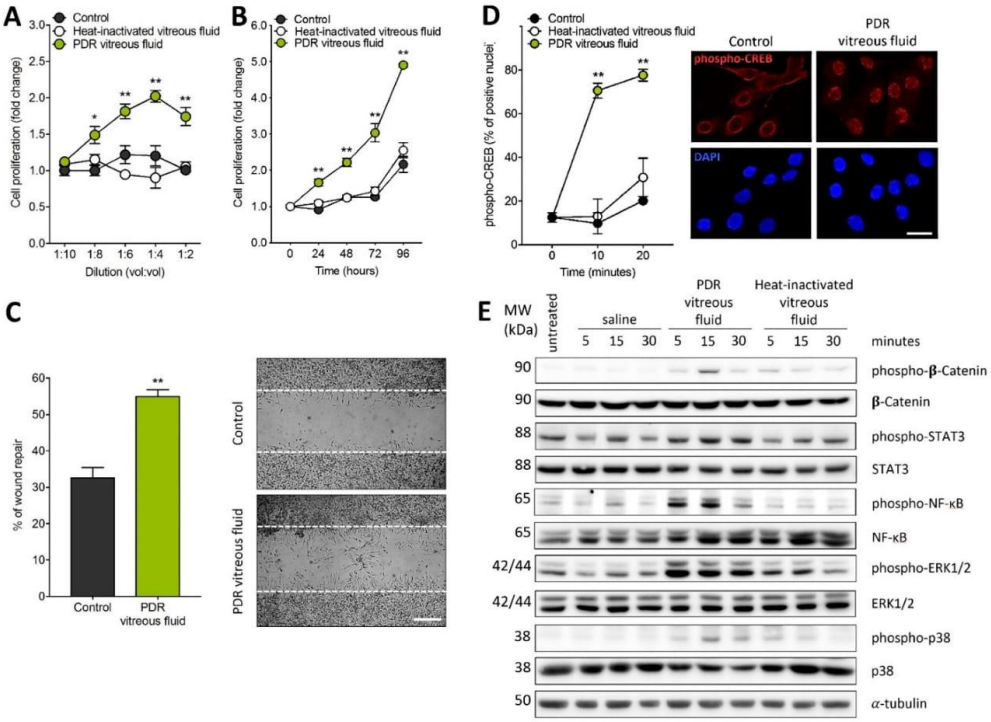

Figure 1. Müller cell activation by proliferative diabetic retinopathy (PDR) vitreous. (**A,B**) MIO-M1 cells were treated with increasing amounts of PDR or heat-inactivated vitreous samples (*vol:vol* dilution in cell culture medium) and counted 72 h thereafter (**A**) or were incubated with 1:4 vitreous dilution and counted at different time points (**B**). Cell proliferation was expressed as fold change in respect to the control. Data are the mean ± SD of 5 independent experiments. * $p < 0.05$ and ** $p < 0.01$ *vs.* control or heat-inactivated vitreous fluid, one-way ANOVA. (**C**) Wounded MIO-M1 monolayers were treated with PDR vitreous fluid. After 24 h, MIO-M1 cells invading the wounded area were quantified by computerized analysis of the digitalized images. Data are the mean ± SD of 2 independent experiments (8 microscopic fields per experimental point). ** $p < 0.01$ *vs.* control, Student's *t* test. Inset: representative images of the repaired area in control cells (upper panel) and PDR vitreous fluid-treated cells (lower panel). Scale bar = 500 μm. (**D**) MIO-M1 cells were treated with PDR or heat-inactivated vitreous samples. After 0–20 min, the percentage of phospho-CREB immunoreactive MIO-M1 nuclei were quantified ($n = 80$ cells per experimental point). ** $p < 0.01$ *vs.* control or heat-inactivated vitreous, one-way ANOVA. Inset: phospho-CREB immunoreactivity (red) in MIO-M1 cells at 10 min in control (left panels) and after PDR vitreous treatment (right panels); nuclei were stained with DAPI (blue). Data are representative of 2 independent experiments. Scale bar = 25 μm. (**E**) Western blot analysis of the phosphorylation of the signaling proteins β-catenin, STAT3, NF-κB, ERK1/2, and p38 in MIO-M1 cells following 0–30 min of stimulation with PDR or heat-inactivated vitreous samples. Data are representative of 2 independent experiments that gave similar results. MW, molecular weight. Densitometric analysis of the Western blot membranes is shown in Figure S2.

In keeping with its capacity to induce Müller cell activation, PDR vitreous induces the rapid nuclear translocation of the proinflammatory transcription factor phospho-cAMP-response element-binding protein (phospho-CREB) (Figure 1D). Accordingly, PDR vitreous rapidly triggers the phosphorylation of a variety of intracellular mediators, including β-catenin, STAT3, ERK1/2, p38, and nuclear factor kappa light chain enhancer of activated B cells (NF-κB) (Figure 1E).

In accordance with its capacity to trigger β-catenin and NF-κB activation, treatment with PDR vitreous induces the overexpression of the inflammasome nucleotide-binding oligomerization domain (NOD), leucine-rich repeat (LRR)-containing proteins 3 (*NLRP3*)

gene. In parallel, activated MIO-M1 cells upregulate the expression of the inflammatory mediators interleukin 1β (*IL1β*), *IL6*, *IL8*, interferon γ (*INFγ*), monocyte chemoattractant protein 1 (*MCP1*), tumor necrosis factor α (*TNFα*), and *VEGF-A* (Figure 2). No modulation was instead observed for *NLRP1*, *NLRP6*, *CASPASE1*, apoptosis-associated speck like protein (*ASC*), and *IL18* genes, or for *IL4*, *IL17*, and transforming growth factor β (*TGFβ*) (data not shown). In all the assays, negligible activity was exerted by heat-inactivated vitreous, pointing to a proteinaceous nature of the vitreal mediators responsible for the biological activity exerted by PDR vitreous on MIO-M1 cells. However, it is interesting to note that heat-inactivated vitreous retains a significant, even though limited, capacity to stimulate the expression of *NLRP3*, *IL8*, and *VEGF-A* in Müller cells (Figure 2), possibly due to the presence in PDR vitreous of non-proteinaceous components, including bioactive lipids or heat-stable cytokines like TGFβ [3]. Further studies will be required to clarify this point.

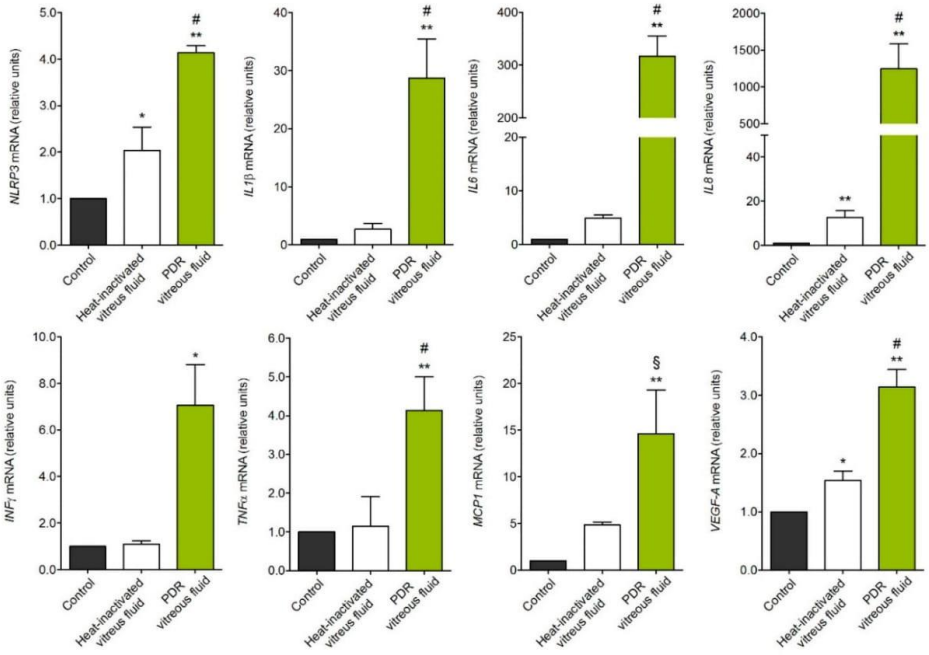

Figure 2. Gene expression analysis of PDR vitreous-activated Müller cells. qPCR analysis of MIO-M1 cells treated with PDR or heat-inactivated vitreous samples. *NLRP3*, *IL1β*, *IL6*, *IL8*, *INFγ*, *MCP1*, and *VEGF-A* expression levels were assessed 4 h after treatment, whereas *TNFα* expression was evaluated at 8 h. Data are representative of 3 independent experiments in triplicate that gave similar results and are expressed as relative units in respect to control. * $p < 0.05$ and ** $p < 0.01$ *vs.* control; § $p < 0.05$ and # $p < 0.01$ *vs.* heat-inactivated vitreous, one-way ANOVA.

2.2. PDR Vitreous-Induced Activation of Müller Cells Is Independent from VEGF

The major therapeutic target in PDR is represented by VEGF, which is thought to play a pivotal role in retinal inflammation, vascular leakage, and neovascularization [3]. To evaluate the effect of VEGF stimulation on Müller cells, MIO-M1 cells were treated with recombinant VEGF-A. As shown in Figure 3, VEGF treatment does not modulate the expression of the analyzed proinflammatory genes. These results prompted us to evaluate the effect of the anti-VEGF drug ranibizumab on PDR vitreous-mediated activation of Müller cells. To obtain a complete inhibition of the activity of VEGF, ranibizumab was administered to MIO-M1 cells at a concentration equal to 10 μM, consistent with the dose

currently used in clinical practice [27]. In keeping with the results obtained following treatment with recombinant VEGF-A, ranibizumab exerted only a negligible inhibitory effect on the activation of MIO-M1 cells induced by PDR vitreous (Figure 3).

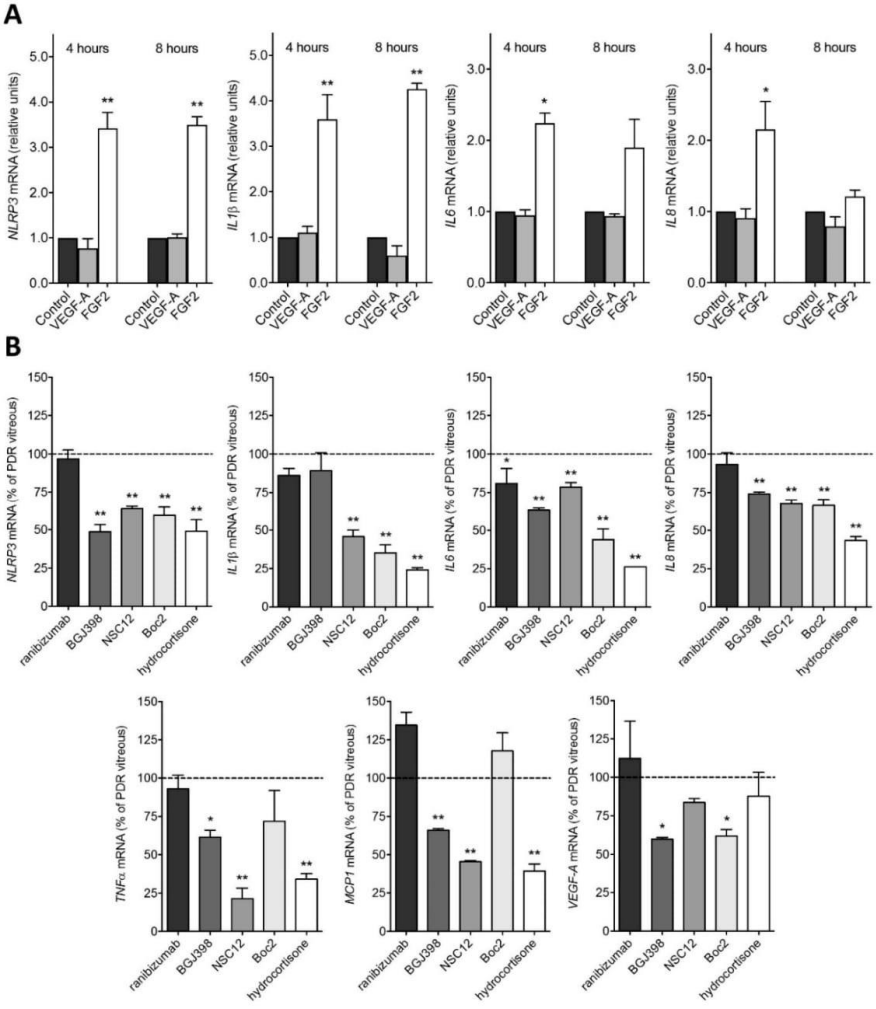

Figure 3. Inhibition of PDR vitreous-induced activation of MIO-M1 cells. (**A**) qPCR analysis of *NLRP3*, *IL1β*, *IL6*, and *IL8* expression in MIO-M1 cells treated with recombinant human VEGF-A or FGF2 for 4 and 8 h. Data are representative of 2 independent experiments in triplicate that gave similar results and are expressed as relative units in respect to control. * $p < 0.05$ and ** $p < 0.01$ *vs.* control or VEGF-A, one-way ANOVA. (**B**) qPCR analysis of *NLRP3*, *IL1β*, *IL6*, *IL8*, *TNFα*, *MCP1*, and *VEGF-A* expression in MIO-M1 cells treated with PDR vitreous for 4 h in the absence or in the presence of 10 μM ranibizumab, 100 nM BGJ398, 10 μM NSC12, 60 μM Boc2, or 10 μM hydrocortisone. Data are representative of 2 independent experiments in triplicate that gave similar results and are expressed as % in respect to PDR vitreous stimulation. * $p < 0.05$ and ** $p < 0.01$ *vs.* PDR vitreous, one-way ANOVA.

Based on these observations, we investigated the expression and activation of VEGFRs in MIO-M1 cells. As shown in Figure 4A, MIO-M1 cells express *VEGFR2* transcripts at levels similar to those detected in human umbilical vein endothelial cells (HUVECs) whereas they fail to express significant levels of *VEGFR1* and *VEGFR3*. However, Western blot analysis of

the cell extracts demonstrate that VEGFR2 protein is present at negligible levels in MIO-M1 cells when compared to HUVECs (Figure 4C). Accordingly, VEGF treatment induces a rapid VEGFR2 phosphorylation and ERK1/2 activation in HUVECs, but not in MIO-M1 cells (Figure 4B,C). Together, these data confirm that MIO-M1 cells are irresponsive to VEGF stimulation in our experimental conditions.

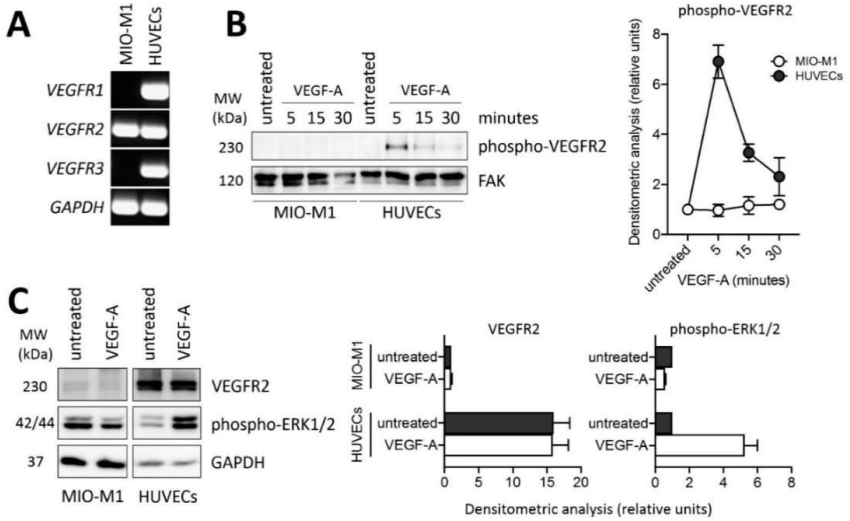

Figure 4. VEGFR2 expression and lack of response in MIO-M1 cells. (**A**) Semi-quantitative RT-PCR analysis of *VEGFR1*, *VEGFR2*, and *VEGFR3* expression in MIO-M1 cells and in human umbilical vein endothelial cells (HUVECs). Data are representative of 2 independent experiments that gave similar results. (**B**) Western blot analysis of VEGFR2 phosphorylation following 0–30 min of stimulation with 30 ng/mL VEGF-A in MIO-M1 cells and HUVECs. Densitometric analysis is shown in the right panel. Data are the mean ± SD of 2 independent experiments. (**C**) Western blot analysis of VEGFR2 protein levels and ERK1/2 phosphorylation following 10 min of stimulation with 30 ng/mL VEGF-A in MIO-M1 cells and HUVECs. Densitometric analysis is shown in the right and far right panel, respectively. Data are the mean ± SD of 2 independent experiments. MW, molecular weight.

FGF2 is the prototypic member of the heparin-binding FGF family [24]. Previous observations showed that FGF2 may induce proliferation and gliotic responses in Müller cells [28]. Accordingly, in contrast with recombinant VEGF-A, recombinant FGF2 induces the overexpression of *NLRP3*, *IL1β*, *IL6*, and *IL8* in MIO-M1 cells, even though to a limited extent when compared to the effect exerted by PDR vitreous (Figure 3). In keeping with these findings, the ATP-competitive tyrosine kinase FGF receptor (FGFR) inhibitor BGJ398 [25] exerts a significant, though partial, inhibition of the overexpression of the proinflammatory genes upregulated by PDR vitreous when administered to MIO-M1 cells at 100 nM, a concentration selective for FGFR1-3 and ineffective for VEGF receptor-2 and various other tyrosine kinase receptors [25] (Figure 3). Similar results were obtained by treating MIO-M1 cells with PDR vitreous in the presence of NSC12, a small FGF-trap molecule which is able to bind and inhibit the activity of all the members of the FGF family [26] (Figure 3). Together, these data raise the hypothesis that stimulation of the FGF/FGFR system triggered by FGF2 and/or by other members of the FGF family may contribute, at least in part, to the activation of Müller cells by PDR vitreous.

Recent observations from our laboratory have shown that the peptide N-tert-butyloxy carbonyl-Phe-Leu-Phe-Leu-Phe (Boc2), widely used as a pan-formyl peptide receptor (FPR) antagonist [29], hampers the angio-inflammatory responses mediated by PDR vitreous on endothelial cells [18]. This FPR-independent effect is due to the capacity of Boc2 to inhibit the binding of a variety of heparin-binding cytokines/growth factors to heparin (including

the heparin-binding VEGF-A_{165} isoform, FGF2, connective tissue growth factor, stromal cell-derived factor-1, placenta-derived growth factor-2, high mobility group box-1, platelet-derived growth factor-BB (PDGF-BB), and hepatocyte growth factor), thus preventing their interaction with cell surface heparan-sulphate proteoglycans and cognate receptors [20]. On this basis, in order to assess the effect exerted by a multi-target growth factor/cytokine inhibitor on the activation triggered by PDR vitreous on Müller cells, MIO-M1 cells were incubated with PDR vitreous samples in the absence or in the presence of Boc2. As shown in Figure 3, Boc2 inhibits the upregulation of *NLRP3*, *IL1β*, *IL6*, *IL8*, and *VEGF-A* expression induced by PDR vitreous, whereas it has no effect on the modulation of *TNFα* and *MCP1*.

Various proinflammatory cytokines/chemokines have been detected in PDR vitreous (see [3] and references therein) that are endowed with the capacity to activate Müller cells [30–32]. Glucocorticoid receptor signaling exerts an anti-inflammatory action in Müller cells via the modulation of the activity of various transcription factors, including STAT3 and NF-κB (reviewed in [33]). Accordingly, the anti-inflammatory steroid drug hydrocortisone prevented to a significant extent the upregulation of NLRP3, IL1β, IL6, IL8, and VEGF-A that occurs in MIO-M1 cells treated with PDR vitreous (Figure 3). Altogether, these observations point to a role for various vitreal modulators beside VEGF in Müller cell activation during PDR.

3. Discussion

The role of retinal glial cells in the pathogenesis of PDR has been thoroughly described [11,12]. In the early stages of DR, Müller cells become hyperactive and start to produce and release angiogenic and neurotrophic factors in order to protect the retina from the insult consequent to the high glucose conditions. However, this response may establish over time an inflammatory milieu that further triggers Müller cell activation and neovascular events typical of the later stages of PDR [11–16]. In this frame, the understanding of the reactive responses of Müller cells and of their protective/detrimental effects in PDR is of pivotal importance to bring new therapeutic strategies to patients.

Here, PDR vitreous humor obtained from diabetic patients after pars plana vitrectomy was used as a tool to explore the activation that occurs in Müller cells during PDR. Previous observations have shown that high glucose concentrations may cause the upregulation of various cytokines in Müller cells [31,34–36]. In our work, all experiments were performed with MIO-M1 cells maintained in culture medium containing 25 mM glucose, thus mimicking more closely a "diabetic-like" microenvironment when cells were treated with PDR vitreous. The results show that PDR vitreous stimulates MIO-M1 cell proliferation and motility, hallmarks of the gliotic response that characterizes Müller cells [11] and may contribute to ERM formation in PDR patients [37]. No significant stimulation was instead exerted by the vitreous obtained from patients affected by rhegmatogenous retinal detachment, pointing to a specificity of the effect. Accordingly, vitreous samples collected from patients undergoing vitrectomy for diabetic and non-diabetic retinal disorders have shown a different ability to drive the contractile activity of Müller cells, PDR vitreous samples being the most effective (reviewed in [37]). Further studies will be required to assess whether the activation observed in MIO-M1 cells following treatment with PDR vitreous can be induced, and to which extent, by vitreous samples obtained from patients affected by other retinal disorders in which Müller cells may exert a pathogenic role, including macular hole and idiopathic ERM [37–39]. Relevant to this point, preliminary observations on a limited set of samples indicate that vitreous from PDR patients with ERM may exert a more potent mitogenic response in MIO-M1 cells when compared to samples from PDR patients without ERM, with no significant difference in their capacity to exert a motogenic stimulus in these cells (data not shown). Analysis of a large cohort of patients will be required to confirm these findings.

Phospho-CREB accumulates in the nucleus of Müller cells in response to acute retinal damage, where it participates in glia de-differentiation, proliferation, and modulation of gene expression [40,41]. Consistent with this observation, treatment with PDR vitreous

causes the rapid nuclear translocation of phospho-CREB in MIO-M1 cells. In addition, PDR vitreous induces the phosphorylation of the intracellular mediators β-catenin, STAT3, p38, ERK1/2, and NF-κB, and upregulates the expression of various proinflammatory cytokines/chemokines, including *IL1β*, *IL6*, *IL8*, *INFγ*, *TNFα*, *MCP1*, and *VEGF-A*. This goes in parallel with the upregulation of *NLRP3*, a key component of the NLRP3 inflammasome [42]. These data extend previous observations about the uncontrolled release of IL1β, IL6, and MCP1 by microglial and macroglial cells in diabetic and Akimba animal models [11,43–45] and the putative role of NLRP3 inflammasome in PDR [44,46,47].

The activity of the NLRP3 inflammasome is mediated at the transcriptional level (priming) by NF-κB activation and at the post-transcriptional level (activation) by a variety of stimuli (reviewed in [48]). Previous observations have shown that tyrosine kinase signaling might exert both stimulatory and inhibitory effects on the activation of the NLRP3 inflammasome [48,49]. Accordingly, our data demonstrate that FGF2 induces NLRP3 upregulation in Müller cells that express high levels of *FGFR1* and *FGFR2* mRNAs and low levels of *FGFR3* transcript under our experimental conditions (Figure S3B). In addition, the selective FGFR tyrosine kinase inhibitor BGJ398 [25] and the pan-FGF trap NSC12 [26] inhibit *NLRP3* upregulation triggered by PDR vitreous in these cells. A similar inhibitory effect was observed following incubation of PDR vitreous-treated MIO-M1 cells with the pan-heparin-binding protein inhibitor Boc2 or with hydrocortisone. In contrast with FGF2, VEGF does not affect *NRLP3* expression in MIO-M1 cells and the anti-VEGF drug ranibizumab does not prevent the upregulation of *NLRP3* in PDR vitreous-treated MIO-M1 cells. These data point to a role for the FGF/FGFR system and possibly for other mediators, but not VEGF, in NLRP3 inflammasome activation in Müller cells during PDR.

As observed for *NLRP3* expression, our data demonstrate that VEGF-A is unable to induce the upregulation of various proinflammatory cytokines/chemokines in MIO-M1 cells. Accordingly, the anti-VEGF drug ranibizumab does not affect the capacity of PDR vitreous to trigger an inflammatory response in Müller cells when administered at 10 μM, the intravitreal concentration commonly used in the clinical practice [27]. It is worth noticing that similar results were obtained also on endothelial cells, where anti-VEGF drugs showed a limited capacity to hamper the pro-angiogenic/proinflammatory responses induced by PDR vitreous in these cells [18,21]. It must be pointed out that the vitreous samples utilized for our experiments were collected only from PDR patients that received the last drug injection at least 15 days before vitrectomy. Given the intravitreal half-life of anti-VEGF drugs (approx. 5–7 days [50]), the residual levels of the drug in these samples do not affect the activity nor the response of PDR vitreous to anti-VEGF interventions when tested on endothelial cells [19].

No matter the presence of VEGF in PDR vitreous, our results indicate that VEGFR2 protein is present at negligible levels in MIO-M1 cells under our experimental conditions, no VEGFR2 phosphorylation and ERK1/2 activation being observed following VEGF treatment. This occurs despite the levels of *VEGFR2* transcripts being similar to those detected in HUVECs, a prototypic cell type responsive to the VEGF/VEGFR2 axis. This apparent discrepancy may be due to an inefficient translation or instability of the *VEGFR2* transcripts or to an increase in VEGFR2 protein degradation by the ubiquitin/proteasome pathway in MIO-M1 cells when compared to HUVECs. Previous observations had shown the presence of the VEGFR2 protein in Müller cells of rat and murine retina, VEGF neutralization or *Vegfr2* disruption under diabetic conditions leading to Müller cell apoptosis in the two animal models, respectively [51,52]. On the other hand, treatment of MIO-M1 cells with anti-VEGF agents have led to contrasting results with modest or no effect on cell viability/apoptosis [53,54]. Further experiments are required to fully elucidate the role of the VEGF/VEGFR2 system in Müller cells.

A variety of pro-angiogenic/proinflammatory mediators beside VEGF accumulate in the vitreous of PDR patients during disease progression (see [3] and references therein). FGF2 has been detected in ERMs [55–57] and pro-inflammatory mediators can induce FGF2 expression in Müller cells [58,59]. Conversely, FGF2 may trigger proliferation and gliotic

responses in these cells [28]. Here, we extend these findings by showing that recombinant FGF2 induces the upregulation of proinflammatory genes in MIO-M1 cells. In keeping with this observation, the FGFR tyrosine kinase inhibitor BGJ398 and the pan-FGF trap NSC12 partially inhibit the activation of MIO-M1 cells by PDR vitreous, thus suggesting that the deregulation of the FGF/FGFR system may play a role in Müller cell activation during PDR. FGF2 is the prototypic member of the canonical FGF family that includes the FGF subfamilies FGF1/2/5, FGF3/4/6, FGF7/10/22, FGF8/17/18, and FGF9/16/20 [60] which are able to induce angiogenic, fibrogenic, and inflammatory responses under various pathological conditions [61]. Together, our data indicate that one or more members of the FGF family are present in PDR vitreous and may contribute to its capacity to trigger a proinflammatory response in MIO-M1 cells. Previous observations have shown the capacity of the FGF/FGFR system to activate the canonical WNT/β-catenin pathway via ERK-MAP kinase signaling [62]. In turn, β-catenin may promote NLRP3 inflammasome activation [63]. Further studies will be required to identify the bioactive vitreal member(s) of the FGF family present in PDR vitreous and to fully dissect the FGF/FGFR-dependent signaling leading to the activation of a putative β-catenin/NF-κB/NLRP3 inflammasome pathway in Müller cells.

Finally, the capacity of the multi-target heparin-binding protein antagonist Boc2 and of the anti-inflammatory agent hydrocortisone to inhibit MIO-M1 cell activation triggered by PDR vitreous indicates that other yet unidentified heparin-binding growth factors and inflammatory cytokines may contribute to Müller cell activation. For instance, TGFβ-1 induces glial-to-mesenchymal transition in Müller cells [64], PDGF acts as an autocrine modulator for Müller cells [65,66], and insulin-like growth factor-1 can induce Müller cell proliferation and contractility [65,67,68]. In addition, Müller cells may proliferate in response to the pro-inflammatory cytokine TNFα [32], and IL1β stimulation mediates the upregulation of CCL2, CXCL1, CXCL10, and IL8 chemokines [30,69], as well as the overexpression of IL6 in MIO-M1 cells [31].

Clinical observations demonstrate that anti-VEGF approaches are only partially efficacious for the treatment of PDR patients [5–7]. Based on the evidence that anti-VEGF drugs show only a limited effect on the activity exerted by PDR vitreous on Müller cells and endothelial cells [18,21], our results indicate that the characterization of novel drug candidates with different mechanisms of action may contribute, in association with anti-VEGF interventions, to the development of more efficacious therapeutic approaches in PDR.

4. Materials and Methods

4.1. Reagents

Dulbecco's modified Eagle medium (DMEM) medium, M199 medium, fetal calf serum (FCS), and SYBR Green PCR master mix were from GIBCO Life Technologies (Grand Island, NY, USA). Endothelial cell growth factor, porcine heparin, penicillin, streptomycin, Triton-X100, BriJ, sodium orthovanadate, protease inhibitor cocktail, 4′,6-diamidino-2-phenylindole (DAPI), hydrocortisone, and anti-α-tubulin antibody were from Sigma-Aldrich (St. Louis, MO, USA). Bradford reagent, enhanced chemiluminescence reagent, and iTaq Universal Syber Green Supermix were from Bio-Rad Laboratories (Hercules, CA, USA). PVP-free polycarbonate filters were obtained from Costar (Cambridge, MA, USA). TRIzol Reagent, Moloney murine leukemia virus (MMLV) reverse transcriptase, anti-phospho-VEGFR2 (pTyr1175), and anti-focal adhesion kinase (FAK) antibodies were from Invitrogen (Carlsbad, CA, USA). ReliaPrep™ RNA Miniprep System was from Promega (Madison, WI, USA). Anti-phospho-NF-κB (pSer311), anti-NF-κB, anti-phospho-STAT3 (pSer727), anti-STAT3, anti-GAPDH, anti-mouse-horseradish peroxidase (HRP), and anti-rabbit-HRP antibodies were from Santa Cruz Biotechnologies (Santa Cruz, CA, USA). Anti-phospho-CREB (pSer133), anti-phospho-β-catenin (pSer552), anti-β-catenin, anti-phospho-ERK1/2 (pThr202/Tyr204), anti-ERK1/2, anti-phospho-p38 (pThr180/pTyr182), anti-p38, and anti-VEGFR2 antibodies were from Cell Signaling Technology (Beverly, MA, USA). Chicken anti-rabbit Alexa Fluor 594 antibody was from Molecular Probes (Eugene,

OR, USA). Boc2 was from Phoenix Europe GmbH (Karlsruhe, Germany). Ranibizumab (Lucentis©) was from Novartis (Horsham, UK). BGJ398 was from Selleckchem (Houston, TX, USA). Recombinant human FGF2 was from Tecnogen (Caserta, Italy). Recombinant human VEGF-A (VEGF-A_{165} isoform) was kindly provided by Dr. K. Ballmer-Hofer (PSI, Villigen, Switzerland). Human dermal fibroblast cDNA was kindly provided by Dr. M. Ritelli (University of Brescia, Brescia, Italy). NSC12 was kindly provided by Dr. M. Mor (University of Parma, Parma, Italy).

4.2. Human Vitreous Fluid Samples

PDR patients (Table 1) underwent *pars plana* vitrectomy at the Clinics of Ophthalmology (University of Brescia) during the period November 2018–August 2020. Samples were stored at −80 °C. All assays were performed on vitreous samples pooled at random from 5–6 patients. Heat-inactivated vitreous samples were prepared by incubating vitreous pools for 20 min at 95 °C. Pools of vitreous samples obtained from patients affected by rhegmatogenous retinal detachment were used as control.

Table 1. PDR patients. Data are n unless indicated otherwise and are expressed as mean ± SD.

Patients/Eyes	39/42
Clinical features	
Gender (male/female)	28/11
Age (years)	65 ± 10
Type 1/type 2 diabetes	4/35
Duration of diabetes (years)	21 ± 6
Oral hypoglycemic drug treatment	10/39
Insulin treatment	10/39
Oral hypoglycemic drug + insulin treatment	19/39
Glycaemia (mg/dL)	161 ± 56
HbA1c (%)	7.9 ± 1.1
Neuropathy	6/39
Nephropathy	13/39
Cardiopathy	15/39
Hypertension	37/39
Dyslipidemia	23/39
Triglycerides (mg/dL)	120 ± 54
Cholesterol (mg/dL)	153 ± 44
Creatinine (mg/dL)	1.4 ± 0.7
Hemoglobin (g/dL)	13.1 ± 1.6
Ophthalmic features	
PDR	42/42
PDR with vitreous hemorrhage	19/42
PDR with macular edema	19/42
PDR with ERM	31/38
Ocular therapies	
Intravitreal injection of anti-VEGF blocker	29/42
Panretinal laser photocoagulation	32/42

Abbreviations: ERM: epiretinal membranes; PDR: proliferative diabetic retinopathy; VEGF: vascular endothelial growth factor.

4.3. Cell Cultures

The human Müller cell line Moorfields/Institute of Ophthalmology-Müller 1 (MIO-M1) was obtained from the UCL Institute of Ophthalmology, London, UK [70]. MIO-M1 cells were immediately amplified and stock aliquots were frozen in liquid nitrogen. After thawing, cells were used for no more than 4–5 passages. MIO-M1 cells were grown in DMEM with 4.5 g/L glucose plus 10% FCS and 1.0 mM glutamine. Cells were maintained in a humidified 5% CO_2 incubator at 37 °C, with medium replaced every 2–3 days until cells reached confluency. Cells were tested regularly for *Mycoplasma* negativity. When compared to human dermal fibroblasts by quantitative PCR (qPCR) analysis, these cells express high levels of the Müller cell markers *vimentin* (*VIM*) and *retinaldehyde binding protein 1* (*RLBP1*, encoding for cellular retinaldehyde binding protein CRALBP) and negligible levels of the *actin α 2* (*ACTA2*) and *S100 calcium-binding protein A4* (*S100A4*) fibroblast markers, encoding for α-smooth muscle actin (α-SMA) and fibroblast-specific protein 1 (S100), respectively (Figure S3A). HUVECs were isolated from human umbilical cords and grown in M199 medium supplemented with 20% FCS, endothelial cell growth factor (100 µg/mL), and porcine heparin (50 µg/mL) as previously described [71].

4.4. MIO-M1 Proliferation Assay

MIO-M1 cells were seeded at 5000 cells/cm^2 in DMEM plus 2.0% FCS. After 3 days, cells were treated with increasing amounts of saline or vitreous diluted in culture medium. After 24, 48, 72, or 96 h, cells were detached with trypsin, suspended in 200 µL of PBS plus 5.0% FCS, and counted with a MACSQuant cytofluorimeter (Milteny Biotec).

4.5. MIO-M1 Wound Healing Assay

MIO-M1 cells were seeded at 100,000 cells/cm^2 in DMEM plus 2.0% FCS. After 3 days, MIO-M1 cell monolayers were scratched with a 200 µL tip to obtain a 2-mm-thick denuded area and cultured in the presence of saline or PDR vitreous diluted 1:4 with culture medium. After 24 h, wounded monolayers were photographed, and the percentage of repaired area was quantified with Fiji software [72].

4.6. Western Blot Analysis

MIO-M1 cells were seeded at 50,000 cells/cm^2 in DMEM *plus* 2.0% FCS. After 3 days of starvation, cells were treated for 0–30 min with saline, 30 ng/mL VEGF or vitreous fluid diluted 1:4 with culture medium. After treatment, cells were lysed in 50 mM Tris–HCl 150 mM NaCl buffer (pH 7.4) containing 1.0% Triton-X100, 0.1% BriJ, 1.0 mM sodium orthovanadate, and protease inhibitor cocktail. Aliquots of each sample containing equal amount of proteins (15–30 µg) were subjected to SDS-PAGE. Gels were transblotted onto a PVDF membrane and blots were blocked with 1.0% BSA for 1 h at room temperature. Western blotting analysis was performed with anti-phospho-β-catenin, anti-β-catenin, anti-phospo-ERK1/2, anti-ERK1/2, anti-phospho-NF-κB, anti-NF-κB, anti-phospho-p38, anti-p38, anti-phospho-STAT3, anti-STAT3, anti-phospho-VEGFR2, anti-VEGFR2, anti-α-tubulin, anti-FAK, or anti-GAPDH antibodies (1:1000). After treating the membranes with appropriate secondary HRP-labeled secondary antibody (1:5000), blots were developed with enhanced chemiluminescence reagent. Images were acquired using a ChemiDoc Touch instrument and band intensity was evaluated with Image Lab 3.0 software (Bio-Rad Laboratories). When specified, MIO-M1 cells were compared to HUVECs for VEGFR2 expression and activation as previously described [73].

4.7. RT-PCR Analyses

Semi-quantitative RT-PCR was used to analyze FGFR1-4 and VEGFR1-3 expression in MIO-M1 cells. To this aim, total RNA was isolated from MIO-M1 cells after 3 days of starvation in DMEM plus 2.0% FCS using TRIzol® Reagent according to manufacturers' instruction. A total of 2.0 µg of total RNA was retro-transcribed with MMLV reverse transcriptase using random hexaprimers in a final 20 µL volume. Then, 1/10th of the

reaction was analyzed by semi-quantitative RT-PCR using the primers listed in Table 2. The PCR products were electrophoresed on a 1.5% agarose gel and visualized by ethidium bromide staining. When specified, MIO-M1 cells were compared to HUVECs for VEGFR expression.

Table 2. Oligonucleotide primers used for RT-PCR analysis.

Gene	Forward	Reverse
ACTA2	5′-AATGGCTCTGGGCTCTGTAA-3′	5′-TTTTGCTCTGTGCTTCGTCA-3′
FGFR1	5′-GGGCTGGAATACTGCTACAA-3′	5′-GCCAAAGTCTGCTATCTTCATC-3′
FGFR2	5′-GGATAACAACACGCCTCTCTT-3′	5′-GCCCAAAGCAACCTTCTC-3′
FGFR3	5′-TGGTGTCCTGTGCCTACC-3′	5′-CCGTTGGTCGTCTTCTTGT-3′
FGFR4	5′-AACCGCATTGGAGGCATT-3′	5′-TCTACCAGGCAGGTGTATGT-3′
GAPDH	5′-GAAGGTCGGAGTCAACGGATT-3′	5′-TGACGGTGCCATGGAATTTG-3′
IL1β	5′-GTGGCAATGAGGATGACTTG-3′	5′-GTGGTGGTCGGAGATTCGTA-3′
IL6	5′-TGTGTGGGTCTGTTGTAGGG-3′	5′-CCCGTGCAATATCTAGGAAAA-3′
IL8	5′-TGTGTGGGTCTGTTGTAGGG-3′	5′-CCCGTGCAATATCTAGGAAAA-3′
INFγ	5′-GCAGGTCATTCAGATGTAGCGG-3′	5′-CCACACTCTTTTGGATGCTCTGG-3′
MCP1	5′-CTCAGCCAGATGCAATCAA-3′	5′-CACTTCTGCTTGGGGTCA-3′
NLRP3	5′-GGACTGAAGCACCTGTTGTGCA-3′	5′-TCCTGAGTCTCCCAAGGCATTC-3′
RLBP1	5′-GCTGCTGGAGAATGAGGAAA-3′	5′-TGGTGGATGAAGTGGATGG-3′
S100A4	5′-CCTGGATGTGATGGTGTCC-3′	5′-TCGTTGTCCCTGTTGCTGT-3′
TNFα	5′-TGCTTGTTCCTCAGCCTCTT-3′	5′-GCTTGTCACTCGGGGTTC-3′
VEGF-A	5′-AATCGAGACCCTGGTGGAC-3′	5′-GGTGAGGTTTGATCCGCATA-3′
VEGFR1	5′-AGCAGTTCCACCACTTTAGA-3′	5′-GAACTTTCCACAGAGCCCTT-3′
VEGFR2	5′-GGAAATGACACTGGAGCCTA-3′	5′-TTTGAAATGGACCCGAGACA-3′
VEGFR3	5′-CAACGACCTACAAAGGCTCT-3′	5′-GTAAAACACCTGGCCTCCTC-3′
VIM	5′-CGCCAGATGCGTGAAATG-3′	5′-ACCAGAGGGAGTGAATCCAGA-3′

Abbreviations. *ACTA2*: actin α 2; *FGFR*: fibroblast growth factor receptor; *GAPDH*: glyceraldehyde-3-phosphate dehydrogenase; *IL*: interleukin; *INFγ*: interferon γ; *MCP1*: monocyte chemoattractant protein 1; *NLRP3*: nucleotide-binding oligomerization domain (NOD), leucine-rich repeat (LRR)-containing proteins 3; *RLBP1*: retinaldehyde-binding protein 1; *S100A4*: S100 calcium-binding protein A4; *TNFα*: tumor necrosis factor α; *VEGF-A*: vascular endothelial growth factor-A; *VEGFR*: vascular endothelial growth factor receptor; *VIM*: vimentin.

For qPCR analysis, MIO-M1 cells were seeded at 50,000 cells/cm^2 in DMEM plus 2.0% FCS. After 3 days of starvation, cells were treated for 4 h or 8 h with 30 ng/mL VEGF-A, 30 ng/mL FGF2, saline, or vitreous diluted 1:4 with culture medium in the absence or in the presence of 10 μM ranibizumab, 100 nM BGJ398, 10 μM NSC12, 60 μM Boc2, or 10 μM hydrocortisone. Total RNA was isolated using TRIzol® Reagent and ReliaPrep™ RNA Miniprep System according to manufacturers' instructions. Then, 2.0 μg of total RNA was retrotranscribed and 1/10th of the retrotranscribed cDNA was used for qPCR that was performed with the ViiA 7 Real-Time PCR System (ThermoFisher) using iTaq Universal Syber Green Supermix according to the manufacturer's instructions. Samples were analyzed in triplicate using the oligonucleotide primers listed in Table 2 and data were normalized to the levels of GAPDH expression.

4.8. MIO-M1 Immunofluorescence Analysis

A total of 50,000 cells/cm^2 was seeded on μ-slide 8-well chambers (Ibidi) in DMEM plus 2.0% FCS. After 3 days of starvation, cells were treated for 0–30 min with saline or vitreous diluted 1:4 with culture medium, fixed in cold methanol, permeabilized with 0.2% Triton-X100, and saturated with 3.0% BSA in PBS (blocking solution). Then, cells were incubated overnight at 4 °C with anti-phospho-CREB antibody (1:800 in blocking solution) and for 1 more hour at room temperature with an anti-rabbit Alexa Fluor 594 secondary antibody (1:500 in blocking solution). Nuclei were counterstained with DAPI and cells were photographed using a Zeiss Axiovert 200M epifluorescence microscope equipped with Apotome and a Plan-Apochromat ×63/1.4 NA oil objective.

4.9. Statistical Analysis

Data are expressed as mean ± SD. Statistical significance was evaluated with the GraphPad Prism 7 software (San Diego, CA, USA) using Student's t test or one-way ANOVA followed by Bonferroni multiple comparison post-test to test the probability of significant differences between 2 or more groups of samples, respectively. Differences were considered significant when p value < 0.05.

Supplementary Materials: The following is available online at https://www.mdpi.com/1422-0067/22/4/2179/s1. Figure S1: Retinal detachment vitreous fluid does not activate MIO-M1 Müller cells; Figure S2: Müller cell signaling activated by PDR vitreous; Figure S3: Molecular characterization of MIO-M1 Müller cells.

Author Contributions: Conceptualization, S.R. and M.P.; investigation, S.R., J.G., A.M.K.C., A.L.; resources, A.C., P.S., F.S.; data curation, S.R. and M.P.; validation, S.R. and M.P.; writing—original draft preparation, S.R. and M.P.; writing—review and editing, S.R., F.S., M.P.; visualization, S.R.; supervision, M.P.; project administration, M.P.; funding acquisition, S.R., F.S., M.P. All authors have read and agreed to the published version of the manuscript.

Funding: This research was funded by Fondazione Diabete Ricerca to S.R. and by Associazione Italiana per la Ricerca sul Cancro, grant number IG 2019 n° 23116 to M.P. SR was supported by Fondazione Umberto Veronesi and by Associazione Garda Vita (R. Tosoni) fellowships.

Institutional Review Board Statement: The study was conducted according to the guidelines of the Declaration of Helsinki, and approved by the Institutional Review of Spedali Civili of Brescia (protocol code NP1276, 6 February 2013).

Informed Consent Statement: Informed consent was obtained from all subjects involved in the study.

Data Availability Statement: The data that support the findings of this study are available from the corresponding authors upon reasonable request.

Acknowledgments: The authors wish to thank D. Bosisio (University of Brescia, Brescia, Italy) for helpful suggestions and criticisms.

Conflicts of Interest: The authors declare no conflict of interest.

Abbreviations

ACTA2	actin α 2
ERM	epiretinal membrane
FGF2	basic fibroblast growth factor
FGFR	fibroblast growth factor receptor
GAPDH	glyceraldehyde-3-phosphate dehydrogenase
HUVECs	human umbilical vein endothelial cells
IL	interleukin
INFγ	interferon γ
MCP1	monocyte chemoattractant protein 1
NLRP3	nucleotide-binding oligomerization domain (NOD), leucine-rich repeat (LRR)-containing proteins 3
PDGF	platelet derived growth factor
PDR	proliferative diabetic retinopathy
RLBP1	retinaldehyde binding protein 1
S100A4	S100 calcium-binding protein A4
TNFα	tumor necrosis factor α
VEGF-A	vascular endothelial growth factor-A
VEGFR	vascular endothelial growth factor receptor
VIM	vimentin

References

1. International Diabetes Federation Diabetes Atlas (9th ed.). Available online: http://www.diabetesatlas.org/ (accessed on 28 December 2020).
2. Al-Kharashi, A.S. Role of oxidative stress, inflammation, hypoxia and angiogenesis in the development of diabetic retinopathy. *Saudi J. Ophthalmol.* **2018**, *32*, 318–323. [CrossRef] [PubMed]
3. Nawaz, I.M.; Rezzola, S.; Cancarini, A.; Russo, A.; Costagliola, C.; Semeraro, F.; Presta, M. Human vitreous in proliferative diabetic retinopathy: Characterization and translational implications. *Prog. Retin. Eye Res.* **2019**, *72*, 100756. [CrossRef]
4. Osaadon, P.; Fagan, X.J.; Lifshitz, T.; Levy, J. A review of anti-VEGF agents for proliferative diabetic retinopathy. *Eye (Lond)* **2014**, *28*, 510–520. [CrossRef] [PubMed]
5. Zhao, Y.; Singh, R.P. The role of anti-vascular endothelial growth factor (anti-VEGF) in the management of proliferative diabetic retinopathy. *Drugs Context.* **2018**, *7*, 212532. [CrossRef]
6. Tan, G.S.; Cheung, N.; Simo, R.; Cheung, G.C.; Wong, T.Y. Diabetic macular oedema. *Lancet Diabetes Endocrinol.* **2017**, *5*, 143–155. [CrossRef]
7. Brown, D.M.; Nguyen, Q.D.; Marcus, D.M.; Boyer, D.S.; Patel, S.; Feiner, L.; Schlottmann, P.G.; Rundle, A.C.; Zhang, J.; Rubio, R.G.; et al. Long-term outcomes of ranibizumab therapy for diabetic macular edema: The 36-month results from two phase III trials: RISE and RIDE. *Ophthalmology* **2013**, *120*, 2013–2022. [CrossRef] [PubMed]
8. Semeraro, F.; Morescalchi, F.; Cancarini, A.; Russo, A.; Rezzola, S.; Costagliola, C. Diabetic retinopathy, a vascular and inflammatory disease: Therapeutic implications. *Diabetes Metab.* **2019**, *45*, 517–527. [CrossRef]
9. Le, Y.Z. VEGF production and signaling in Müller glia are critical to modulating vascular function and neuronal integrity in diabetic retinopathy and hypoxic retinal vascular diseases. *Vision Res.* **2017**, *139*, 108–114. [CrossRef]
10. Reichenbach, A.; Bringmann, A. New functions of Müller cells. *Glia* **2013**, *61*, 651–678. [CrossRef]
11. Bringmann, A.; Iandiev, I.; Pannicke, T.; Wurm, A.; Hollborn, M.; Wiedemann, P.; Osborne, N.N.; Reichenbach, A. Cellular signaling and factors involved in Muller cell gliosis: Neuroprotective and detrimental effects. *Prog. Retin. Eye Res.* **2009**, *28*, 423–451. [CrossRef] [PubMed]
12. Bringmann, A.; Pannicke, T.; Grosche, J.; Francke, M.; Wiedemann, P.; Skatchkov, S.N.; Osborne, N.N.; Reichenbach, A. Muller cells in the healthy and diseased retina. *Prog. Retin. Eye Res.* **2006**, *25*, 397–424. [CrossRef]
13. Oberstein, S.Y.; Byun, J.; Herrera, D.; Chapin, E.A.; Fisher, S.K.; Lewis, G.P. Cell proliferation in human epiretinal membranes: Characterization of cell types and correlation with disease condition and duration. *Mol. Vis.* **2011**, *17*, 1794–1805.
14. Roy, S.; Amin, S.; Roy, S. Retinal fibrosis in diabetic retinopathy. *Exp. Eye Res.* **2016**, *142*, 71–75. [CrossRef] [PubMed]
15. Rodrigues, M.; Xin, X.; Jee, K.; Babapoor-Farrokhran, S.; Kashiwabuchi, F.; Ma, T.; Bhutto, I.; Hassan, S.J.; Daoud, Y.; Baranano, D.; et al. VEGF secreted by hypoxic Muller cells induces MMP-2 expression and activity in endothelial cells to promote retinal neovascularization in proliferative diabetic retinopathy. *Diabetes* **2013**, *62*, 3863–3873. [CrossRef]
16. Portillo, J.C.; Lopez Corcino, Y.; Miao, Y.; Tang, J.; Sheibani, N.; Kern, T.S.; Dubyak, G.R.; Subauste, C.S. CD40 in Retinal Muller Cells Induces P2X7-Dependent Cytokine Expression in Macrophages/Microglia in Diabetic Mice and Development of Early Experimental Diabetic Retinopathy. *Diabetes* **2017**, *66*, 483–493. [CrossRef]
17. Rezzola, S.; Nawaz, M.I.; Cancarini, A.; Semeraro, F.; Presta, M. Vascular Endothelial Growth Factor in the Vitreous of Proliferative Diabetic Retinopathy Patients: Chasing a Hiding Prey? *Diabetes Care* **2019**, *42*, e105–e106. [CrossRef]
18. Rezzola, S.; Corsini, M.; Chiodelli, P.; Cancarini, A.; Nawaz, I.M.; Coltrini, D.; Mitola, S.; Ronca, R.; Belleri, M.; Lista, L.; et al. Inflammation and N-formyl peptide receptors mediate the angiogenic activity of human vitreous humour in proliferative diabetic retinopathy. *Diabetologia* **2017**, *60*, 719–728. [CrossRef] [PubMed]
19. Rezzola, S.; Nawaz, I.M.; Cancarini, A.; Ravelli, C.; Calza, S.; Semeraro, F.; Presta, M. 3D endothelial cell spheroid/human vitreous humor assay for the characterization of anti-angiogenic inhibitors for the treatment of proliferative diabetic retinopathy. *Angiogenesis* **2017**, *20*, 629–640. [CrossRef]
20. Nawaz, I.M.; Chiodelli, P.; Rezzola, S.; Paganini, G.; Corsini, M.; Lodola, A.; Lodola, A.; Di Ianni, A.; Mor, M.; Presta, M. N-tert-butyloxycarbonyl-Phe-Leu-Phe-Leu-Phe (BOC2) inhibits the angiogenic activity of heparin-binding growth factors. *Angiogenesis* **2018**, *21*, 47–59. [CrossRef]
21. Rezzola, S.; Dal Monte, M.; Belleri, M.; Bugatti, A.; Chiodelli, P.; Corsini, M.; Cammalleri, M.; Cancarini, A.; Morbidelli, L.; Oreste, P.; et al. Therapeutic Potential of Anti-Angiogenic Multitarget, N,O-Sulfated E. Coli K5 Polysaccharide in Diabetic Retinopathy. *Diabetes* **2015**, *64*, 2581–2592. [CrossRef]
22. Rezzola, S.; Loda, A.; Corsini, M.; Semeraro, F.; Annese, T.; Presta, M.; Ribatti, D. Angiogenesis-Inflammation Cross Talk in Diabetic Retinopathy: Novel Insights from the Chick Embryo Chorioallantoic Membrane/Human Vitreous Platform. *Front. Immunol.* **2020**, *11*, 581288. [CrossRef]
23. Dal Monte, M.; Rezzola, S.; Cammalleri, M.; Belleri, M.; Locri, F.; Morbidelli, L.; Corsini, M.; Paganini, G.; Semeraro, F.; Cancarini, A.; et al. Antiangiogenic Effectiveness of the Urokinase Receptor-Derived Peptide UPARANT in a Model of Oxygen-Induced Retinopathy. *Investig. Ophthalmol. Vis. Sci.* **2015**, *56*, 2392–2407. [CrossRef]
24. Presta, M.; Dell'Era, P.; Mitola, S.; Moroni, E.; Ronca, R.; Rusnati, M. Fibroblast growth factor/fibroblast growth factor receptor system in angiogenesis. *Cytokine Growth Factor Rev.* **2005**, *16*, 159–178. [CrossRef]

25. Guagnano, V.; Furet, P.; Spanka, C.; Bordas, V.; Le Douget, M.; Stamm, C.; Brueggen, J.; Jensen, M.R.; Schnell, C.; Schmid, H.; et al. Discovery of 3-(2,6-dichloro-3,5-dimethoxy-phenyl)-1-{6-[4-(4-ethyl-piperazin-1-yl)-phenylamin o]-pyrimidin-4-yl}-1-methyl-urea (NVP-BGJ398), a potent and selective inhibitor of the fibroblast growth factor receptor family of receptor tyrosine kinase. *J. Med. Chem.* **2011**, *54*, 7066–7083. [CrossRef] [PubMed]
26. Ronca, R.; Giacomini, A.; Di Salle, E.; Coltrini, D.; Pagano, K.; Ragona, L.; Matarazzo, S.; Rezzola, S.; Maiolo, D.; Torrella, R.; et al. Long-Pentraxin 3 Derivative as a Small-Molecule FGF Trap for Cancer Therapy. *Cancer Cell* **2015**, *28*, 225–239. [CrossRef] [PubMed]
27. Bressler, S.B.; Liu, D.; Glassman, A.R.; Blodi, B.A.; Castellarin, A.A.; Jampol, L.M.; Kaufman, P.L.; Melia, M.; Singh, H.; Wells, J.A.; et al. Change in Diabetic Retinopathy Through 2 Years: Secondary Analysis of a Randomized Clinical Trial Comparing Aflibercept, Bevacizumab, and Ranibizumab. *JAMA Ophthalmol.* **2017**, *135*, 558–568. [CrossRef] [PubMed]
28. Hollborn, M.; Jahn, K.; Limb, G.A.; Kohen, L.; Wiedemann, P.; Bringmann, A. Characterization of the basic fibroblast growth factor-evoked proliferation of the human Muller cell line, MIO-M1. *Graefes Arch. Clin. Exp. Ophthalmol.* **2004**, *242*, 414–422. [CrossRef]
29. Toniolo, C.; Bonora, G.M.; Showell, H.; Freer, R.J.; Becker, E.L. Structural requirements for formyl homooligopeptide chemoattractants. *Biochemistry* **1984**, *23*, 698–704. [CrossRef]
30. Liu, X.; Ye, F.; Xiong, H.; Hu, D.; Limb, G.A.; Xie, T.; Peng, L.; Yang, W.; Sun, Y.; Zhou, M.; et al. IL-1beta Upregulates IL-8 Production in Human Muller Cells Through Activation of the p38 MAPK and ERK1/2 Signaling Pathways. *Inflammation* **2014**, *37*, 1486–1495. [CrossRef]
31. Liu, X.; Ye, F.; Xiong, H.; Hu, D.N.; Limb, G.A.; Xie, T.; Peng, L.; Zhang, P.; Wei, Y.; Zhang, W.; et al. IL-1beta induces IL-6 production in retinal Muller cells predominantly through the activation of p38 MAPK/NF-kappaB signaling pathway. *Exp. Cell Res.* **2015**, *331*, 223–231. [CrossRef]
32. Nelson, C.M.; Ackerman, K.M.; O'Hayer, P.; Bailey, T.J.; Gorsuch, R.A.; Hyde, D.R. Tumor necrosis factor-alpha is produced by dying retinal neurons and is required for Muller glia proliferation during zebrafish retinal regeneration. *J. Neurosci.* **2013**, *33*, 6524–6539. [CrossRef] [PubMed]
33. Ghaseminejad, F.; Kaplan, L.; Pfaller, A.M.; Hauck, S.M.; Grosche, A. The role of Muller cell glucocorticoid signaling in diabetic retinopathy. *Graefes Arch. Clin. Exp. Ophthalmol.* **2020**, *258*, 221–230. [CrossRef] [PubMed]
34. Zong, H.; Ward, M.; Madden, A.; Yong, P.H.; Limb, G.A.; Curtis, T.M.; Stitt, A.W. Hyperglycaemia-induced pro-inflammatory responses by retinal Muller glia are regulated by the receptor for advanced glycation end-products (RAGE). *Diabetologia* **2010**, *53*, 2656–2666. [CrossRef]
35. Mu, H.; Zhang, X.M.; Liu, J.J.; Dong, L.; Feng, Z.L. Effect of high glucose concentration on VEGF and PEDF expression in cultured retinal Muller cells. *Mol. Biol Rep.* **2009**, *36*, 2147–2151. [CrossRef]
36. Wang, J.; Xu, X.; Elliott, M.H.; Zhu, M.; Le, Y.Z. Muller cell-derived VEGF is essential for diabetes-induced retinal inflammation and vascular leakage. *Diabetes* **2010**, *59*, 2297–2305. [CrossRef] [PubMed]
37. Guidry, C. The role of Muller cells in fibrocontractive retinal disorders. *Prog. Retin. Eye Res.* **2005**, *24*, 75–86. [CrossRef] [PubMed]
38. Chen, Q.; Liu, Z.X. Idiopathic Macular Hole: A Comprehensive Review of Its Pathogenesis and of Advanced Studies on Metamorphopsia. *J. Ophthalmol.* **2019**, *2019*, 7294952. [CrossRef] [PubMed]
39. Bu, S.C.; Kuijer, R.; van der Worp, R.J.; Postma, G.; Renardel de Lavalette, V.W.; Li, X.R.; Hooymans, J.M.M.; Los, L.I. Immunohistochemical Evaluation of Idiopathic Epiretinal Membranes and In Vitro Studies on the Effect of TGF-beta on Muller Cells. *Investig. Ophthalmol. Vis. Sci.* **2015**, *56*, 6506–6514. [CrossRef] [PubMed]
40. Mayr, B.; Montminy, M. Transcriptional regulation by the phosphorylation-dependent factor CREB. *Nat. Rev. Mol. Cell Biol.* **2001**, *2*, 599–609. [CrossRef]
41. Fischer, A.J.; Scott, M.A.; Tuten, W. Mitogen-activated protein kinase-signaling stimulates Muller glia to proliferate in acutely damaged chicken retina. *Glia* **2009**, *57*, 166–181. [CrossRef]
42. Swanson, K.V.; Deng, M.; Ting, J.P. The NLRP3 inflammasome: Molecular activation and regulation to therapeutics. *Nat. Rev. Immunol.* **2019**, *19*, 477–489. [CrossRef] [PubMed]
43. Liu, Y.; Biarnes Costa, M.; Gerhardinger, C. IL-1beta is upregulated in the diabetic retina and retinal vessels: Cell-specific effect of high glucose and IL-1beta autostimulation. *PLoS ONE* **2012**, *7*, e36949. [CrossRef]
44. Chaurasia, S.S.; Lim, R.R.; Parikh, B.H.; Wey, Y.S.; Tun, B.B.; Wong, T.Y.; Luu, C.D.; Agrawal, R.; Ghosh, A.; Mortellaro, A.; et al. The NLRP3 Inflammasome May Contribute to Pathologic Neovascularization in the Advanced Stages of Diabetic Retinopathy. *Sci Rep.* **2018**, *8*, 2847. [CrossRef] [PubMed]
45. Yang, L.P.; Sun, H.L.; Wu, L.M.; Guo, X.J.; Dou, H.L.; Tso, M.O.; Zhao, L.; Li, S. Baicalein reduces inflammatory process in a rodent model of diabetic retinopathy. *Investig. Ophthalmol. Vis. Sci.* **2009**, *50*, 2319–2327. [CrossRef]
46. Loukovaara, S.; Piippo, N.; Kinnunen, K.; Hytti, M.; Kaarniranta, K.; Kauppinen, A. NLRP3 inflammasome activation is associated with proliferative diabetic retinopathy. *Acta Ophthalmol.* **2017**, *95*, 803–808. [CrossRef] [PubMed]
47. Chen, H.; Zhang, X.; Liao, N.; Mi, L.; Peng, Y.; Liu, B.; Zhang, S.; Wen, F. Enhanced Expression of NLRP3 Inflammasome-Related Inflammation in Diabetic Retinopathy. *Investig. Ophthalmol. Vis. Sci.* **2018**, *59*, 978–985. [CrossRef]
48. He, Y.; Hara, H.; Nunez, G. Mechanism and Regulation of NLRP3 Inflammasome Activation. *Trends Biochem. Sci.* **2016**, *41*, 1012–1021. [CrossRef] [PubMed]

49. Chung, I.C.; Yuan, S.N.; OuYang, C.N.; Lin, H.C.; Huang, K.Y.; Chen, Y.J.; Chung, A.K.; Chu, C.L.; Ojcius, D.M.; Chang, Y.S.; et al. Src-family kinase-Cbl axis negatively regulates NLRP3 inflammasome activation. *Cell Death Dis.* **2018**, *9*, 1109. [CrossRef] [PubMed]
50. Fogli, S.; Del Re, M.; Rofi, E.; Posarelli, C.; Figus, M.; Danesi, R. Clinical pharmacology of intravitreal anti-VEGF drugs. *Eye (Lond)* **2018**, *32*, 1010–1020. [CrossRef] [PubMed]
51. Fu, S.; Dong, S.; Zhu, M.; Sherry, D.M.; Wang, C.; You, Z.; Haigh, J.J.; Le, Y.Z. Muller Glia Are a Major Cellular Source of Survival Signals for Retinal Neurons in Diabetes. *Diabetes* **2015**, *64*, 3554–3563. [CrossRef]
52. Saint-Geniez, M.; Maharaj, A.S.; Walshe, T.E.; Tucker, B.A.; Sekiyama, E.; Kurihara, T.; Darland, D.C.; Young, M.J.; D'Amore, P.A. Endogenous VEGF is required for visual function: Evidence for a survival role on muller cells and photoreceptors. *PLoS ONE* **2008**, *3*, e3554. [CrossRef] [PubMed]
53. Caceres-Del-Carpio, J.; Moustafa, M.T.; Toledo-Corral, J.; Hamid, M.A.; Atilano, S.R.; Schneider, K.; Fukuhara, P.S.; Donato Costa, R.; Norman, J.L.; Malik, D.; et al. In vitro response and gene expression of human retinal Muller cells treated with different anti-VEGF drugs. *Exp. Eye Res.* **2020**, *191*, 107903. [CrossRef] [PubMed]
54. Matsuda, M.; Krempel, P.G.; Marquezini, M.V.; Sholl-Franco, A.; Lameu, A.; Monteiro, M.L.R.; de Oliveira Miguel, N.C. Cellular stress response in human Muller cells (MIO-M1) after bevacizumab treatment. *Exp. Eye Res.* **2017**, *160*, 1–10. [CrossRef]
55. Hueber, A.; Wiedemann, P.; Esser, P.; Heimann, K. Basic fibroblast growth factor mRNA, bFGF peptide and FGF receptor in epiretinal membranes of intraocular proliferative disorders (PVR and PDR). *Int. Ophthalmol.* **1996**, *20*, 345–350. [CrossRef]
56. Liang, X.; Li, C.; Li, Y.; Huang, J.; Tang, S.; Gao, R.; Li, S. Platelet-derived growth factor and basic fibroblast growth factor immunolocalized in proliferative retinal diseases. *Chin. Med. J.* **2000**, *113*, 144–147.
57. Coltrini, D.; Belleri, M.; Gambicorti, E.; Romano, D.; Morescalchi, F.; Krishna Chandran, A.M.; Calza, S.; Semeraro, F.; Presta, M. Gene expression analysis identifies two distinct molecular clusters of idiopatic epiretinal membranes. *Biochim. Biophys. Acta Mol. Basis Dis.* **2020**, *1866*, 165938. [CrossRef]
58. Yoshida, S.; Yoshida, A.; Ishibashi, T. Induction of IL-8, MCP-1, and bFGF by TNF-alpha in retinal glial cells: Implications for retinal neovascularization during post-ischemic inflammation. *Graefes Arch. Clin. Exp. Ophthalmol.* **2004**, *242*, 409–413. [CrossRef] [PubMed]
59. Cheng, T.; Cao, W.; Wen, R.; Steinberg, R.H.; LaVail, M.M. Prostaglandin E2 induces vascular endothelial growth factor and basic fibroblast growth factor mRNA expression in cultured rat Muller cells. *Investig. Ophthalmol. Vis. Sci.* **1998**, *39*, 581–591.
60. Itoh, N.; Ornitz, D.M. Functional evolutionary history of the mouse Fgf gene family. *Developmental. Dyn.* **2008**, *237*, 18–27. [CrossRef]
61. Beenken, A.; Mohammadi, M. The FGF family: Biology, pathophysiology and therapy. *Nat. Rev. Drug Discov.* **2009**, *8*, 235–253. [CrossRef] [PubMed]
62. Krejci, P.; Aklian, A.; Kaucka, M.; Sevcikova, E.; Prochazkova, J.; Masek, J.K.; Mikolka, P.; Pospisilova, T.; Spoustova, T.; Weis, M.; et al. Receptor tyrosine kinases activate canonical WNT/beta-catenin signaling via MAP kinase/LRP6 pathway and direct beta-catenin phosphorylation. *PLoS ONE* **2012**, *7*, e35826. [CrossRef] [PubMed]
63. Huang, L.; Luo, R.; Li, J.; Wang, D.; Zhang, Y.; Liu, L.; Zhang, N.; Xu, X.; Lu, B.; Zhano, K. beta-catenin promotes NLRP3 inflammasome activation via increasing the association between NLRP3 and ASC. *Mol. Immunol.* **2020**, *121*, 186–194. [CrossRef] [PubMed]
64. Kanda, A.; Noda, K.; Hirose, I.; Ishida, S. TGF-beta-SNAIL axis induces Muller glial-mesenchymal transition in the pathogenesis of idiopathic epiretinal membrane. *Sci. Rep.* **2019**, *9*, 673. [CrossRef]
65. Guidry, C.; Bradley, K.M.; King, J.L. Tractional force generation by human muller cells: Growth factor responsiveness and integrin receptor involvement. *Investig. Ophthalmol. Vis. Sci.* **2003**, *44*, 1355–1363. [CrossRef] [PubMed]
66. Bringmann, A.; Wiedemann, P. Involvement of Muller glial cells in epiretinal membrane formation. *Graefes Arch. Clin. Exp. Ophthalmol.* **2009**, *247*, 865–883. [CrossRef]
67. Guidry, C.; Feist, R.; Morris, R.; Hardwick, C.W. Changes in IGF activities in human diabetic vitreous. *Diabetes* **2004**, *53*, 2428–2435. [CrossRef]
68. Romaniuk, D.; Kimsa, M.W.; Strzalka-Mrozik, B.; Kimsa, M.C.; Kabiesz, A.; Romaniuk, W.; Mazurek, U. Gene expression of IGF1, IGF1R, and IGFBP3 in epiretinal membranes of patients with proliferative diabetic retinopathy: Preliminary study. *Mediat. Inflamm.* **2013**, *2013*, 986217. [CrossRef] [PubMed]
69. Natoli, R.; Fernando, N.; Madigan, M.; Chu-Tan, J.A.; Valter, K.; Provis, J.; Rutar, M. Microglia-derived IL-1beta promotes chemokine expression by Muller cells and RPE in focal retinal degeneration. *Mol. Neurodegener.* **2017**, *12*, 31. [CrossRef] [PubMed]
70. Limb, G.A.; Salt, T.E.; Munro, P.M.; Moss, S.E.; Khaw, P.T. In vitro characterization of a spontaneously immortalized human Muller cell line (MIO-M1). *Investig. Ophthalmol. Vis. Sci.* **2002**, *43*, 864–869.
71. Ravelli, C.; Grillo, E.; Corsini, M.; Coltrini, D.; Presta, M.; Mitola, S. beta3 Integrin Promotes Long-Lasting Activation and Polarization of Vascular Endothelial Growth Factor Receptor 2 by Immobilized Ligand. *Arter. Thromb. Vasc. Biol.* **2015**, *35*, 2161–2171. [CrossRef]
72. Schindelin, J.; Arganda-Carreras, I.; Frise, E.; Kaynig, V.; Longair, M.; Pietzsch, T.; Preibisch, S.; Rueden, C.; Saalfeld, S.; Schimd, B.; et al. Fiji: An open-source platform for biological-image analysis. *Nat. Methods* **2012**, *9*, 676–682. [CrossRef]
73. Rezzola, S.; Di Somma, M.; Corsini, M.; Leali, D.; Ravelli, C.; Polli, V.A.B.; Grillo, E.; Presta, M.; Mitola, S. VEGFR2 activation mediates the pro-angiogenic activity of BMP4. *Angiogenesis* **2019**, *22*, 521–533. [CrossRef]

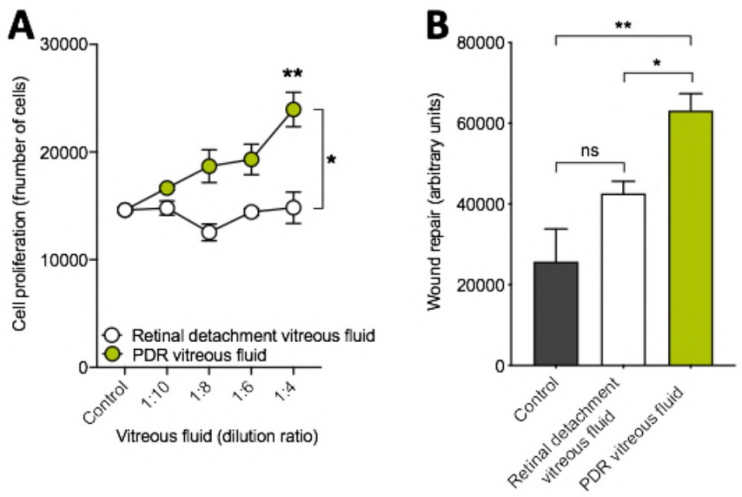

Supplementary Figure 1. Retinal detachment vitreous fluid does not activate MIO-M1 Müller cells. **(A)** MIO-M1 cells were treated with increasing amounts of PDR or retinal detachment vitreous samples (*vol:vol* dilution in cell culture medium) and counted 72 hours thereafter. Data are the mean ± SD of 2 independent experiments in triplicate. * $p < 0.05$ *vs* retinal detachment vitreous fluid, Student's *t* test, and ** $p < 0.01$ *vs* control, 1-way ANOVA. **(B)** Wounded MIO-M1 monolayers were treated with PDR or retinal detachment vitreous fluid. After 24 hours, MIO-M1 cells invading the wounded area were quantified by computerized analysis of the digitalized images. Data are the mean ± SD of 2 independent experiments (8 microscopic fields per experimental point). * $p < 0.05$ *vs* retinal detachment vitreous fluid, Student's *t* test, and ** $p < 0.01$ *vs* control, 1-way ANOVA; ns, non-significant.

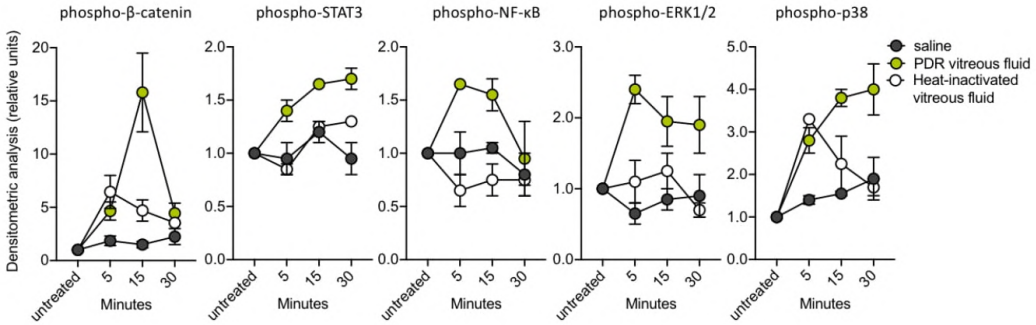

Supplementary Figure 2. Müller cell signaling activated by PDR vitreous. Densitometric analysis of the phosphorylation of the signaling proteins β-catenin, STAT3, NF-κB, ERK1/2, and p38 in MIO-M1 cells following 0-30 minutes of stimulation with PDR or heat-inactivated vitreous samples (see Figure 1E). Data are the mean ± SD of 2 independent experiments.

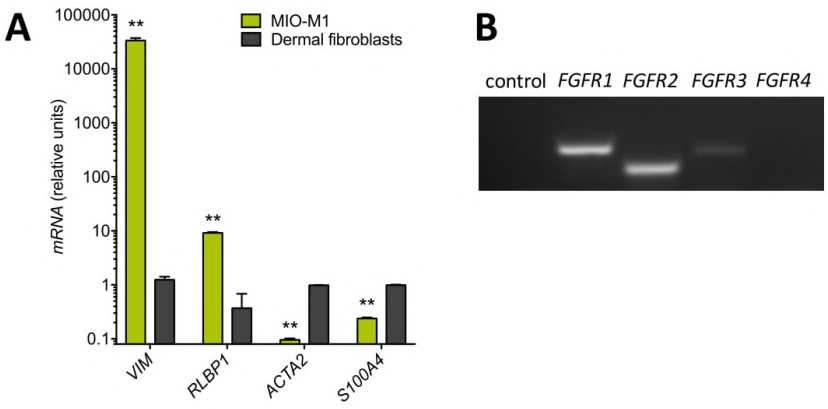

Supplementary Figure 3. Molecular characterization of MIO-M1 Müller cells. (A) qPCR analysis of *VIM*, *RLBP1*, *ACTA2*, and *S100A4* expression in MIO-M1 cells and human dermal fibroblasts. Data are representative of 2 independent experiments in triplicate and are expressed as relative units in respect to *GAPDH* expression. ** $p < 0.01$ *vs* dermal fibroblasts, Student's *t* test. **(B)** Semi-quantitative RT-PCR analysis of *FGFR1*, *FGFR2*, *FGFR3*, and *FGFR4* expression in MIO-M1 cells. Data are representative of 2 independent experiments that gave similar results.

CONCLUSIONS

MOLECULAR CLASSIFICATION OF iERMs

Here, we performed a retrospective study in which the expression levels of iERM-related genes were analyzed in a cohort of 56 iERM samples. The genes encode for proteins representing biomarkers of different aspects of the pathogenesis of iERM, including markers of iERM cell populations and ECM components and markers of the biological events relevant to the pathogenesis of iERM, including various cytokines and growth factors. The results showed high variability in the expression levels of all the genes investigated. We observed a significant correlation between the expression levels of the Müller cell/glial markers GLUL and RLBP1. Similarly, a significant correlation was observed among the fibroblast/myofibroblast markers ACTA2, TAGLN, and S100A4 and between the hyalocyte/macrophage markers PTPRC and CD163. These data confirm and extend previous morphological and immunohistochemical analyses showing these cell types in iERMs.

qPCR analysis of the expression of genes encoding for putative biomarkers of the cellular and molecular events occurring in iERMs identified two molecular clusters of iERMs, herewith named iERM-A and iERM-B. When compared to iERM-A specimens, iERM-B samples showed higher levels of cytokine and growth factor transcripts and higher expression of glial and fibrogenic markers, with no difference in the expression levels of myofibroblast and hyalocyte markers [101]. Notably, the information present in the clinical charts indicated that the patients belonging to the iERM-A Cluster showed less severe clinical features when compared to iERM-B patients, including higher preoperative decimal BCVA, a better and faster improvement of IS/OS visualization after surgery, and more favorable SD-OCT features following the Hwang et al. [19] Classification. Based on these observations, it seems possible to hypothesize that two different statuses of activation may exist in iERMs, one characterized by a more pro-fibrotic phenotype driven, among others, by TGFB1, NGF, and IGF gene products, and a second one in which glial cell activation plays a prominent role.

iERMs VITREOUS INDUCES GMT IN MÜLLER MIO-M1 CELLS

To investigate the capacity of iERM vitreous to activate Müller cells, MIO-M1 cells were treated with a pool of vitreous samples obtained before membrane peeling from the same iERM-A and iERM-B patients. Here, we demonstrate that a pool of vitreous fluid harvested from iERM patients before membrane peeling induces proliferation, migration, and GMT in MIO-M1 cells, a phenotype consistent with Müller cell behavior during iERM progression. We also analyzed the vitreous fluid

from iERM patients that were part of a cohort belonging to a previous retrospective study aimed to attempt the molecular characterization of iERM specimens obtained after membrane peeling. When aliquots of the same samples utilized to generate the iERM vitreous pool were assessed individually for their capacity to induce GMT in MIO-M1 cells, the results indicated that all iERM vitreous samples were able to cause the downregulation of the Müller cell/glial markers. However, these samples differ in their capacity to affect the expression of the myofibroblast markers. Indeed, a cluster of iERM vitreous samples induced Müller cell/glial marker downregulation paralleled by a significant upregulation of the pro-fibrotic myofibroblast markers, leading to a GMT ^{complete} response in MIO-M1 cells. The second Cluster of iERM vitreous samples exerted instead no effect or an inhibitory response on the expression of pro-fibrotic myofibroblast markers together with a significant upregulation of the proliferation marker, thus inducing glial dedifferentiation in the absence of the acquisition of mesenchymal markers. This latter phenotype may represent a transitional GMT ^{partial} state. Notably, all the vitreous samples belonging to the GMT ^{complete} cluster were derived from iERM-A patients, whereas all the samples belonging to the GMT ^{partial} cluster were obtained from iERM-B patients. In keeping with our previous observations, iERM-B patients with vitreous fluid able to induce a GMT ^{partial} response in MIO-M1 cells were characterized by more severe clinical and morphological features when compared to GMT ^{complete} /iERM-A patients.

Together, these data indicate that both the molecular analysis of iERMs and the study of the impact of the corresponding vitreous fluids on Müller cells provide congruent information that allows the identification of two clusters of iERM patients with distinct clinical features.

PDR VITREOUS-INDUCED ACTIVATION OF MÜLLER CELLS IS INDEPENDENT OF VEGF

We further analysed the role of Müller glial cells in the pathogenesis of PDR as it is thoroughly described [59]. Understanding the reactive responses of Müller cells and their protective/detrimental effects in PDR is of pivotal importance to bringing new therapeutic strategies to patients. Here, PDR vitreous humor obtained from diabetic patients after pars plana vitrectomy was used as a tool to explore the activation that occurs in Müller cells during PDR. The results show that PDR vitreous stimulates MIO-M1 cell proliferation and motility, hallmarks of the gliotic response that characterizes Müller cells [59] and may contribute to ERM formation in PDR patients.

In addition, our results indicate that such responses are not due to VEGF, which is unable to cause VEGFR2 phosphorylation and ERK1/2 activation in MIO-M1 cells under our experimental

conditions. These data suggest that other mediators, distinct from VEGF, are responsible for the Müller cell activation that occurs following PDR vitreous treatment.

A variety of pro-angiogenic/proinflammatory mediators besides VEGF accumulate in the vitreous of PDR patients during disease progression [72]. FGF2 has been detected in ERMs [102, 103], and proinflammatory mediators can induce FGF2 expression in Müller cells [70, 71]. Conversely, FGF2 may trigger proliferation and gliotic responses in these cells [104]. Here, we extended these findings by showing that recombinant FGF2 induces the upregulation of proinflammatory genes in MIO-M1 cells. In keeping with this observation, the FGFR tyrosine kinase inhibitor BGJ398 and the pan-FGF trap NSC12 partially inhibit the activation of MIO-M1 cells by PDR vitreous, thus suggesting that the deregulation of the FGF/FGFR system may play a role in Müller cell activation during PDR. Together, our data indicate that one or more members of the FGF family are present in PDR vitreous and may contribute to its capacity to trigger a proinflammatory response in MIO-M1 cells.

Finally, the capacity of the multi-target heparin-binding protein antagonist Boc2 and the anti-inflammatory agent hydrocortisone to inhibit MIO-M1 cell activation triggered by PDR vitreous indicates that other yet unidentified heparin-binding growth factors and inflammatory cytokines may contribute to Müller cell activation.

Clinical observations demonstrate that anti-VEGF approaches are only partially efficacious for treating PDR patients[105-107]. Based on the evidence that anti-VEGF drugs show only a limited effect on the activity exerted by PDR vitreous on Müller cells and endothelial cells[81, 84], our results indicate that the characterization of novel drug candidates with different mechanisms of action may contribute, in association with anti-VEGF interventions, to the development of more efficacious therapeutic approaches in PDR.

BIBLIOGRAPHY

[1] S.C. Bu, R. Kuijer, X.R. Li, J.M. Hooymans, L.I. Los, Idiopathic epiretinal membrane, Retina 34(12) (2014) 2317-35.

[2] E. Tsotridou, E. Loukovitis, K. Zapsalis, I. Pentara, S. Asteriadis, P. Tranos, Z. Zachariadis, G. Anogeianakis, A Review of Last Decade Developments on Epiretinal Membrane Pathogenesis, Med Hypothesis Discov Innov Ophthalmol 9(2) (2020) 91-110.

[3] B. George, S. Chen, V. Chaudhary, J. Gonder, S. Chakrabarti, Extracellular matrix proteins in epiretinal membranes and in diabetic retinopathy, Curr Eye Res 34(2) (2009) 134-44.

[4] A. Russo, M. Ragusa, C. Barbagallo, A. Longo, T. Avitabile, M.G. Uva, V. Bonfiglio, M.D. Toro, R. Caltabiano, C. Mariotti, F. Boscia, M. Romano, C. Di Pietro, D. Barbagallo, M. Purrello, M. Reibaldi, miRNAs in the vitreous humor of patients affected by idiopathic epiretinal membrane and macular hole, PLoS One 12(3) (2017) e0174297.

[5] C.H. Ng, N. Cheung, J.J. Wang, A.F. Islam, R. Kawasaki, S.M. Meuer, M.F. Cotch, B.E. Klein, R. Klein, T.Y. Wong, Prevalence and risk factors for epiretinal membranes in a multi-ethnic United States population, Ophthalmology 118(4) (2011) 694-9.

[6] C.S. Fong, P. Mitchell, E. Rochtchina, T. Hong, T. de Loryn, J.J. Wang, Incidence and progression of epiretinal membranes in eyes after cataract surgery, Am J Ophthalmol 156(2) (2013) 312-318.e1.

[7] W. Xiao, X. Chen, W. Yan, Z. Zhu, M. He, Prevalence and risk factors of epiretinal membranes: a systematic review and meta-analysis of population-based studies, BMJ Open 7(9) (2017) e014644.

[8] P. Maitra, D.A. Kumar, A. Agarwal, Epiretinal membrane profile on spectral domain optical coherence tomography in patients with uveitis, Indian J Ophthalmol 67(3) (2019) 376-381.

[9] C.I. Falkner-Radler, C. Glittenberg, S. Hagen, T. Benesch, S. Binder, Spectral-domain optical coherence tomography for monitoring epiretinal membrane surgery, Ophthalmology 117(4) (2010) 798-805.

[10] Y. Hirano, T. Yasukawa, Y. Ogura, Optical coherence tomography guided peeling of macular epiretinal membrane, Clin Ophthalmol 5 (2010) 27-9.

[11] A. Govetto, R.A. Lalane, D. Sarraf, M.S. Figueroa, J.P. Hubschman, Insights Into Epiretinal Membranes: Presence of Ectopic Inner Foveal Layers and a New Optical Coherence Tomography Staging Scheme, Am J Ophthalmol 175 (2017) 99-113.

[12] V. Konidaris, S. Androudi, A. Alexandridis, A. Dastiridou, P. Brazitikos, Optical coherence tomography-guided classification of epiretinal membranes, Int Ophthalmol 35(4) (2015) 495-501.

[13] W. Stevenson, C.M. Prospero Ponce, D.R. Agarwal, R. Gelman, J.B. Christoforidis, Epiretinal membrane: optical coherence tomography-based diagnosis and classification, Clin Ophthalmol 10 (2016) 527-34.

[14] J.W. Yau, S.L. Rogers, R. Kawasaki, E.L. Lamoureux, J.W. Kowalski, T. Bek, S.J. Chen, J.M. Dekker, A. Fletcher, J. Grauslund, S. Haffner, R.F. Hamman, M.K. Ikram, T. Kayama, B.E. Klein, R. Klein, S. Krishnaiah, K. Mayurasakorn, J.P. O'Hare, T.J. Orchard, M. Porta, M. Rema, M.S. Roy, T. Sharma, J. Shaw, H. Taylor, J.M. Tielsch, R. Varma, J.J. Wang, N. Wang, S. West, L. Xu, M. Yasuda, X. Zhang, P. Mitchell, T.Y. Wong, M.-A.f.E.D.M.-E.S. Group, Global prevalence and major risk factors of diabetic retinopathy, Diabetes Care 35(3) (2012) 556-64.

[15] N. Cheung, P. Mitchell, T.Y. Wong, Diabetic retinopathy, Lancet 376(9735) (2010) 124-36.

[16] K.Z. Aung, G. Makeyeva, M.K. Adams, E.W. Chong, L. Busija, G.G. Giles, D.R. English, J. Hopper, P.N. Baird, R.H. Guymer, L.D. Robman, The prevalence and risk factors of epiretinal membranes: the Melbourne Collaborative Cohort Study, Retina 33(5) (2013) 1026-34.

[17] Q. You, L. Xu, J.B. Jonas, Prevalence and associations of epiretinal membranes in adult Chinese: the Beijing eye study, Eye (Lond) 22(7) (2008) 874-9.

[18] S. Fraser-Bell, M. Guzowski, E. Rochtchina, J.J. Wang, P. Mitchell, Five-year cumulative incidence and progression of epiretinal membranes: the Blue Mountains Eye Study, Ophthalmology 110(1) (2003) 34-40.

[19] J.U. Hwang, J. Sohn, B.G. Moon, S.G. Joe, J.Y. Lee, J.G. Kim, Y.H. Yoon, Assessment of macular function for idiopathic epiretinal membranes classified by spectral-domain optical coherence tomography, Invest Ophthalmol Vis Sci 53(7) (2012) 3562-9.

[20] N. Cheung, S.P. Tan, S.Y. Lee, G.C.M. Cheung, G. Tan, N. Kumar, C.Y. Cheng, T.Y. Wong, Prevalence and risk factors for epiretinal membrane: the Singapore Epidemiology of Eye Disease study, Br J Ophthalmol 101(3) (2017) 371-376.

[21] A. Salminen, J. Ojala, K. Kaarniranta, A. Haapasalo, M. Hiltunen, H. Soininen, Astrocytes in the aging brain express characteristics of senescence-associated secretory phenotype, Eur J Neurosci 34(1) (2011) 3-11.

[22] R.I. Kohno, Y. Hata, S. Kawahara, T. Kita, R. Arita, Y. Mochizuki, L.P. Aiello, T. Ishibashi, Possible contribution of hyalocytes to idiopathic epiretinal membrane formation and its contraction, Br J Ophthalmol 93(8) (2009) 1020-6.

[23] M. Karlstetter, R. Scholz, M. Rutar, W.T. Wong, J.M. Provis, T. Langmann, Retinal microglia: just bystander or target for therapy?, Prog Retin Eye Res 45 (2015) 30-57.

[24] L.G. Fritsche, R.N. Fariss, D. Stambolian, G.R. Abecasis, C.A. Curcio, A. Swaroop, Age-related macular degeneration: genetics and biology coming together, Annu Rev Genomics Hum Genet 15 (2014) 151-71.

[25] M. Joshi, S. Agrawal, J.B. Christoforidis, Inflammatory mechanisms of idiopathic epiretinal membrane formation, Mediators Inflamm 2013 (2013) 192582.

[26] Q. Huang, J. Li, With or without internal limiting membrane peeling during idiopathic epiretinal membrane surgery: A meta-analysis, PLoS One 16(1) (2021) e0245459.

[27] F. Rommel, M.P. Brinkmann, J.A.M. Sochurek, M. Prasuhn, S. Grisanti, M. Ranjbar, Ocular Blood Flow Changes Impact Visual Acuity Gain after Surgical Treatment for Idiopathic Epiretinal Membrane, J Clin Med 9(6) (2020).

[28] K. Ogurtsova, J.D. da Rocha Fernandes, Y. Huang, U. Linnenkamp, L. Guariguata, N.H. Cho, D. Cavan, J.E. Shaw, L.E. Makaroff, IDF Diabetes Atlas: Global estimates for the prevalence of diabetes for 2015 and 2040, Diabetes Res Clin Pract 128 (2017) 40-50.

[29] R. Klein, B.E. Klein, S.E. Moss, M.D. Davis, D.L. DeMets, The Wisconsin epidemiologic study of diabetic retinopathy. III. Prevalence and risk of diabetic retinopathy when age at diagnosis is 30 or more years, Arch Ophthalmol 102(4) (1984) 527-32.

[30] Y. Zheng, M. He, N. Congdon, The worldwide epidemic of diabetic retinopathy, Indian J Ophthalmol 60(5) (2012) 428-31.

[31] P. Kroll, E.B. Rodrigues, S. Hoerle, Pathogenesis and classification of proliferative diabetic vitreoretinopathy, Ophthalmologica 221(2) (2007) 78-94.

[32] F. Semeraro, A. Cancarini, R. dell'Omo, S. Rezzola, M.R. Romano, C. Costagliola, Diabetic Retinopathy: Vascular and Inflammatory Disease, J Diabetes Res 2015 (2015) 582060.

[33] M.S. Ola, M.I. Nawaz, M.M. Siddiquei, S. Al-Amro, A.M. Abu El-Asrar, Recent advances in understanding the biochemical and molecular mechanism of diabetic retinopathy, J Diabetes Complications 26(1) (2012) 56-64.

[34] M.S. Ola, M.I. Nawaz, H.A. Khan, A.S. Alhomida, Neurodegeneration and neuroprotection in diabetic retinopathy, Int J Mol Sci 14(2) (2013) 2559-72.

[35] X.L. Du, D. Edelstein, L. Rossetti, I.G. Fantus, H. Goldberg, F. Ziyadeh, J. Wu, M. Brownlee, Hyperglycemia-induced mitochondrial superoxide overproduction activates the hexosamine pathway and induces plasminogen activator inhibitor-1 expression by increasing Sp1 glycosylation, Proc Natl Acad Sci U S A 97(22) (2000) 12222-6.

[36] S. Satofuka, A. Ichihara, N. Nagai, K. Noda, Y. Ozawa, A. Fukamizu, K. Tsubota, H. Itoh, Y. Oike, S. Ishida, (Pro)renin receptor-mediated signal transduction and tissue renin-angiotensin system contribute to diabetes-induced retinal inflammation, Diabetes 58(7) (2009) 1625-33.

[37] E.D. Schleicher, E. Wagner, A.G. Nerlich, Increased accumulation of the glycoxidation product N(epsilon)-(carboxymethyl)lysine in human tissues in diabetes and aging, J Clin Invest 99(3) (1997) 457-68.

[38] Y. Ido, C. Kilo, J.R. Williamson, Cytosolic NADH/NAD+, free radicals, and vascular dysfunction in early diabetes mellitus, Diabetologia 40 Suppl 2 (1997) S115-7.

[39] C.N. Serhan, Resolution phase of inflammation: novel endogenous anti-inflammatory and proresolving lipid mediators and pathways, Annu Rev Immunol 25 (2007) 101-37.

[40] T. Kuwano, S. Nakao, H. Yamamoto, M. Tsuneyoshi, T. Yamamoto, M. Kuwano, M. Ono, Cyclooxygenase 2 is a key enzyme for inflammatory cytokine-induced angiogenesis, FASEB J 18(2) (2004) 300-10.

[41] K. Tamura, T. Sakurai, H. Kogo, Relationship between prostaglandin E2 and vascular endothelial growth factor (VEGF) in angiogenesis in human vascular endothelial cells, Vascul Pharmacol 44(6) (2006) 411-6.

[42] J. Tang, T.S. Kern, Inflammation in diabetic retinopathy, Prog Retin Eye Res 30(5) (2011) 343-58.

[43] H.W. Flynn, E.Y. Chew, B.D. Simons, F.B. Barton, N.A. Remaley, F.L. Ferris, Pars plana vitrectomy in the Early Treatment Diabetic Retinopathy Study. ETDRS report number 17. The Early Treatment Diabetic Retinopathy Study Research Group, Ophthalmology 99(9) (1992) 1351-7.

[44] A.Y. Zhou, C.J. Zhou, J. Yao, Y.L. Quan, B.C. Ren, J.M. Wang, Panretinal photocoagulation versus panretinal photocoagulation plus intravitreal bevacizumab for high-risk proliferative diabetic retinopathy, Int J Ophthalmol 9(12) (2016) 1772-1778.

[45] N. Cheung, I.Y. Wong, T.Y. Wong, Ocular anti-VEGF therapy for diabetic retinopathy: overview of clinical efficacy and evolving applications, Diabetes Care 37(4) (2014) 900-5.

[46] M. Zhao, Y. Sun, Y. Jiang, Anti-VEGF therapy is not a magic bullet for diabetic retinopathy, Eye (Lond) 34(4) (2020) 609-610.

[47] P. DALE, NEUROSCIENCE THIRD EDITION, 2004.

[48] H. Kolb, E. Fernandez, R. Nelson, Webvision: The Organization of the Retina and Visual System, 1995.

[49] K. Peynshaert, J. Devoldere, A.K. Minnaert, S.C. De Smedt, K. Remaut, Morphology and Composition of the Inner Limiting Membrane: Species-Specific Variations and Relevance toward Drug Delivery Research, Curr Eye Res 44(5) (2019) 465-475.

[50] R. Gelman, W. Stevenson, C. Prospero Ponce, D. Agarwal, J.B. Christoforidis, Retinal Damage Induced by Internal Limiting Membrane Removal, J Ophthalmol 2015 (2015) 939748.

[51] D. Goldman, Müller glial cell reprogramming and retina regeneration, Nat Rev Neurosci 15(7) (2014) 431-42.

[52] A. Bringmann, P. Wiedemann, Müller glial cells in retinal disease, Ophthalmologica 227(1) (2012) 1-19.

[53] E. Vecino, F.D. Rodriguez, N. Ruzafa, X. Pereiro, S.C. Sharma, Glia-neuron interactions in the mammalian retina, Prog Retin Eye Res 51 (2016) 1-40.

[54] A. Bringmann, T. Pannicke, J. Grosche, M. Francke, P. Wiedemann, S.N. Skatchkov, N.N. Osborne, A. Reichenbach, Müller cells in the healthy and diseased retina, Prog Retin Eye Res 25(4) (2006) 397-424.

[55] E. Newman, A. Reichenbach, The Müller cell: a functional element of the retina, Trends Neurosci 19(8) (1996) 307-12.

[56] J.W. Rich-Edwards, M.B. Goldman, W.C. Willett, D.J. Hunter, M.J. Stampfer, G.A. Colditz, J.E. Manson, Adolescent body mass index and infertility caused by ovulatory disorder, Am J Obstet Gynecol 171(1) (1994) 171-7.

[57] A. Kanda, K. Noda, I. Hirose, S. Ishida, TGF-β-SNAIL axis induces Müller glial-mesenchymal transition in the pathogenesis of idiopathic epiretinal membrane, Sci Rep 9(1) (2019) 673.

[58] K. Rashid, I. Akhtar-Schaefer, T. Langmann, Microglia in Retinal Degeneration, Front Immunol 10 (2019) 1975.

[59] A. Bringmann, P. Wiedemann, Involvement of Müller glial cells in epiretinal membrane formation, Graefes Arch Clin Exp Ophthalmol 247(7) (2009) 865-83.

[60] C.S. Sethi, G.P. Lewis, S.K. Fisher, W.P. Leitner, D.L. Mann, P.J. Luthert, D.G. Charteris, Glial remodeling and neural plasticity in human retinal detachment with proliferative vitreoretinopathy, Invest Ophthalmol Vis Sci 46(1) (2005) 329-42.

[61] C. Haritoglou, R.G. Schumann, A. Kampik, A. Gandorfer, Glial cell proliferation under the internal limiting membrane in a patient with cellophane maculopathy, Arch Ophthalmol 125(9) (2007) 1301-2.

[62] C. Guidry, The role of Müller cells in fibrocontractive retinal disorders, Prog Retin Eye Res 24(1) (2005) 75-86.

[63] P. Wiedemann, Growth factors in retinal diseases: proliferative vitreoretinopathy, proliferative diabetic retinopathy, and retinal degeneration, Surv Ophthalmol 36(5) (1992) 373-84.

[64] B.A. Coughlin, D.J. Feenstra, S. Mohr, Müller cells and diabetic retinopathy, Vision Res 139 (2017) 93-100.

[65] C. Guidry, R. Feist, R. Morris, C.W. Hardwick, Changes in IGF activities in human diabetic vitreous, Diabetes 53(9) (2004) 2428-35.

[66] C. Guidry, K.M. Bradley, J.L. King, Tractional force generation by human müller cells: growth factor responsiveness and integrin receptor involvement, Invest Ophthalmol Vis Sci 44(3) (2003) 1355-63.

[67] J. Zhang, X. Chen, L. Zhang, Y. Peng, gene polymorphisms associated with diabetic retinopathy risk in Chinese Han population, Oncotarget 8(50) (2017) 88034-88042.

[68] G.A. Limb, H. Jayaram, Regulatory and Pathogenic Roles of Müller Glial Cells in Retinal Neovascular Processes and Their Potential for Retinal Regeneration, Frontiers in Diabetes 20 (2010) 98-108.

[69] H. Kimura, C. Spee, T. Sakamoto, D.R. Hinton, Y. Ogura, Y. Tabata, Y. Ikada, S.J. Ryan, Cellular response in subretinal neovascularization induced by bFGF-impregnated microspheres, Invest Ophthalmol Vis Sci 40(2) (1999) 524-8.

[70] S. Yoshida, A. Yoshida, T. Ishibashi, Induction of IL-8, MCP-1, and bFGF by TNF-alpha in retinal glial cells: implications for retinal neovascularization during post-ischemic inflammation, Graefes Arch Clin Exp Ophthalmol 242(5) (2004) 409-13.

[71] T. Cheng, W. Cao, R. Wen, R.H. Steinberg, M.M. LaVail, Prostaglandin E2 induces vascular endothelial growth factor and basic fibroblast growth factor mRNA expression in cultured rat Müller cells, Invest Ophthalmol Vis Sci 39(3) (1998) 581-91.

[72] I.M. Nawaz, S. Rezzola, A. Cancarini, A. Russo, C. Costagliola, F. Semeraro, M. Presta, Human vitreous in proliferative diabetic retinopathy: Characterization and translational implications, Prog Retin Eye Res 72 (2019) 100756.

[73] S.Y. Oberstein, J. Byun, D. Herrera, E.A. Chapin, S.K. Fisher, G.P. Lewis, Cell proliferation in human epiretinal membranes: characterization of cell types and correlation with disease condition and duration, Mol Vis 17 (2011) 1794-805.

[74] S. Roy, S. Amin, Retinal fibrosis in diabetic retinopathy, Exp Eye Res 142 (2016) 71-5.

[75] M. Rodrigues, X. Xin, K. Jee, S. Babapoor-Farrokhran, F. Kashiwabuchi, T. Ma, I. Bhutto, S.J. Hassan, Y. Daoud, D. Baranano, S. Solomon, G. Lutty, G.L. Semenza, S. Montaner, A. Sodhi, VEGF secreted by hypoxic Müller cells induces MMP-2 expression and activity in endothelial cells to promote retinal neovascularization in proliferative diabetic retinopathy, Diabetes 62(11) (2013) 3863-73.

[76] J.C. Portillo, Y. Lopez Corcino, Y. Miao, J. Tang, N. Sheibani, T.S. Kern, G.R. Dubyak, C.S. Subauste, CD40 in Retinal Müller Cells Induces P2X7-Dependent Cytokine Expression in Macrophages/Microglia in Diabetic Mice and Development of Early Experimental Diabetic Retinopathy, Diabetes 66(2) (2017) 483-493.

[77] P.N. Bishop, Structural macromolecules and supramolecular organisation of the vitreous gel, Prog Retin Eye Res 19(3) (2000) 323-44.

[78] J.P. Monteiro, F.M. Santos, A.S. Rocha, J.P. Castro-de-Sousa, J.A. Queiroz, L.A. Passarinha, C.T. Tomaz, Vitreous humor in the pathologic scope: insights from proteomic approaches, Proteomics Clin Appl 9(1-2) (2015) 187-202.

[79] T. Shitama, H. Hayashi, S. Noge, E. Uchio, K. Oshima, H. Haniu, N. Takemori, N. Komori, H. Matsumoto, Proteome Profiling of Vitreoretinal Diseases by Cluster Analysis, Proteomics Clin Appl 2(9) (2008) 1265-1280.

[80] S. Rezzola, M.I. Nawaz, A. Cancarini, F. Semeraro, M. Presta, Vascular Endothelial Growth Factor in the Vitreous of Proliferative Diabetic Retinopathy Patients: Chasing a Hiding Prey?, Diabetes Care 42(7) (2019) e105-e106.

[81] S. Rezzola, M. Corsini, P. Chiodelli, A. Cancarini, I.M. Nawaz, D. Coltrini, S. Mitola, R. Ronca, M. Belleri, L. Lista, D. Rusciano, M. De Rosa, V. Pavone, F. Semeraro, M. Presta, Inflammation and N-formyl peptide receptors mediate the angiogenic activity of human vitreous humour in proliferative diabetic retinopathy, Diabetologia 60(4) (2017) 719-728.

[82] S. Rezzola, I.M. Nawaz, A. Cancarini, C. Ravelli, S. Calza, F. Semeraro, M. Presta, 3D endothelial cell spheroid/human vitreous humor assay for the characterization of anti-angiogenic inhibitors for the treatment of proliferative diabetic retinopathy, Angiogenesis 20(4) (2017) 629-640.

[83] I.M. Nawaz, P. Chiodelli, S. Rezzola, G. Paganini, M. Corsini, A. Lodola, A. Di Ianni, M. Mor, M. Presta, N-tert-butyloxycarbonyl-Phe-Leu-Phe-Leu-Phe (BOC2) inhibits the angiogenic activity of heparin-binding growth factors, Angiogenesis 21(1) (2018) 47-59.

[84] S. Rezzola, M. Dal Monte, M. Belleri, A. Bugatti, P. Chiodelli, M. Corsini, M. Cammalleri, A. Cancarini, L. Morbidelli, P. Oreste, P. Bagnoli, F. Semeraro, M. Presta, Therapeutic Potential of Anti-Angiogenic Multitarget N,O-Sulfated E. Coli K5 Polysaccharide in Diabetic Retinopathy, Diabetes 64(7) (2015) 2581-92.

[85] M. Dal Monte, S. Rezzola, M. Cammalleri, M. Belleri, F. Locri, L. Morbidelli, M. Corsini, G. Paganini, F. Semeraro, A. Cancarini, D. Rusciano, M. Presta, P. Bagnoli, Antiangiogenic Effectiveness of the Urokinase Receptor-Derived Peptide UPARANT in a Model of Oxygen-Induced Retinopathy, Invest Ophthalmol Vis Sci 56(4) (2015) 2392-407.

[86] S. Aretz, T.U. Krohne, K. Kammerer, U. Warnken, A. Hotz-Wagenblatt, M. Bergmann, B.V. Stanzel, T. Kempf, F.G. Holz, M. Schnölzer, J. Kopitz, In-depth mass spectrometric mapping of the human vitreous proteome, Proteome Sci 11(1) (2013) 22.

[87] A. Pollreisz, M. Funk, F.P. Breitwieser, K. Parapatics, S. Sacu, M. Georgopoulos, R. Dunavoelgyi, G.J. Zlabinger, J. Colinge, K.L. Bennett, U. Schmidt-Erfurth, Quantitative proteomics of aqueous and vitreous fluid from patients with idiopathic epiretinal membranes, Exp Eye Res 108 (2013) 48-58.

[88] A. Dongre, R.A. Weinberg, New insights into the mechanisms of epithelial-mesenchymal transition and implications for cancer, Nat Rev Mol Cell Biol 20(2) (2019) 69-84.

[89] J. Roche, The Epithelial-to-Mesenchymal Transition in Cancer, Cancers (Basel) 10(2) (2018).

[90] R. Kalluri, R.A. Weinberg, The basics of epithelial-mesenchymal transition, J Clin Invest 119(6) (2009) 1420-8.

[91] V. Das, S. Bhattacharya, C. Chikkaputtaiah, S. Hazra, M. Pal, The basics of epithelial-mesenchymal transition (EMT): A study from a structure, dynamics, and functional perspective, J Cell Physiol (2019).

[92] G.D. Marconi, L. Fonticoli, T.S. Rajan, S.D. Pierdomenico, O. Trubiani, J. Pizzicannella, F. Diomede, Epithelial-Mesenchymal Transition (EMT): The Type-2 EMT in Wound Healing, Tissue Regeneration and Organ Fibrosis, Cells 10(7) (2021).

[93] Y. Koike, M. Yozaki, A. Utani, H. Murota, Fibroblast growth factor 2 accelerates the epithelial-mesenchymal transition in keratinocytes during wound healing process, Sci Rep 10(1) (2020) 18545.

[94] D. Haensel, X. Dai, Epithelial-to-mesenchymal transition in cutaneous wound healing: Where we are and where we are heading, Dev Dyn 247(3) (2018) 473-480.

[95] B. Gawronska-Kozak, A. Grabowska, A. Kur-Piotrowska, M. Kopcewicz, Foxn1 Transcription Factor Regulates Wound Healing of Skin through Promoting Epithelial-Mesenchymal Transition, PLoS One 11(3) (2016) e0150635.

[96] P. Savagner, K.M. Yamada, J.P. Thiery, The zinc-finger protein slug causes desmosome dissociation, an initial and necessary step for growth factor-induced epithelial-mesenchymal transition, J Cell Biol 137(6) (1997) 1403-19.

[97] M.A. Nieto, R.Y. Huang, R.A. Jackson, J.P. Thiery, EMT: 2016, Cell 166(1) (2016) 21-45.

[98] K.A. Bielefeld, S. Amini-Nik, B.A. Alman, Cutaneous wound healing: recruiting developmental pathways for regeneration, Cell Mol Life Sci 70(12) (2013) 2059-81.

[99] S. Lamouille, J. Xu, R. Derynck, Molecular mechanisms of epithelial-mesenchymal transition, Nat Rev Mol Cell Biol 15(3) (2014) 178-96.

[100] D. Wu, A. Kanda, Y. Liu, K. Noda, M. Murata, S. Ishida, Involvement of Müller Glial Autoinduction of TGF-β in Diabetic Fibrovascular Proliferation Via Glial-Mesenchymal Transition, Invest Ophthalmol Vis Sci 61(14) (2020) 29.

[101] A.M. Abu El-Asrar, L. Missotten, K. Geboes, Expression of hypoxia-inducible factor-1alpha and the protein products of its target genes in diabetic fibrovascular epiretinal membranes, Br J Ophthalmol 91(6) (2007) 822-6.

[102] A. Hueber, P. Wiedemann, P. Esser, K. Heimann, Basic fibroblast growth factor mRNA, bFGF peptide and FGF receptor in epiretinal membranes of intraocular proliferative disorders (PVR and PDR), Int Ophthalmol 20(6) (1996) 345-50.

[103] X. Liang, C. Li, Y. Li, J. Huang, S. Tang, R. Gao, S. Li, Platelet-derived growth factor and basic fibroblast growth factor immunolocalized in proliferative retinal diseases, Chin Med J (Engl) 113(2) (2000) 144-7.

[104] M. Hollborn, K. Jahn, G.A. Limb, L. Kohen, P. Wiedemann, A. Bringmann, Characterization of the basic fibroblast growth factor-evoked proliferation of the human Müller cell line, MIO-M1, Graefes Arch Clin Exp Ophthalmol 242(5) (2004) 414-22.

[105] Y. Zhao, R.P. Singh, The role of anti-vascular endothelial growth factor (anti-VEGF) in the management of proliferative diabetic retinopathy, Drugs Context 7 (2018) 212532.

[106] G.S. Tan, N. Cheung, R. Simó, G.C. Cheung, T.Y. Wong, Diabetic macular oedema, Lancet Diabetes Endocrinol 5(2) (2017) 143-155.

[107] D.M. Brown, Q.D. Nguyen, D.M. Marcus, D.S. Boyer, S. Patel, L. Feiner, P.G. Schlottmann, A.C. Rundle, J. Zhang, R.G. Rubio, A.P. Adamis, J.S. Ehrlich, J.J. Hopkins, R.a.R.R. Group, Long-term outcomes of ranibizumab therapy for diabetic macular edema: the 36-month results from two phase III trials: RISE and RIDE, Ophthalmology 120(10) (2013) 2013-22.

ADDENDUM

During my Ph.D. tenure, I have co-authored the following paper (manuscript under preparation).

β-GALACTOSYLCERAMIDASE DEFICIENCY CAUSES UPREGULATION OF LONG PENTRAXIN-3 IN THE CENTRAL NERVOUS SYSTEM OF *TWITCHER* MICE AND KRABBE PATIENTS

Daniela Coltrini[1], **Adwaid Manu Krishna Chandran**[1], Mirella Belleri[1], Pietro L. Poliani[2], Manuela Cominelli[2], Francesca Pagani[2], Stefano Calza[3], Julia K. Kofler[4], Maria L. Escolar[4], Marco Presta[1]

β-GALACTOSYLCERAMIDASE DEFICIENCY CAUSES UPREGULATION OF LONG PENTRAXIN-3 IN THE CENTRAL NERVOUS SYSTEM OF *TWITCHER* MICE AND KRABBE PATIENTS.

Daniela Coltrini[1], **Adwaid Manu Krishna Chandran**[1], Mirella Belleri[1], Pietro L. Poliani[2], Manuela Cominelli[2], Francesca Pagani[2], Stefano Calza[3], Julia K. Kofler[4], Maria L. Escolar[4], Marco Presta[1]

[1]Unit of Experimental Oncology and Immunology, [2]Unit of Pathology and [3]Unit of Statistics, Department of Molecular and Translational Medicine, School of Medicine, University of Brescia, Italy.
[4]Program for Neurodevelopmental Function in Rare Disorders, Clinical Center for the Study of Development and Learning, University of North Carolina at Chapel Hill, Chapel Hill, USA.

Address correspondence to:
Marco Presta
Department of Molecular and Translational Medicine, University of Brescia, Viale Europa 11, 25123 Brescia, Italy.
E-mail: marco.presta@unibs.it

Running title: PTX3 in Krabbe disease

INTRODUCTION

The acute phase protein long pentraxin-3 (PTX3) is an important regulator of peripheral innate immunity and a key mediator of inflammation during cardiovascular and cerebrovascular diseases [108]. Growing evidence point to the involvement of PTX3 in neurodegenerative disorders [109]. *PTX3* expression is upregulated in the central nervous system (CNS) following pro-inflammatory cytokine stimulation [110], seizure-induced neurodegeneration [111], and ischemia [112]. Accordingly, peripheral PTX3 levels are increased after experimental stroke in mice [113] whilst plasma PTX3 levels correlate with mortality after ischemic stroke in humans [114]. In addition, serum levels of PTX3 have been proposed as a novel biochemical marker in Parkinson's disease [115].

Globoid cell leukodystrophy (GLD), or Krabbe disease, is an autosomal recessive sphingolipidosis caused by genetic deficiency of the lysosomal hydrolase *β-galactosylceramidase* (*GALC*) [116].

GALC degrades galactosylceramide (a major component of myelin) and other terminal β-galactose-containing sphingolipids, including β-galactosylsphingosine (psychosine), leading to a pro-inflammatory/neurodegenerative condition characterized by degeneration of oligodendroglia and progressive demyelination of the central and peripheral nervous system. The pathogenesis of GLD has been proposed to arise from the accumulation of the neurotoxic metabolite psychosine present at high levels in the CNS of Krabbe patients [117-120]. The disease is characterized by loss of oligodendroglia and Schwann cells with demyelination in the brain, spinal cord, nerve roots and peripheral nerves [121]. A pathognomonic feature of GLD is the presence in the white matter of globoid cells [122, 123], giant multinucleated cells likely originated from resident microglia [124]. Clinically, GLD may manifest in early infancy with fatal neurological dysfunctions [121, 125, 126]. The current standard of care for this disease is hematopoietic stem cell transplantation derived from bone marrow or umbilical cord blood [127, 128].

Here, the expression of PTX3 was investigated in the CNS of GALC deficient *twitcher* ($Galc^{twi/twi}$) mice, an authentic murine model of GLD [129, 130], and in the brain of Krabbe patients. The results demonstrate that *Ptx3* expression levels increase in the cerebrum, cerebellum, and spinal cord of $Galc^{twi/twi}$ mice throughout the course of the disease. This was paralleled by the upregulation of various proinflammatory genes, including cytokine/chemokine-encoding genes, and M1-polarized macrophage/microglia markers. Accordingly, the levels of PTX3 protein are significantly increased in the CNS and plasma of *twitcher* animals. In keeping with the data obtained in *twitcher* mice, immunohistochemical analysis of autopsy brain samples from Krabbe patients shows that macrophages and globoid cells are intensely immunoreactive for PTX3, which was absent in control brain samples. Finally, crossing of $Galc^{twi/twi}$ *twitcher* mice with transgenic *PTX3* overexpressing animals (*hPTX3* mice) caused an amelioration of clinical features and attenuated spinal cord inflammation in the *hPTX3/*$Galc^{twi/twi}$ offspring when compared to $Galc^{twi/twi}$ littermates.
In conclusion, our results provide the first evidence that PTX3 is produced in the CNS of GALC deficient *twitcher* mice and Krabbe patients and it may exert a protective role by reducing the neuroinflammatory response that occurs in the spinal cord of $Galc^{twi/twi}$ animals with possible implications for GLD therapy.

MATERIALS AND METHODS

Animals. Breeder *twitcher* heterozygous mice (C57BL/6J, $Galc^{twi/+}$; Jackson Laboratories, ME, USA) were maintained under standard housing conditions. Experiments were performed according

to the Italian laws (D.L. 116/92 and following additions) that enforce the EU 86/109 Directive and were approved by the local animal ethics committee (OPBA, Università degli Studi di Brescia, Italy). *Twitcher* mutation was determined by polymerase chain reaction (PCR) on DNA extracted from clipped tails [131]. In all the experiments, littermate wild type ($Galc^{wt}$) and homozygous ($Galc^{twi/twi}$) animals were used. To generate *PTX3*-overexpressing *twitcher* mice, syngeneic TgN(Tie2-hPTX3) male mice (*hPTX3* mice) that ubiquitously express human PTX3 under the control of the *Tie2* promoter [132] were bred with female $Galc^{twi/+}$ mice to obtain $hPTX3/Galc^{twi/+}$ animals. Next, $hPTX3/Galc^{wt}$ and $hPTX3/Galc^{twi/twi}$ mice were generated by crossing $hPTX3/Galc^{twi/+}$ breeder mice that were genotyped for *Galc* status by PCR and for *hPTX3* overexpression by RT-PCR.

Quantitative RT-PCR analysis. Cerebrum, cerebellum, and spinal cord specimens were analysed for gene expression by quantitative RT-PCR (qPCR) at P15, P24 and P35, and data were normalized for *Gapdh* expression [133]. To this purpose, total RNA was extracted from frozen samples using TRIzol Reagent according to manufacturer's instructions (Invitrogen Carlsbad, CA), and contaminating DNA was digested using DNAse (Promega). Total RNA (2 □g) was retrotranscribed with MMLV reverse transcriptase (Invitrogen,) using random hexaprimers in a final 20 □l volume. Quantitative PCR was performed with a ViiA™ 7 Real-Time PCR Detection System (Applied Biosystems) using an iQTM SYBR Green Supermix (Biorad) according to manufacturer's instructions. *Ptx3* expression levels were analysed by qPCR also in kidneys, liver, and lungs from $Galc^{wt}$ and $Galc^{twi/twi}$ mice at P35. In each experiment, an arbitrary value equal to 1.0 was assigned to the levels of expression of the gene(s) measured in one sample that was used as reference. The specific primers are shown in **Supplementary Table 1**.

PTX3 double-immunofluorescence analysis. Formalin-fixed, paraffin-embedded tissue sections (7 µm) of the brain cortex, cerebellum, and spinal cord from P35 $Galc^{wt}$ and $Galc^{twi/twi}$ mice were incubated overnight at 4°C with an anti-PTX3 polyclonal antibody from B. Bottazzi (Humanitas Clinical Institute, Rozzano, Italy) followed by 1 h incubation with biotin anti-rabbit antibody and by 1 h incubation with streptavidin Alexa Fluor 594. Sections were then incubated for 2 h with an anti-GFAP (Dako) or with an anti-Iba1 monoclonal antibody (Genetex), followed by 1 h incubation with Alexa Fluor 488 anti-mouse antibody. All tissue sections were incubated for 30 min with DAPI for nuclear staining and mounted in Dako fluorescent mounting medium. Images were taken using an Axiovert 200 M microscope equipped with ApoTome optical sectioning device (CarlZeiss, Oberkochen, Germany, EU).

Western blotting. Cerebrum, cerebellum, and spinal cord specimens from *Galc*^{wt} and *Galc*$^{twi/twi}$ mice at P35 were used for Western blotting analysis. The tissues were homogenized in lysis buffer (1.0% NP-40, 20 mM Tris-HCl pH 8, 137 mM NaCl, 10% glycerol, 2.0 mM EDTA, 1.0 mM sodium orthovanadate, 10 mg/ml aprotinin, 10 mg/ml leupeptin). For PTX3 expression analysis, tissue extracts (40 mg of protein) were analyzed using an anti-PTX3 polyclonal antibody. Monoclonal anti-vinculin antibody (Sigma-Aldrich) was used as the loading control.

Serum PTX3. The blood levels of PTX3 were evaluated by ELISA (R&D Systems) using 7.0 □l serum from *Galc*^{wt} and *Galc*$^{twi/twi}$ mice at P28-34.

Assessment of clinical features. Body weight, life span, twitching and hind limbs clenching were monitored daily from day P8 till mice reached a moribund condition. Each mouse was observed for at least 1 min by two trained observers. The extent of frequency and severity of twitching was scored as: 1, fine; 2, mild; 3, mild-moderate; 4, moderate; 5, severe. Hind limbs clenching frequency was scored: 1, rare; 2, mild; 3, intermittent; 4, moderate; 5, severe [134].

Histopathology of human GLD biopsies. Autopsy brain specimens of GLD patients (**Supplementary Table 2**) were obtained from the Program for Neurodevelopmental Function in Rare Disorders, Clinical Center for the Study of Development and Learning, University of North Carolina at Chapel Hill (Chapel Hill, USA). Two matched control brains from 4- year-old and 11-year-old patients who died for unrelated non neurological complications were obtained from the Archive of Pathological Department of Spedali Civili of Brescia. Their use was approved by the Ethics Board of Spedali Civili di Brescia [patient consent was not needed for retrospective and exclusively observational study on archival material obtained for diagnostic purposes (Delibera del Garante n. 52 del 24/7/2008 and DL 193/2003)]. Formalin-fixed, paraffin-embedded tissue sections were submitted to H&E and single or double immunohistochemical staining. Briefly, sections were de-waxed, rehydrated and endogenous peroxidase activity blocked with 0,3% H_2O_2 in methanol for 20 minutes. Antigen retrieval was performed using a microwave-oven or thermostatic bath in 1.0 mM EDTA buffer (pH 8.0). Sections were then washed in TBS (pH 7,4) and incubated for one hour in the specific primary antibody diluted in TBS 1% Bovine Serum Albumin (BSA). Signal has been revealed using the DAKO Envision+System-HRP Labelled Polymer Anti-Mouse or Anti-Rabbit (Dako Cytomation), followed by Diaminobenzydine (DAB) as chromogen and Hematoxylin as counterstain. For double immunostains, after completing the first immune reaction, the second primary antibody was applied and labelled using MACH 4^{TM} Universal AP Polymer Kit (Biocare

Medical); chromogen reaction was developed with Ferangi Blue^{TM} Chromogen System (Biocare Medical) and nuclei were faintly counterstained with Methyl Green. Images were then acquired with Olympus DP70 camera mounted on Olympus Bx60 microscope using AnalySIS imaging software (Soft Imaging System GmbH). The following primary antibodies were used: rabbit anti-PTX3 polyclonal antibody (1:500, kindly provided by B. Bottazzi Humanitas Clinical Institute, Rozzano, Italy), monoclonal mouse anti human CD68, clone PG-M1 (1:200, Dako Cytomation), and monoclonal mouse anti human GFAP, clone 6F2 (1:100, Dako Cytomation).

RESULTS

Ptx3 upregulation in *twitcher* CNS

In a first set of experiments, *Ptx3* expression was assessed by qPCR analysis in the cerebrum of littermate *Galc*^{wt} and homozygous *Galc*$^{twi/twi}$ mice. Measurements were performed at postnatal day P15 before the onset of evident neurologic signs, at P24 when pathologic alterations are occasionally detectable, and at P35 when *Galc*$^{twi/twi}$ mice show clear neurologic defects, including tremor and hind limb paralysis [130, 135, 136]. As shown in **Figure 1A**, the brain levels of *Ptx3* transcripts start to increase at P15, to further increase at P24 and P35. This was paralleled by the upregulation of the inflammatory cytokines *Tnf*□, *Cxcl1* and *Il1*α and of the CCAAT/enhancer binding protein delta (*Cebpd*) gene, which encodes for a transcription factor mediating *PTX3* expression in astrocytes during neuroinflammation [137]. Accordingly, a progressive increase of the levels of the astrocytic marker of gliosis *Gfap* and of the microglial marker *ionized calcium-binding adaptor molecule-1* (*Iba1*) [138] occurs in *Galc*$^{twi/twi}$ cerebrum when compared to controls. In keeping with the neuroinflammatory response that occurs in *twitcher* brain, we observed an increase of the levels of expression of the classical M1 macrophage polarization/microglia markers *Fc receptor, IgG, low affinity III* and *II (Fcgr3/CD16* and *Fcgr2/CD32)* [139] with no changes in the expression of the alternative M2 macrophage polarization markers *arginase-1* (*Arg1*) and *mannose receptor C-type1* (*Mrc1*/*CD206*) [140]. A similar transcriptional profile was observed in the cerebellum (**Supplementary Figure 1**) and spinal cord (**Figure 1B**) of *Galc*$^{twi/twi}$ mice that also showed an increase of the M2 polarization markers *Arg1* and *CD206*, with *Ptx3* mRNA levels that are significantly higher than those measured in the brain counterpart at all the time points investigated. This appears to be in keeping with the higher levels of psychosine detected in the spinal cord of *twitcher* mice when compared to cerebrum and cerebellum [141]. Western blot analysis confirmed that *Ptx3* upregulation in the CNS of *twitcher* mice resulted in an increase expression of the PTX3

protein in cerebrum, cerebellum, and spinal cord of these animals when compared to controls (**Figure 2A**).

At variance with the results obtained by the analysis of the *twitcher* CNS, no *Ptx3* upregulation occurs in the peripheral tissues of *Galc*$^{twi/twi}$ mice, including kidney, liver, and lungs, in which only limited psychosine accumulation and inflammatory responses occur as a consequence of GALC deficiency [130, 135, 142, 143] (**Supplementary Figure 2**). Nevertheless, in keeping with the observation that the serum levels of PTX3 are increased after stroke [113, 114] and in Parkinson's disease [115], the levels of PTX3 in the blood of P35 *twitcher* mice are significantly increased when compared to *Galc*^{wt} animals (**Figure 2B**).

Previous observations had shown that activated astrocytes and microglia represent a major source of PTX3 in the brain [110, 144]. On this basis, immunohistochemical analysis of CNS was performed in *twitcher* mice and control littermates at P35. As shown in **Figure 3A**, double immunostains indicate that PTX3 immunoreactivity is prevalently detectable in IBA1-positive globoid cells in the white matter of the brain cortex and spinal cord of P35 *Galc*$^{twi/twi}$ animals (**Figure 3A**), no significant expression being observed in control samples that lack signs of gliosis (**Supplementary Figure 3**). In addition, PTX3 is also expressed by GFAP-positive astrocytes in the grey matter of the CNS of *twitcher* animals (**Figure 3B**) but not in *Galc*^{wt} animals (**Supplementary Figure 3**). Similar results were obtained in *twitcher* cerebellum samples (**Supplementary Figure 4**).

Figure 1. *Ptx3* and proinflammatory gene expression in the cerebrum and spinal cord of *twitcher* mice. Steady state mRNA levels of the indicated genes were evaluated by qPCR in the cerebrum (A) and spinal cord (B) of *Galc*^{wt} and *Galc*$^{twi/twi}$ mice harvested at P15, P24 and P35. Data were normalized to *Gapdh* expression and are the mean ± S.D. of 3-6 animals per group, *, P< 0.05; #, P < 0.01; §, P < 0.001, *Galc*^{wt} *versus Galc*$^{twi/twi}$, Student's t-test.

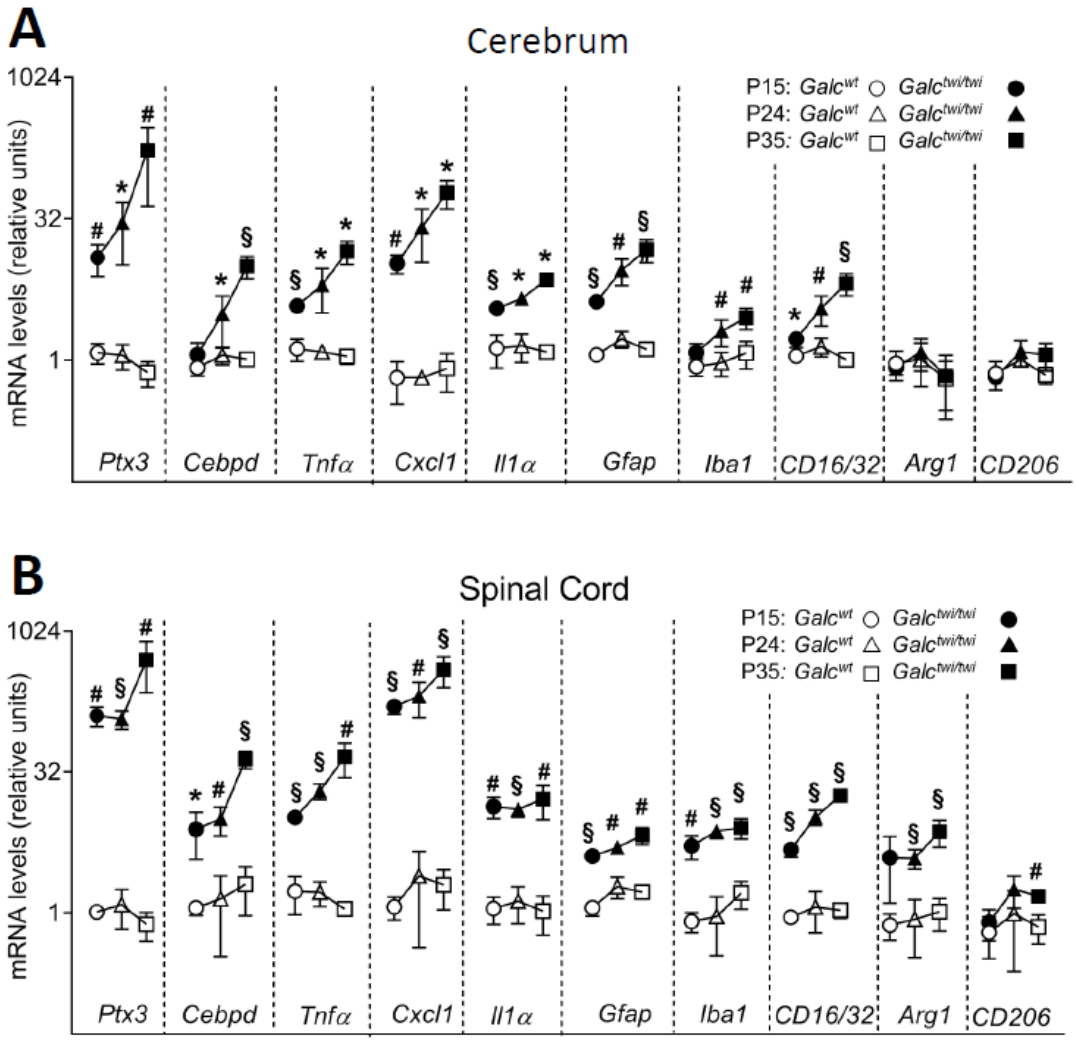

Figure 2. PTX3 protein levels in *twitcher* mice. A) Western blot analysis of PTX3 immunoreactivity in the CNS of *Galc*^{wt} and *Galc*$^{twi/twi}$ mice at P35. Vimentin was used as a loading control. **B**) Blood samples were collected from 22 *Galc*^{wt} and 27 *Galc*$^{twi/twi}$ mice at P28-34 and serum levels of PTX3 were assessed by ELISA. Each point represents one animal. Data are shown as mean ± S.D. ***, $P < 0.001$, Student's t test.

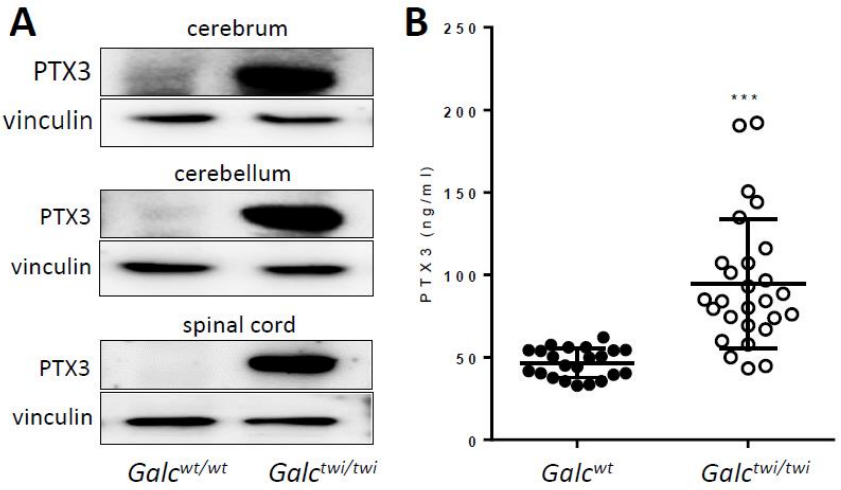

Figure 3. PTX3 immunolocalization in the CNS of *twitcher* mice. Paraffin-embedded sections of the white (**A**) and grey (**B**) matter of the brain cortex and spinal cord of P35 *Galc*$^{twi/twi}$ mice were double-immunostained with anti-PTX3/GFAP or anti-PTX3/IBA1 antibodies. Scale bar, 50 µm, scale bar in inserts, 5 µm.

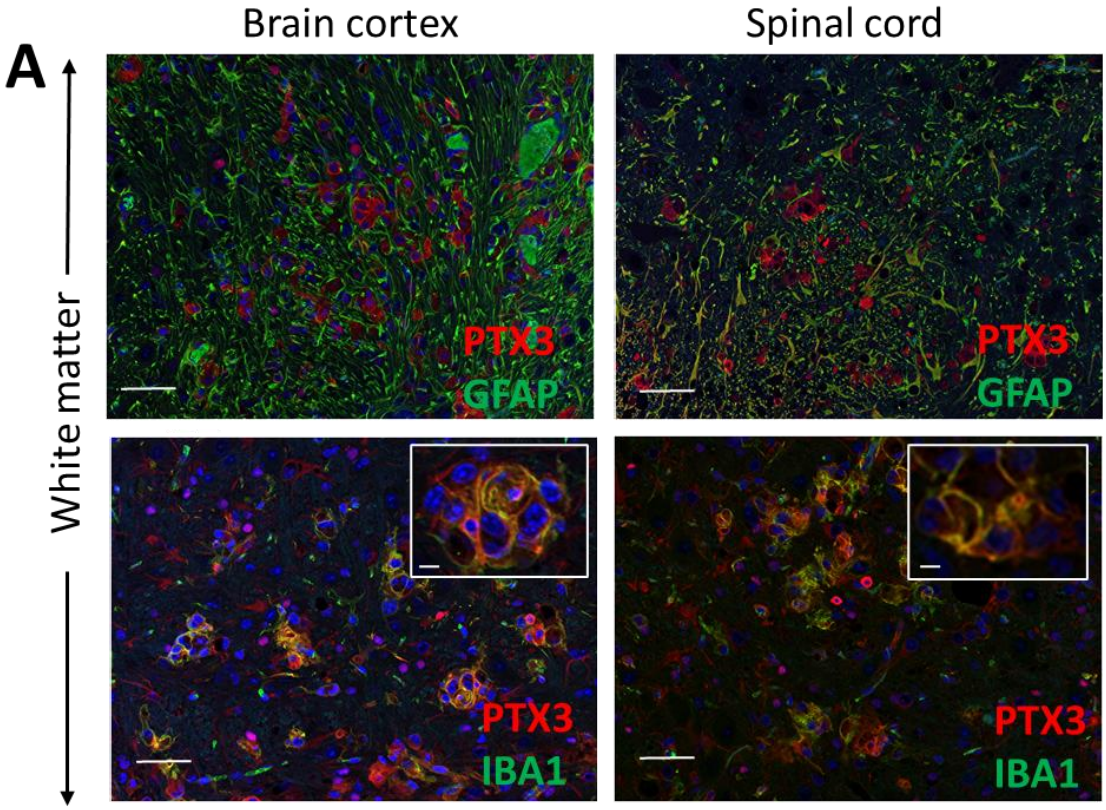

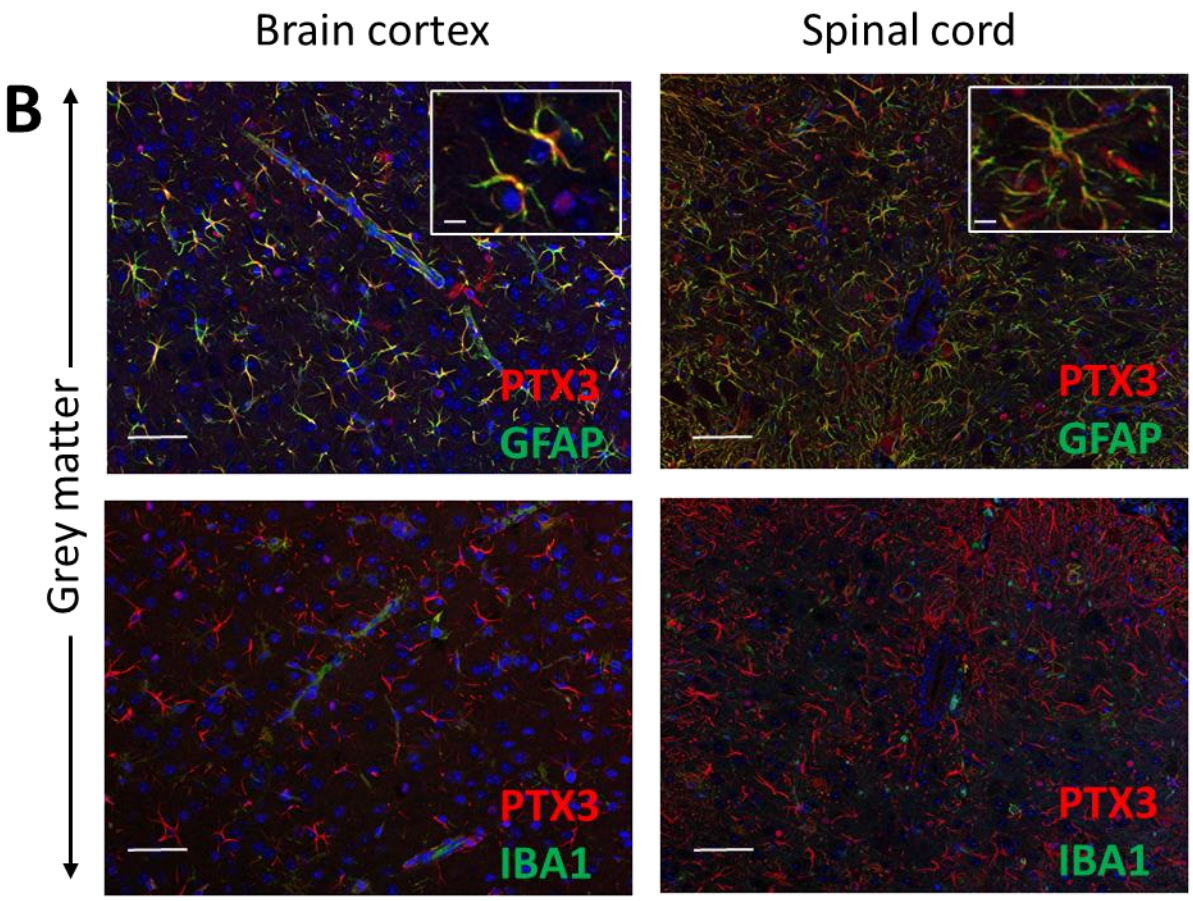

PTX3 is expressed in the brain of Krabbe patients

To assess whether GALC deficiency may cause *PTX3* expression also in human CNS, we analyzed autopsy brain samples from 9 Krabbe patients and 2 matched controls (**Table 1)**. Most of the Krabbe samples showed the classical histopathological hallmarks of the disease, such as diffuse demyelination along with marked loss of oligodendrocytes, intense reactive gliosis, and infiltration of globoid cells (**Figure 4A**). Single immunostains indicate that macrophages and globoid cells are diffusely and intensely immunoreactive for PTX3. Double immunostains confirmed that PTX3 is mainly expressed within macrophages and globoid cells in human samples, while GFAP double positive astrocytes are barely detected. Control brain samples did not show double positive PTX3 immunoreactive cells (**Figure 4B**). Overall, in keeping with the data obtained in *twitcher* mice, these findings demonstrate that PTX3 is upregulated in the brain of GLD patients, its immunoreactivity being mainly expressed in monocyte-derived cells.

Figure 4. PTX3 immunolocalization in the brain of Krabbe patients. A) Representative images from Krabbe disease brain specimens showing the classical histopathological hallmarks of the disease with diffuse infiltration of macrophages mainly distributed around the blood vessels and referred as "globoid cells" (left image, H&E staining). Immunostains for PTX3 and GFAP (middle and right images, respectively) show intense and diffuse expression of PTX3 and gliosis. B) Double immunostainings from representative Krabbe disease and matched control brain samples. The large majority of CD68+ monocyte-derived cells are intensely immunoreactive for PTX3 within the white matter of Krabbe disease patients (left image) while reactive GFAP+ astrocytes expressing PTX3 are barely detected (middle left image; see arrow). Conversely, no PTX3+ or CD68+ cells were detected in these samples, except for rare circulating CD68-PTX3+ monocytes within the vessels (middle right image) and PTX3 was not detected in resident GFAP+ astrocytes from control matched brains (right image). Images are from 40x (panel A) and 60x (panel B) original magnification.

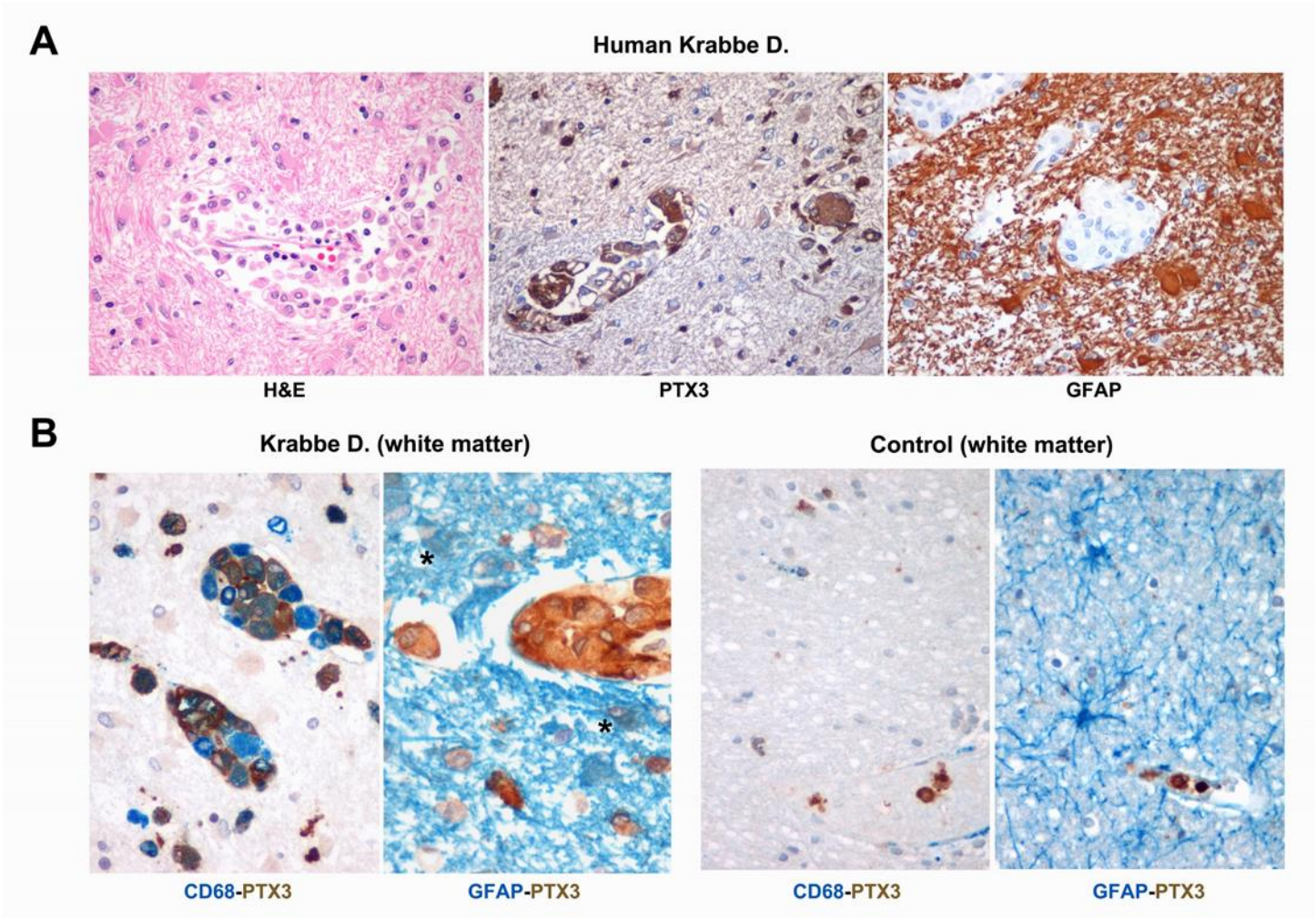

Table 1. PTX3 immunostaining in Krabbe patients

Deidentified case ID	Presence of pathology (perivascular globoid cells)		GFAP staining		PTX3 staining	
CW15 103	-	No evidence	+/-	Mild gliosis	-	
CW18 064	+/-	Modest	++	Gliosis	+/-	Only few inflammatory cells
CW16 061	++	Moderate	++	Gliosis	++	Mainly in perivascular globoid cells
CW16 064	+++	Severe	++	Gliosis	++	Mainly in perivascular globoid cells
CW17 060	+++	Severe	++	Gliosis	++	Mainly in perivascular globoid cells
CW18 060	+++	Severe	++	Gliosis	++	Mainly in perivascular globoid cells
CW16 062	-	No evidence	+	Moderate gliosis	+/-	Only few inflammatory cells
CW16 065	+	Mild to moderate	++	Gliosis	+	Mainly in perivascular globoid cells
CW16 066	+++	Severe	++	Gliosis	++	Mainly in perivascular globoid cells

PTX3 overexpression reduces clinical symptoms and attenuates spinal cord inflammation in *twitcher* mice

TgN(Tie2-hPTX3) mice (*hPTX3* mice) ubiquitously express human *PTX3* under the control of the *Tie2* promoter, leading to a significant accumulation of the PTX3 protein in serum and tissues of the transgenic animals [132]. The constitutive *hPTX3* expression does not result in apparent defects in embryonic development, adult animals are normal and fertile, and no macroscopic or microscopic morphological abnormalities have been observed in organs and tissues of *hPTX3* mice [132]. On this basis, to assess a possible impact of PTX3 overexpression in *twitcher* mice, syngeneic *PTX3*-overexpressing *hPTX3* male mice were crossed with female $Galc^{twi/+}$ animals to obtain $hPTX3/Galc^{twi/+}$ breeders that were then crossed to generate $hPTX3/Galc^{wt}$ and $hPTX3/Galc^{twi/twi}$ animals. Next, $hPTX3/Galc^{wt}$ and $hPTX3/Galc^{twi/twi}$ mice were compared to the corresponding $Galc^{wt}$ and $Galc^{twi/twi}$ littermates. As shown in **Supplementary Figure 5,** constitutive *hPTX3* overexpression does not affect the body weight gain of both $hPTX3/Galc^{wt}$ and $hPTX3/Galc^{twi/twi}$ mice when compared to the corresponding control $Galc^{wt}$ and $Galc^{twi/twi}$ animals, *Galc* deficiency leading to a similar decrease in body weight starting from approximately day P20 and P28 both in the absence or in the presence of constitutive *hPTX3* overexpression in male and female animals, respectively. Nevertheless, *hPTX3* overexpression resulted in statistically significant, albeit limited 4 day-increase of the overall survival of *twitcher* animals, with the life span extending from 42 to 46 days ($P< 0.001$) (**Figure 5A**), thus suggesting that PTX3 may exert an impact on the disease course. Indeed, when compared to $Galc^{twi/twi}$ animals, $hPTX3/Galc^{twi/twi}$ mice showed a reduced frequency and severity of twitching, which appeared around day P22 in both groups of animals (**Figure 5B, C**). In addition, $hPTX3/Galc^{twi/twi}$ mice displayed a less severe atypical tail suspension reflex (hind limbs clenching)

(**Figure 5D**). No animal death and appearance of clinical symptoms were instead observed in *hPTX3/Galc*^{wt} and *Galc*^{wt} mice during the same investigation period.

Figure 5. Impact of hPTX3 overexpression on the clinical features of twitcher mice. A) The life span of hPTX3/Galctwi/twi mice (n = 15) was compared to that of Galctwi/twi mice (n = 11). hPTX3 overexpressing animals had a significant extension of life span compared to control twitcher mice. P < 0.001, Gehan-Breslow-Wilcoxon test. B-D) The extent of frequency (B) and severity (C) of twitching and hind limbs clenching frequency (D) were scored in hPTX3/Galctwi/twi mice (n = 15) and Galctwi/twi mice (n = 11). No neurological signs were observed before day P20 in both groups of animals. No animal death and appearance of clinical symptoms were observed in hPTX3/Galcwt and Galcwt mice throughout the whole experimental period. *, P < 0.05; #, P < 0.01; §, P < 0.001, Student's t-test.

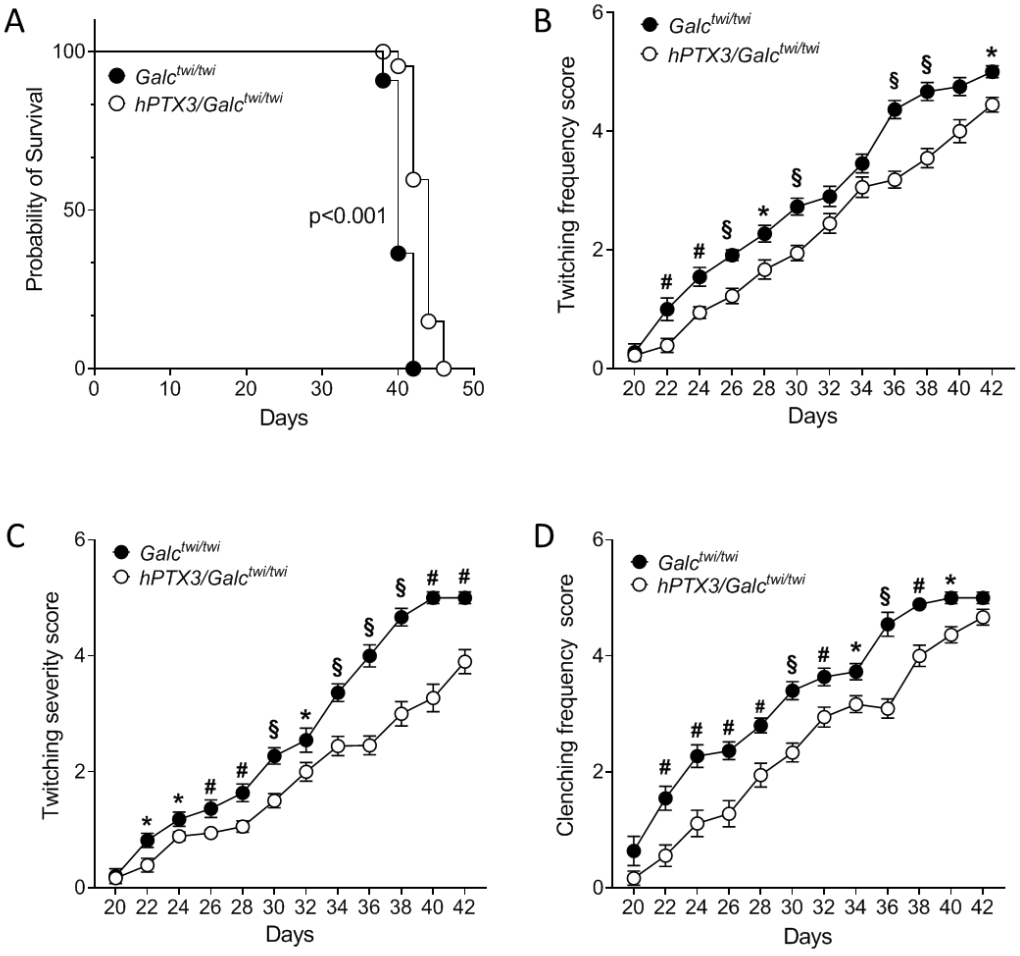

Finally, qPCR analysis of cerebrum, cerebellum, and spinal cord of P35 animals was performed to assess the impact of *hPTX3* overexpression on the inflammatory response of the CNS in GALC-deficient mice. As shown in **Figure 6**, a reduced upregulation of the expression of the inflammatory

mediators *Tnfα*, *Il1α*, and *Cxcl1*, as well as of the M1 polarization macrophage/microglia markers *CD16/CD32*, was observed in the spinal cord of *hPTX3/Galc*$^{twi/twi}$ mice when compared to the *Galc*$^{twi/twi}$ counterpart, with no difference in *Gfap* and *Iba1* expression. At variance, no differences in gene expression were detected in the cerebrum and cerebellum of the two groups of animals, the only exceptions being represented by a decreased cerebellar expression of the M2 polarization markers *Arg1* and *CD206* and a slight increase of cerebrum expression of *TNFa* in *hPTX3/Galc*$^{twi/twi}$ mice when compared to *Galc*$^{twi/twi}$ animals (**Supplementary Figure 6**). In keeping with these observations, the levels of endogenous murine *Ptx3* transcript and of its transcription factor *Cebpd* were significantly reduced in the spinal cord of *hPTX3/Galc*$^{twi/twi}$ mice when compared to *Galc*$^{twi/twi}$ animals (**Figure 6**), no differences being instead observed between the two groups in the cerebrum and cerebellum (**Supplementary Figure 6**).

Figure 6. qPCR analysis of the spinal cord of hPTX3/Galcwt and hPTX3/Galctwi/twi mice. Steady state mRNA levels of the indicated genes were evaluated by qPCR in the spinal cord of hPTX3/Galcwt and hPTX3/Galctwi/twi mice and compared to those measured in the corresponding control Galcwt and Galctwi/twi mice harvested at P35. Data were normalized to Gapdh expression and are the mean ± SEM of 7-10 animals per group. *, P < 0.1; **, P < 0.05; ***, P < 0.01,****, P < 0.001 for Galctwi/twi versus hPTX3/Galctwi/twi ; §, P < 0.001 for Galcwt versus Galctwi/twi or hPTX3/Galcwt versus hPTX3/Galctwi/twi. One-way ANOVA with post-hoc comparisons with adjustment for multiple comparisons (Sidak).

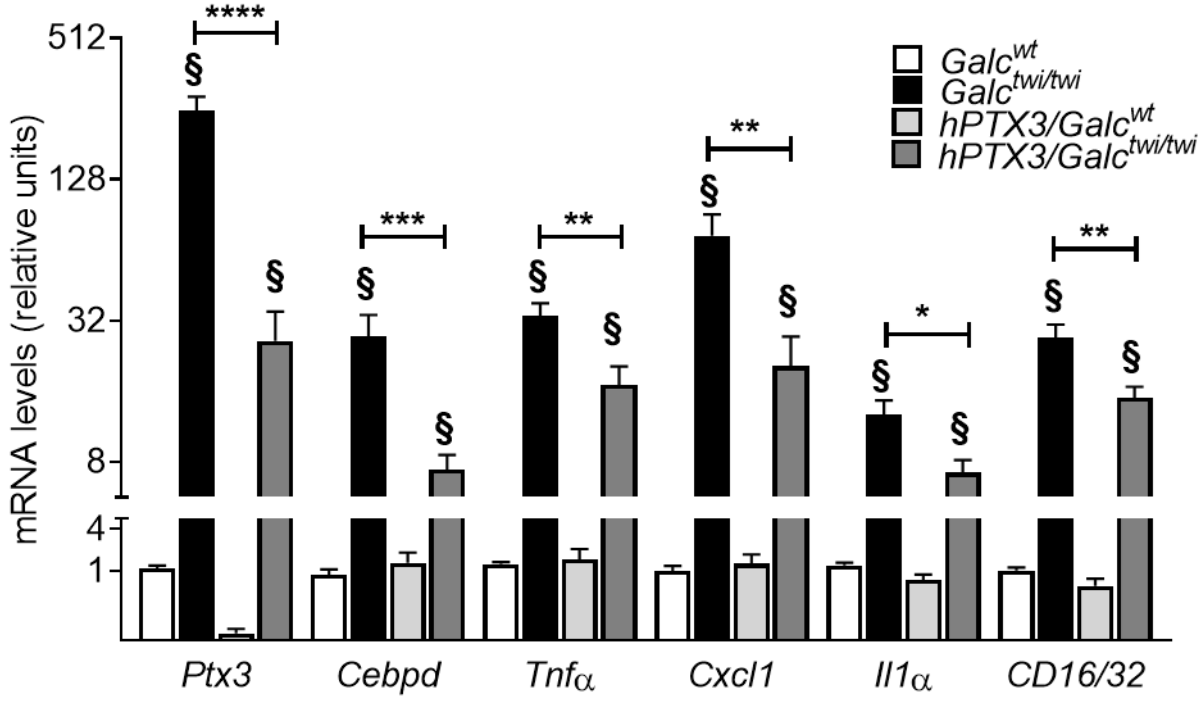

DISCUSSION

In humans, genetic deficiency of the sphingolipid-metabolizing enzyme GALC leads to Krabbe disease, a neuroinflammatory degenerative disorder. Here, we demonstrate that *twitcher* mice, an authentic model of Krabbe disease [129, 130], is characterized by the progressive upregulation of the expression of the soluble pattern recognition receptor PTX3 along the CNS caudal-rostral axis, with no changes in the peripheral organs. The upregulation of the *Ptx3* transcript levels in cerebrum, cerebellum, and spinal cord of *twitcher* mice results in the increase of PTX3 protein levels in the affected tissues and plasma. In keeping with these observations, PTX3 is expressed by monocyte-derived cells in brain specimens from Krabbe patients but not in controls.

Ptx3 expression can be induced in the CNS following stimulation by LPS or pro-inflammatory cytokines [110]. Accordingly, *Ptx3* upregulation is observed under various experimental neuroinflammatory conditions, including neurotrauma [145], ischemia [112], limbic seizure [111] and autoimmune encephalomyelitis [146]. In addition, serum levels of PTX3 are increased in patients affected by neurodegenerative disorders, including Parkinson's disease [115], ischemic stroke [114], and multiple sclerosis [146].

Our data extend these observations and demonstrate for the first time that *Ptx3* upregulation occurs in the CNS of *twitcher* mice in parallel with an increased expression of neuroinflammation-related genes, including various cytokines/chemokines, the marker of gliosis *Gfap*, the microglial marker *Iba1*, and the M1 macrophage polarization/microglia markers *CD16/CD32*. These changes were detectable at postnatal day P15, before the onset of evident neurologic signs, and were increased at P24, when pathologic alterations are occasionally noticeable, and at P35, when clear neurologic defects occur, including tremor and hind limb paralysis [130, 135, 136]. These findings indicate that the inflammatory environment which is progressively established after birth in the CNS of GALC deficient mice drives the expression of *Ptx3*, as confirmed by the observed upregulation of *Cebpd*, a transcription factor known to mediate *PTX3* expression in astrocytes during neuroinflammation [137]. Previous findings had shown that PTX3 can be expressed by neurons, astrocytes, and/or microglia following cytokine stimulation or under neuroinflammatory conditions depending on the specific disorder and acute *versus* chronic phase of the disease [see [109, 145, 146] and references therein]. Here, immunohistochemical analysis has demonstrated that PTX3 immunoreactivity is prevalently detectable in IBA1-positive globoid cells in the white matter of the brain cortex, cerebellum, and

spinal cord, as well as in GFAP-positive astrocytes of the grey matter of *Galc*$^{twi/twi}$ animals. These observations were confirmed by the analysis of autopsy brain specimens from Krabbe infants that were characterized by an intense gliosis and in which PTX3 immunoreactivity was detectable in macrophages and globoid cells, a hallmark of Krabbe disease [124].

PTX3 is an important mediator of innate immunity responses, produced locally at the site of inflammation [147]. In CNS, PTX3 modulates the activity of microglia by inhibiting phagocytosis of apoptotic cells and favoring the uptake of pathogens [144]. PTX3 binding helps the rescue of neurons from phagocytic clearance by macrophages [137] and protects them from ischemic damage [113, 148], trauma [149], and in Parkinson's disease [150]. Accordingly, neurogenesis and angiogenesis are inhibited after cerebral ischemia in *Ptx3* null mice and neuronal damage is increased after limbic seizure when GALC deficient animals were compared to controls [111, 112]. Together, these data point to a protective role of PTX3 during neuroinflammation.

In keeping with this hypothesis, our data demonstrate that constitutive *PTX3* overexpression attenuates the severity of clinical signs in *twitcher* mice, such as twitching and hind limbs clenching, and it causes a limited, albeit significant increase of their life span. Accordingly, *PTX3* overexpression reduced the upregulation of proinflammatory genes in the spinal cord of *hPTX3/Galc*$^{twi/twi}$ mice when compared to *Galc*$^{twi/twi}$ animals, including endogenous *Ptx3* and its transcription factor *Cebpd*. Of note, at variance with the results obtained for the spinal cord, *PTX3* overexpression did not affect the neuroinflammatory response observed in the cerebrum and cerebellum of *hPTX3/Galc*$^{twi/twi}$ *versus* *Galc*$^{twi/twi}$ animals. Relevant to this point, neurohistopathological and neurochemical alterations caused by GALC deficiency in the CNS of *twitcher* mice have been shown to occur in a temporal and regional-dependent fashion, the first alterations being observed in the spinal cord to progress along the caudal-rostral axis in the cerebellum and cerebrum [see [151] and references therein]. In addition, spinal cord alterations are already observed in 18–21-week-old GLD fetuses [152, 153]. Thus, the spinal cord appears to represent the earliest and most susceptible tissue affected by GALC deficiency in murine and human CNS. Different hypotheses can be raised to attempt to explain why such tissue is also more responsive to the protective role exerted by genetic, constitutive *PTX3* upregulation. In *hPTX3* animals the ubiquitous production of PTX3 is under the control of the *Tie2* promoter [132] that drives the vascular expression of the transgene throughout embryogenesis and adulthood [154]. Thus, the early *PTX3* overexpression that occurs in *hPTX3/Galc*$^{twi/twi}$ animals may prevent, at least in part, the first lesions that arise in the spinal cord of GALC deficient mice, being instead less effective against the later CNS lesions. In addition, the metabolic alterations that occur in parallel with the

progression of gliosis, neurodegeneration, microglial activation, and apoptosis along the rostral-caudal axis in a regional and age-dependent fashion [151] may exert a different impact on the protective activity of PTX3 in *hPTX3/Galc*$^{twi/twi}$ mice. A further hypothesis can be based on the fact that PTX3 may also exert detrimental effects following CNS damage [see [109] and references therein], indicating that the activity of PTX3 in neuroinflammation may represent the result of a fine tuning in different areas of the CNS between pro and anti-neurodegenerative mechanisms of action that remain poorly defined. Finally, other members of the long pentraxin family, represented by the neuronal pentraxin NP1, NP2 and NPR, may exert an impact on neurodegeneration and interfere with PTX3 activity [145]. Further studies, including experiments performed in a *Ptx3* null background, will be required to assess these hypotheses.

In conclusion, our results provide the first evidence that PTX3 is produced in the CNS of GALC deficient *twitcher* mice and Krabbe patients and it may exert a protective role by reducing the neuroinflammatory response that occurs in the spinal cord of *Galc*$^{twi/twi}$ animals with possible implications for GLD therapy.

REFERENCES

[1] S.C. Bu, R. Kuijer, X.R. Li, J.M. Hooymans, L.I. Los, Idiopathic epiretinal membrane, Retina 34(12) (2014) 2317-35.
[2] E. Tsotridou, E. Loukovitis, K. Zapsalis, I. Pentara, S. Asteriadis, P. Tranos, Z. Zachariadis, G. Anogeianakis, A Review of Last Decade Developments on Epiretinal Membrane Pathogenesis, Med Hypothesis Discov Innov Ophthalmol 9(2) (2020) 91-110.
[3] B. George, S. Chen, V. Chaudhary, J. Gonder, S. Chakrabarti, Extracellular matrix proteins in epiretinal membranes and in diabetic retinopathy, Curr Eye Res 34(2) (2009) 134-44.
[4] A. Russo, M. Ragusa, C. Barbagallo, A. Longo, T. Avitabile, M.G. Uva, V. Bonfiglio, M.D. Toro, R. Caltabiano, C. Mariotti, F. Boscia, M. Romano, C. Di Pietro, D. Barbagallo, M. Purrello, M. Reibaldi, miRNAs in the vitreous humor of patients affected by idiopathic epiretinal membrane and macular hole, PLoS One 12(3) (2017) e0174297.
[5] C.H. Ng, N. Cheung, J.J. Wang, A.F. Islam, R. Kawasaki, S.M. Meuer, M.F. Cotch, B.E. Klein, R. Klein, T.Y. Wong, Prevalence and risk factors for epiretinal membranes in a multi-ethnic United States population, Ophthalmology 118(4) (2011) 694-9.
[6] C.S. Fong, P. Mitchell, E. Rochtchina, T. Hong, T. de Loryn, J.J. Wang, Incidence and progression of epiretinal membranes in eyes after cataract surgery, Am J Ophthalmol 156(2) (2013) 312-318.e1.
[7] W. Xiao, X. Chen, W. Yan, Z. Zhu, M. He, Prevalence and risk factors of epiretinal membranes: a systematic review and meta-analysis of population-based studies, BMJ Open 7(9) (2017) e014644.
[8] P. Maitra, D.A. Kumar, A. Agarwal, Epiretinal membrane profile on spectral domain optical coherence tomography in patients with uveitis, Indian J Ophthalmol 67(3) (2019) 376-381.
[9] C.I. Falkner-Radler, C. Glittenberg, S. Hagen, T. Benesch, S. Binder, Spectral-domain optical coherence tomography for monitoring epiretinal membrane surgery, Ophthalmology 117(4) (2010) 798-805.
[10] Y. Hirano, T. Yasukawa, Y. Ogura, Optical coherence tomography guided peeling of macular epiretinal membrane, Clin Ophthalmol 5 (2010) 27-9.

[11] A. Govetto, R.A. Lalane, D. Sarraf, M.S. Figueroa, J.P. Hubschman, Insights Into Epiretinal Membranes: Presence of Ectopic Inner Foveal Layers and a New Optical Coherence Tomography Staging Scheme, Am J Ophthalmol 175 (2017) 99-113.
[12] V. Konidaris, S. Androudi, A. Alexandridis, A. Dastiridou, P. Brazitikos, Optical coherence tomography-guided classification of epiretinal membranes, Int Ophthalmol 35(4) (2015) 495-501.
[13] W. Stevenson, C.M. Prospero Ponce, D.R. Agarwal, R. Gelman, J.B. Christoforidis, Epiretinal membrane: optical coherence tomography-based diagnosis and classification, Clin Ophthalmol 10 (2016) 527-34.
[14] J.W. Yau, S.L. Rogers, R. Kawasaki, E.L. Lamoureux, J.W. Kowalski, T. Bek, S.J. Chen, J.M. Dekker, A. Fletcher, J. Grauslund, S. Haffner, R.F. Hamman, M.K. Ikram, T. Kayama, B.E. Klein, R. Klein, S. Krishnaiah, K. Mayurasakorn, J.P. O'Hare, T.J. Orchard, M. Porta, M. Rema, M.S. Roy, T. Sharma, J. Shaw, H. Taylor, J.M. Tielsch, R. Varma, J.J. Wang, N. Wang, S. West, L. Xu, M. Yasuda, X. Zhang, P. Mitchell, T.Y. Wong, M.-A.f.E.D.M.-E.S. Group, Global prevalence and major risk factors of diabetic retinopathy, Diabetes Care 35(3) (2012) 556-64.
[15] N. Cheung, P. Mitchell, T.Y. Wong, Diabetic retinopathy, Lancet 376(9735) (2010) 124-36.
[16] K.Z. Aung, G. Makeyeva, M.K. Adams, E.W. Chong, L. Busija, G.G. Giles, D.R. English, J. Hopper, P.N. Baird, R.H. Guymer, L.D. Robman, The prevalence and risk factors of epiretinal membranes: the Melbourne Collaborative Cohort Study, Retina 33(5) (2013) 1026-34.
[17] Q. You, L. Xu, J.B. Jonas, Prevalence and associations of epiretinal membranes in adult Chinese: the Beijing eye study, Eye (Lond) 22(7) (2008) 874-9.
[18] G. JDM., Stereoscopic atlas of macular disease, 1987:716-717.
[19] J.U. Hwang, J. Sohn, B.G. Moon, S.G. Joe, J.Y. Lee, J.G. Kim, Y.H. Yoon, Assessment of macular function for idiopathic epiretinal membranes classified by spectral-domain optical coherence tomography, Invest Ophthalmol Vis Sci 53(7) (2012) 3562-9.
[20] N. Cheung, S.P. Tan, S.Y. Lee, G.C.M. Cheung, G. Tan, N. Kumar, C.Y. Cheng, T.Y. Wong, Prevalence and risk factors for epiretinal membrane: the Singapore Epidemiology of Eye Disease study, Br J Ophthalmol 101(3) (2017) 371-376.
[21] A. Salminen, J. Ojala, K. Kaarniranta, A. Haapasalo, M. Hiltunen, H. Soininen, Astrocytes in the aging brain express characteristics of senescence-associated secretory phenotype, Eur J Neurosci 34(1) (2011) 3-11.
[22] R.I. Kohno, Y. Hata, S. Kawahara, T. Kita, R. Arita, Y. Mochizuki, L.P. Aiello, T. Ishibashi, Possible contribution of hyalocytes to idiopathic epiretinal membrane formation and its contraction, Br J Ophthalmol 93(8) (2009) 1020-6.
[23] M. Karlstetter, R. Scholz, M. Rutar, W.T. Wong, J.M. Provis, T. Langmann, Retinal microglia: just bystander or target for therapy?, Prog Retin Eye Res 45 (2015) 30-57.
[24] L.G. Fritsche, R.N. Fariss, D. Stambolian, G.R. Abecasis, C.A. Curcio, A. Swaroop, Age-related macular degeneration: genetics and biology coming together, Annu Rev Genomics Hum Genet 15 (2014) 151-71.
[25] M. Joshi, S. Agrawal, J.B. Christoforidis, Inflammatory mechanisms of idiopathic epiretinal membrane formation, Mediators Inflamm 2013 (2013) 192582.
[26] Q. Huang, J. Li, With or without internal limiting membrane peeling during idiopathic epiretinal membrane surgery: A meta-analysis, PLoS One 16(1) (2021) e0245459.
[27] F. Rommel, M.P. Brinkmann, J.A.M. Sochurek, M. Prasuhn, S. Grisanti, M. Ranjbar, Ocular Blood Flow Changes Impact Visual Acuity Gain after Surgical Treatment for Idiopathic Epiretinal Membrane, J Clin Med 9(6) (2020).
[28] K. Ogurtsova, J.D. da Rocha Fernandes, Y. Huang, U. Linnenkamp, L. Guariguata, N.H. Cho, D. Cavan, J.E. Shaw, L.E. Makaroff, IDF Diabetes Atlas: Global estimates for the prevalence of diabetes for 2015 and 2040, Diabetes Res Clin Pract 128 (2017) 40-50.
[29] R. Klein, B.E. Klein, S.E. Moss, M.D. Davis, D.L. DeMets, The Wisconsin epidemiologic study of diabetic retinopathy. III. Prevalence and risk of diabetic retinopathy when age at diagnosis is 30 or more years, Arch Ophthalmol 102(4) (1984) 527-32.

[30] Y. Zheng, M. He, N. Congdon, The worldwide epidemic of diabetic retinopathy, Indian J Ophthalmol 60(5) (2012) 428-31.
[31] P. Kroll, E.B. Rodrigues, S. Hoerle, Pathogenesis and classification of proliferative diabetic vitreoretinopathy, Ophthalmologica 221(2) (2007) 78-94.
[32] F. Semeraro, A. Cancarini, R. dell'Omo, S. Rezzola, M.R. Romano, C. Costagliola, Diabetic Retinopathy: Vascular and Inflammatory Disease, J Diabetes Res 2015 (2015) 582060.
[33] M.S. Ola, M.I. Nawaz, M.M. Siddiquei, S. Al-Amro, A.M. Abu El-Asrar, Recent advances in understanding the biochemical and molecular mechanism of diabetic retinopathy, J Diabetes Complications 26(1) (2012) 56-64.
[34] M.S. Ola, M.I. Nawaz, H.A. Khan, A.S. Alhomida, Neurodegeneration and neuroprotection in diabetic retinopathy, Int J Mol Sci 14(2) (2013) 2559-72.
[35] X.L. Du, D. Edelstein, L. Rossetti, I.G. Fantus, H. Goldberg, F. Ziyadeh, J. Wu, M. Brownlee, Hyperglycemia-induced mitochondrial superoxide overproduction activates the hexosamine pathway and induces plasminogen activator inhibitor-1 expression by increasing Sp1 glycosylation, Proc Natl Acad Sci U S A 97(22) (2000) 12222-6.
[36] S. Satofuka, A. Ichihara, N. Nagai, K. Noda, Y. Ozawa, A. Fukamizu, K. Tsubota, H. Itoh, Y. Oike, S. Ishida, (Pro)renin receptor-mediated signal transduction and tissue renin-angiotensin system contribute to diabetes-induced retinal inflammation, Diabetes 58(7) (2009) 1625-33.
[37] E.D. Schleicher, E. Wagner, A.G. Nerlich, Increased accumulation of the glycoxidation product N(epsilon)-(carboxymethyl)lysine in human tissues in diabetes and aging, J Clin Invest 99(3) (1997) 457-68.
[38] Y. Ido, C. Kilo, J.R. Williamson, Cytosolic NADH/NAD+, free radicals, and vascular dysfunction in early diabetes mellitus, Diabetologia 40 Suppl 2 (1997) S115-7.
[39] C.N. Serhan, Resolution phase of inflammation: novel endogenous anti-inflammatory and proresolving lipid mediators and pathways, Annu Rev Immunol 25 (2007) 101-37.
[40] T. Kuwano, S. Nakao, H. Yamamoto, M. Tsuneyoshi, T. Yamamoto, M. Kuwano, M. Ono, Cyclooxygenase 2 is a key enzyme for inflammatory cytokine-induced angiogenesis, FASEB J 18(2) (2004) 300-10.
[41] K. Tamura, T. Sakurai, H. Kogo, Relationship between prostaglandin E2 and vascular endothelial growth factor (VEGF) in angiogenesis in human vascular endothelial cells, Vascul Pharmacol 44(6) (2006) 411-6.
[42] J. Tang, T.S. Kern, Inflammation in diabetic retinopathy, Prog Retin Eye Res 30(5) (2011) 343-58.
[43] H.W. Flynn, E.Y. Chew, B.D. Simons, F.B. Barton, N.A. Remaley, F.L. Ferris, Pars plana vitrectomy in the Early Treatment Diabetic Retinopathy Study. ETDRS report number 17. The Early Treatment Diabetic Retinopathy Study Research Group, Ophthalmology 99(9) (1992) 1351-7.
[44] A.Y. Zhou, C.J. Zhou, J. Yao, Y.L. Quan, B.C. Ren, J.M. Wang, Panretinal photocoagulation versus panretinal photocoagulation plus intravitreal bevacizumab for high-risk proliferative diabetic retinopathy, Int J Ophthalmol 9(12) (2016) 1772-1778.
[45] N. Cheung, I.Y. Wong, T.Y. Wong, Ocular anti-VEGF therapy for diabetic retinopathy: overview of clinical efficacy and evolving applications, Diabetes Care 37(4) (2014) 900-5.
[46] M. Zhao, Y. Sun, Y. Jiang, Anti-VEGF therapy is not a magic bullet for diabetic retinopathy, Eye (Lond) 34(4) (2020) 609-610.
[47] P. DALE, NEUROSCIENCE THIRD EDITION, 2004.
[48] H. Kolb, E. Fernandez, R. Nelson, Webvision: The Organization of the Retina and Visual System, 1995.
[49] K. Peynshaert, J. Devoldere, A.K. Minnaert, S.C. De Smedt, K. Remaut, Morphology and Composition of the Inner Limiting Membrane: Species-Specific Variations and Relevance toward Drug Delivery Research, Curr Eye Res 44(5) (2019) 465-475.
[50] R. Gelman, W. Stevenson, C. Prospero Ponce, D. Agarwal, J.B. Christoforidis, Retinal Damage Induced by Internal Limiting Membrane Removal, J Ophthalmol 2015 (2015) 939748.

[51] D. Goldman, Müller glial cell reprogramming and retina regeneration, Nat Rev Neurosci 15(7) (2014) 431-42.
[52] A. Bringmann, P. Wiedemann, Müller glial cells in retinal disease, Ophthalmologica 227(1) (2012) 1-19.
[53] E. Vecino, F.D. Rodriguez, N. Ruzafa, X. Pereiro, S.C. Sharma, Glia-neuron interactions in the mammalian retina, Prog Retin Eye Res 51 (2016) 1-40.
[54] A. Bringmann, T. Pannicke, J. Grosche, M. Francke, P. Wiedemann, S.N. Skatchkov, N.N. Osborne, A. Reichenbach, Müller cells in the healthy and diseased retina, Prog Retin Eye Res 25(4) (2006) 397-424.
[55] E. Newman, A. Reichenbach, The Müller cell: a functional element of the retina, Trends Neurosci 19(8) (1996) 307-12.
[56] J.W. Rich-Edwards, M.B. Goldman, W.C. Willett, D.J. Hunter, M.J. Stampfer, G.A. Colditz, J.E. Manson, Adolescent body mass index and infertility caused by ovulatory disorder, Am J Obstet Gynecol 171(1) (1994) 171-7.
[57] A. Kanda, K. Noda, I. Hirose, S. Ishida, TGF-β-SNAIL axis induces Müller glial-mesenchymal transition in the pathogenesis of idiopathic epiretinal membrane, Sci Rep 9(1) (2019) 673.
[58] K. Rashid, I. Akhtar-Schaefer, T. Langmann, Microglia in Retinal Degeneration, Front Immunol 10 (2019) 1975.
[59] A. Bringmann, P. Wiedemann, Involvement of Müller glial cells in epiretinal membrane formation, Graefes Arch Clin Exp Ophthalmol 247(7) (2009) 865-83.
[60] C.S. Sethi, G.P. Lewis, S.K. Fisher, W.P. Leitner, D.L. Mann, P.J. Luthert, D.G. Charteris, Glial remodeling and neural plasticity in human retinal detachment with proliferative vitreoretinopathy, Invest Ophthalmol Vis Sci 46(1) (2005) 329-42.
[61] C. Haritoglou, R.G. Schumann, A. Kampik, A. Gandorfer, Glial cell proliferation under the internal limiting membrane in a patient with cellophane maculopathy, Arch Ophthalmol 125(9) (2007) 1301-2.
[62] C. Guidry, The role of Müller cells in fibrocontractive retinal disorders, Prog Retin Eye Res 24(1) (2005) 75-86.
[63] P. Wiedemann, Growth factors in retinal diseases: proliferative vitreoretinopathy, proliferative diabetic retinopathy, and retinal degeneration, Surv Ophthalmol 36(5) (1992) 373-84.
[64] B.A. Coughlin, D.J. Feenstra, S. Mohr, Müller cells and diabetic retinopathy, Vision Res 139 (2017) 93-100.
[65] C. Guidry, R. Feist, R. Morris, C.W. Hardwick, Changes in IGF activities in human diabetic vitreous, Diabetes 53(9) (2004) 2428-35.
[66] C. Guidry, K.M. Bradley, J.L. King, Tractional force generation by human müller cells: growth factor responsiveness and integrin receptor involvement, Invest Ophthalmol Vis Sci 44(3) (2003) 1355-63.
[67] J. Zhang, X. Chen, L. Zhang, Y. Peng, gene polymorphisms associated with diabetic retinopathy risk in Chinese Han population, Oncotarget 8(50) (2017) 88034-88042.
[68] G.A. Limb, H. Jayaram, Regulatory and Pathogenic Roles of Müller Glial Cells in Retinal Neovascular Processes and Their Potential for Retinal Regeneration, Frontiers in Diabetes 20 (2010) 98-108.
[69] H. Kimura, C. Spee, T. Sakamoto, D.R. Hinton, Y. Ogura, Y. Tabata, Y. Ikada, S.J. Ryan, Cellular response in subretinal neovascularization induced by bFGF-impregnated microspheres, Invest Ophthalmol Vis Sci 40(2) (1999) 524-8.
[70] S. Yoshida, A. Yoshida, T. Ishibashi, Induction of IL-8, MCP-1, and bFGF by TNF-alpha in retinal glial cells: implications for retinal neovascularization during post-ischemic inflammation, Graefes Arch Clin Exp Ophthalmol 242(5) (2004) 409-13.
[71] T. Cheng, W. Cao, R. Wen, R.H. Steinberg, M.M. LaVail, Prostaglandin E2 induces vascular endothelial growth factor and basic fibroblast growth factor mRNA expression in cultured rat Müller cells, Invest Ophthalmol Vis Sci 39(3) (1998) 581-91.

[72] I.M. Nawaz, S. Rezzola, A. Cancarini, A. Russo, C. Costagliola, F. Semeraro, M. Presta, Human vitreous in proliferative diabetic retinopathy: Characterization and translational implications, Prog Retin Eye Res 72 (2019) 100756.
[73] S.Y. Oberstein, J. Byun, D. Herrera, E.A. Chapin, S.K. Fisher, G.P. Lewis, Cell proliferation in human epiretinal membranes: characterization of cell types and correlation with disease condition and duration, Mol Vis 17 (2011) 1794-805.
[74] S. Roy, S. Amin, Retinal fibrosis in diabetic retinopathy, Exp Eye Res 142 (2016) 71-5.
[75] M. Rodrigues, X. Xin, K. Jee, S. Babapoor-Farrokhran, F. Kashiwabuchi, T. Ma, I. Bhutto, S.J. Hassan, Y. Daoud, D. Baranano, S. Solomon, G. Lutty, G.L. Semenza, S. Montaner, A. Sodhi, VEGF secreted by hypoxic Müller cells induces MMP-2 expression and activity in endothelial cells to promote retinal neovascularization in proliferative diabetic retinopathy, Diabetes 62(11) (2013) 3863-73.
[76] J.C. Portillo, Y. Lopez Corcino, Y. Miao, J. Tang, N. Sheibani, T.S. Kern, G.R. Dubyak, C.S. Subauste, CD40 in Retinal Müller Cells Induces P2X7-Dependent Cytokine Expression in Macrophages/Microglia in Diabetic Mice and Development of Early Experimental Diabetic Retinopathy, Diabetes 66(2) (2017) 483-493.
[77] P.N. Bishop, Structural macromolecules and supramolecular organisation of the vitreous gel, Prog Retin Eye Res 19(3) (2000) 323-44.
[78] J.P. Monteiro, F.M. Santos, A.S. Rocha, J.P. Castro-de-Sousa, J.A. Queiroz, L.A. Passarinha, C.T. Tomaz, Vitreous humor in the pathologic scope: insights from proteomic approaches, Proteomics Clin Appl 9(1-2) (2015) 187-202.
[79] T. Shitama, H. Hayashi, S. Noge, E. Uchio, K. Oshima, H. Haniu, N. Takemori, N. Komori, H. Matsumoto, Proteome Profiling of Vitreoretinal Diseases by Cluster Analysis, Proteomics Clin Appl 2(9) (2008) 1265-1280.
[80] S. Rezzola, M.I. Nawaz, A. Cancarini, F. Semeraro, M. Presta, Vascular Endothelial Growth Factor in the Vitreous of Proliferative Diabetic Retinopathy Patients: Chasing a Hiding Prey?, Diabetes Care 42(7) (2019) e105-e106.
[81] S. Rezzola, M. Corsini, P. Chiodelli, A. Cancarini, I.M. Nawaz, D. Coltrini, S. Mitola, R. Ronca, M. Belleri, L. Lista, D. Rusciano, M. De Rosa, V. Pavone, F. Semeraro, M. Presta, Inflammation and N-formyl peptide receptors mediate the angiogenic activity of human vitreous humour in proliferative diabetic retinopathy, Diabetologia 60(4) (2017) 719-728.
[82] S. Rezzola, I.M. Nawaz, A. Cancarini, C. Ravelli, S. Calza, F. Semeraro, M. Presta, 3D endothelial cell spheroid/human vitreous humor assay for the characterization of anti-angiogenic inhibitors for the treatment of proliferative diabetic retinopathy, Angiogenesis 20(4) (2017) 629-640.
[83] I.M. Nawaz, P. Chiodelli, S. Rezzola, G. Paganini, M. Corsini, A. Lodola, A. Di Ianni, M. Mor, M. Presta, N-tert-butyloxycarbonyl-Phe-Leu-Phe-Leu-Phe (BOC2) inhibits the angiogenic activity of heparin-binding growth factors, Angiogenesis 21(1) (2018) 47-59.
[84] S. Rezzola, M. Dal Monte, M. Belleri, A. Bugatti, P. Chiodelli, M. Corsini, M. Cammalleri, A. Cancarini, L. Morbidelli, P. Oreste, P. Bagnoli, F. Semeraro, M. Presta, Therapeutic Potential of Anti-Angiogenic Multitarget N,O-Sulfated E. Coli K5 Polysaccharide in Diabetic Retinopathy, Diabetes 64(7) (2015) 2581-92.
[85] M. Dal Monte, S. Rezzola, M. Cammalleri, M. Belleri, F. Locri, L. Morbidelli, M. Corsini, G. Paganini, F. Semeraro, A. Cancarini, D. Rusciano, M. Presta, P. Bagnoli, Antiangiogenic Effectiveness of the Urokinase Receptor-Derived Peptide UPARANT in a Model of Oxygen-Induced Retinopathy, Invest Ophthalmol Vis Sci 56(4) (2015) 2392-407.
[86] S. Aretz, T.U. Krohne, K. Kammerer, U. Warnken, A. Hotz-Wagenblatt, M. Bergmann, B.V. Stanzel, T. Kempf, F.G. Holz, M. Schnölzer, J. Kopitz, In-depth mass spectrometric mapping of the human vitreous proteome, Proteome Sci 11(1) (2013) 22.
[87] A. Pollreisz, M. Funk, F.P. Breitwieser, K. Parapatics, S. Sacu, M. Georgopoulos, R. Dunavoelgyi, G.J. Zlabinger, J. Colinge, K.L. Bennett, U. Schmidt-Erfurth, Quantitative proteomics

of aqueous and vitreous fluid from patients with idiopathic epiretinal membranes, Exp Eye Res 108 (2013) 48-58.
[88] A. Dongre, R.A. Weinberg, New insights into the mechanisms of epithelial-mesenchymal transition and implications for cancer, Nat Rev Mol Cell Biol 20(2) (2019) 69-84.
[89] J. Roche, The Epithelial-to-Mesenchymal Transition in Cancer, Cancers (Basel) 10(2) (2018).
[90] R. Kalluri, R.A. Weinberg, The basics of epithelial-mesenchymal transition, J Clin Invest 119(6) (2009) 1420-8.
[91] V. Das, S. Bhattacharya, C. Chikkaputtaiah, S. Hazra, M. Pal, The basics of epithelial-mesenchymal transition (EMT): A study from a structure, dynamics, and functional perspective, J Cell Physiol (2019).
[92] G.D. Marconi, L. Fonticoli, T.S. Rajan, S.D. Pierdomenico, O. Trubiani, J. Pizzicannella, F. Diomede, Epithelial-Mesenchymal Transition (EMT): The Type-2 EMT in Wound Healing, Tissue Regeneration and Organ Fibrosis, Cells 10(7) (2021).
[93] Y. Koike, M. Yozaki, A. Utani, H. Murota, Fibroblast growth factor 2 accelerates the epithelial-mesenchymal transition in keratinocytes during wound healing process, Sci Rep 10(1) (2020) 18545.
[94] D. Haensel, X. Dai, Epithelial-to-mesenchymal transition in cutaneous wound healing: Where we are and where we are heading, Dev Dyn 247(3) (2018) 473-480.
[95] B. Gawronska-Kozak, A. Grabowska, A. Kur-Piotrowska, M. Kopcewicz, Foxn1 Transcription Factor Regulates Wound Healing of Skin through Promoting Epithelial-Mesenchymal Transition, PLoS One 11(3) (2016) e0150635.
[96] P. Savagner, K.M. Yamada, J.P. Thiery, The zinc-finger protein slug causes desmosome dissociation, an initial and necessary step for growth factor-induced epithelial-mesenchymal transition, J Cell Biol 137(6) (1997) 1403-19.
[97] M.A. Nieto, R.Y. Huang, R.A. Jackson, J.P. Thiery, EMT: 2016, Cell 166(1) (2016) 21-45.
[98] K.A. Bielefeld, S. Amini-Nik, B.A. Alman, Cutaneous wound healing: recruiting developmental pathways for regeneration, Cell Mol Life Sci 70(12) (2013) 2059-81.
[99] S. Lamouille, J. Xu, R. Derynck, Molecular mechanisms of epithelial-mesenchymal transition, Nat Rev Mol Cell Biol 15(3) (2014) 178-96.
[100] D. Wu, A. Kanda, Y. Liu, K. Noda, M. Murata, S. Ishida, Involvement of Müller Glial Autoinduction of TGF-β in Diabetic Fibrovascular Proliferation Via Glial-Mesenchymal Transition, Invest Ophthalmol Vis Sci 61(14) (2020) 29.
[101] A.M. Abu El-Asrar, L. Missotten, K. Geboes, Expression of hypoxia-inducible factor-1alpha and the protein products of its target genes in diabetic fibrovascular epiretinal membranes, Br J Ophthalmol 91(6) (2007) 822-6.
[102] A. Hueber, P. Wiedemann, P. Esser, K. Heimann, Basic fibroblast growth factor mRNA, bFGF peptide and FGF receptor in epiretinal membranes of intraocular proliferative disorders (PVR and PDR), Int Ophthalmol 20(6) (1996) 345-50.
[103] X. Liang, C. Li, Y. Li, J. Huang, S. Tang, R. Gao, S. Li, Platelet-derived growth factor and basic fibroblast growth factor immunolocalized in proliferative retinal diseases, Chin Med J (Engl) 113(2) (2000) 144-7.
[104] M. Hollborn, K. Jahn, G.A. Limb, L. Kohen, P. Wiedemann, A. Bringmann, Characterization of the basic fibroblast growth factor-evoked proliferation of the human Müller cell line, MIO-M1, Graefes Arch Clin Exp Ophthalmol 242(5) (2004) 414-22.
[105] Y. Zhao, R.P. Singh, The role of anti-vascular endothelial growth factor (anti-VEGF) in the management of proliferative diabetic retinopathy, Drugs Context 7 (2018) 212532.
[106] G.S. Tan, N. Cheung, R. Simó, G.C. Cheung, T.Y. Wong, Diabetic macular oedema, Lancet Diabetes Endocrinol 5(2) (2017) 143-155.
[107] D.M. Brown, Q.D. Nguyen, D.M. Marcus, D.S. Boyer, S. Patel, L. Feiner, P.G. Schlottmann, A.C. Rundle, J. Zhang, R.G. Rubio, A.P. Adamis, J.S. Ehrlich, J.J. Hopkins, R.a.R.R. Group, Long-term outcomes of ranibizumab therapy for diabetic macular edema: the 36-month results from two phase III trials: RISE and RIDE, Ophthalmology 120(10) (2013) 2013-22.

[108] C. Garlanda, B. Bottazzi, A. Bastone, A. Mantovani, Pentraxins at the crossroads between innate immunity, inflammation, matrix deposition, and female fertility, Annu Rev Immunol 23 (2005) 337-66.
[109] F. Fornai, A. Carrizzo, M. Ferrucci, A. Damato, F. Biagioni, A. Gaglione, A.A. Puca, C. Vecchione, Brain diseases and tumorigenesis: The good and bad cops of pentraxin3, The international journal of biochemistry & cell biology 69 (2015) 70-4.
[110] N. Polentarutti, B. Bottazzi, E. Di Santo, E. Blasi, D. Agnello, P. Ghezzi, M. Introna, T. Bartfai, G. Richards, A. Mantovani, Inducible expression of the long pentraxin PTX3 in the central nervous system, Journal of neuroimmunology 106(1-2) (2000) 87-94.
[111] T. Ravizza, D. Moneta, B. Bottazzi, G. Peri, C. Garlanda, E. Hirsch, G.J. Richards, A. Mantovani, A. Vezzani, Dynamic induction of the long pentraxin PTX3 in the CNS after limbic seizures: evidence for a protective role in seizure-induced neurodegeneration, Neuroscience 105(1) (2001) 43-53.
[112] B. Rodriguez-Grande, L. Varghese, F. Molina-Holgado, O. Rajkovic, C. Garlanda, A. Denes, E. Pinteaux, Pentraxin 3 mediates neurogenesis and angiogenesis after cerebral ischaemia, Journal of neuroinflammation 12 (2015) 15.
[113] B. Rodriguez-Grande, M. Swana, L. Nguyen, P. Englezou, S. Maysami, S.M. Allan, N.J. Rothwell, C. Garlanda, A. Denes, E. Pinteaux, The acute-phase protein PTX3 is an essential mediator of glial scar formation and resolution of brain edema after ischemic injury, Journal of cerebral blood flow and metabolism : official journal of the International Society of Cerebral Blood Flow and Metabolism 34(3) (2014) 480-8.
[114] W.S. Ryu, C.K. Kim, B.J. Kim, C. Kim, S.H. Lee, B.W. Yoon, Pentraxin 3: a novel and independent prognostic marker in ischemic stroke, Atherosclerosis 220(2) (2012) 581-6.
[115] H.W. Lee, J. Choi, K. Suk, Increases of pentraxin 3 plasma levels in patients with Parkinson's disease, Movement disorders : official journal of the Movement Disorder Society 26(13) (2011) 2364-70.
[116] K. Suzuki, Y. Suzuki, Globoid cell leucodystrophy (Krabbe's disease): deficiency of galactocerebroside beta-galactosidase, Proc Natl Acad Sci U S A 66(2) (1970) 302-9.
[117] A. Ballabio, V. Gieselmann, Lysosomal disorders: from storage to cellular damage, Biochim Biophys Acta 1793(4) (2009) 684-96.
[118] K. Suzuki, Twenty five years of the "psychosine hypothesis": a personal perspective of its history and present status, Neurochem Res 23(3) (1998) 251-9.
[119] H. Igisu, K. Suzuki, Progressive accumulation of toxic metabolite in a genetic leukodystrophy, Science 224(4650) (1984) 753-5.
[120] Y. Li, Y. Xu, B.A. Benitez, M.S. Nagree, J.T. Dearborn, X. Jiang, M.A. Guzman, J.C. Woloszynek, A. Giaramita, B.K. Yip, J. Elsbernd, M.C. Babcock, M. Lo, S.C. Fowler, D.F. Wozniak, C.A. Vogler, J.A. Medin, B.E. Crawford, M.S. Sands, Genetic ablation of acid ceramidase in Krabbe disease confirms the psychosine hypothesis and identifies a new therapeutic target, Proc Natl Acad Sci U S A 116(40) (2019) 20097-20103.
[121] D.A. Wenger, M.A. Rafi, P. Luzi, J. Datto, E. Costantino-Ceccarini, Krabbe disease: genetic aspects and progress toward therapy, Mol Genet Metab 70(1) (2000) 1-9.
[122] T. Kanazawa, S. Nakamura, M. Momoi, T. Yamaji, H. Takematsu, H. Yano, H. Sabe, A. Yamamoto, T. Kawasaki, Y. Kozutsumi, Inhibition of cytokinesis by a lipid metabolite, psychosine, J Cell Biol 149(4) (2000) 943-50.
[123] Y. Kozutsumi, T. Kanazawa, Y. Sun, T. Yamaji, H. Yamamoto, H. Takematsu, Sphingolipids involved in the induction of multinuclear cell formation, Biochim Biophys Acta 1582(1-3) (2002) 138-43.
[124] A.M. Nicaise, E.R. Bongarzone, S.J. Crocker, A microglial hypothesis of globoid cell leukodystrophy pathology, J Neurosci Res 94(11) (2016) 1049-61.
[125] K. Suzuki, Globoid cell leukodystrophy (Krabbe's disease): update, Journal of child neurology 18(9) (2003) 595-603.

[126] M.C. Loonen, O.P. Van Diggelen, H.C. Janse, W.J. Kleijer, W.F. Arts, Late-onset globoid cell leucodystrophy (Krabbe's disease). Clinical and genetic delineation of two forms and their relation to the early-infantile form, Neuropediatrics 16(3) (1985) 137-42.
[127] C.H. Hill, S.C. Graham, R.J. Read, J.E. Deane, Structural snapshots illustrate the catalytic cycle of beta-galactocerebrosidase, the defective enzyme in Krabbe disease, Proc Natl Acad Sci U S A 110(51) (2013) 20479-84.
[128] M.L. Escolar, M.D. Poe, J.M. Provenzale, K.C. Richards, J. Allison, S. Wood, D.A. Wenger, D. Pietryga, D. Wall, M. Champagne, R. Morse, W. Krivit, J. Kurtzberg, Transplantation of umbilical-cord blood in babies with infantile Krabbe's disease, N Engl J Med 352(20) (2005) 2069-81.
[129] T. Kobayashi, T. Yamanaka, J.M. Jacobs, F. Teixeira, K. Suzuki, The Twitcher mouse: an enzymatically authentic model of human globoid cell leukodystrophy (Krabbe disease), Brain research 202(2) (1980) 479-83.
[130] K. Suzuki, The twitcher mouse: a model for Krabbe disease and for experimental therapies, Brain Pathology 5(3) (1995) 249-58.
[131] N. Sakai, K. Inui, N. Tatsumi, H. Fukushima, T. Nishigaki, M. Taniike, J. Nishimoto, H. Tsukamoto, I. Yanagihara, K. Ozono, S. Okada, Molecular cloning and expression of cDNA for murine galactocerebrosidase and mutation analysis of the twitcher mouse, a model of Krabbe's disease, J Neurochem 66(3) (1996) 1118-24.
[132] R. Ronca, A. Giacomini, E. Di Salle, D. Coltrini, K. Pagano, L. Ragona, S. Matarazzo, S. Rezzola, D. Maiolo, R. Torrella, E. Moroni, R. Mazzieri, G. Escobar, M. Mor, G. Colombo, M. Presta, Long-Pentraxin 3 Derivative as a Small-Molecule FGF Trap for Cancer Therapy, Cancer cell 28(2) (2015) 225-39.
[133] P. Marmiroli, V. Rodriguez-Menendez, L. Rigamonti, E. Tonoli, R. Rigolio, G. Cavaletti, G. Tredici, A. Vercelli, Neuropathological changes in the peripheral nervous system and spinal cord in a transgenic mouse model of Niemann-Pick disease type A, Clin Neuropathol 28(4) (2009) 263-74.
[134] J.S. Shen, K. Watabe, T. Ohashi, Y. Eto, Intraventricular administration of recombinant adenovirus to neonatal twitcher mouse leads to clinicopathological improvements, Gene Ther 8(14) (2001) 1081-7.
[135] K. Suzuki, The twitcher mouse. A model of human globoid cell leukodystrophy (krabbe's disease), Am J Pathol 111(3) (1983) 394-7.
[136] M. Belleri, R. Ronca, D. Coltrini, B. Nico, D. Ribatti, P.L. Poliani, A. Giacomini, P. Alessi, S. Marchesini, M.B. Santos, E.R. Bongarzone, M. Presta, Inhibition of angiogenesis by beta-galactosylceramidase deficiency in globoid cell leukodystrophy, Brain : a journal of neurology 136(Pt 9) (2013) 2859-75.
[137] C.Y. Ko, L.H. Chang, Y.C. Lee, E. Sterneck, C.P. Cheng, S.H. Chen, A.M. Huang, J.T. Tseng, J.M. Wang, CCAAT/enhancer binding protein delta (CEBPD) elevating PTX3 expression inhibits macrophage-mediated phagocytosis of dying neuron cells, Neurobiology of aging 33(2) (2012) 422 e11-25.
[138] D. Ito, Y. Imai, K. Ohsawa, K. Nakajima, Y. Fukuuchi, S. Kohsaka, Microglia-specific localisation of a novel calcium binding protein, Iba1, Brain research. Molecular brain research 57(1) (1998) 1-9.
[139] K.I. Claycomb, P.N. Winokur, K.M. Johnson, A.M. Nicaise, A.W. Giampetruzzi, A.V. Sacino, E.Y. Snyder, E. Barbarese, E.R. Bongarzone, S.J. Crocker, Aberrant production of tenascin-C in globoid cell leukodystrophy alters psychosine-induced microglial functions, Journal of neuropathology and experimental neurology 73(10) (2014) 964-74.
[140] K. Yao, H.B. Zu, Microglial polarization: novel therapeutic mechanism against Alzheimer's disease, Inflammopharmacology 28(1) (2020) 95-110.
[141] C.H. Hill, G.M. Cook, S.J. Spratley, S. Fawke, S.C. Graham, J.E. Deane, The mechanism of glycosphingolipid degradation revealed by a GALC-SapA complex structure, Nature communications 9(1) (2018) 151.

[142] T. Kobayashi, H. Shinoda, I. Goto, T. Yamanaka, Y. Suzuki, Globoid cell leukodystrophy is a generalized galactosylsphingosine (psychosine) storage disease, Biochem Biophys Res Commun 144(1) (1987) 41-6.
[143] P.D. Whitfield, P.C. Sharp, R. Taylor, P. Meikle, Quantification of galactosylsphingosine in the twitcher mouse using electrospray ionization-tandem mass spectrometry, J Lipid Res 42(12) (2001) 2092-5.
[144] H. Jeon, S. Lee, W.H. Lee, K. Suk, Analysis of glial secretome: the long pentraxin PTX3 modulates phagocytic activity of microglia, Journal of neuroimmunology 229(1-2) (2010) 63-72.
[145] M. Oggioni, D. Mercurio, D. Minuta, S. Fumagalli, K. Popiolek-Barczyk, M. Sironi, A. Ciechanowska, S. Ippati, D. De Blasio, C. Perego, J. Mika, C. Garlanda, M.G. De Simoni, Long pentraxin PTX3 is upregulated systemically and centrally after experimental neurotrauma, but its depletion leaves unaltered sensorimotor deficits or histopathology, Scientific reports 11(1) (2021) 9616.
[146] K. Ummenthum, L.A. Peferoen, A. Finardi, D. Baker, G. Pryce, A. Mantovani, M. Bsibsi, B. Bottazzi, R. Peferoen-Baert, P. van der Valk, C. Garlanda, M. Kipp, R. Furlan, J.M. van Noort, S. Amor, Pentraxin-3 is upregulated in the central nervous system during MS and EAE, but does not modulate experimental neurological disease, European journal of immunology 46(3) (2016) 701-11.
[147] K. Daigo, A. Inforzato, I. Barajon, C. Garlanda, B. Bottazzi, S. Meri, A. Mantovani, Pentraxins in the activation and regulation of innate immunity, Immunological reviews 274(1) (2016) 202-217.
[148] H.W. Park, H.E. Moon, H.S. Kim, S.L. Paek, Y. Kim, J.W. Chang, Y.S. Yang, K. Kim, W. Oh, J.H. Hwang, J.W. Kim, D.G. Kim, S.H. Paek, Human umbilical cord blood-derived mesenchymal stem cells improve functional recovery through thrombospondin1, pantraxin3, and vascular endothelial growth factor in the ischemic rat brain, J Neurosci Res 93(12) (2015) 1814-25.
[149] C. Zhou, H. Chen, J.F. Zheng, Z.D. Guo, Z.J. Huang, Y. Wu, J.J. Zhong, X.C. Sun, C.J. Cheng, Pentraxin 3 contributes to neurogenesis after traumatic brain injury in mice, Neural regeneration research 15(12) (2020) 2318-2326.
[150] C. Lian, Q. Huang, X. Zhong, Z. He, B. Liu, H. Zeng, N. Xu, Z. Yang, C. Liao, Z. Fu, H. Guo, Pentraxin 3 secreted by human adipose-derived stem cells promotes dopaminergic neuron repair in Parkinson's disease via the inhibition of apoptosis, FASEB J 35(7) (2021) e21748.
[151] T.W. Meisingset, A. Ricca, M. Neri, U. Sonnewald, A. Gritti, Region- and age-dependent alterations of glial-neuronal metabolic interactions correlate with CNS pathology in a mouse model of globoid cell leukodystrophy, Journal of cerebral blood flow and metabolism : official journal of the International Society of Cerebral Blood Flow and Metabolism 33(7) (2013) 1127-37.
[152] H. Ida, O.M. Rennert, K. Watabe, Y. Eto, K. Maekawa, Pathological and biochemical studies of fetal Krabbe disease, Brain Dev 16(6) (1994) 480-4.
[153] J.J. Martin, J.G. Leroy, C. Ceuterick, J. Libert, P. Dodinval, L. Martin, Fetal Krabbe leukodystrophy. A morphologic study of two cases, Acta Neuropathol 53(2) (1981) 87-91.
[154] T.M. Schlaeger, S. Bartunkova, J.A. Lawitts, G. Teichmann, W. Risau, U. Deutsch, T.N. Sato, Uniform vascular-endothelial-cell-specific gene expression in both embryonic and adult transgenic mice, Proc Natl Acad Sci U S A 94(7) (1997) 3058-63.

Supplementary Material

Supplementary Table 1. qPCR oligonucleotide primers

Gene	Forward	Reverse
Ptx3	5'-GACCTCGGATGACTACGAG	5'-CTCCGAGTGCTCCTGGCG

Deidentified case ID	Age of Onset	Asympto-matic	Krabbe disease Classification	Trans-planted	Age of transplant	Initial symptoms after transplant if asymptomatic	Age of death	Stage
CW15-060	N/A	Yes	Early Infantile	Yes	1 month 6 days	6 months 17 days	15 years 5 months 30 days	N/A
CW16-061	5 months	No	Early Infantile	No			6 years 9 months 12 days	IV at 19 months
CW16-064	3.5 months	No	Early Infantile	No	N/A	N/A	1 year 6 months	II-III at 5 months
CW17-060	4 months	No	Early Infantile	No	N/A	N/A	1 year 2 months 13 days	IV at 10 months
CW18-060	5 months	No	Early Infantile	No	N/A	N/A	3 years 1 month 8 days	ND
CW18-070	6 months	No	Early Infantile	No	N/A	N/A	7 years 3 months 25 days	IV at 5 years 5 months
CW15-061	12 months	No	Late Infantile	No	N/A	N/A	11 years 1 month 29 days	III at last visit at 6 years
CW16-062	12 months	No	Late Infantile	No	N/A	N/A	9 years 8 months 20 days	IV at 5 years 7 months
CW16-065	8 months	No	Late Infantile	No	N/A	N/A	2 years 4 months 18 days	IV at 20 months
CW16-066	9 months	No	Late Infantile	No	N/A	N/A	2 years 2 months 9 days	IV at 22 months

Cepbd	5’-TCGACTTCAGCGCCTACATT	5’-CTAGCGACAGACCCCACAC
Tnfa	5’-GCCTCTTCTCATTCCTGCTT	5’-TGATCTGAGTGTGAGGGTCTG
Cxcl1	5’-GCTGGGATTCACCTCAAGAA	5’-TGGGGACACCTTTTAGCATC
IL1a	5’-CAGTTCTGCCATTGACCATC	5’-GAATCTTCCCGTTGCTTGAC
Gfap	5’-AGAAAACCGCATCACCATTC	5’-CGTCCTTGTGCTCCTGCT
Iba1	5’-CGAATGCTGGAGAAACTTGG	5’-ACCAGTTGGCCTCTTGTGTT
CD16/32	5’CTGGGAGTGATTTCTGACTGG	5’-TGGTTGGCTTTTGGGATAGA
Arg1	5’GCAGAGGTCCAGAAGAATGG	5’-TTGTCAGGGGAGTGTTGATG
CD206	5’-TGGCGAGCATCAAGAGTAAA	5’-CATAGGAAACGGGAGAACCA
Gapdh	5’GAAGGTCGGTGTGAACGGATT	5’-TGACTGTGCCGTTGAATTTG

Supplementary Table 2. Krabbe Patients

N/A= Not applicable, ND= No Data

Stage II- increased tone irritability, difficulty eating; Stage III- hypotonia, unable to eat; Stage IV- blind, deafness and quadriplegia, dysautonomia.

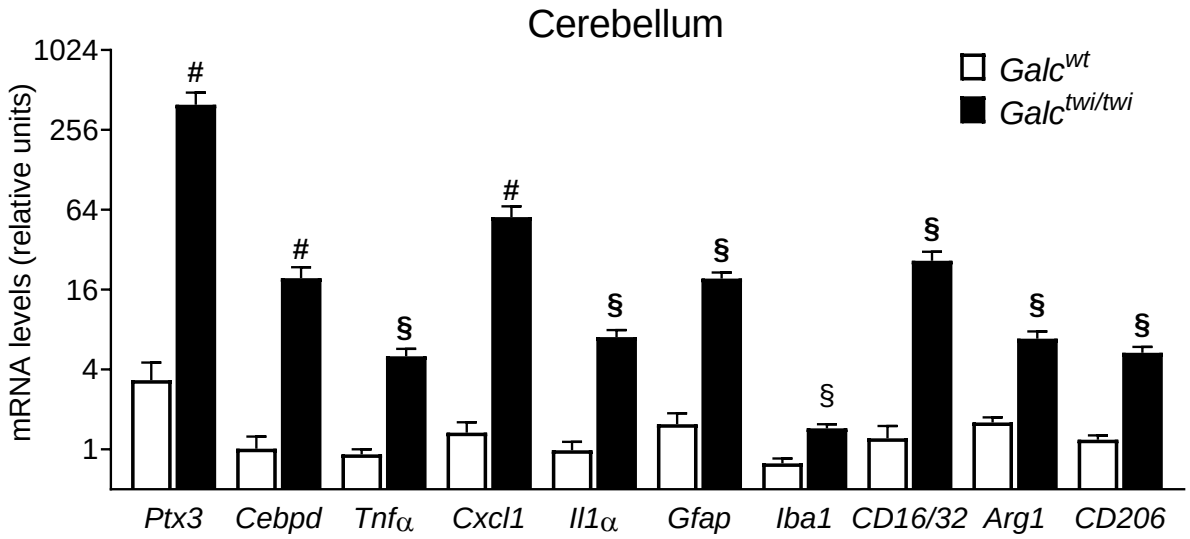

Supplementary Figure 1. *Ptx3* and proinflammatory gene expression in the cerebellum of *twitcher* mice. Steady state mRNA levels of the indicated genes were evaluated by qPCR in the cerebellum of *Galc*^{wt} and *Galc*$^{twi/twi}$ mice harvested at P35. Data were normalized to *Gapdh* expression and are the mean ± SEM of 7-10 animals per group, #, P < 0.01; §, P < 0.001, *Galc*^{wt} *versus Galc*$^{twi/twi}$, Student's t-test.

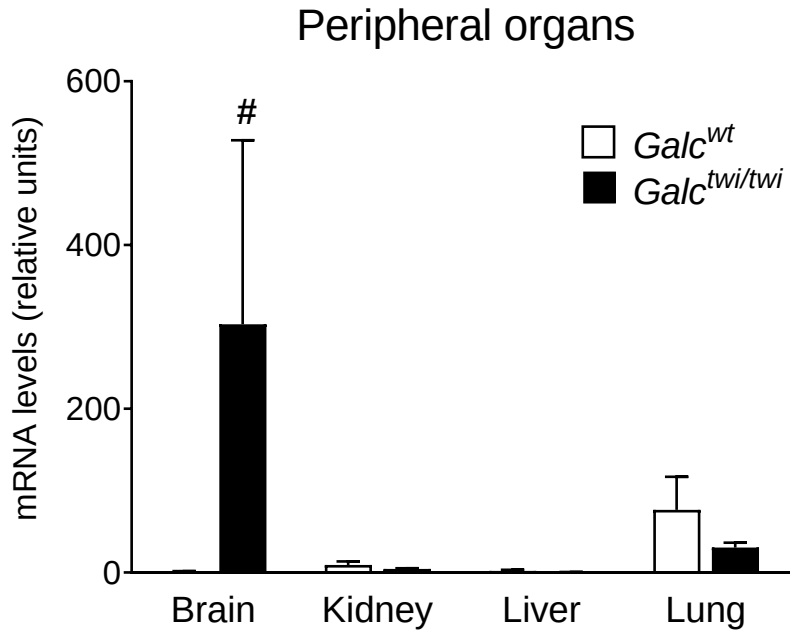

Supplementary Figure 2. *Ptx3* expression in the peripheral organs of *twitcher* mice. *Ptx3* expression was evaluated by qPCR in the brain, kidney, liver, and lungs *Galc*^{wt} and *Galc*$^{twi/twi}$ mice at P35. Data are the mean ± S.D. of 3-6 animals per group. #, P< 0.01, *Galc*^{wt} versus *Galc*$^{twi/twi}$, Student's t-test.

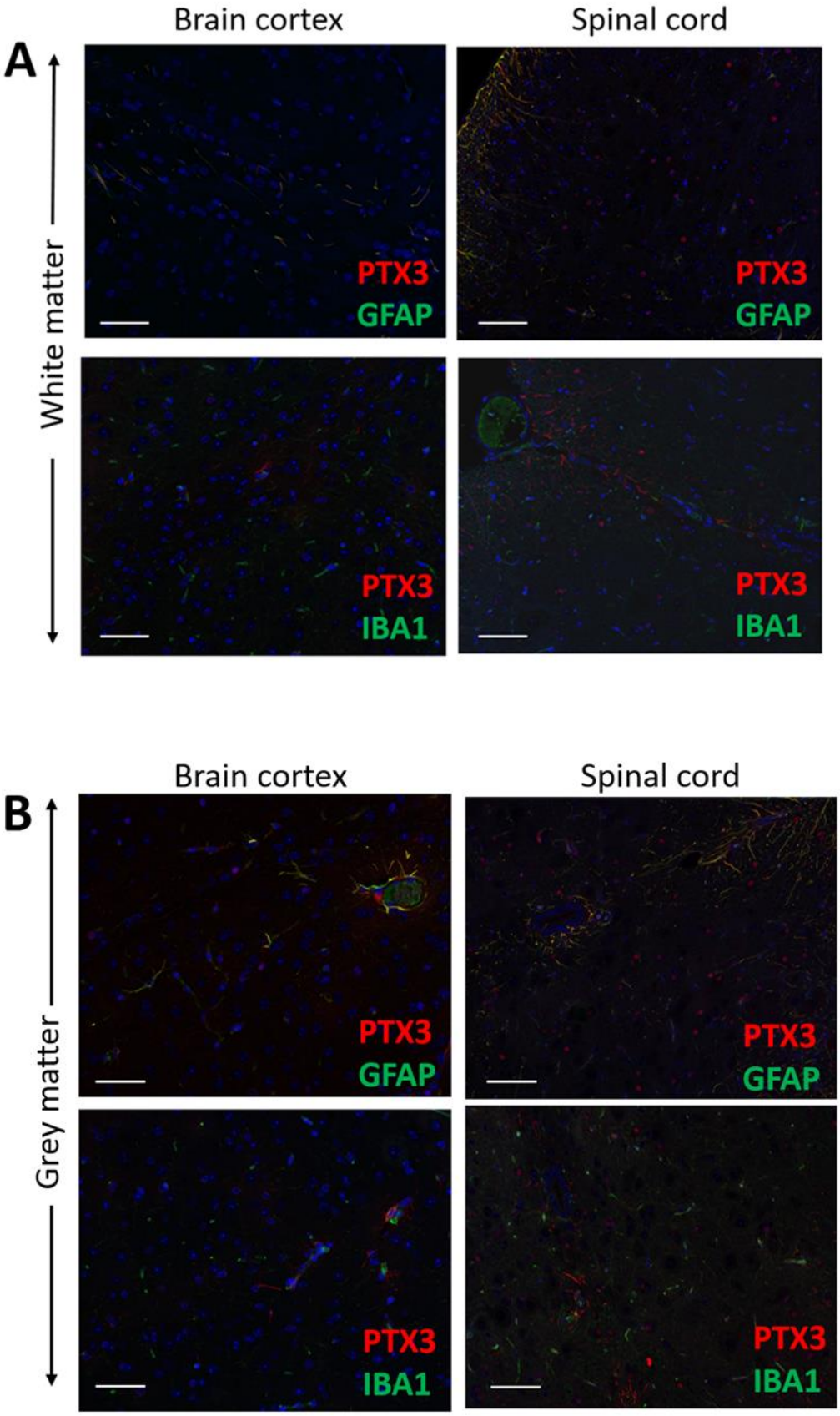

Supplementary Figure 3. Immunohistochemical analysis of the CNS of *Galc*^{wt} mice. Paraffin-embedded sections of the white (**A**) and grey (**B**) matter of the brain cortex and spinal cord of P35

Galc^{wt} mice were double-immunostained with anti-PTX3/GFAP or anti-PTX3/IBA1 antibodies. Scale bar, 50 μm.

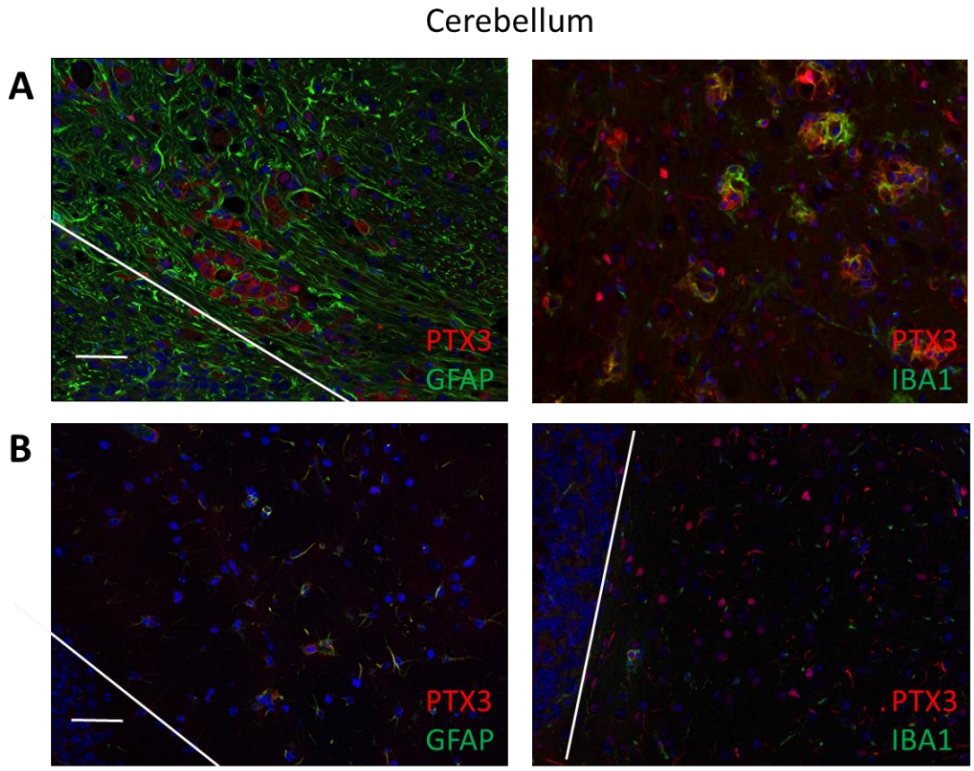

Supplementary Figure 4. PTX3 immunolocalization in the cerebellum of *Galc*$^{twi/twi}$ *and Galc*^{wt} mice. Paraffin-embedded sections of cerebellum of P35 *Galc*$^{twi/twi}$ (**A**) and *Galc*^{wt} (**B**) mice were double-immunostained with anti-PTX3/GFAP or anti-PTX3/IBA1 antibodies. Line indicates the boundary between white and gray matter. Scale bar, 50 μm.

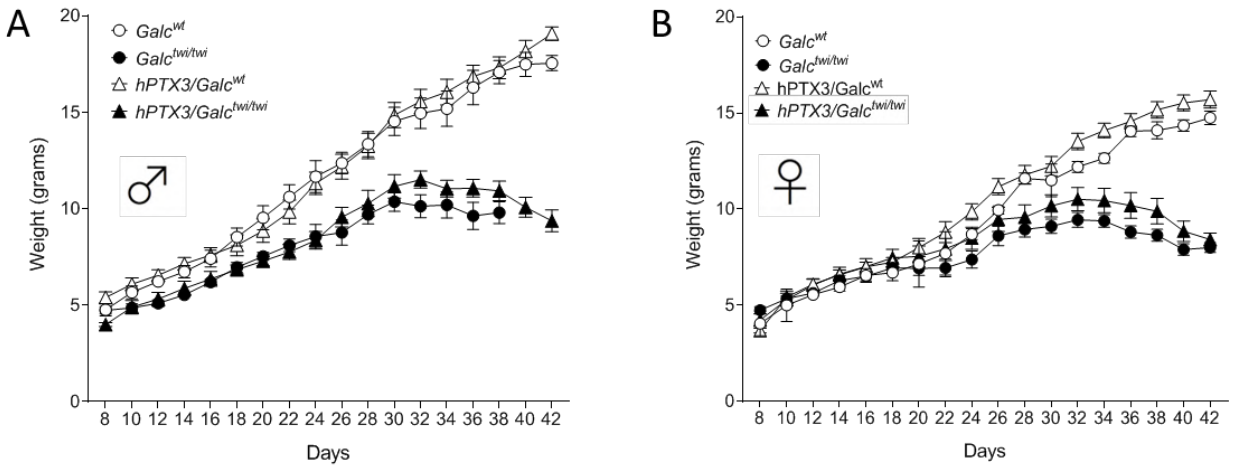

Supplementary Figure 5. Body weight of *hPTX3/Galc^{wt}* and *hPTX3/Galc$^{twi/twi}$* mice. The body weight gain of male (**A**) and female (**B**) hPTX3 overexpressing *hPTX3/Galc^{wt}* and *hPTX3/Galc$^{twi/twi}$* mice was compared to that of the corresponding control *Galc^{wt}* and *Galc$^{twi/twi}$* animals. Data are the mean ± SEM. of 2-12 animals per group

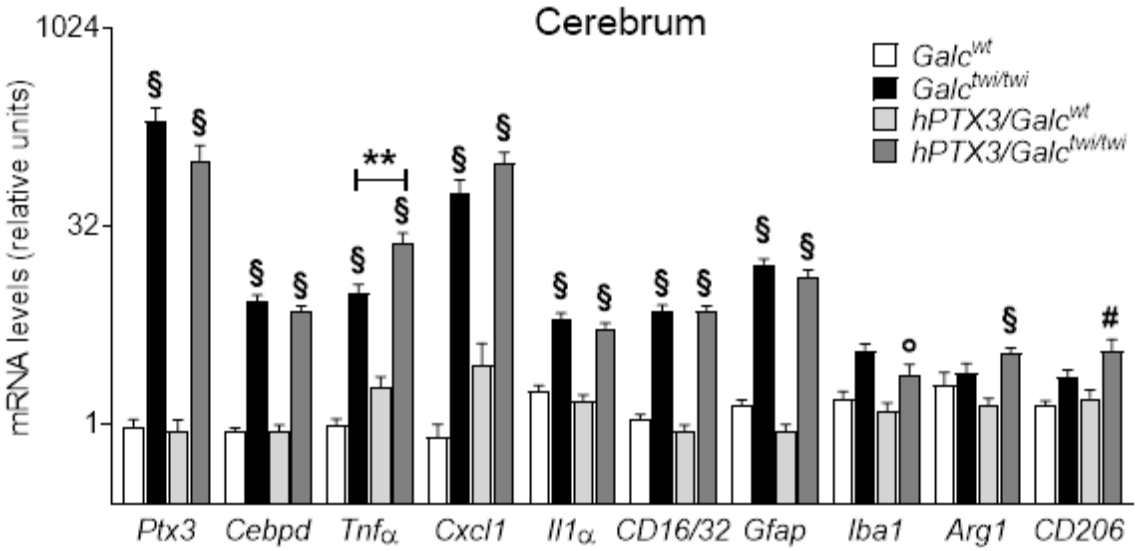

Supplementary Figure 6. qPCR analysis of the cerebrum and cerebellum of hPTX3/Galcwt and hPTX3/Galctwi/twi mice. Steady state mRNA levels of the indicated genes were evaluated by qPCR in the cerebrum and cerebellum of hPTX3/Galcwt and hPTX3/Galctwi/twi mice and compared to those measured in the corresponding control Galcwt and Galctwi/twi mice harvested at P35. Data were normalized to Gapdh expression and are the mean ± SEM. of 7-10 animals per group. **, P < 0.01; ***, P < 0.001, for Galctwi/twi versus hPTX3/Galctwi/twi ; °, P < 0.05; #, P < 0.01; §, P < 0.001 for Galcwt versus Galctwi/twi or hPTX3/Galcwt versus hPTX3/Galctwi/twi. One-way ANOVA with post-hoc comparisons with adjustment for multiple comparisons (Sidak).

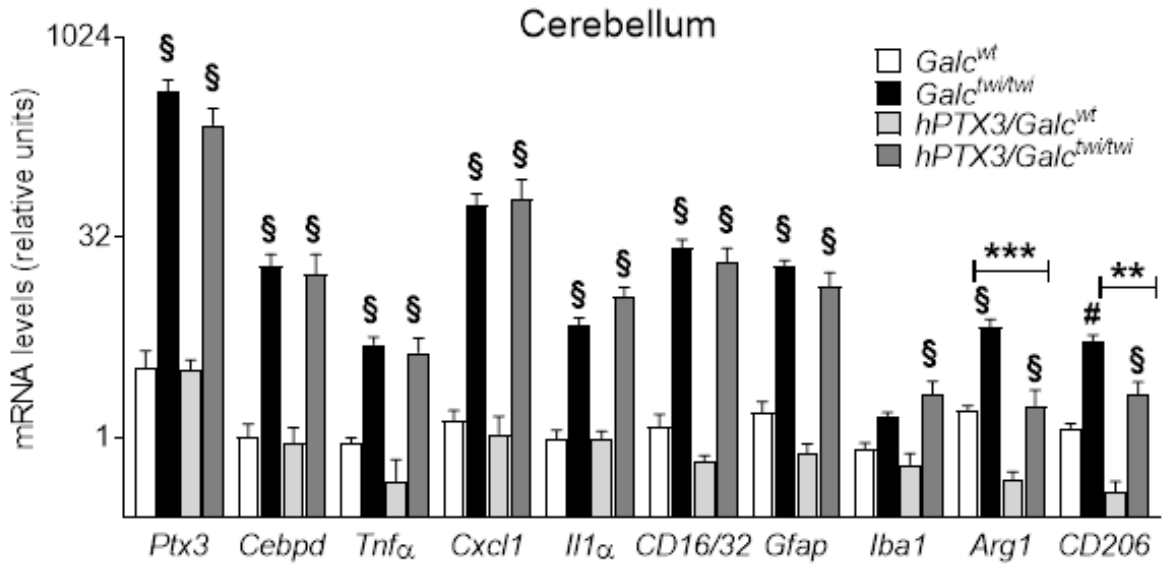
Cerebellum
mRNA levels (relative units)
1024
32
1
Galc^wt
Galc^twi/twi
hPTX3/Galc^wt
hPTX3/Galc^twi/twi
Ptx3
Cebpd
Tnfα
Cxcl1
Il1α
CD16/32
Gfap
Iba1
Arg1
CD206
§
#
***
**

CURRICULUM VITAE

Adwaid Manu Krishna Chandran

Address: Unit of Experimental Oncology and Immunology, Dept. of Molecular and Translational Medicine, Univer, 25133, Brescia, Italy

Email address: adwaid.krishna@unibs.it **Email address:** adwaidmanu1992@gmail.com

Phone number: (+39) 3202288683 **Skype:** adwaidmanu1992

Gender: Male **Date of birth:** 14/08/1992 **Nationality:** Indian

EDUCATION AND TRAINING

[2019 – 2022] **PhD in Precision Medicine**

University of Brescia

Address: Brescia, Italy

[2013 – 2015] **Master of science in Biomedical Genetics**

VIT University

Address: Vellore, India

[2010 – 2013] **Bachelor of Science in Biotechnology**

Bharathiar University

Address: Coimbatore, India

RESEARCH AND PROFESSIONAL EXPERIENCE

November 2018-Current:

- Characterization of cellular and molecular mechanisms involved in ERMs.
- Investigate the role of PTX3 in Krabbe disease

June 2019 - September 2019:

- Early-stage researcher in a "SCAFFY European project "(n° 645640)", MARIE SKŁODOWSKA-CURIE, Research, and Innovation Staff Exchange (RISE), HORIZON 2020

May 2016 –May 2018:

- ·Junior research fellow Manipal Academy of Higher Education, INDIA.
- The project involves a detailed neurological, systemic and molecular profiling of the animals exposed to EMF radiation and Heavy metal toxicity during fetal development, neonates and adults.

June 2015 – December 2015(mater thesis):

- Association of polymorphism in homocysteine regulatory genes with intracranial aneurysm patients in Kerala population – Rajiv Gandhi Centre for Biotechnology (RGCB), INDIA.

June 2014 –April 2015 (mini project):

- Genotoxicity of tetrodotoxin extracted from different organs of diodon hystrix puffer fish from south east Indian coast – VIT University, INDIA.

July 2013 – December 2013 (mini project):

- Antihaemolytic and antioxidant activity of piper longum – VIT University, INDIA.

PUBLICATIONS

1.) **Krishna Chandran AM**, Coltrini D, Belleri M, Rezzola S, Gambicorti E, Romano D, Morescalchi F, Calza S, Semeraro F, Presta M. Vitreous from idiopathic epiretinal membrane patients induces glial-to-mesenchymal transition in Müller cells. Biochim Biophys Acta Mol Basis Dis. 2021 Oct 1;1867(10):166181.

2.) Rezzola S, Guerra J, **Krishna Chandran AM**, Loda A, Cancarini A, Sacristani P, Semeraro F, Presta M. VEGF-Independent Activation of Müller Cells by the Vitreous from Proliferative Diabetic Retinopathy Patients. Int J Mol Sci. 2021 Feb 22;22(4):2179.

3.) Coltrini D, Belleri M, Gambicorti E, Romano D, Morescalchi F, **Krishna Chandran AM**, Calza S, Semeraro F, Presta M. Gene expression analysis identifies two distinct molecular clusters of idiopatic epiretinal membranes. Biochim Biophys Acta Mol Basis Dis. 2020 Dec 1;1866(12):165938.

4.) **Krishna Chandran AM**, Christina H, Das S, Mumbrekar KD, Satish Rao BS. Neuroprotective role of naringenin against methylmercury induced cognitive impairment and mitochondrial damage in a mouse model. Environ Toxicol Pharmacol. 2019 Oct; 71:103224.

CONFERENCES AND SEMINARS

1.) 104th Oxford Ophthalmological Congress (OOC),2021 virtual meeting - Poster presentation.

2.) 7th Italian experience in biomedical research: young minds at work,2019 at Park Hotel - Desenzano del Garda, Brescia, ITALY-Oral presentation.

3.) 5th Manipal Research Colloquium ,2018 at Manipal Academy of Higher Education, Manipal, India-Oral presentation

4.) XXXXII Annual Conference of Environmental Mutagen Society of India (EMSI) and National Conference on "Environmental

Mutagenesis: Integration of Basic Biology & Omics to improve Human Health,2018 at BARC, Mumbai, India-Poster presentation.

5.) 9th international Conference on science, Engineering and Technology, 2014 at VIT University, Vellore, India- Poster presentation.

6.) 7th international Conference on science, Engineering and Technology, 2013 at VIT University, Vellore, India – Oral Presentation.

7.) National Conference on "Confluence of Research and Ethics in Biological Sciences-A Scenario on the Emerging Trends" (NCBS- 2013) – Poster presentation

LANGUAGE SKILLS

Mother tongue(s): Malayalam

Other language(s):

English

LISTENING C2 **READING** C2 **WRITING** C2

SPOKEN PRODUCTION C1 **SPOKEN INTERACTION** C2

JOB-RELATED SKILLS

Animal handling: Breeding and maintenance of laboratory animals

Biochemistry: Western blot, ELISA, biochemical and enzymatic assays.

Cell biology: In Vitro cell experiments using primary cell and cell lines.

Cytogenetics: leukocyte culturing, Analysis of induced chromosome aberration in Leukocyte Culture by chemicals and radiation, Sister chromatid exchange analysis, Micronucleus test, Sperm abnormality Analysis, Chromosome Preparation from Mouse bone marrow, karyotyping, staining (giemsa and silver staining), banding techniques (GTG banding, NOR banding, centromere banding), DNA damage analysis.

Microscopy: fluorescence and light microscopy.

Molecular biology: Primer designing, PCR, RFLP, Real-Time PCR, Long Range PCR, Bisulphite Sequencing, Sanger Sequencing and analysis.

Neurobiology: Behavioural studies and neurological staining

RECOMMENDATIONS

1. Prof.Presta Marco

Professor

Experimental Oncology and Immunology,

Department of Molecular and Translational Medicine

University of Brescia, Italy

Email ID: marco.presta@unibs.it

2. Prof.B. S. Satish Rao,

Directorate of Research

Manipal Academy of Higher Education, Manipal, India

Email ID: rao.satish@manipal.edu